# Assessing diversity of prairie plants using remote sensing

by

RAN WANG

A thesis submitted in partial fulfillment of the requirements for the degree of

Doctor of Philosophy

Department of Earth and Atmospheric Sciences
University of Alberta

## Abstract

Biodiversity loss endangers ecosystem services and is considered as a global change that may generate unacceptable environmental consequences on the Earth system. Global biodiversity observations are needed to provide a deep understanding of the biodiversity - ecosystem services relationship and conserve the Earth's biodiversity. Traditionally, in situ biodiversity monitoring is limited in time and space and is usually a costly and time-consuming enterprise. Remote sensing can provide data over a large area in a consistent, objective manner and has been used to detect plant biodiversity in a range of ecosystems based on the varying spectral properties of different species or functional groups. Studies estimating biodiversity using remote sensing can be generally categorized into three types: estimating biodiversity indirectly with habitat mapping; mapping distribution of individuals as a basis for assessing community composition and diversity; and assessing species richness directly from patterns of spectral variation to yield α-diversity. However, key questions remain: 1) can the diversity-productivity relationship be assessed using remote sensing? 2) what drives the variation of optical signal among species or functional groups? and 3) what is the appropriate spectral and spatial scale for biodiversity detection using remote sensing?

To answer these questions, a series studies were accomplished at Cedar Creek Ecosystem Science Reserve, Minnesota, where the biodiversity manipulation of prairie plants provided a proper diversity gradient. First, the productivity-biodiversity relationship was tested from a remote sensing perspective. Results indicated that NDVI and biodiversity

were positively related, and that the NDVI-biodiversity relationship varied slightly across the growing season and was affected by other factors including canopy structure, short-term water stress, and shifting flowering patterns. Second, proximal remote sensing revealed rapid information loss with increasing pixel size. The best resolution to detect α diversity using spectral diversity at this prairie ecosystem was at a size close to a typical herbaceous plant leaf or single canopy. Furthermore, results from a combination of field spectral measurements and a modeling framework indicated that both species richness and evenness influenced spectral diversity metrics. Species identities also showed substantial effects on spectral diversity metrics at the fine scale. Background (e.g., soil) effects on spectral diversity varied with metrics: spectral diversity metrics based on information theory were sensitive to the background, while background had no effects on classification-based indices at this fine scale. Using full range spectra (400 – 2500nm) slightly increased the species separability over using visible-NIR wavelength only. Additionally, the primary spectral diversity metric, the coefficient of variation of spectral reflectance in space, was also tested in a prairie ecosystem in Southern Alberta to detect the biodiversity in a natural landscape. Overall, the plant optical signal was influenced by both leaf traits and canopy structure, and the ability to use spectral diversity metrics in biodiversity estimation depended on the species richness, evenness, composition, associated spectral properties, sensor characteristics, and the particular spectral diversity metrics selected. This project provides a critical foundation for assessing biodiversity using imaging spectrometry and these findings can be used to guide regional studies of biodiversity estimation using high spatial and spectral resolution remote sensing.

## Preface

This thesis is an original work by Ran Wang. The ongoing research project, of which this thesis is a part, is funded by NASA and NSF, Project Name "Linking remotely sensed optical diversity to genetic, phylogenetic and functional diversity to predict ecosystem processes", No. DEB-1342872. Chapters 2 through 5 were co-authored, with research, analysis and writing led by Ran Wang. Co-authors were involved in scoping the project, assisting data collection and data analysis and providing editorial comments.

A version of Chapter 2 has been published as: Ran Wang, John A. Gamon, Rebecca Montgomery, Philip A. Townsend, Arthur I. Zygielbaum, Keren Bitan, David Tilman and Jeannine Cavender-Bares. 2016. "Seasonal variation in the NDVI–species richness relationship in a prairie grassland experiment (Cedar Creek)". *Remote Sensing*. 8: 128. R.W. was the primary author, and J.G., J.C.-B., R.M., P.T., and A.Z. all contributed to the writing; R.W., J.G., K.B. collected the optical data; R.M. contributed flowering and height (phenology) data; R.W. provided most of the data analysis, with a contribution from R.M. on the analysis of phenology data; R.W., J.G., J.C.-B., R.M., D.T. contributed to the design of the experiment.

A version of Chapter 3 has been published as: Ran Wang, John A. Gamon, Craig A. Emmerton, Haitao Li, Enrica Nestola, Gilberto Z. Pastorello and Olaf Menzer. 2016. "Integrated analysis of productivity and biodiversity in a southern Alberta prairie". *Remote Sensing*. 8: 214. R.W. was the primary author, and J.A.G., C.A.E., E.N., G.Z.P., O.M. all contributed to the writing. J.A.G., H.L., E.N., G.Z.P. collected the field data. H.L., G.Z.P., and J.A.G. assisted in collecting the airborne data. C.A.E. conducted the eddy covariance data analysis. O.M. conducted the flux tower footprint analysis. R.W. conducted the airborne data analysis. R.W. and J.A.G. conceived and designed the experiment.

A version of Chapter 4 has been accepted for publication as: Ran Wang, John A. Gamon, Jeannine Cavender-Bares, Philip A. Townsend, Arthur I. Zygielbaum. "The spatial sensitivity of the spectral diversity-biodiversity relationship: an experimental test in a prairie grassland". – *Ecological Applications (in press)*. R.W. was the primary author, and J.G., J.C.-B., P.T., and A.Z. all contributed to the writing; R.W. and J.G. collected

the optical data; R.W. provided the data analysis; R.W., J.G., J.C.-B., P.T., and A.Z. contributed to the design of the experiment.

A version of Chapter 5 is in preparation for publication as: Ran Wang, John A. Gamon, Anna K. Schweiger, Jeannine Cavender-Bares, Shan Kothari, Philip A. Townsend, Arthur I. Zygielbaum. “Investigating the effect of species richness, evenness and composition on spectral diversity using simulated hyperspectral images”. R.W. was the primary author, and J.G., A.S., J.C.-B., S.K., P.T., and A.Z. all contributed to the writing; R.W. and J.G. collected the image-derived optical data; A.S. and S.K. collected the leaf clip-derived optical data, R.W. provided the data analysis; R.W., J.G., A.S., J.C.-B., P.T., and A.Z. contributed to the design of the experiment.

## Acknowledgements

Decades ago, “scientist” might have been one of the most popular dream professions among kids in China, even though most people didn’t have an idea about what scientists were supposed to do. At that time, I could hardly imagine that I could work so closely with scientists someday. During the last four years, I have been training to be a scientist as a Ph.D. student in University of Alberta. Whether or not I’ll stay in the academia, I really appreciate this special experience.

I would first like to thank my supervisor Dr. John Gamon, who certainly has a profound influence on my academic career. I see a scientist’s professional knowledge and rigorous working attitude from Dr. Gamon. Dr. Gamon is always patient with my terrible writing and keeps giving detailed comments on my every manuscript. In my eyes, he is constantly trying to make the perfect better. All this impressed me and pushed me to be better.

I would also like to thank my committee members Dr. James Cahill and Dr. Alberto Reyes for giving constructive comments and suggestions on my research. I expanded my knowledge on ecology from Dr. Cahill’s lab meetings and I enjoyed the atmosphere where people in the lab are always willing to share ideas and help each other. I learned how a young scientist should look like from the wonderful working experiences with Dr. Reyes: enthusiastic, open-minded and hard working. I’m also grateful to Dr. Jeannine Cavender-Bares, Dr. Philip Townsend, and Dr. Arthur Zygielbaum in the project for helping design the experiments and providing advice on the manuscripts.

I have had great pleasure to work with every member in our group, Chris Wong, Kyle Springer, Craig Emmerton, Scott Williamson and Donnette Thayer in the last four years. I appreciate all the assistance from staff and interns at the Cedar Creek Ecosystem Science Reserve. The research cannot be achieved without their help.

A special gratitude to my family. It has been a tough decision to study aboard and I have not been able to spend as much time as I wanted with my parents. I appreciate their understanding and they always have my back through my life. My girlfriend, Xiaomeng Li, is the first and most patient audience for all my weird thoughts at all times. Her

continuous support and encouragement make me go through this special journey. I love you all.

# Table of contents

# List of Tables

# List of Figures

# Chapter 1 Introduction

"*The **Eremocene**, the Age of Loneliness, is basically the age of people, our domesticated plants and animals, and our croplands all around the world as far as the eye you can see.*"
Edward O. Wilson: Half Earth: Our Planet's Fight for Life

## 1.1 Biodiversity

A widely-cited definition of biological diversity is "the variety and variability among living organism and the ecological complexes in which they occur" (US Congress Office of Technology 1987). Broadly, biodiversity is the total variability of living organisms on Earth, including diversity within species, between species and of ecosystems (Heywood 1995).

The question *why do different regions on Earth have different numbers and types of species* has puzzled ecologists and biologists for centuries. Species richness and distribution vary with latitude, climate, productivity, and a host of other physical and biological variables. The latitudinal diversity gradient exists in almost all taxonomic groups (Hillebrand 2004). Dozens of hypotheses including "Null-Model", and hypotheses from ecological, historical, and evolutionary perspectives, have been proposed to explain this latitudinal gradient (Mittelbach 2012). An awareness of how species diversity varies across space and time provides a foundation from which to explore the mechanisms of species interactions and to understand the processes that drive variation in species numbers and their distribution (Mittelbach 2012).

Understanding the processes that drive the variation in number of species and their distribution have challenged community ecologists, while an equal challenge exists in assessing species diversity at different spatial scales. Biodiversity can be defined at different spatial scales (Whittaker 1960, 1972): Alpha (α) diversity is diversity at a defined place (habitat); Beta (β) diversity describes the variation among habitats; Gamma (γ) diversity is the total diversity of a region or other spatial units (landscape level). α and γ diversity measure the number of species or other suitable measures of diversity at local

and regional spatial scales respectively, and β diversity presents the community dissimilarity. These three diversity measures are simple in principle but can be problematic when applied in the real world. For α diversity, while it seems straightforward to define the concept, the boundaries of a habitat or site are often subjective, and getting an accurate measure of species richness at a site involves important sampling considerations. β diversity measures the difference in species composition, or species turnover, among sites. But contentious discussions remain in how to define and measure β diversity (Tuomisto 2010a, b, Anderson et al. 2011). Finally, γ diversity refers to the total number of species in a landscape or a region. The concept of region, however, varies with particular studies or applications (Whittaker et al. 2001).

### 1.2 Loss of biodiversity

The advance of ecology has caused scientist to realize, the relative rate of biodiversity loss. By the late 1980s, reports stated the loss rate of the world's biodiversity "is *likely* to increase over the next several decades" (US Congress Office of Technology 1987) and the American public "sees biodiversity needs to be protected" (Nash 1989). In the late 1990s to early this century, biodiversity was related to its effects on ecosystem function, and began to be seen as an important global change issue in its own right (Pimm et al. 1995, Sala et al. 2000). Now, biodiversity loss is treated as a global change with consequences that may exceed that of climate change in generating unacceptable environmental change to the Earth system (Rockström et al. 2009).

Extinction has always been a part of the history of life on Earth and would happen without human activities. However, the numbers of species, notably the vertebrate animals and flowering plants, are being lost at an accelerating rate since the last mass extinction (65 Mya) that claimed the lives of dinosaurs (Wake and Vredenburg 2008). The estimated current species extinction rate is 100-1000 times faster than the background rate of species extinction, which is approx. 0.1-1 species per million species per year for marine life and 0.2-0.5 extinctions per million species per year for mammals (Rockström et al. 2009). The current extinction has been called the sixth mass extinction (Barnosky et al. 2011), and by the mid of the current century, up to half of the Earth's

species may disappear due to habitat modification and destruction, overuse of fertilizers and pesticides, global warming and increased climatic variability, overharvesting, invasive species, and other effects of human activities (Thomas et al. 2004, Wake and Vredenburg 2008).

Species extinctions are not the only aspect of changing biodiversity. The changing of species richness, abundance and community structure, habitat loss and degradation, invasive species and shift in the distribution of species and biomes affect the global biodiversity distribution (Pereira et al. 2010). In the short term, extinction of some species may have limited links to ecosystem services comparing to other metrics, such as changes in species abundances and community structure and, at a higher organizational level, habitat loss or biome changes (Hooper et al. 2005, Pereira et al. 2010). However, extinction might be able to cause a future ecological cost that is called the extinction debt (Tilman et al. 1994). For example, the range of a species can decline shortly after habitat change, but that species may not immediately become extinct. However, extinctions might occur generations after the habitat loss and the most abundant species can be the most vulnerable to the habitat change and can, consequently, lead to insidious effects on ecosystem functions (Tilman et al. 1994).

Biodiversity loss endangers ecosystem services that maintain human wellbeing. Conservation of biodiversity is important on account of the distribution and abundance of species over space and time and the functional roles each species plays in an ecosystem (Hooper et al. 2005). The functional characteristics varies among species and the relative abundance of each species alone may not always represent the importance of a species to the ecosystem, because relatively rare species (e.g., keystone species (Power et al. 1996)) can have strong influences on the energy and material flows within the ecosystem (Hooper et al. 2005). Other than the effects of biodiversity on ecosystem functions and services, loss of biodiversity can also cause ethical and aesthetic concerns for example, each species is unique and represents a particular part of millions of years Earth history, and the extinction of a species means its history will be buried forever. It took at least 3.7 billion years to build the world our species inherited (Ohtomo et al. 2014) and

understanding the patterns of biodiversity could serve as a basis for preserving biodiversity.

### 1.3 Biodiversity and ecosystem function

Community ecologists have long focused on understanding how ecosystem biotic and abiotic factors affects biodiversity within it (Hillebrand and Matthiessen 2009). The influence of diversity on ecosystem function gained attention following two papers published in 1990s (Naeem et al. 1994, Tilman and Downing 1994). Although Tilman's work (Tilman and Downing 1994) was criticized due to the possibly artifacts caused by added nitrogen, they paved a new road to investigate the biodiversity-ecosystem relationship from a different direction (Hooper et al. 2005, Balvanera et al. 2006, Cardinale et al. 2007). Succinctly, biodiversity affects ecosystem function in terms of productivity (Tilman et al. 1996, Isbell et al. 2009, 2015), community and ecosystem stability (Tilman and Downing 1994, Tilman et al. 2006), nutrient use and nutrient retention (Hector and Bagchi 2007, Maestre et al. 2012, Midgley 2012), and invasibility (Naeem and Li 1997, Naeem et al. 2000).

Much of the cutting edge biodiversity-productivity research has developed from experiments and models (Thompson 2015). Three large scale experiments, Cedar Creek Ecosystem Science Reserve in Minnesota, USA (Tilman 1997, Tilman et al. 2001), BIODEPTH in Europe (Hector et al. 1999), and the Jena Biodiversity Experiment in Germany (Hector et al. 2011), consistently demonstrated that biodiversity enhanced productivity. Two likely hypotheses have been presented to explain this positive relationship between biodiversity and productivity: 1) species selection effects, and 2) Niche complementarity (Lehman and Tilman 2000, Loreau and Hector 2001). The selection effects hypothesis (also called "selection probability effects") states that adding species increases the probability of having a productive species, especially when creating a community with high richness within a small size pool of candidate species (Huston 1997). The complementarity hypothesis suggests that the presence of multiple species increases production via more efficient resource capture.

Although the productivity-biodiversity relationships are often positive at broad spatial scales, a variety of productivity-biodiversity relationships, including positive, negative, hump-shaped and U-shaped have been reported at local scales (Adler et al. 2011, Fraser et al. 2015). This relationship can be affected by community composition, resource levels (e.g., fertilizer or irrigation levels) and nature of disturbance (Waide et al. 1999, Mittelbach et al. 2001, Fraser et al. 2015). In some cases, highly productive sites are known to be resource rich and species poor. These high productivity and low diversity sites are typically highly managed via irrigation or fertilizer application (Fraser et al. 2015) and often lead to declines in the species richness relationships at high productivity. Variation in the relationship between biodiversity and ecosystem function is known to depend on resource availability (Reich and Hobbie 2013) and environmental drivers, particularly drought stress, have been shown to constrain biomass in prairie systems (Tilman and Haddi 1992, Isbell et al. 2015).

### 1.4 Measuring biodiversity in nature

Several approaches have been used to measure biodiversity. However, it is difficult to define or apply a single metric in biodiversity estimation. Diversity indices may be criticized for losing information and may not by themselves be very informative in summarizing community characteristics. Considerable information about community characteristics can be lost when using a single value to measure biodiversity (Noss 1990). Species richness – the number of species at a site - is the oldest, simplest and among the most widely used measures of α diversity and has been used to drive many ecological models (Gotelli and Colwell 2001). Other than species richness, many diversity metrics describe the entire distribution of species abundance (e.g. a rank abundance plot, which contains the maximum amount of information about a community's diversity). Some metrics quantify the richness of the sample or assemblage (e.g. species accumulation curves), or provide a statistic that takes account of the evenness of the species abundances (the richness and evenness are both taken into consideration by the Shannon's index and Simpson's Index) (Magurran 2004, 2013, Hamilton 2005). Note that ecologists can and do measure other aspects of biodiversity besides numbers of

species, like genetic diversity and functional group diversity (Magurran and McGill 2011).

Typical methods of measuring biodiversity need experienced researchers working in the field. However, field biodiversity sampling is always a downward estimator of the real species richness due to the limited sample size, and the impracticality of finding all the species, especially when the diversity is high and most species are rare, as is typical of tropical rainforests (Gotelli and Colwell 2010). While an explicit survey of all the subjects can provide detailed information, it is infeasible to apply this kind of census for every case. Therefore, a proper sampling method must be taken to estimate the diversity (Bonar et al. 2010). Even so, it generally costs a lot of time and energy to execute the sampling work and can be remarkably expensive when sampling over a large area. It has been estimated that 0.6 to 4 million Euros per year are needed to accomplish a species monitor program in France (Levrel et al. 2010) and as little as 0.5 million USD are needed to integrate species-monitoring programs for selected terrestrial vertebrates, butterflies, and plants in regions such as sub-Saharan Africa, South America, and East Asia (Pereira et al. 2010). However, for most regions, a large amount of government investment is needed to support biodiversity monitoring, and new methods/technologies are needed to make such monitoring more effective for large areas.

### 1.5 Remote sensing of biodiversity

"*Remote sensing, a stepchild of the space age, is prying out many of Earth's innermost secrets.*" – National Geographic: Eye in the Sky—History of Satellites

Although the early terrestrial observation satellites were launched in the 1970s, the potential of using remote sensing to measure, map, monitor, and model spatial patterns and trends in biodiversity was largely ignored until 1990s (Stoms and Estes 1993). A simple survey of the number of published articles using "*Remote Sensing*" and "*Biodiversity*" as *Topic* in Web of Science reveals the increasing interest in remote sensing for assessing biodiversity. By 1990, only one publication was found that used

satellite remote sensing to track the effects of tropical forest loss on the changes in species abundance (Westman et al. 1989). A larger number of studies on this topic started to emerge in the 1990s (65 publications in 1990 - 2000) and the numbers increased steadily in the first 15 years of this century (173 publications in 2001 – 2005; 450 publications in 2006 – 2010; 777 publications in 2011 - 2015) (Figure 1.1). Clearly, remote sensing is playing an ever-increasing role in studies of biodiversity.

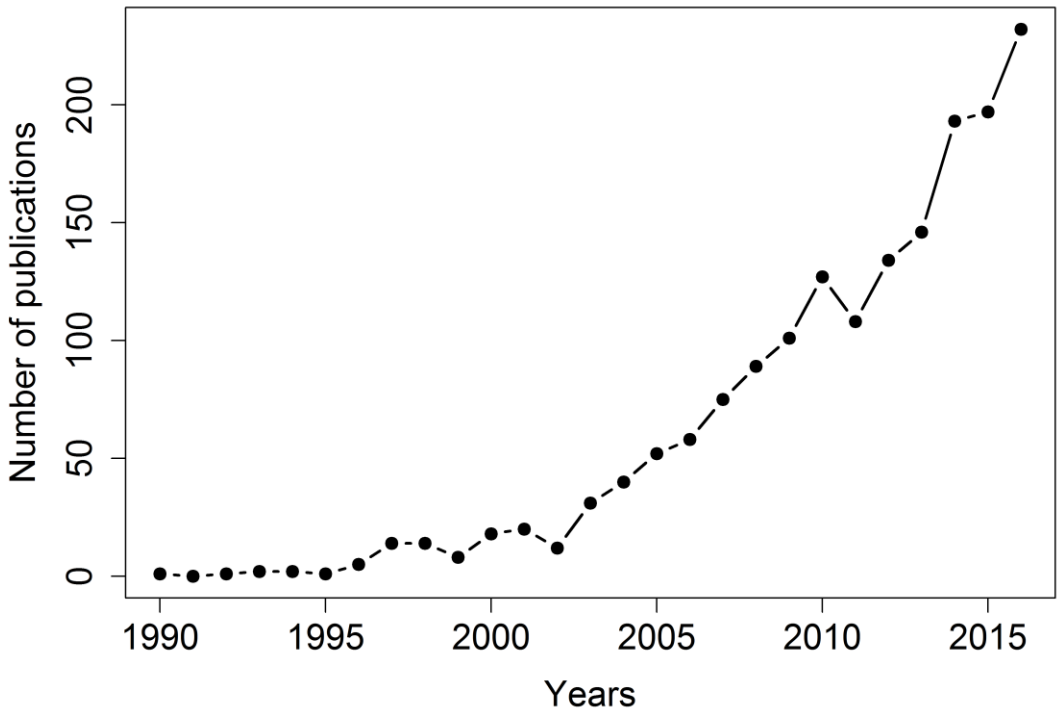


Figure 1.1 The number of publications on remote sensing of biodiversity in Web of Science (1990 - 2016)

The early applications of remote sensing in biodiversity estimation mainly focused on mapping landscape or habitat through landcover classification. But little was accomplished on detailed verification of the statistical or ecological significance of the indices linking the habitat diversity – biodiversity relationship (Stoms and Estes 1993). This was due to a limited ecological understanding of the effects of biodiversity on

ecosystem function, the limited information provided by the early remote sensing sensors, insufficient imaging processing techniques (e.g., simple classification methods with no particular indices designed for biodiversity assessment), and lack of understanding of how to interpret ecological information contained in the remote sensing products (Stoms and Estes 1993).

Traditionally, our ability to detect biodiversity with remote sensing is restricted by spatial, spectral, and temporal resolution of the techniques involved. Imaging spectrometry and Light Detection and Ranging (LiDAR) systems have been both used in vegetation remote sensing and are relevant to biodiversity assessment in recent years. These new tools are expanding the range of detectable plant physiological and structural properties that can contribute to an assessment of functional diversity (Ustin and Gamon 2010).

Studies estimating biodiversity using remote sensing can be generally categorized into three types: estimating biodiversity indirectly with habitat mapping; mapping distribution of individuals as a basis for assessing community composition and diversity; and assessing species richness directly from patterns of spectral variation to yield α-diversity (Table 1.1).

### 1.5.1 Estimating biodiversity indirectly with habitat mapping

Landcover mapping is one of the earliest and most widely used applications of optical remote sensing. At the beginning of this century, landcover data had been found helpful for predicting the distribution of both individual species (Jennings 2000, Saveraid et al. 2001) and species assemblages (Kerr et al. 2001). In Europe, the Earth Observation Data for Habitat Monitoring (EODHaM) system was launched to provide a framework for integrating Earth observation and *in situ* data to monitor biodiversity and habitat (Lucas et al. 2015).

Estimating biodiversity through habitat mapping applies remote sensing indices to assess environmental parameters (e.g., productivity, climate and habitat structure) and either relates the heterogeneity of the habitats to biodiversity (Kerr et al. 2001, Bailey 2004) or integrates these remote sensed environmental parameters with GIS (Austin et al. 1996, Luoto et al. 2002, Foody 2005, Costanza et al. 2011) using national models (e.g.,

National GAP Analysis Program (GAP) (Jennings 2000) or local models (Parviainen et al. 2009)) to estimate biodiversity.

The accuracy of biodiversity mapping or species distribution estimation using habitat mapping is highly affected by characteristics of the species involved. Landcover mapping might only estimate potential rather than the real species distributions for species that do not occupy all suitable habitats (Kerr and Ostrovsky 2003). For example, the estimation of distribution of particular butterfly, plant or bird species in Yellowstone National Park is possible when their distributions fit a specific habitat requirement, the number of their individuals are abundant, or both (Saveraid et al. 2001). It is less practical to assess distribution of rare species or species that are not specific to particular habitats even from remarkably accurate and detailed land cover data (Kerr and Ostrovsky 2003).

Habitat mapping using remote sensing techniques is generally done at coarse scales (Wulder et al. 2004, Corbane et al. 2015). Global land cover data can be provided by using MODIS satellite at 500 m pixel size (Friedl et al. 2010), while regional landcover data have been retrieved using moderate resolution satellite products such as Landsat that has a 30 m spatial resolution (Tiede et al. 2010). Detailed information on landscape complexity is lost when using such relatively low spatial resolution satellite products. While higher spatial resolution satellites with sub-meter pixels are available now, mostly from commercial satellites, the limited spectral information contained in those products limited the accuracy of habitat mapping and their high cost precludes widespread usage. Also, the limited spectral bands may further restrict their power to detect diversity.

### 1.5.2 Mapping distributions of individuals

A fundamental premise in mapping the distribution of individuals or particular species using remote sensing is a deep understanding of the relationship between the spectral response measured by the remote sensing sensor and the parameters of interest (Wulder 2004, Asner et al. 2008). For example, in order to predict the distribution of invasive species, the native and exotic species should be, at least, separable by their spectral reflectance. However, the necessary spectral information has been limited until only very recently.

The task of species mapping has generally been done by applying airborne imaging spectroscopy that can provide high spatial resolution images with detailed spectral information at local or regional scales (Roberts et al. 1998, Ustin et al. 2004, Xiao et al. 2004, Asner et al. 2008). Imaging spectroscopy can now cover the whole range of the visible and short-wave infrared reflectance spectrum (400 – 2500 nm) at high spectral resolution, and absorption features of leaves in specific tiny bands can be detected (Ustin et al. 2004). Airborne spectra have been successfully related to plant leaf chemical properties in tropical forests (Asner and Martin 2009, Féret and Asner 2014). Although it might be impossible to distinguish every species using remote sensing (Price 1994), it is often feasible to differentiate dominant species or community types based on the images using spectral differences (Ustin and Gamon 2010). For example, invasive species may have unique spectroscopic reflectance properties from that of native species, and plants of different functional types, e.g., nitrogen-fixing and non-fixing species, can be separable due to their biochemical composition (Asner et al. 2008). Moreover, particular leaf traits can affect canopy architecture which can accentuate the leaf spectral properties through multiple scattering and contrasting illumination (Ollinger 2011). By integrating imaging spectroscopy and LiDAR, both biochemical traits and canopy structure properties can be captured. As a consequence, mapping individual species can succeed when there are biochemical and/or structural variations between species (Ustin and Gamon 2010) and complete *a priori* knowledge about the optical properties of all the possible present species (Price 1994).

### 1.5.3 Estimating alpha diversity directly through spectral diversity

'Spectral diversity' (Palmer et al. 2002), sometimes called "optical diversity" (Ustin and Gamon 2010) indicates the variation in spectral patterns detected by remote sensing. Instead of mapping species *per se*, spectral diversity detects functional and structural properties, which vary among species or functional groups ("optical types") (Ustin and Gamon 2010). The spectral diversity hypothesis can be tied to the 'functional convergence' hypothesis, which considers that the observable properties of plants are determined by different evolutionary histories (phylogeny) and the variety of ways in which plants respond to resources through different ecophysiological strategies (Field 1991). Despite phylogenetic differences, resource limitations (e.g., light, water, nutrients)

can affect the growth of plants and lead to patterns in leaf traits (carbon and nitrogen composition, pigment, water content, dry mass and structural parameters, e.g. lignin), canopy structure (leaf area and leaf angle distribution) and phenology. Plants adjust their properties, such as leaf life span, allocation to defense, photosynthesis and respiration, to adapt to the environment or limitation of resource (Wright et al. 2004). As a result, an individual organism's phenotypic activity or state represents the interaction between its genome, the changing environment, and random events (Fusco and Minelli 2010). Characteristic plant traits affect plant light absorption and scattering and consequently, cause variation in plant optical properties that can be detected with remote sensing (Ustin and Gamon 2010).

The spectral diversity hypothesis links ecological resource theory to fundamental physical principles to provide a rapid and accurate approach to measure variation in functional types via optical patterns (Ustin & Gamon, 2010). If optical type is regarded not only as an indicator of plant physiological and biochemical properties but a fundamental vegetation property, resulting from "ecological rules" driven by resource allocation, there should be predictable interrelationships among the plant traits and optical properties. If this effect leads to predictable (repeatable) patterns across time and space, then the principle of functional convergence enables remote sensing to characterize plant functional traits based on objective optical signals. As a consequence, variation in these optical properties and their associated traits in time and space might enable us to detect biodiversity at different scales.

Many remote sensing metrics based on spectral patterns have been proposed to assess biodiversity (Table 1.1). These metrics can be grouped into two major categories: 1) metrics based on information theory (e.g. spectral entropy (Rocchini et al. 2015)) and 2) metrics based on classification results (Féret and Asner 2014, Schäfer et al. 2016). The information theory based metrics either extract information from the spectral space by calculating the variance of vegetation reflectance indices (e.g., NDVI) (Gould 2000, Carlson et al. 2007), the coefficient of variation of the reflectance across space (Wang et al. 2016a), or the distance from the spectral centroid (Palmer et al. 2002). Alternatively, these metrics can be based on patterns in principal component space that compacts

spectral information and removes noise and band collinearity. Examples include the distance from the centroid in principal component space (Rocchini 2007). The classification based metrics apply a classification, either unsupervised classification (Féret and Asner 2014) or object-based classification (Schäfer et al. 2016), to the remotely sensed images and relate the metrics calculated based on the resulting "spectral species" to actual biodiversity metrics.

Table 1.1 Examples of alpha diversity assessment using remote sensing, showing types of methods, ecosystems, sensors and platforms, specific methods used, and references

| Type of methods | Ecosystem & location | Sensor & Platform | Metrics (information/classification) | Reference |
|---|---|---|---|---|
| Habitat mapping | | | | |
| | Grassland and deciduous woodland (Scotland) | Landsat | Unsupervised classification | (Austin et al. 1996) |
| | Grassland and deciduous woodland (Great Britain) | Landsat | Classification | (Griffiths and Lee 2000) |
| | Greater Yellowstone Ecosystem (USA) | SPOT | Classification | (Saveraid et al. 2001) |
| | Pan Canada | AVHRR<br>SPOT | Classification by Canada Centre for Remote Sensing and Canadian Forest Service | (Kerr et al. 2001) |
| | Boreal agricultural landscape (Finland | Landsat | Supervised classification | (Luoto et al. 2002) |
| | Great Basis (USA) | Landsat | Maximum and heterogeneity of productivity | (Bailey and Bailey 2004) |
| | Great Britain | AVHRR | NDVI, temperature | (Foody 2005) |
| | Pine/aspen forest (South Dakota, USA) | LiDAR | Vegetation index | (Clawges et al. 2008) |

| | | | | |
|---|---|---|---|---|
| | | IKOMOS | | |
| | Evergreen forest, transitional between lowland rain forest and montane forest (Uganda) | Landsat Quickbird | NDVI, PCA | (Stickler and Southworth 2008) |
| | Northern boreal forest (Finland) | Landsat | NDVI and local greenness models | (Parviainen et al. 2009) |
| | Coastal plain (Carolina, USA) | Landsat<br>MODIS | Mean NDVI - productivity | (Costanza et al. 2011) |
| Species distribution | | | | |
| | California Chaparral (California, USA) | AVIRIS | End member spectral mixture analysis (classification) | (Roberts et al. 1998) |
| | Forest tree species in urban area | AVIRIS | Spectral mixture analysis (Classification) | (Xiao et al. 2004) |
| | Invasive forest species (Hawaii, USA) | AVIRIS | Link reflectance to leaf traits using PLSR | (Asner et al. 2008) |
| | Wetland (California, USA) | PROBE | Classification | (Zomer et al. 2009) |
| | Invasive species urban area (British Columbia, Canada) | CASI | Spectral angle mapper classification | (Chance et al. 2016) |
| Alpha diversity | | | | |
| | Low-shrub tundra (NWT, Canada) | Landsat | Variation in NDVI | (Gould 2000) |
| | Tallgrass prairie (Oklahoma, USA) | Aerial photograph | Spectral diversity | (Palmer et al. 2002) |
| | Subtropical vegetation communities | AVHRR | Variation in NDVI | (Fairbanks and McGwire |

| | | | |
|---|---|---|---|
| (California, USA) | | | 2004) |
| Tropical forest (Florida, USA) | Landsat | Mean and standard deviation of NDVI | (Gillespie 2005) |
| Wetland (Tuscany, Italy) | Quickbird, Landsat | PCA | (Rocchini 2007) |
| Lowland rain forest (Hawaii, USA) | AVIRIS | Range of spectral values | (Carlson et al. 2007) |
| Evergreen Mediterranean plants (Mount Hermon, Israel) | Landsat<br>Aster<br>Quickbird | Mean and standard deviation of NDVI | (Levin et al. 2007) |
| Grassland (Inner Mongolia, China) | MODIS | MODIS-derived GPP and NDSVI | (John et al. 2008) |
| Meadows and woodland (Mississippi, USA) | HyMap | CV of reflectance indices | (Lucas and Carter 2008) |
| Dry, moist, and wet forest (Panama) | Landsat<br>AIRSAR | Mean and standard deviation of NDVI, radar backscatter | (Gillespie et al. 2009) |
| Savannah (Central Namibia) | HyMap | PCA | (Oldeland et al. 2010) |
| Meadow (Central Alps, Valtellina, Italy) | Handhold spectrometer (ASD) | PLSR | (Fava et al. 2010) |
| Vascular plants (Switzerland) | Landsat | PCA | (Rocchini et al. 2011) |
| Mediterranean forests and crops (Tuscany, Italy) | Landsat | PCA | (Rocchini and Neteler 2012) |
| Peruvian Amazon | AVIRIS | Unsupervised classification | (Féret and Asner 2014) |
| Deciduous forest (Chile) | EO1-Hyperion | Use NDVI, topological, and structural data train classification | (Ceballos et al. 2015) |

| | | | |
|---|---|---|---|
| | LiDAR | model | |
| Wildland forest – agriculture (Michigan, USA) | AVIRIS | PCA | (Dahlin 2016) |
| Vascular plants (Sweden) | HySpex | PCA | (Möckel et al. 2016) |
| Ngangao Forest (Kenya) | AisaEagle | Image segmentation and unsupervised classification | (Schäfer et al. 2016) |

### 1.6 Bridging the ecological and remote sensing agendas

The potential for collaborations between remote sensing and ecological communities has been proposed for a long time (Stoms and Estes 1993, Kerr and Ostrovsky 2003, Turner et al. 2003, de Araujo Barbosa et al. 2015). Yet, these two communities have only recently started to coordinate and much work remains to be done (Pettorelli et al. 2014). A couple reasons exist for this delayed and rare collaborative between the two communities. One issue is the gap between the backgrounds needed for the two subjects. Each community has its own knowledge system and language. For example, remote sensing scientists may not always have a deep understanding of ecosystem function or know the meaning of ecological terminology, while widely used remote sensing terms like “imaging spectroscopy” are often not familiar to ecologists. Even the same term can have slightly different meanings in the two communities. For example, spatial scale usually means grain and extent in ecology but typically refers to the pixel size in remote sensing. Therefore, it is often difficult to find an appropriate terminology when combining disciplines. Also, there are only limited conferences and journals accommodating topics in both disciplines, hampering the direct communication between the two communities.

Another issue relates to data dispersion and accessibility. “Open data” or “open science” that not only means that data but also analyses and methods are preserved (Reichman et al. 2011) has been proposed for years, but it is still a long way off. In ecology, only a small fraction of data is accessible and there is still a lack of standards for collecting and

archiving data (Reichman et al. 2011). In remote sensing, data affordability and access limited the usage of remote sensing products (Turner et al. 2015). Although institutes like United States Geological Survey (USGS), National Aeronautics and Space Administration (NASA), Oak Ridge National Laboratory Distributed Active Archive Center (ORNL DAAC), and European Space Agency (ESA) provide open access to some satellite products e.g., Landsat, MODIS and SENTINEL, commercial satellite products are still very expensive. Meanwhile, airborne remote sensing data that can provide detailed spectral and spatial information are limited in geographic scope and too expensive for most researchers. Furthermore, some remote sensing products are too big or complicated for easy usage, in part due to the shortage of accessible data and software tools. There is a need for better sharing tools e.g., sophisticated algorithms, open-source software, and public databases for ecologists to obtain and process remote sensing images and extract information they want. More cross-community interactions are needed between the biodiversity and remote sensing communities to really push biodiversity assessment using remote sensing (Turner 2014, Jetz et al. 2016).

### 1.7 Research objectives

Given the projected decline in biodiversity in the Anthropocene (Crutzen 2002) and the importance of biodiversity to human societies and economies, better methods of assessing biodiversity over large areas are needed. This study aims to provide a solid theoretical foundation for the spectral diversity hypothesis and a deeper understanding of the spectral diversity-biodiversity relationship at local scales relevant to alpha diversity. If operational remote sensing methods can be developed for wider application, we could more readily apply spectral diversity to detect biodiversity (species richness and functional diversity) of ecosystems though remote sensing. To accomplish this, hyperspectral reflectance data were collected using both ground based and airborne platforms at different scales (Figure 1.2).

This project was accomplished at Cedar Creek Ecosystem Science Reserve, Minnesota, USA (45.41° N, 93.20° W) and Mattheis Research Ranch, Alberta, Canada (50.90° N, 111.88° W). The biodiversity manipulation of prairie plants in Cedar Creek BioDIV

experiment provided an ideal diversity gradient for testing the spectral diversity hypothesis, while Mattheis Research Ranch served as a proper site for examining how the experiment-scale findings performed in a natural landscape. Meanwhile, both sites have a history of biodiversity research by ecologists so that working in these sites enhances links between remote sensing and ecology.


Figure 1.2 Different sampling platforms and scales, from ground sampling to airborne remote sensing. (a): Hand-held non-imaging spectrometer sampling; (b): Fine scale imaging spectrometer sampling; (c): Airborne sampling.

The biodiversity-productivity relationship is an important example of the link between biodiversity and ecosystem function. Species richness generally promotes ecosystem productivity, although the shape of the relationship varies and remains the subject of debate. Chapter 2 and 3 examine the diversity-productivity relationship in two prairie ecosystems from a remote sensing perspective. Chapter 2 tests the species richness–productivity relationship using a common vegetation index, Normalized Difference Vegetation Index (NDVI), as a measure of productivity in experimental prairie grassland plots (Cedar Creek). The study spanned a growing season (May to October 2014) to evaluate dynamic changes in the NDVI–species richness relationship through time and in relation to environmental variables and phenology.

Chapter 3 illustrates a study using flux data and field optical data to help calibrate airborne imagery and map ecosystem productivity in a grazed prairie ecosystem in southern Alberta, Canada. Airborne NDVI measurements were calibrated against $CO_2$ flux measurements and above-ground biomass to estimate landscape productivity. Combining three metrics of biodiversity (airborne data, vegetation map and field sampling) to evaluate broad relationships between diversity and productivity across the landscape provided a unique test of the diversity-productivity hypothesis over a large area (10 $km^2$) of this managed prairie ecosystem.

Remote sensing has been used to detect plant biodiversity in a range of ecosystems based on the varying spectral properties of different species or functional groups. However, the most appropriate spatial resolution and spectral bands necessary to detect diversity remain unclear. At low resolution, differences among spectral patterns may be too weak to detect. Alternatively, at high resolution, redundant information may be introduced. To explore the effect of spatial resolution, Chapter 4 presents a study of the scale-dependence of spectral diversity in a prairie ecosystem experiment at Cedar Creek Ecosystem Science Reserve, Minnesota, USA. This study involved a scaling exercise comparing spectral diversity from pixels sampled at different spatial scales to standard metrics of alpha diversity within manipulated diversity treatments. The study also considered the effect of different spectral regions on biodiversity estimation using remote

sensing. To accomplish these goals, hyperspectral data were collected using several instruments from both ground and airborne platforms.

From current publications in this field, and from Chapters 2 and 3 in this thesis, we know that remote sensing of biodiversity works in the Cedar Creek experiments and in natural landscapes. But we need to know the mechanisms behind this relationship rather than simply calculating a biodiversity index using airborne or satellite images and relating it to the ground sampling results for a single instance. Chapter 5 explores this need by applying a theoretical test using simulated plot data to understand how species composition, richness, and evenness affect spectral diversity. Leaf and canopy reflectance measurements collected from the Cedar Creek BioDIV experimental prairie plots were used to simulate synthetic plots with different community structures (species richness, evenness, and composition). Two types of spectral diversity metrics, CV and metrics calculated based on a Partial Least Squares Discriminant Analysis (PLSDA) classification method, were used to compare to the conventional diversity metrics. This study also explored contributions of leaf- vs. canopy-level information to spectral diversity and compared effects of spectral bands on spectral diversity indices.

Following the data chapters, conclusions and recommendations for future work are provided in a final summary chapter.

### 1.8 References

Adler, P. B. et al. 2011. Productivity Is a Poor Predictor of Plant Species Richness. - Science. 1750: 1750–1754.

Anderson, M. J. et al. 2011. Navigating the multiple meanings of β diversity: a roadmap for the practicing ecologist. - Ecol. Lett. 14: 19–28.

Asner, G. P. and Martin, R. E. 2009. Airborne spectranomics: mapping canopy chemical and taxonomic diversity in tropical forests. - Front. Ecol. Environ. 7: 269–276.

Asner, G. P. et al. 2008. Remote sensing of native and invasive species in Hawaiian forests. - Remote Sens. Environ. 112: 1912–1926.

Austin, G. E. et al. 1996. Predicting the spatial distribution of buzzard Buteo buteo nesting areas using a geographical information system and remote sensing. - J. Appl. Ecol. 33: 1541–1550.

Bailey, S. and Bailey, S. 2004. Primary productivity and species richness: relationships among functional guilds, residency groups and vagility classes at multiple spatial scales. - Ecography. 27: 207–217.

Balvanera, P. et al. 2006. Quantifying the evidence for biodiversity effects on ecosystem functioning and services. - Ecol. Lett. 9: 1146–1156.

Barnosky, A. D. et al. 2011. Has the Earth's sixth mass extinction already arrived? - Nature 471: 51–57.

Bonar, S. et al. 2010. An overview of sampling issues in species diversity and abundance surveys. - In: Magurran, A. E. and McGill, B. J. (eds), Biological Diversity: frontiers in measurement and assessment. Oxford University Press, pp. 376.

Cardinale, B. J. et al. 2007. Impacts of plant diversity on biomass production increase through time because of species complementarity. - Proc. Natl. Acad. Sci. U. S. A. 104: 18123–18128.

Carlson, K. M. et al. 2007. Hyperspectral remote sensing of canopy biodiversity in Hawaiian lowland rainforests. - Ecosystems 10: 536–549.

Ceballos, A. et al. 2015. Comparison of airborne LiDAR and satellite hyperspectral remote sensing to estimate vascular plant richness in deciduous mediterranean forests of central Chile. - Remote Sens. 7: v.

Chance, C. M. et al. 2016. Spectral Wavelength Selection and Detection of Two Invasive Plant Species in an Urban Area. - Can. J. Remote Sens. 42: 1–14.

Clawges, R. et al. 2008. The use of airborne lidar to assess avian species diversity, density, and occurrence in a pine/aspen forest. - Remote Sens. Environ. 112: 2064–2073.

Corbane, C. et al. 2015. Remote sensing for mapping natural habitats and their conservation status - New opportunities and challenges. - Int. J. Appl. Earth Obs. Geoinf. 37: 7–16.

Costanza, J. K. et al. 2011. Multi-scale environmental heterogeneity as a predictor of plant species richness. - Landsc. Ecol. 26: 851–864.

Crutzen, P. J. 2002. Geology of mankind. - Nature 415: 2002.

Dahlin, K. M. 2016. Spectral diversity area relationships for assessing biodiversity in a wildland-agriculture matrix. - Ecol. Appl. 26: 2756–2766.

de Araujo Barbosa, C. C. et al. 2015. Remote sensing of ecosystem services: A systematic review. - Ecol. Indic. 52: 430–443.

Fairbanks, D. H. K. and McGwire, K. C. 2004. Patterns of floristic richness in vegetation communities of California: regional scale analysis with multi-temporal NDVI. - Glob. Ecol. Biogeogr. 13: 221–235.

Fava, F. et al. 2010. Fine-scale assessment of hay meadow productivity and plant diversity in the European Alps using field spectrometric data. - Agric. Ecosyst. Environ. 137: 151–157.

Féret, J.-B. and Asner, G. P. 2014. Mapping tropical forest canopy diversity using high-fidelity imaging spectroscopy. - Ecol. Appl. 24: 1289–1296.

Field, C. B. 1991. Ecological scaling of carbon gain to stress and resource availability.

Foody, G. M. 2005. Mapping the richness and composition of British breeding birds from coarse spatial resolution satellite sensor imagery. - Int. J. Remote Sens. 26: 3943–3956.

Fraser, L. H. et al. 2015. Worldwide evidence of a unimodal relationship between productivity and plant species richness. - Science (80-. ). 349: 302–306.

Friedl, M. A. et al. 2010. MODIS Collection 5 global land cover: Algorithm refinements and characterization of new datasets. - Remote Sens. Environ. 114: 168–182.

Fusco, G. and Minelli, A. 2010. Phenotypic plasticity in development and evolution: facts and concepts. Introduction. - Philos. Trans. R. Soc. Lond. B. Biol. Sci. 365: 547–556.

Gamon, J. A. 2008. Tropical sensing — opportunities and challenges. - In: M, K. and GA, S.-A. (eds), Hyperspectral remote sensing of tropical and subtropical forests. CRC Press Taylor&Francis Group, pp. 297–304.

Gillespie, T. W. 2005. Predicting woody-plant species richness in tropical dry forests: A case study from south Florida, USA. - Ecol. Appl. 15: 27–37.

Gillespie, T. W. et al. 2009. Towards quantifying tropical tree species richness in tropical forests. - Int. J. Remote Sens. 30: 1629–1634.

Gotelli, N. J. and Colwell, R. K. 2001. Quantifyinf biodiversity: procedures and pitfalls in the measurement and comparison of species richness. - Ecol. Lett. 4: 379–391.

Gotelli, N. J. and Colwell, R. K. 2010. Estimating species richness. - In: Magurran, A. E. and McGill, B. J. (eds), Biological Diversity: Frontiers In Measurement And Assessment. pp. 39–54.

Gould, W. 2000. Remote sensing of vegetation , plant species richness , and regional biodiversity hotspots. - Ecol. Appl. 10: 1861–1870.

Griffiths, G. H. and Lee, J. 2000. Landscape pattern and species richness; regional scale analysis from remote sensing. - Int. J. Remote Sens. 21: 2685–2704.

Hamilton, A. J. 2005. Species diversity or biodiversity? - J. Environ. Manage. 75: 89–92.

Hector, A. and Bagchi, R. 2007. Biodiversity and ecosystem multifunctionality. - Nature 448: 188–190.

Hector, A. et al. 1999. Plant diversity and productivity experiments en European grasslands. - Science. 286: 1123–1127.

Hector, A. et al. 2011. BUGS in the analysis of biodiversity experiments: Species richness and composition are of similar importance for grassland productivity. - PLoS One in press.

Heywood, V. H. 1995. Global Biodiversity Assessment. - Cambridge University Press.

Hillebrand, H. 2004. On the generality of the latitudinal diversity gradient. - Am. Nat. 163: 192–211.

Hillebrand, H. and Matthiessen, B. 2009. Biodiversity in a complex world: Consolidation and progress in functional biodiversity research. - Ecol. Lett. 12: 1405–1419.

Hooper, D. U. et al. 2005. Effects of biodiversity on ecosystem functioning: a consensus of current knowledge. - Ecol. Monogr. 75: 3–35.

Huston, M. A. 1997. Hidden treatments in ecological experiments: re-evalutating the ecosystem function of biodiverstiy. - Oecologia 110: 449–460.

Isbell, F. I. et al. 2009. Biodiversity, productivity and the temporal stability of productivity: Patterns and processes. - Ecol. Lett. 12: 443–451.

Isbell, F. et al. 2015. Biodiversity increases the resistance of ecosystem productivity to climate extremes. - Nature 526: 574–577.

Jennings, M. D. 2000. Gap analysis: Concepts, methods, and recent results. - Landsc. Ecol. 15: 5–20.

Jetz, W. et al. 2016. Monitoring plant functional diversity from space. - Nat. Plants 2: 16024.

John, R. et al. 2008. Predicting plant diversity based on remote sensing products in the semi-arid region of Inner Mongolia. - Remote Sens. Environ. 112: 2018–2032.

Kerr, J. T. and Ostrovsky, M. 2003. From space to species: Ecological applications for remote sensing. - Trends Ecol. Evol. 18: 299–305.

Kerr, J. T. et al. 2001. Remotely sensed habitat diversity predicts butterfly species richness and community similarity in Canada. - Proc. Natl. Acad. Sci. U. S. A. 98: 11365–11370.

Lehman, C. L. and Tilman, D. 2000. Biodiversity, stability, and productivity in competitive communities. - Am. Nat. 156: 534–552.

Levin, N. et al. 2007. Predicting mountain plant richness and rarity from space using satellite-derived vegetation indices. - Divers. Distrib. 13: 692–703.

Levrel, H. et al. 2010. Balancing state and volunteer investment in biodiversity monitoring for the implementation of CBD indicators: A French example. - Ecol. Econ. 69: 1580–1586.

Loreau, M. and Hector, A. 2001. Partitioning selection and complementarity in biodiversity experiments. - Nature 412: 72–76.

Lucas, K. and Carter, G. 2008. The use of hyperspectral remote sensing to assess vascular plant species richness on Horn Island, Mississippi. - Remote Sens. Environ. 112: 3908–3915.

Lucas, R. et al. 2015. The Earth Observation Data for Habitat Monitoring (EODHaM) system. - Int. J. Appl. Earth Obs. Geoinf. 37: 17–28.

Luoto, M. et al. 2002. Modelling butterfly distribution based on remote sensing data. - J Biogeogr. 29: 1027–1037.

Maestre, F. T. et al. 2012. Plant Species Richness and Ecosystem Multifunctionality in Global Drylands. - Science. 335: 214–218.

Magurran, A. E. 2004. Measuring Biological Diversity. - Blackwell Publishing.

Magurran, A. E. 2013. Open questions: some unresolved issues in biodiversity. - BMC Biol. 11: 118.

Magurran, A. E. and McGill, B. J. 2011. Biological diversity: frontiers in measurement and assessment. - Oxford University Press.

Midgley, G. F. 2012. Biodiversity and Ecosystem Function. - Science (80-. ). 335: 174–176.

Mittelbach, G. G. 2012. Biodiversity and Ecosystem Functioning. - In: Community Ecology. 1st ed.n. Sinauer Associates, Inc., pp. 41–62.

Mittelbach, G. G. et al. 2001. What is the observed relationship between species richness and productivity? - Ecology 82: 2381–2396.

Möckel, T. et al. 2016. Airborne Hyperspectral Data Predict Fine-Scale Plant Species Diversity in Grazed Dry Grasslands. - Remote Sens. 8: 133.

Naeem, S. and Li, S. 1997. Biodiversity enhances ecosystem reliability. - Nature 390: 507–510.

Naeem, S. et al. 1994. Declining biodiversity can alter the performance of ecosystem. - Nature 368: 734–737.

Naeem, S. et al. 2000. Plant diversity increases resistance to invasion in the absence of covarying extrinsic factors. - Oikos 91: 97–108.

Nash, R. F. 1989. The rights of nature: A history of environmental ethics. - University of Wisconsin Press.

Noss, R. 1990. Indicators for monitoring biodiversity: A hierarchical approach. - Conserv. Biol. 4: 355–364.

Ohtomo, Y. et al. 2014. Evidence for biogenic graphite in early Archaean Isua metasedimentary rocks. - Nat. Geosci. 7: 25–28.

Oldeland, J. et al. 2010. Does using species abundance data improve estimates of species diversity from remotely sensed spectral heterogeneity? - Ecol. Indic. 10: 390–396.

Ollinger, S. V 2011. Sources of variability in canopy reflectance and the convergent properties of plants. - New Phytol. 189: 375–394.

Palmer, M. W. et al. 2002. Quantitative tools for perfecting species lists. - Environmetrics 13: 121–137.

Parviainen, M. et al. 2009. The role of local and landscape level measures of greenness in modelling boreal plant species richness. - Ecol. Modell. 220: 2690–2701.

Pereira, H. M. et al. 2010. Global biodiversity monitoring. - Front. Ecol. Environ. 8: 458–460.

Pettorelli, N. et al. 2014. Satellite remote sensing, biodiversity research and conservation of the future. - Philos. Trans. R. Soc. B Biol. Sci. 369: 1–5.

Pimm, S. L. et al. 1995. The future of biodiversity. - Science (80-. ). 269: 347–350.

Power, M. E. et al. 1996. Challenges in the Quest for Keystones. - Bioscience 46: 609–620.

Price, J. C. 1994. How unique are spectral signatures? - Remote Sens. Environ. 49: 181–186.

Reich, P. B. and Hobbie, S. E. 2013. Decade-long soil nitrogen constraint on the CO2 fertilization of plant biomass. - Nat. Clim. Chang. 3: 278–282.

Reichman, O. J. et al. 2011. Challenges and opportunities of open data in ecology. - Science. 331: 703–705.

Roberts, D. A. et al. 1998. Mapping Chaparral in the Santa Monica Mountains Using Multiple Endmember Spectral Mixture Models. - Remote Sens. Environ. 65: 267–279.

Rocchini, D. 2007. Effects of spatial and spectral resolution in estimating ecosystem α-diversity by satellite imagery. - Remote Sens. Environ. 111: 423–434.

Rocchini, D. and Neteler, M. 2012. Spectral rank–abundance for measuring landscape diversity. - Int. J. Remote Sens. 33: 4458–4470.

Rocchini, D. et al. 2011. Landscape complexity and spatial scale influence the relationship between remotely sensed spectral diversity and survey-based plant species richness. - J. Veg. Sci. 22: 688–698.

Rocchini, D. et al. 2015. Advancing species diversity estimate by remotely sensed proxies: a conceptual review. - Ecol. Inform. 25: 22–28.

Rockström, J. et al. 2009. A safe operating space for humanity. - Nature 461: 472--475.

Sala, O. E. et al. 2000. Global biodiversity scenarios for the year 2100. - Science (80-. ). 287: 1770–1774.

Saveraid, E. H. et al. 2001. A comparison of satellite data and landscape variables in predicting bird species occurrences in the Greater Yellowstone Ecosystem, USA. - Landsc. Ecol. 16: 71–83.

Schäfer, E. et al. 2016. Mapping tree species diversity of a tropical montane forest by unsupervised clustering of airborne imaging spectroscopy data. - Ecol. Indic. 64: 49–58.

Stickler, C. M. and Southworth, J. 2008. Application of multi-scale spatial and spectral analysis for predicting primate occurrence and habitat associations in Kibale National Park, Uganda. - Remote Sens. Environ. 112: 2170–2186.

Stoms, D. M. and Estes, J. E. 1993. A remote sensing research agenda for mapping and monitoring biodiversity. - Int. J. Remote Sens. 14: 1839–1860.

Thomas, C. D. et al. 2004. Extinction risk from climate change. - Nature 427: 145–148.

Thompson, S. D. 2015. Mapping and monitering indicators of terrestrial biodiversity with remote sensing.

Tiede, D. et al. 2010. Object-based Class Modeling for Cadastre-constrained Delineation of Geo-objects. - Photogramm. Eng. Remote Sens. 76: 193–202.

Tilman, D. 1997. The influence of functional diversity and composition on ecosystem processes. - Science. 277: 1300–1302.

Tilman, D. and Haddi, A. El 1992. Drought and biodiversity in Grasslands. - Oecologia 89: 257–264.

Tilman, D. and Downing, J. A. 1994. Biodiversity and stability in grasslands. - Nature 367: 363–365.

Tilman, D. et al. 1994. Habitat destruction and the extinction debt. - Nature 371: 65–66.

Tilman, D. et al. 1996. Productivity and sustainability influenced by biodiversity in grassland ecosystems. - Nature 379: 718–720.

Tilman, D. et al. 2001. Diversity and productivity in a long-term grassland experiment. - Science. 294: 843–845.

Tilman, D. et al. 2006. Biodiversity and ecosystem stability in a decade-long grassland experiment. - Nature 441: 629–632.

Tuomisto, H. 2010a. A diversity of beta diversities: Straightening up a concept gone awry. Part 1. Defining beta diversity as a function of alpha and gamma diversity. - Ecography. 33: 2–22.

Tuomisto, H. 2010b. A diversity of beta diversities: Straightening up a concept gone awry. Part 2. Quantifying beta diversity and related phenomena. - Ecography. 33: 23–45.

Turner, W. 2014. Sensing biodiversity. - Science. 346: 301–303.

Turner, W. et al. 2003. Remote sensing for biodiversity science and conservation. - Trends Ecol. Evol. 18: 306–314.

Turner, W. et al. 2015. Free and open-access satellite data are key to biodiversity conservation. - Biol. Conserv. 182: 173–176.

US Congress Office of Technology 1987. Technologies To Maintain Biological Diversity.

Ustin, S. L. and Gamon, J. A. 2010. Remote sensing of plant functional types. - New Phytol. 186: 795–816.

Ustin, S. L. et al. 2004. Using imaging spectroscopy to study ecosystem processes and properties. - Bioscience 54: 523–534.

Waide, R. B. et al. 1999. The relationship between productivity and species richness. - Annu. Rev. Ecol Syst 30: 257–300.

Wake, D. B. and Vredenburg, V. T. 2008. Are we in the midst of the sixth mass extinction? A view from the world of amphibians. - Proc. Natl. Acad. Sci. U. S. A. 105: 11466–11473.

Wang, R. et al. 2016. Integrated analysis of productivity and biodiversity in a southern Alberta prairie. - Remote Sens. 8: 214.

Westman, W. E. et al. 1989. Tropical deforestation and species endangerment: the role of remote sensing. - Landsc. Ecol. 3: 97–109.

Whittaker, R. H. 1960. Vegetation of the Sisiyou Mountains, Orgeon and California. - Ecol. Monogr. 30: 279–338.

Whittaker, R. H. 1972. Evolution and Measurement of Species Diversity. - Taxon 21: 213–251.

Whittaker, R. J. et al. 2001. Scale and species richness : towards a general , theory of species diversity hierarchical. - Diversity 28: 453–470.

Wright, I. J. et al. 2004. The worldwide leaf economics spectrum. - Nature 428: 821–827.

Wulder, M. A. et al. 2004. High spatial resolution remotely sensed data for ecosystem characterization. - Bioscience 54: 511–521.

Xiao, Q. et al. 2004. Using AVIRIS data and multiple-masking techniques to map urban forest tree species. - Int. J. Remote Sens. 25: 5637–5654.

Zomer, R. et al. 2009. Building spectral libraries for wetlands land cover classification and hyperspectral remote sensing. - J. Environ. Manage. 90: 2170–2177.

# Chapter 2 Seasonal Variation in the NDVI–Species Richness Relationship in a Prairie Grassland Experiment (Cedar Creek)


## Abstract

Species richness generally promotes ecosystem productivity, although the shape of the relationship varies and remains the subject of debate. One reason for this uncertainty lies in the multitude of methodological approaches to sampling biodiversity and productivity, some of which can be subjective. Remote sensing offers new, objective ways of assessing productivity and biodiversity. In this study, we tested the species richness–productivity relationship using a common remote sensing index, the Normalized Difference Vegetation Index (NDVI), as a measure of productivity in experimental prairie grassland plots (Cedar Creek). Our study spanned a growing season (May to October, 2014) to evaluate dynamic changes in the NDVI–species richness relationship through time and in relation to environmental variables and phenology. We show that NDVI, which is strongly associated with vegetation percent cover and biomass, is related to biodiversity for this prairie site, but it is also strongly influenced by other factors, including canopy growth stage, short-term water stress and shifting flowering patterns. Remarkably, the NDVI-biodiversity correlation peaked at mid-season, a period of warm, dry conditions and anthesis, when NDVI reached a local minimum. These findings confirm a positive, but dynamic, productivity–diversity relationship and highlight the benefit of optical remote sensing as an objective and non-invasive tool for assessing diversity–productivity relationships.


## 2.1 Introduction

The species richness–productivity relationship has long been of interest in ecology. Much of the recent Biodiversity-Ecosystem Function (BEF) research has developed from a series of landmark experiments at Cedar Creek that consistently demonstrated that biodiversity enhances productivity in experimental grassland systems (Tilman et al. 1996, 2001, Tilman 1997). Two hypotheses have been proposed to explain the positive relationship between biodiversity and productivity: 1) selection effects, and 2)

complementarity (Lehman and Tilman 2000, Loreau and Hector 2001). The selection effects hypothesis (also called "selection probability effects") states that adding species increases the probability of having a productive species, especially when creating a community with high richness within a small size pool of candidate species (Huston 1997). The complementarity hypothesis suggests that the presence of multiple species in a high richness community can increase production via more efficient resource capture.

In reviews of the BEF literature, a variety of biodiversity–productivity relationships have been reported (Adler et al. 2011, Fraser et al. 2015). Both unimodal and positive relationships are commonly reported between productivity and richness, and this relationship can be affected by community composition, resource levels (e.g., fertilizer or irrigation levels) and nature of disturbance (Waide et al. 1999, Mittelbach et al. 2001, Fraser et al. 2015). In some cases, highly productive sites are known to be resource rich and species poor. These high productivity and low diversity sites are typically highly managed via irrigation or fertilizer application (Fraser et al. 2015) and often lead to declines in the species richness relationships at high productivity. Indeed, variation in the relationship between biodiversity and ecosystem function is known to depend on resource availability (Reich and Hobbie 2013) and environmental drivers, particularly drought stress, has been shown to constrain biomass in prairie systems (Tilman and Haddi 1992, Isbell et al. 2015).

One goal of BEF research is to understand the underlying ecological mechanisms behind the biodiversity–productivity relationship. However, the assessment of the relationship itself and changes in the relationship through time pose additional challenges. Determining the nature of these relationships is of increasing importance in natural systems, given that unmanipulated grasslands show a range of productivity–diversity relationships, depending on site conditions and composition (Adler et al. 2011). Prairie productivity is often estimated through biomass harvests that are time-consuming due to the effort in harvesting, sorting and weighing live vegetation in the sampling region (Bork et al. 1999, Booth and Tueller 2003, Piñeiro et al. 2006). There are also limits to the number of samples that can be taken in a single season without altering the experiment. Moreover, the traditional methods of estimating biomass - and their

repeatability—can be subjective due to the dependence on the knowledge and skill of those conducting sampling (Booth and Tueller 2003). This estimation is further affected by sample size and method (Clark et al. 2001). Due to these constraints, only a small area can typically be harvested to obtain the biomass and richness. As a consequence, it has been difficult to observe changes in biomass in response to external drivers through time and the seasonal dynamics of the diversity–productivity relationship.

Remote sensing provides a useful tool to estimate vegetation productivity over large areas and has been used to estimate prairie production. A large number of studies have led to well-established methods that estimate the percent cover, biomass, and productivity of grasslands using remote sensing (Gamon et al. 1993, 1995, Bork et al. 1999, Booth and Tueller 2003). These studies have shown that the Normalized Difference Vegetation Index (NDVI) (Tucker 1979) is highly correlated with green biomass, green leaf area index, and radiation absorption (APAR) by green canopy material in grasslands (Gamon et al. 1995, Piñeiro et al. 2006). Remote sensing also provides an objective method that can assess productivity rapidly, repeatedly and following consistent methods, without damaging or altering the target vegetation.

The Cedar Creek Ecosystem Science Reserve (CCESR; Minnesota, USA) has a long, rich history of biodiversity studies. The ongoing BioDIV experiment has been maintained for more than 20 years to investigate the effects of species and functional biodiversity on community and ecosystem function, and has included assessment of productivity, stability and nutrient dynamics (Tilman 1997, Tilman et al. 2006). Previous studies at this site have reported a significant, positive relationship between diversity (either species richness or functional diversity) and biomass (e.g., (Tilman 1997)).

In this study, we revisited the species richness–productivity relationship for these experimental prairie grassland plots covering a range of biodiversity levels (nominal species richness ranging from 1 to 16 plant species per plot) using NDVI, a common remote sensing metric of ecosystem productivity and green vegetation biomass. Our study spanned a summer growing season (May to October, 2014), allowing us to evaluate dynamic changes in the NDVI–species richness relationship through time and in relation to environmental variables, including temperature, precipitation and soil moisture. We

tested the hypotheses that (1) remote estimates of productivity would be positively associated with species richness, as reported by previous studies based on traditional field sampling methods (Tilman et al. 1996, Tilman 1997); and (2) the relationship would change dynamically throughout the growing season in response to the progression of plants through shifting phenological stages and according to environmental fluctuations (e.g., as a consequence of summer drought).

## 2.2 Methods

### 2.2.1 Field Site and Experimental Design

This study was conducted at the Cedar Creek Ecosystem Science Reserve, Minnesota, US (45.4086° N, 93.2008° W). The BioDIV experiment has maintained 168 prairie plots (9 m × 9 m) with nominal plant species richness ranging from 1 to 16 since 1994 (Mittelbach 2012). The species planted in each plot were originally randomly selected from a pool of 18 grassland perennial species, including $C_3$ and $C_4$ grasses, legumes, forbs and trees. Of the original 168 plots, 35 plots with species richness ranging from 1 to 16 were selected for our study. These 35 plots included 11 monoculture plots and six replicates of every other richness level (2, 4, 8, and 16) but with differing species combinations. Weeding was done 3 to 4 times each year for all the plots to maintain the species richness. A more complete accounting of the methods and history of the BioDIV experiment can be found in the published literature on this site (e.g., (Tilman et al. 2001, Reich et al. 2012)).

### 2.2.2 Reflectance Sampling

In the 35 study plots, canopy spectral reflectance was measured every two weeks over most of the 2014 growing season (late May to late August) and once a month during senescence (September to October) with a hand-held, dual channel spectrometer (Unispec DC, PP Systems, Amesbury, MA, USA) (Figure 2.1a). With this instrument, both upwelling radiance and downwelling irradiance were collected simultaneously, and these measurements were cross-calibrated using a white reference calibration panel (Spectralon, Labsphere, North Sutton, NH, USA), allowing us to correct for the atmospheric variation (Gamon et al. 2006). The detectors measured irradiance and radiance from 350 to 1130 nm with a nominal bandwidth (band-to-band spacing) of approximately 3 nm, and actual

bandwidth (FWHM) of 10 nm. The upward-looking channel included a fibre optic and a cosine head to record the solar irradiance. The downward-looking channel included a fibre optic and a field-of-view restrictor that limited the field of view (FOV) to a nominal value of 20 degrees, although empirical tests indicated the actual FOV was closer to 15 degrees (not shown). In this application, the spatial resolution on the ground (IFOV) was approximately 0.5 $m^2$. The reflectance at each wavelength was calculated as:

$$\rho_\lambda = \frac{(L_{target,\lambda}/E_{target,\lambda})}{(L_{panel,\lambda}/E_{panel,\lambda})} \quad (2.1)$$

where $L_{target,\lambda}$ indicates the radiance measured at each wavelength ($\lambda$ , in nm) by a downward-pointed detector sampling the surface ("target"), and $E_{target,\lambda}$ indicates the irradiance measured simultaneously by an upward-looking detector sampling the downwelling radiation. $L_{panel,\lambda}$ indicates the radiance measured by a downward-pointed detector sampling the calibration panel, and $E_{panel,\lambda}$ indicates the irradiance measured simultaneously by an upward-pointed detector sampling the downwelling radiation.

A linear interpolation was applied to the reflectance spectra to obtain reflectance values at 680 and 800 nm and calculate NDVI:

$$\text{NDVI} = \frac{\rho_{800} - \rho_{680}}{\rho_{800} + \rho_{680}} \quad (2.2)$$

where $\rho_{680}$ and $\rho_{800}$ indicate the reflectance at 680 and 800 nm respectively. To determine seasonal NDVI patterns, 17 reflectance measurements were taken along the northern-most row on each sampling date (Figure 2.1a) in each of the 35 plots, providing a consistent subsample of each plot over the growing season. To estimate the NDVI values on August 1 (the day that vegetation percent cover was measured) a linear interpolation was applied to NDVl measurements made on July 18 and August 4.

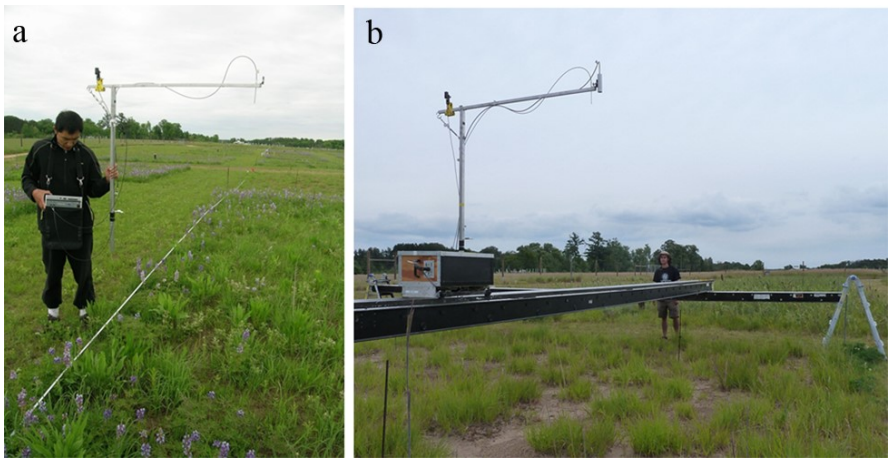


Figure 2.1 Sampling spectral reflectance using (a) the handheld method, applied biweekly to obtain reflectance phenology over the season; and (b) the tram cart on track (Gamon et al. 2006) used to sample entire plots once near midsummer peak biomass. For the first method, only the northern-most row of each plot was sampled for reflectance phenology over the growing season. The second method is further illustrated in Figure 2.2.

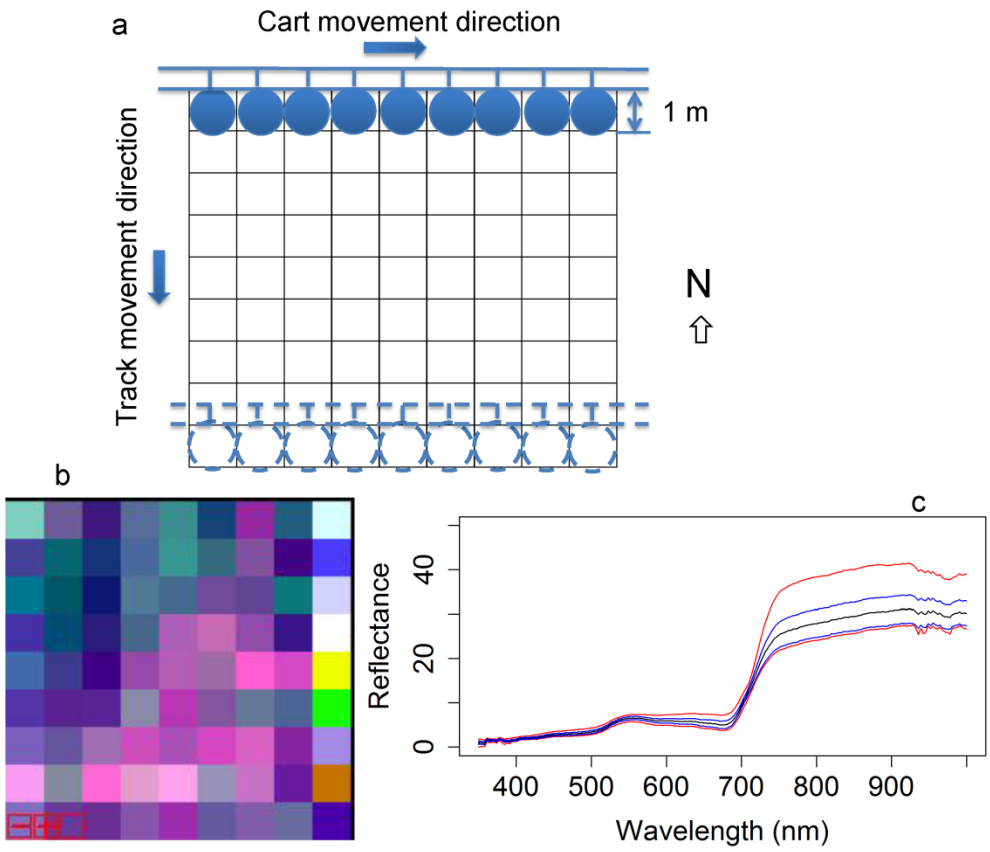


Figure 2.2 Design of whole-plot reflectance sampling (**a**) and example of synthetic image (plot 168, richness = 16) (**b**); and resulting reflectance spectra (**c**). Colored lines indicate mean (black), standard deviation (blue) and min/max (red) reflectance values. Reflectance spectra were used to calculate NDVI through time for comparison with nominal species richness (1–16).

### 2.2.3 Whole-Plot Reflectance Sampling

Once at peak season (July 23 to August 3), we sampled canopy reflectance of 33 entire plots using a tram system (Gamon et al. 2006) (Figure 2.1b). The tram consisted of a mobile cart on a movable track supported by scaffolding (Figure 2.1b), allowing a systematic measurement of each 1-$m^2$ portion of each plot (Figure 2.2a). This resulted in a total of 81 measurements (9 × 9 m) for each plot with approximately 1 $m^2$ spatial resolution, creating a synthetic image (Figure 2.2b) that provided a full sample of each of the 33 plots, comparable to what could be obtained with airborne imaging spectrometry. The speed of the tram cart was 0.167 m/s. It took approx. 10 minutes (including time to

move the scaffolding) to cover a plot (9 × 9 m). During the (whole-plot) sampling period, data were collected from 10 am to 4 pm every day until all 33 plots were completely sampled. We skipped midday (12:30 pm to 1 pm) to avoid possible self-shadow effects of the fiber when measuring the white reference. While some data reported were collected under clear skies, clouds were unavoidable, and their influence on NDVI calculations were largely reduced through the cross-calibration procedure described above. A quantum sensor (LI-190SB, LI-COR, Lincoln, NE, USA) was used to track the sky condition when running the tram cart. To avoid possible edge effects, 49 (7 × 7 m) of the 81 measurements in the center were used to calculate the average reflectance of each plot (Figure 2.2c). NDVI from each reflectance spectrum was calculated using Equation (2.2) and the average NDVI was determined for each plot.

### 2.2.4 Biomass and Vegetation Percent Cover

Above-ground living plant biomass of the selected 35 plots was measured on 4 August 2014. Plots were sampled by clipping, drying and weighing four parallel and evenly spaced 0.1 m × 6 m strips per plot. The biomass of each strip was sorted to species, but presented here as total plot biomass. Ground vegetation percent cover measurements were taken on June 19 and August 1 in 2014. Percent cover was determined by visual inspection within nine 0.5 m × 0.5 m quadrats, placed every meter, starting 50 cm from the north facing edge of the plot for a total of nine subsamples per plot. Percent cover was estimated for each individual species as the nearest 10 percent that each species occupied of the total quadrat area, and then summed. Vegetation coverage did not necessarily sum to 100% if bare ground was exposed, or if species overlapped. To avoid affecting seasonal NDVI patterns, biomass measurements in each plot were sampled in a separate area from the reflectance sampling locations, both of which were assumed to be representative of the whole plot. For mid-season NDVI assessment of *entire* plots, the biomass sampling was conducted a few days after the optical sampling to avoid affecting the NDVI.

### 2.2.5 Height

We monitored height of focal species at each NDVI census as an independent measure of canopy growth. We measured the height of three randomly selected individuals of each

species present in each plot unless there were less than three individuals, in which case we measured all individuals. Individuals were not marked, so different individuals may have been measured at different census intervals. To calculate average height of vegetation in each plot we used percent cover data collected in June and August to create an abundance-weighted plot vegetation height. Plot vegetation height was calculated as the sum of the abundance weighted height of each species in the plot, where abundance was quantified as percent cover and height was measured in centimeters. For all but *Lupinus perennis*, percent cover did not differ between the two percent cover census dates and so we used average cover. For *Lupinus perennis*, we used percent cover from June for all census dates in June and July then used August percent cover data for August, September and October census dates.

### 2.2.6 Flowering Phenology

We monitored flowering phenology of all focal species at each NDVI census. We used USA-NPN protocols for monitoring (www.usanpn.org/natures_notebook). Here we focus on flowering phenophases due to their potential to influence spectra. Briefly, each species in each plot was scored for whether they had flowers and whether any flowers were open. For each of these phenophases we also scored abundance. For flowers, we scored the number of flowers in the following categories: <3, 3–10, 11–100, >101). For open flowers, we scored the percentage of flowers that were open in the following categories: Less than 5%; 5%–24%; 25%–49%; 50%–74%; 75%–94%; 95% or more.

For data analysis, we took the mid-point of each category, except >101 for which we arbitrarily set as 110. For each species, plot and census we multiplied the number of flowers by the decimal percent of those flowers that were open to get an abundance-weighted number of open flowers per species. These were then summed for each plot giving a total number of open flowers per plot.

### 2.2.7 Environmental Conditions

Meteorological conditions (temperature, rainfall) and soil moisture were tracked during the experimental period. Temperature and precipitation records were collected from Cedar Creek weather station (approximately 0.76 km away from the BioDIV experimental plots), while time domain reflectometry (TDR) was used to measure soil

moisture at four different depths in a subset of 38 BioDIV experimental plots across all diversity treatment levels. These were not necessarily the same plots as those used for subsampling NDVI but are a representative subset of the ambient conditions in the BioDIV experiment and site. We used the moisture sensor (Trime FM, IMKO GmbH, Ettlingen, Germany), with a 17 cm long probe inserted vertically into the soil inside a 2 m long PVC tube at 4 depths: 3–20 cm, 20–37 cm, 80–97 cm, and 140–157 cm. The sensor was calibrated at two endpoints using the same setup with dry and wet glass beads in a large volume (19L) following manufacturers instructions.

### 2.2.8 Statistical Analysis

Species richness–biomass, species richness–vegetation percent cover and species richness–NDVI relationships were fitted using linear regression model within R software (Team 2015).

A multiple linear regression model within R software (Team 2015) was applied to fit the NDVI with species richness and vegetation percent cover measurements. We analyzed height data using a two-way ANOVA with species and census as main effects. We used Tukey's HSD to test pairwise contrasts. Phenological data were not normally distributed and transformation did not result in normally distributed data. We therefore used a non-parametric Kruskall-Wallis test to examine the effect of date on the total number of open flowers and then used the Steel-Dwass (non-parametric equivalent to Tukey's HSD) to test pairwise contrasts. These analyses were conducted in JMP® Pro 11.0 (SAS Institute Inc., Cary, NC, USA, 27513).

## 2.3 Results

Consistent with previous studies at this site (Tilman 1997), high species richness plots tended to have higher biomass and percent cover, but biomass was more strongly related to species richness than was percent cover (Figure 2.3). Both biomass and vegetation percent cover showed logarithmic relationships with species richness (Figure 2.3), similar to previous patterns observed at BioDIV (Tilman 1997). Although the mean vegetation percent cover increased with increasing species richness, the variation of percent cover among low species richness plots was higher than the variation of biomass, with some of the low richness plots having a very high vegetation percent cover, causing a weak (but

significant) relationship between species richness and cover (Figure 2.3b). Species composition clearly affected the species richness—percent cover relationship, as evidenced by the high scatter in percent cover for the monoculture plots. For example, one monoculture plot (*Amorpha canescens*, plot 20 in Table S2.1 in Appendices), had the highest vegetation percent cover (95%), but the biomass of this plot was 200 g/m$^2$, which was only 51.3% of the most productive polyculture, whose richness was 16 (plot 169 in Table S2.1 in Appendices). On the other hand, the *Liatris aspera* monoculture plot (plot 129 in Table S2.1 in Appendices) has a biomass of 159.97 g/m$^2$ (41% of the most productive polyculture) while the vegetation percent cover of this plot was only 15%.

NDVI showed a linear relationship with biomass (Figure 2.4a) but a log relationship with vegetation percent cover (Figure 2.4b). The NDVI-percent cover relationships had stronger correlations than the NDVI-species richness relationship on both sampling dates (Table 2.1), illustrating the strong dependence of NDVI on canopy structure. Adding species richness as a variable improved the performance of the NDVI-percent cover relationships on both sampling dates (Table 2.1), demonstrating that the NDVI was affected by species composition in addition to canopy structure. These results suggest a potentially confounding effect of vegetation structure (e.g., percent cover) on the NDVI-species richness relationships reported above. NDVI was particularly sensitive to vegetation percent cover in sparse canopies (below 60% cover) and showed less sensitivity to vegetation percent cover in dense canopies (above 60% cover) (Figure 2.4b), as has been shown by the tendency of NDVI to "saturate" with increasing quantities of vegetation (whether biomass, percent cover or LAI) in previous studies (Gamon et al. 1995). The NDVI–cover relationship also varied with season, with NDVI values declining between mid-June and early August (Figure 2.4b). The NDVI and percent cover values were higher earlier in the growing season (June 19) than later (August 1) (Figures 2.3 and 2.4), when senescence reduced NDVI (Figure 2.5).

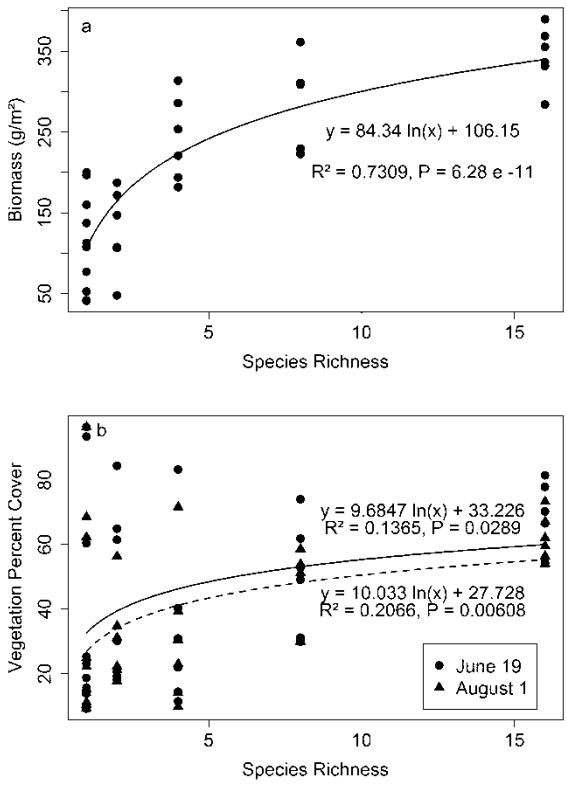


Figure 2.3 Species richness *versus* biomass (**a**) and vegetation percent cover (**b**). Biomass was measured on 4 August and percent cover was measured on 19 June and 1 August 2014.

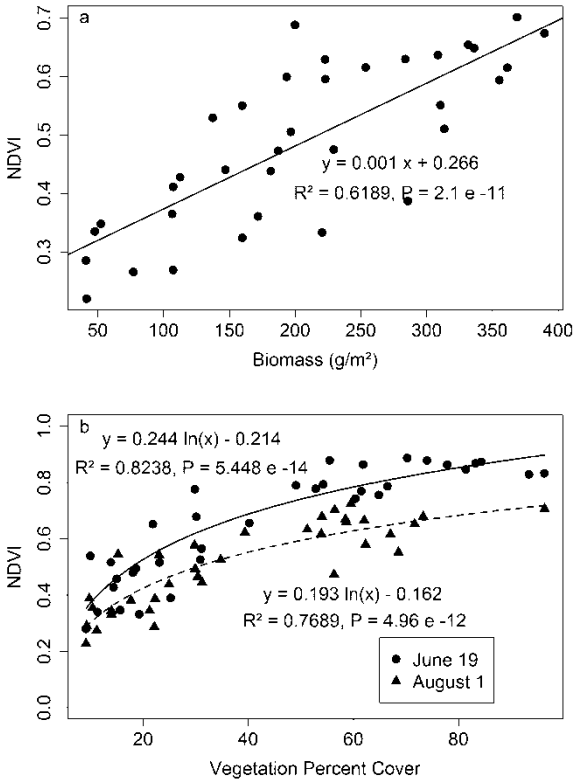


Figure 2.4 NDVI *versus* biomass (**a**) and vegetation percent cover (**b**). Biomass was measured on 4 August and percent cover was measured on 19 June and 1 August 2014.

Table 2.1 Dependence of NDVI on species richness and vegetation percent cover. Values shown are multiple linear regression parameters, including intercept, coefficients for log(species richness) and log(percent cover), $R^2$ and $F$ values. Regressions have degree of freedom = 32. Significant codes: NS, $0.05 < p$, *, $0.01 < p < 0.05$, **, $0.001 < p < 0.01$ and ***, $P < 0.001$. 0619 and 0801 represent the sampling dates (19 June and 1 August 2014).

| Date & Model Inputs | Regression Parameters | | | Overall $R^2$ | Overall $F$ Value |
|---|---|---|---|---|---|
| | Intercept | log (Species Richness) | log (Percent Cover) | | |
| 0619-Percent cover | −0.21415 ** | 0 | 0.24357 *** | 0.8238 *** | 154.3 *** |
| 0619-Richness | 0.53337 *** | 0.10391 *** | 0 | 0.3129 | 15.03 *** |
| 0619-Both | −0.17454 * | 0.03296 * | 0.22154 *** | 0.8486 *** | 89.67 *** |
| 0801-Percent cover | −0.14260 * | 0 | 0.18095 *** | 0.7387 *** | 93.28 *** |
| 0801-Richness | 0.37723 *** | 0.09317 *** | 0 | 0.4766 *** | 30.05 *** |
| 0801-Both | −0.08934NS | 0.04280 ** | 0.15750 *** | 0.835 *** | 80.98 *** |

Reflectance measurements revealed clear NDVI dynamics and subtle changes in the NDVI–diversity relationship that were affected by trends in weather conditions and flowering over the growing season (Figure 2.5). NDVI showed early-season increases in May and June (Figure 2.5d), a period of canopy growth and development, as indicated by increases in plant height (Figure 2.5b). Plants in 16-species plots were significantly taller than those in 8-species plots and both were significantly taller than 4, 2 and 1 species plots (Tukey's HSD, $p < 0.05$). The latter three did not differ from each other (Tukey's HSD, $p > 0.05$).

By August 1, NDVI showed a deep decline accompanied by a coincident decline in surface soil moisture following a period of high temperatures and lack of precipitation, but then recovered briefly during a subsequent period of lower temperature and high precipitation in mid to late August (Figure 2.5). After this second, smaller August rise, NDVI continued to decline gradually as plants senesced into the fall.

NDVI also appeared to be affected by flowering, with the mid-season NDVI dip coincident with the period of anthesis (flower opening) for many of the dominant species (Figure 2.5c). The total number of open flowers varied significantly with date ($\chi^2_8 = 65.7$, $p < 0.001$). Pairwise comparisons (Steel-Dwass method) revealed that there were significantly more flowers at the 6 August 2014 census (close to the NDVI dip) than five of the eight other census times. All but May 29, July 21 and September 4 had significantly lower numbers of flowers.

Over most of the season, NDVI was higher for high-species-richness plots, and the NDVI–species richness relationship shifted over the growing season (Figure 2.5d). This difference in NDVI for plots with different species richness largely disappeared by October, when plants had largely senesced, at a time of advanced canopy growth (Figure 2.5b).

The seasonal change in the NDVI–species richness relationship is shown in more detail in Figure 2.6, further demonstrating that plots with high richness tended to have a higher mean NDVI and lower variation in NDVI than plots with low species richness (Figures 2.6 and 2.7). The variation of NDVI among the high richness plots became visibly

smaller as the growing season progressed (Figure 2.6). NDVI showed the strongest relationship with species richness at peak season (Figures 2.6 and 2.8 and Table 2.2). Similarly, whole-plot measurements (Figure 2.7) based on full-plot sampling (49 measurements) in the middle of the summer showed a clearer trend than any of the individual monthly measurements (Figure 2.6, Table 2.2) that were based on smaller sample sizes (17 *vs.* 49 measurements).

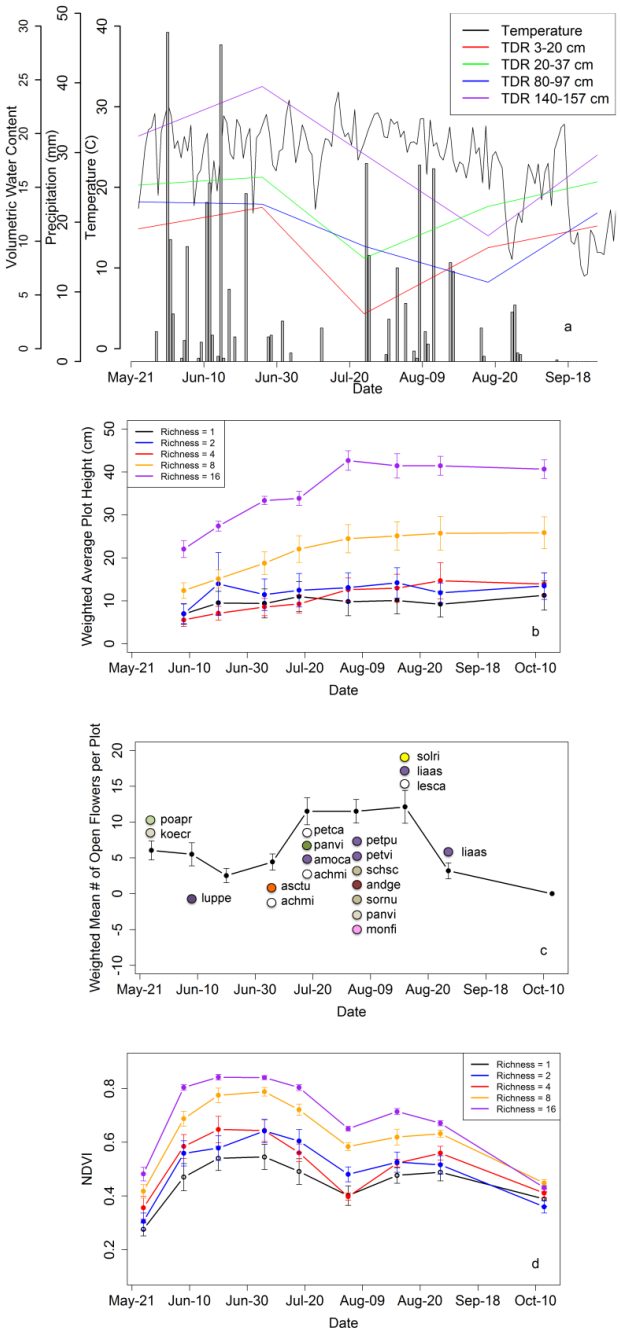


Figure 2.5**.** Time series of air temperature (maximum temperature of the day), precipitation, soil moisture expressed as volumetric water content (**a**); weighted average plot height (**b**); weighted mean number of open flowers per plot (**c**) and NDVI plotted by species richness (**d**) over the growing season in 2014. In Figure 2.5c, the approximate flower color is indicated by the colored circles, and the species names are indicated by 5-letter abbreviations (see Table S2.2 in Appendices for full species names).

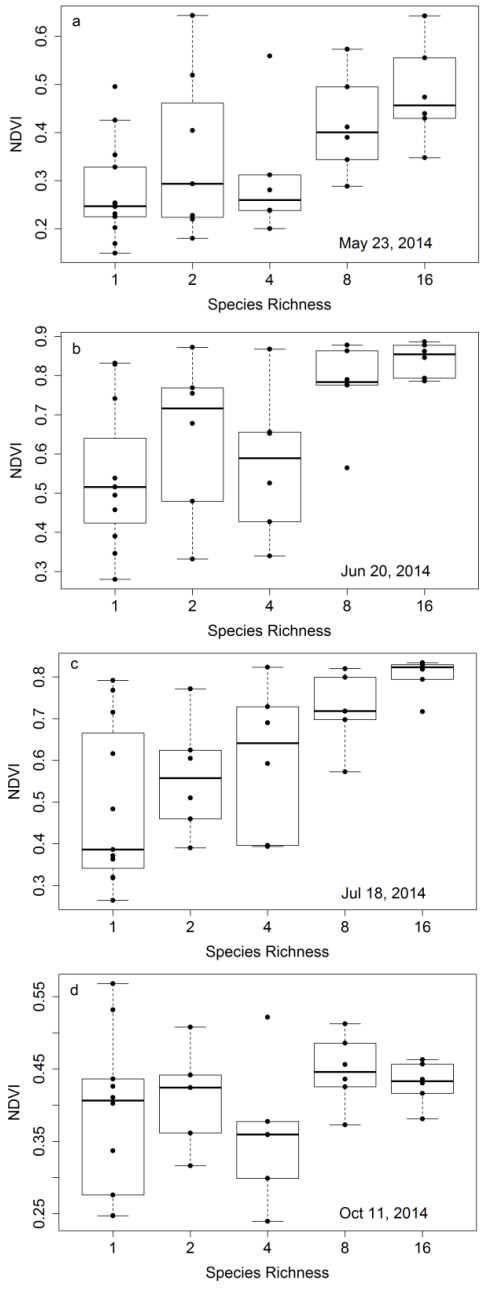


Figure 2.6**.** Representative examples of NDVI *versus* species richness at four time points (plots **a**–**d**) in the 2014 growing season. These figures were derived from plot subsamples (17 measurements along the north most row of each plot) for 35 plots. Species richness represents the planted number of species per plot. Each richness treatment had a sample size of 6, except monoculture plots, which had a sample size of 11. In this figure, box plots were overlaid on actual data points (dots) that represent the average values for each plot. The regression statistics are provided in Table 2.1.

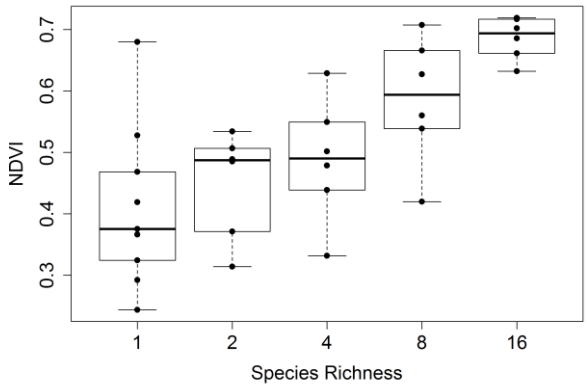


Figure 2.7 Mid-season whole-plot NDVI *versus* species richness (collected over several dates spanning 23 July to 3 August 2014). For this figure, 49 (7 m × 7 m) of the 81 measurements in the center of each plot were used to calculate the average reflectance and NDVI, yielding a more representative sampling than shown in Figure 2.6. Species richness represents the planted number of species per plot. Each richness treatment had a sample size of 6, except monoculture plots, which had a sample size of 9. In this figure, box plots were overlaid on actual data points (dots) that represent the average values for each plot. The regression statistics are provided in Table 2.2.

Table 2.2 Species richness–NDVI relationships for various dates in 2014 compared to the whole plot results obtained at mid-summer (23 July–2 August 2014).

| **Sampling** | **Regression Equation** | **$R^2$** | ***p* Value** |
|---|---|---|---|
| May-23 | y = 0.0132x + 0.2821 | 0.2587 | 0.001 |
| June-08 | y = 0.0211x + 0.4841 | 0.3312 | 0.0003 |
| June-20 | y = 0.0199x + 0.548 | 0.3137 | 0.0005 |
| July-06 | y = 0.0193x + 0.5651 | 0.3325 | 0.0003 |
| July-18 | y = 0.0207x + 0.5022 | 0.374 | $9.51 \times 10^{-5}$ |
| August-04 | y = 0.0178x + 0.3909 | 0.4728 | $5.04 \times 10^{-6}$ |
| August-21 | y = 0.0157x + 0.4725 | 0.3789 | 0.0001 |
| September-05 | y = 0.0119x + 0.4957 | 0.2737 | 0.001 |
| October-11 | y = 0.0034x + 0.3854 | 0.05 | 0.209 |
| Whole-plot Sampling | y = 0.0177x + 0.4114 | 0.5136 | $6.07 \times 10^{-7}$ |

A more complete summary of the effects of sample date and size on the NDVI-species richness relationship is provided in Table 2.2, clearly illustrating that the strongest relationships were obtained towards mid-summer when plants were fully mature and before the onset of senescence, and that larger sample sizes based on whole-plot data

improved the relationships. The seasonal pattern in the NDVI-species richness relationship (expressed as $R^2$ values) can be compared to the NDVI time trend, showing a peak in the correlation during the mid-season dip in NDVI, a time of warm, dry conditions and peak anthesis (Figures 2.5 & 2.8).

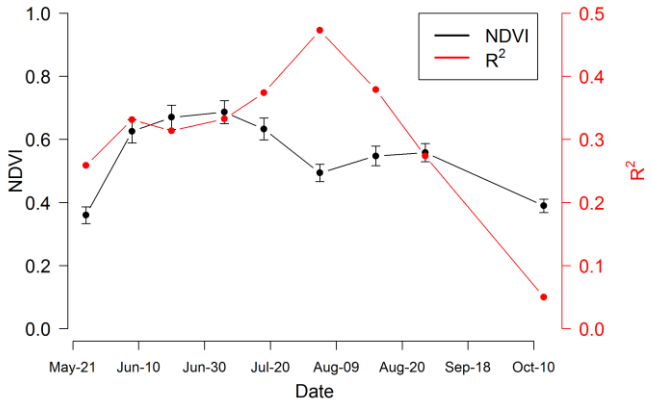


Figure 2.8 Time series of NDVI (black line) and $R^2$ of the NDVI-species richness regression (red line) over the growing season in 2014. NDVI was the average value (±SEM) of all the plots on each sampling date.

## 2.4 Discussion

### 2.4.1 Biomass–NDVI Relationship

In this study, the significant relationship between biomass and NDVI (Figure 2.4) agrees with previous research, and has been discussed in multiple systems from both theoretical (Sellers 1987) and empirical approaches (Gamon et al. 1995). NDVI provides a rapid and non-destructive method of estimating biomass and percent cover, providing an empirical relationship between spectral information and biomass and percent cover (Gitelson et al. 2002). Both vegetation percent cover and biomass have been broadly used as surrogates of vegetation productivity (Mittelbach et al. 2001), especially in grasslands (Scurlock et al. 2002). Using NDVI, remote sensing can assess continuous dynamics of biomass productivity over the growing season at a large scale.

The correlation between NDVI and biomass in our study, while significant, was lower than is often reported (Gamon et al. 1995). One reason for this scatter is that we did not harvest the biomass from the same plot location as NDVI sampling, but assumed that the plots were homogeneous in order to get continuous phenology NDVI measurements in the whole growing season. The NDVI–biomass relationship (Figure 2.4) could have been improved by matching the exact locations of NDVI and biomass sampling (Gamon et al. 1995) but this would have precluded time-series analysis of NDVI phenology. Variation in the NDVI–biomass relationship can also be caused by variation in canopy structure, with different canopy architectures having slightly different NDVI–biomass relationships. Another reason for the scatter may be that NDVI is more closely related to $fPAR_{green}$, a measure of light absorption by green canopy material and hence potential production (Gamon et al. 1995, Gitelson and Gamon 2015), than biomass *per se*. Like biomass harvesting, $fPAR_{green}$ measurement is also destructive and was not measured in our study (but can be inferred from NDVI).

### 2.4.2 Productivity–Richness Relationship

The productivity-biodiversity relationship is a much-discussed topic in the ecological literature (Huston 1997, Tilman 1997, Wardle 1999, Adler et al. 2011, Fraser et al. 2015), and undoubtedly is influenced by many factors. Biodiversity can affect the production of ecosystems due to the complementary roles played by different species (Tilman et al. 1996). For example, adding species within a community can enhance the ability of vegetation to capture resources (Cardinale et al. 2007). Similar to what has been previously reported with the biomass–species richness relationships (Tilman 1997), the NDVI-species richness relationship tended to approach saturation at the high richness end (8 to 16 species). This may be because when all functional groups are present, the addition of species with redundant function has little effect on ecosystem properties (Waide et al. 1999).

Selection effects result from the increased probability of adding a productive species in higher diversity polycultures and can also contribute to the explanation of high biomass in polycultures. In the Cedar Creek BioDIV experiment, both selection effects and complementarity of species have been shown to affect the community productivity

(Fargione et al. 2007, Reich et al. 2012). Our goal in this study was not to further analyze the respective contributions of selection and complementarity effects (Loreau and Hector 2001), but rather to use a remotely sensed measure of vegetation to examine the dynamics of the biodiversity–productivity relationship through time. We note that most of the productive monocultures may have equivalent or even higher biomass than some of the polycultures (shown as higher NDVI in some of the monoculture in our study), that species express different growth and phenological stages at any given point in time (Figure 2.5), and that the most productive species can change though time within one growing season (data not shown). Moreover, it is unlikely that a monoculture can be more productive than a diverse community when considering a long time span (Cardinale et al. 2007). When a long time period (>10 years) is considered, accumulation of complementarity effects can dominate the productivity–richness relationship and lead to a more positive relationship (Fargione et al. 2007, Reich et al. 2012).

At present, remote sensing does not necessarily inform the mechanisms underlying the biodiversity–productivity relationship. However, the non-destructive nature of remote assessment assists our understanding of the dynamics of the richness–productivity relationship through time and in relationship to environmental constraints by permitting repeated landscape-level assessments beyond the scope of typical field plots. In our study, only a small number of species was considered at a local scale, but these methods can also be readily applied to larger regions. In a parallel study of prairie grassland in southern Alberta, Wang *et al.* (Wang et al. 2016a) found a similar, positive relationship between productivity and biodiversity over a large landscape using airborne imaging spectrometry coupled with field sampling. Understanding the mechanisms underlying the richness–productivity relationship, while beyond the scope of this particular study, can help maintain and conserve biodiversity (Mittelbach et al. 2001).

### 2.4.3 Richness-Percent Cover and Effects

In this study, NDVI was affected by both species richness and vegetation percent cover, and vegetation percent cover had a stronger effect than species richness (Table 2.1). The Cedar Creek BioDIV prairie ecosystem experiment is maintained at nominal species richness via burning and weeding every year. Fecundity and dispersal feedbacks over

time have resulted in patchiness and low percent cover of some of the low richness plots (Naeem et al. 2000). As a result, the low richness plots may have increased exposed soil and moss-covered patches. This factor, in addition to vegetation composition effects on NDVI, may have contributed to the reduced NDVI in low richness plots. Further studies could focus on plots with different species richness but similar vegetation percent cover, or on manipulating different species composition at same richness level to control for plant density, to better understand how species richness, cover and composition affect the optical diversity signal separately. The potential to apply remote sensing to address these questions over larger regions and natural landscapes is high (Wang et al. 2016a) and critical to understanding these relationships in natural systems, and ultimately to managing ecosystems for resiliency in the face of rapid global change.

### 2.4.4 Seasonal NDVI Variation

Many factors, including changing canopy display, leaf pigmentation, and flowering, can all influence NDVI. In our study, the drop of NDVI in early August was coincident with the high temperature and lack of precipitation in late July (Figure 2.5). In the short term, water stress can affect NDVI by causing vegetation wilting and leaf rolling. These changes in canopy structure tend to decrease vegetation visibility and increase soil visibility to the sensor, decreasing NIR reflectance and increasing visible reflectance, and thus reducing NDVI. This temporary effect of water stress can be reversed by precipitation, allowing vegetation to recover to some extent, and this helps explain the early August NDVI dip and subsequent increase (Figure 2.5). Similarly, the mid-season NDVI drop was coincident with anthesis, the time of maximum flower opening, which has also been shown to reduce NDVI depending upon flower color and its influence on the reflectance spectrum (Joel et al. 1997, Naeem et al. 2000, Shen et al. 2010).

### 2.4.5 Sample Size

Sample size also affects the NDVI-richness relationship. In our study, the mid-season whole plot results that had a higher sample size ($n$ = 49) showed a stronger NDVI-richness relationship than any of the repeated monthly measurements in a similar subset of plots with a smaller sample size ($n$ = 17) (Figures 2.6 & 2.7, Table 2.2). Most likely, the whole-plot measurements were more representative of the Cedar Creek BioDIV study

than the time-series results that only included a subsample of the full plot areas. Similarly, previous studies (Magurran 2004) and models (Pavlick et al. 2013) showed increasing accuracy with increasing number of sampling strategies. Considering that remote sensing can readily obtain large regions while providing a systematic view of the Earth at regular time intervals, it holds the promise of becoming a feasible, convenient and cost-effective way to conduct biodiversity research (Nagendra 2001).

### 2.4.6 Seasonality of the NDVI-Species Richness Relationship

Compared to the spatial patterns of biodiversity, less attention has been paid to the seasonal patterns of biodiversity (Magurran 2008) or the effect of phenology on the ability to assess biodiversity with remote sensing. In our study, the NDVI-richness relationship was dynamic and the best regression between NDVI and species richness occurred near peak season, although the exact reasons for this deserve further study. This dynamic relationship was most likely affected by canopy development, as well as by prevailing conditions (mid-season warm, dry conditions) and flowering phenology (timing of anthesis). While both short-term drought and mid-season anthesis clearly reduced NDVI, their effect on the NDVI-biodiversity patterns was less clear, and could have even enhanced this relationship, as illustrated by the enhanced NDVI-biodiversity correlations at mid-season (Figures 2.6–2.8, Table 2.2), or at least not interfered with it. Multi-year data may be helpful to separate the confounding effects of short term drought and anthesis on NDVI–biodiversity relationship because the seasonal meteorology can vary year to year. The exact impact of these multiple factors on the timing of the NDVI–biodiversity relationship, while beyond the scope of this study, might yield additional insights into the mechanisms driving the productivity–biodiversity relationship.

## 2.5. Conclusions

Remote sensing provides an efficient and inexpensive way to assess biomass and biodiversity. This study further confirms earlier studies at this site, and illustrates the potential of remote sensing to assess the diversity–productivity relationship. The Cedar Creek experiments provide a convenient test of this relationship in a human-maintained prairie ecosystem. Considering the two hypotheses proposed in the introduction, this study shows that NDVI can be related to species richness, but it is also strongly affected

by other factors, including canopy structure (cover or biomass) and short-term water stress and shifting flowering patterns that can confound the NDVI-richness relationship. Interestingly, the strongest NDVI–biodiversity relationship occurred in mid-summer, when NDVI showed a temporary decline associated with warm, dry conditions and anthesis.

While remote sensing has the potential to be used in biodiversity assessment, it also adds additional capabilities and complexity by being able to assess this diversity at multiple scales. Further work should address the optical-biodiversity relationship in more detail, in part by addressing the scale-dependence. As well, future studies should take advantage of the full spectral power of imaging spectrometry to evaluate the diversity–productivity relationship for a larger variety of ecosystems.

**Acknowledgments**
We thank staff at the Cedar Creek Ecosystem Science Reserve, particularly Troy Mielke and Kally Worm, and research assistant, Jonathan Anderson. We also thank Aidan Mazur and Melanie Sitten from University of Wisconsin-Madison for helping collect the whole plot reflectance data. This study was supported by a NASA and NSF grant DEB-1342872 to J. Cavender-Bares, a NSF-LTER grant to D. Tilman, J. Cavender-Bares and R. Montgomery DEB-1234162 and by iCORE/AITF and NSERC grants to J. Gamon, and a China Scholarship Council fellowship to R. Wang.

## 2.6. References

Adler, P. B. et al. 2011. Productivity Is a Poor Predictor of Plant Species Richness. - Science. 1750: 1750–1754.

Booth, D. T. and Tueller, P. T. 2003. Rangeland monitoring using remote sensing. - Arid L. Res. Manag. 17: 455–467.

Bork, E. W. et al. 1999. Rangeland cover component quantification using broad (TM) and narrow-band (1.4 NM) spectrometry. - J. Range Manag. 52: 249–257.

Cardinale, B. J. et al. 2007. Impacts of plant diversity on biomass production increase through time because of species complementarity. - Proc. Natl. Acad. Sci. U. S. A. 104: 18123–18128.

Clark, D. A. et al. 2001. Measuring net primary production in forest: concepts and field methods. - Ecol. Appl. 11: 356 – 370.

Fargione, J. et al. 2007. From selection to complementarity: shifts in the causes of biodiversity-productivity relationships in a long-term biodiversity experiment. - Proc. Biol. Sci. 274: 871–876.

Fraser, L. H. et al. 2015. Worldwide evidence of a unimodal relationship between productivity and plant species richness. - Science. 349: 302–306.

Gamon, J. A. et al. 1993. Functional patterns in an annual grassland during an AVIRIS overflight *. - Remote Sens. Environ. 44: 239–253.

Gamon, J. A. et al. 1995. Relationships between NDVI, canopy structure, and photosynthesis in three californian vegetation types. - Ecol. Appl. 5: 28–41.

Gamon, J. A. et al. 2006. A mobile tram system for systematic sampling of ecosystem optical properties. - Remote Sens. Environ. 103: 246–254.

Gitelson, A. A. and Gamon, J. A. 2015. The need for a common basis for defining light-use efficiency: Implications for productivity estimation. - Remote Sens. Environ. 156: 196–201.

Gitelson, A. a. et al. 2002. Novel algorithms for remote estimation of vegetation fraction. - Remote Sens. Environ. 80: 76–87.

Huston, M. A. 1997. Hidden treatments in ecological experiments: re-evalutating the ecosystem function of biodiverstiy. - Oecologia 110: 449–460.

Isbell, F. et al. 2015. Biodiversity increases the resistance of ecosystem productivity to climate extremes. - Nature 526: 574–577.

Joel, G. et al. 1997. Production efficiency in sunflower: The role of water and nitrogen stress. - Remote Sens. Environ. 62: 176–188.

Lehman, C. L. and Tilman, D. 2000. Biodiversity, stability, and productivity in competitive communities. - Am. Nat. 156: 534–552.

Loreau, M. and Hector, A. 2001. Partitioning selection and complementarity in biodiversity experiments. - Nature 412: 72–76.

Magurran, A. E. 2004. Measuring biological diversity. - Blackwell Publishing.

Magurran, A. E. 2008. Diversity over time. - Folia Geobot. 43: 319–327.

Mittelbach, G. G. 2012. Biodiversity and ecosystem functioning. - In: Community Ecology. 1st ed.n. Sinauer Associates, Inc., pp. 41–62.

Mittelbach, G. G. et al. 2001. What is the observed relationship between species richness and productivity? - Ecology 82: 2381–2396.

Naeem, S. et al. 2000. Plant diversity increases resistance to invasion in the absence of covarying extrinsic factors. - Oikos 91: 97–108.

Nagendra, H. 2001. Using remote sensing to assess biodiversity. - Int. J. Remote Sens. 22: 2377–2400.

Pavlick, R. et al. 2013. The Jena Diversity-Dynamic Global Vegetation Model (JeDi-DGVM): a diverse approach to representing terrestrial biogeography and biogeochemistry based on plant functional trade-offs. - Biogeosciences 10: 4137–4177.

Piñeiro, G. et al. 2006. Seasonal variation in aboveground production and radiation-use efficiency of temperate rangelands estimated through remote sensing. - Ecosystems 9: 357–373.

Reich, P. B. and Hobbie, S. E. 2013. Decade-long soil nitrogen constraint on the CO2 fertilization of plant biomass. - Nat. Clim. Chang. 3: 278–282.

Reich, P. B. et al. 2012. Impacts of biodiversity loss escalate through time as redundancy fades. - Science. 336: 589–592.

Scurlock, J. M. O. et al. 2002. Estimating net primary productivity from grassland biomass dynamics measurements. - Glob. Chang. Biol. 8: 736–753.

Sellers, P. J. 1987. Canopy reflectance, photosynthesis, and transpiration. II - The role of biophysics in the linearity of their interdependence. - Remote Sens. Environ. 21: 143–183.

Shen, M. et al. 2010. Do flowers affect biomass estimate accuracy from NDVI and EVI? - Int. J. Remote Sens. 31: 2139–2149.

Team, R. C. 2015. R: A language and environment for statistical computing. in press.

Tilman, D. 1997. The influence of functional diversity and composition on ecosystem processes. - Science. 277: 1300–1302.

Tilman, D. and Haddi, A. El 1992. Drought and biodiversity in grasslands. - Oecologia 89: 257–264.

Tilman, D. et al. 1996. Productivity and sustainability influenced by biodiversity in grassland ecosystems. - Nature 379: 718–720.

Tilman, D. et al. 2001. Diversity and productivity in a long-term grassland experiment. - Science. 294: 843–845.

Tilman, D. et al. 2006. Biodiversity and ecosystem stability in a decade-long grassland experiment. - Nature 441: 629–632.

Tucker, C. J. 1979. Red and photographic infrared linear combinations for monitoring vegetation. - Remote Sens. Environ. 8: 127–150.

Waide, R. B. et al. 1999. The relationship between productivity and species richness. - Annu. Rev. Ecol Syst 30: 257–300.

Wang, R. et al. 2016. Integrated analysis of productivity and biodiversity in a southern Alberta prairie. - Remote Sens. 8: 214.

Wardle, D. A. 1999. Is “sampling effect” a problem for experiments investigating biodiversity-ecosystem function relationships? - Oikos 87: 403–407.

# Chapter 3 Integrated Analysis of Productivity and Biodiversity in a Southern Alberta Prairie

**Abstract:**

Grasslands play important roles in ecosystem production and support a large farming and grazing industry. An accurate and efficient way is needed to estimate grassland health and production for monitoring and adjusting management to get sustainable products and other ecosystem services. Previous studies of grasslands have shown varying relationships between productivity and biodiversity, with most showing either a positive or a hump-shaped relationship where productivity peaks at intermediate diversity. In this study, we used airborne imaging spectrometry combined with ground sampling and eddy covariance measurements to estimate the spatial pattern of production and biodiversity for two sites of contrasting productivity in a southern Alberta prairie ecosystem. Resulting patterns revealed that more diverse sites generally had greater productivity, supporting the hypothesis of a positive relationship between production and biodiversity for this site. We showed that the addition of evenness to richness (using the Shannon Index of dominant species instead of the number of dominant species alone) improved the correlation with optical diversity, an optically derived metric of biodiversity based on the coefficient of variation in spectral reflectance across space. Similarly, the Shannon Index was better correlated with productivity (estimated via NDVI (Normalized Difference Vegetation Index)) than the number of dominant species alone. Optical diversity provided a potent proxy for other more traditional biodiversity metrics (richness and Shannon index). Coupling field measurements and imaging spectrometry provides a method for assessing grassland productivity and biodiversity at a larger scale than can be sampled from the ground, and allows the integrated analysis of the productivity–biodiversity relationship over large areas.

## 3.1 Introduction

Grasslands occur on all continents except Antarctica and occupy nearly 25% of the land surface of the Earth (Sala et al. 1996). In North America, the Great Plains is the broad

expanse of flat land located east of the Rocky Mountains and west of the Mississippi River in the United States and Canada. This land is mainly covered in steppe and grassland, and is often referred to as "prairie." In the United States, prairie area is $1.62 \times 10^6$ km$^2$, or 21 percent of the total area of the country (Hunt et al. 2003). In Canada, prairie area is $5 \times 10^5$ km$^2$, 5 percent of the total area of the country (Sims and Risser 2000). In Alberta, approximately 7% of the area is covered by dry mixed grass prairie (Adams et al. 2013), most of which is found in southern Alberta and is contiguous with the Great Plains.

In North America, prairie is an important biome for agriculture and grazing (rangeland). Prairies typically are less productive than croplands but play important roles in carbon sequestration and food supplement for animals. Healthy prairies also sustain soil quality, maintain biodiversity, and provide clean water (Hunt et al. 2003). Among all the ecosystem services provided by prairies, biomass yield is typically the factor that most interests humans due to the direct relationship with the prairie's major products, food and fiber (Bernhardt-Römermann et al. 2011). Prairie management typically focuses on maintaining or improving the output of consumable products along with other ecosystem services (Adams et al. 2013).

Prairie productivity is often estimated through biomass harvesting, which is expensive and time consuming (Bork et al. 1999, Booth and Tueller 2003, Piñeiro et al. 2006). Traditional methods of estimating prairie biomass can be subjective because they depend on the experience and skill of the field staff (Booth and Tueller 2003). The estimation is also affected by the sample size and sampling method (Clark et al. 2001). Accurate and fast methods of prairie production estimation that quickly acquire information over large areas are needed for range managers to evaluate the condition of prairies and adjust their management regimes (Booth and Tueller 2003).

The classic Light Use Efficiency (LUE) model, which originated with Monteith's work (Monteith 1972, Monteith and Moss 1977), is often used to address the spatial and temporal dynamics of production from remote sensing (Yuan et al. 2007). The LUE model considers that primary production largely depends on the absorbed

photosynthetically active radiation (APAR) captured by plants and the efficiency with which the absorbed energy is converted to fixed carbon. APAR is affected by the solar irradiance, leaf pigment concentration and canopy structure (e.g., leaf area index and leaf angle distribution). The efficiency term is affected by the light energy distribution within the leaf, and is often influenced by pigment composition and activity (Gitelson and Gamon 2015). The LUE model parameterized by remote sensing measurements generally works well for grasslands, where the APAR term dominates and the efficiency term can often be treated as a constant, particularly for short periods (Gamon et al. 1993, Flanagan et al. 2015). While some challenges remain in scaling, this provides a simple route to determining grassland productivity for comparison with diversity.

There is a long history of using remote sensing to estimate vegetation properties from satellite or airborne platforms (Tucker et al. 1985, DeFries and Townshend 1994, Hill 2013). A number of studies have used remote sensing to estimate the percent cover, production and biophysical properties of grasslands (Gamon et al. 1995, Bork et al. 1999, Booth and Tueller 2003). Many of these studies have shown that the Normalized Difference Vegetation Index (NDVI) is highly correlated with green biomass, leaf area index, and radiation absorption by green vegetation ($APAR_{green}$) in grasslands (Gamon et al. 1995, Piñeiro et al. 2006), consistent with the simple LUE model approach, and allowing ready production estimates over large grassland areas. However, a major limitation in the application of satellite remote sensing in prairie management is the mismatch between the information that range managers need and the spatial scale of most satellite remote sensing. Due to the coarse pixel size (often several tens of meters to kilometers) (Booth and Tueller 2003) and broad bands of most satellite images, satellite remote sensing can best provide land cover or production estimates over large landscapes, or over regional or continental scales (Hunt et al. 2003), but satellite data often have trouble providing detailed species distribution and prairie health information at the scale of small management units.

The high spatial and spectral resolution of airborne imaging spectrometry can reflect fine-scale features by detecting physical and biochemical properties of plants in specific narrow bands at small (sub-meter) image pixel sizes. Consequently, airborne imaging

spectrometry provides an effective tool to map prairie patterns related to photosynthetic function (Gamon et al. 1993) and species distribution patterns in grassland ecosystems (Pottier et al. 2014). One way to derive detailed spatial and temporal patterns of productivity from such imagery is to calibrate the image data against ground measurements using eddy covariance and field spectral measurements (Gamon et al. 1993). Airborne remote sensing, with its high spatial resolution, provides an ideal tool to address these issues of scale when addressing productivity and diversity.

There is now a large body of literature indicating that biodiversity affects ecosystem production (Tilman et al. 1996) and stability (Isbell et al. 2009, de Mazancourt et al. 2013). Particularly in the face of disturbance, the relationship between diversity and productivity, typically measured as biomass, has been controversial for grassland ecosystems. Some studies report a positive relationship between biomass and biodiversity, whereas others indicate a "hump-shaped" relationship, with biodiversity peaking at intermediate biomass levels (Fraser et al. 2015). This relationship can be affected by resource levels (e.g., fertilizer or irrigation levels) and the degree and nature of disturbance. High productivity and low diversity sites are often highly managed via irrigation or fertilizer application (Fraser et al. 2015). For rangelands, grazing levels can confound this relationship, and highest species richness often occurs at light to moderate grazing levels, which is consistent with the "intermediate disturbance hypothesis" (Grime 1973, Connell 1978). Heavy to very heavy grazing can cause a decline in species richness, often due to the invasion of exotic species that lead to a decrease in species diversity while maintaining high levels of productivity (Adams et al. 2013).

Airborne remote sensing provides an efficient and inexpensive way to assess biodiversity. Traditionally, three basic methods have been used to estimate biodiversity with remote sensing: (1) mapping habitat for key species; (2) mapping species distribution (Roberts et al. 1998, Xiao et al. 2004, Clark et al. 2005, Clark and Roberts 2012) or community composition (Lucas et al. 2008); and (3) assessing species richness (Palmer et al. 2002, Rocchini et al. 2004, Rocchini 2007), α-diversity (Rocchini 2007) or β-diversity (Oldeland et al. 2010) through spatial variation in vegetation optical properties (optical diversity in space), sometimes referred to as "spectral heterogeneity" (Rocchini et al.

2010). Using this latter approach, which we call "optical diversity," a variety of methods have been used to capture optical variation as a way to estimate biodiversity. For example, Féret and Asner (Féret and Asner 2014) defined "spectral species" by applying a clustering model to high spatial resolution airborne imagery to map α-diversity and β-diversity in tropical forests.

The spectral species approach assumes that there are unique, definable spectral types ("species") that can be distinguished in image processing, allowing an estimate of biodiversity. A similar concept can be applied in a more abstract level of image information content, without resorting to identifying particular spectral types. We propose that the information content of the imagery itself, which can be expressed as optical diversity, relates to the spatial variation in the spectral data (Palmer et al. 2002, Rocchini et al. 2004) and provides an indicator of relative diversity. The advantage of this approach is that it provides an objective method that can conceivably be applied to any image or ecosystem, without having to define categorical species or spectral types, which are likely to change seasonally or spatially.

In this study, we used flux data and field optical data to help calibrate airborne imagery and map ecosystem productivity in a grazed prairie ecosystem in southern Alberta, Canada. Airborne NDVI measurements were calibrated against $CO_2$ flux measurements and above-ground biomass to estimate landscape productivity, with particular attention to potential errors associated with spatial scale due to various flux footprint assumptions. We also sampled relative levels of biodiversity using optical diversity and field measurements, and by combining airborne data with a vegetation distribution map. Combining three metrics of biodiversity (airborne data, vegetation map and field sampling) to evaluate broad relationships between diversity and productivity across the landscape provided a unique test of the diversity-productivity hypothesis (Tilman et al. 1996) over a large area (10 $km^2$) of this managed prairie ecosystem.

## 3.2 Methods

### 3.2.1 Study Site

The Mattheis Research Ranch is located 150 km east of Calgary, Alberta, Canada (Centre Latitude: 50.90° N, Centre Longitude: 111.88° W) (Figure 3.1). It covers approximately

5000 hectares, 4/5 of which is native prairie. The vegetation distribution map and code for major vegetation communities (based on dominant vegetation type) in the Mattheis Research Ranch are provided in Appendices (Figure S3.1 and Table S3.1). The landscape included two calibration sites, designated “E3” and “E5” (Figure 3.1), where eddy covariance, vegetation biomass, species composition, and field optical measurements (APAR and spectral reflectance) were made.

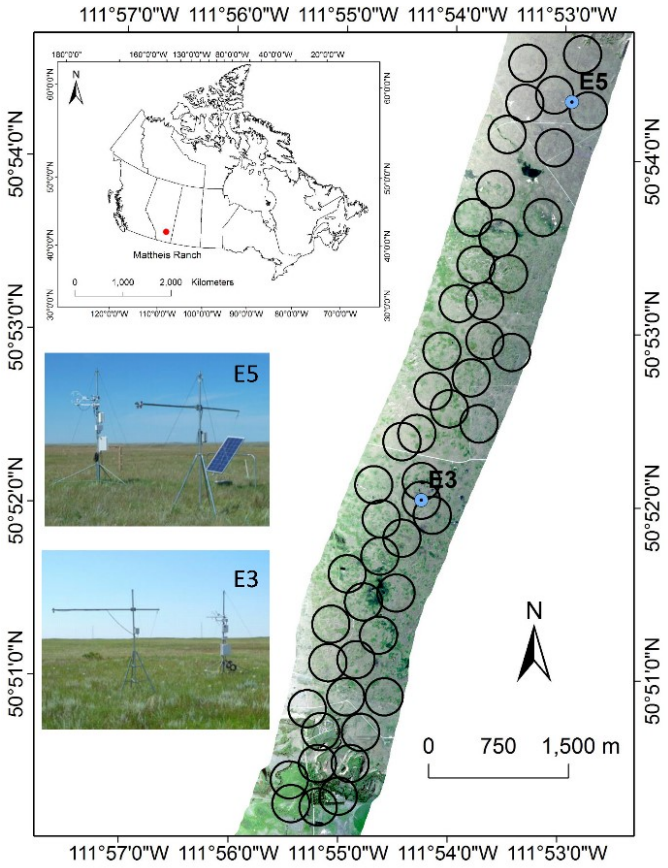


Figure 3.1 Location of Mattheis Research Ranch (50.9038 N, 111.8799 W) and airborne true-color image with 50 randomly selected 200-meter-radius circles in the flight line used for evaluating the productivity-diversity relationship. E5 and E3 labels showed the two flux towers within this area used for calibrating the productivity map, and inset photographs illustrate the flux tower and phenology station for each site. The Canada map was provided by the Statistics Canada.

The landscape in this region is covered mainly by dry mixed grass prairie (Becker 2013). The study area consisted primarily of grazed prairie, with some nearby wetlands and

cultivated areas (largely out of the immediate study area). The grazing regime is a rotational system with relatively short grazing periods of 7–12 days, followed by long recovery periods (6–8 weeks) between grazing periods at moderate stocking. In 2012, grazing commenced in early May–late November, and cattle were outside the direct study area during the overflight. The grazing effects on species composition and structure are not visible from the historical aerial photos, indicating a history of a light grazing regime for this site (Becker 2013).

### 3.2.2 Optical Phenology and Flux Measurements

Two flux towers were established within the ranch at two calibration sites labeled "E3" (50.8672 N, 111.9045 W) and "E5" (50.9056 N, 111.8823 W), located approximately 4.5 km apart. A phenology station was set within 10 m of the flux tower at each site. The optical phenology stations measured reflectance of broadband solar radiation and PAR every fifteen minutes. Each optical station had a data logger (H21-001, Onset Computer Corporation, Bourne, Massachusetts, USA) and two-band radiometer. One band had two PAR sensors (S-LIA, Onset Computer Corporation, Bourne, Massachusetts, USA) and the other band consisted of two PYR (pyranometer) sensors (S-LIB, Onset Computer Corporation, Bourne, Massachusetts, USA). Both the upward and downward sensors have cosine foreoptics, providing a relatively large optical footprint (approximately 100 $m^2$) around the flux tower. These data were used to calculate a proxy NDVI (Huemmrich et al. 1999, Gamon et al. 2010):

$$\text{NDVI proxy} = (\varrho_{PYR} - \varrho_{PAR})/(\varrho_{PYR} + \varrho_{PAR}) \quad (3.3)$$

where $\rho_{PYR}$ is the reflectance of the PYR band (solar radiation), calculated as the ratio of the reflected solar radiation to the incoming solar radiation across a spectral range from 300 to 1100 nm and $\rho_{PAR}$ is the reflectance of the PAR band that is the ratio between the reflected PAR and the incoming PAR within 400 – 700 nm. The proxy NDVI values were subsequently used to derive APAR for the LUE model, as described below (Figure 3.2).

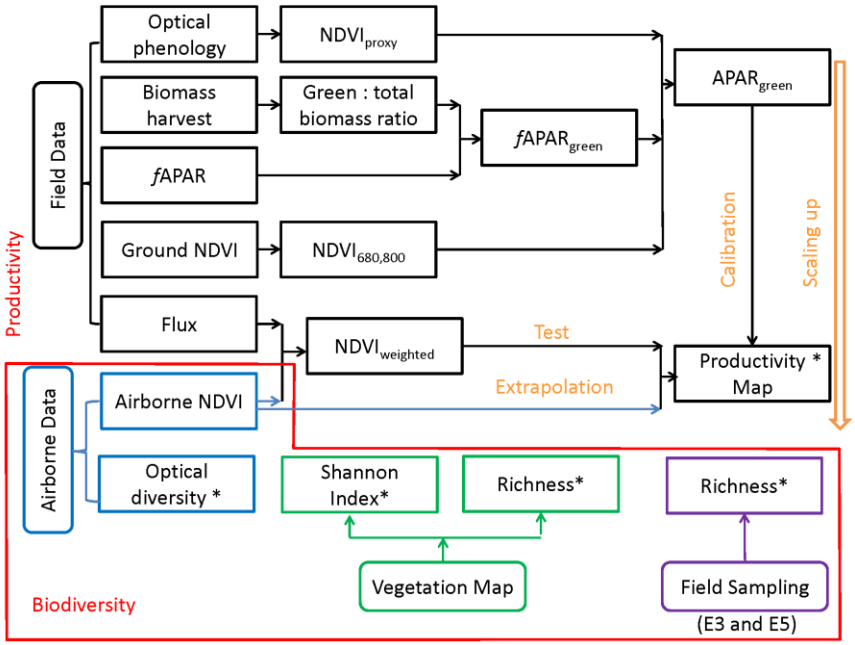


Figure 3.2 Experimental design and data used in this study. The linear relationship between NDVI, biomass and NEE (Net Ecosystem Exchange) allowed us to use NDVI (Normalized Difference Vegetation Index) as a proxy for productivity (*) that was then compared to several metrics of biodiversity indicated by asterisks (*).

Eddy covariance data were collected at both sites using an open-path infrared gas analyzer (IRGA; LI-7500, LI-COR, Lincoln NE, USA) and a three-dimensional sonic anemometer (CSAT3; Campbell Scientific, Logan UT, USA), at 2.9 m (E3 site) and 3.0 m (E5 site) above ground. The raw flux data recorded at 10 Hz was aggregated at thirty-minute time intervals as a measure of net ecosystem productivity (NEP = −Net Ecosystem Exchange, NEE) using the EddyPro (LI-COR, v. 5.1) software package. In our study, we used the sign convention of positive NEP fluxes indicating a net uptake of $CO_2$ by the biosphere and negative NEP fluxes signifying a net release of $CO_2$ to the atmosphere, with the reverse convention used for NEE.

Flux and optical data from the E3 site was used to create the APAR-NEE model, instead of data from E5, which had an extensive flux data gap in the growing season. The flux data at E3 site was collected continuously from 16 May to 19 October 2012. At the E3

site, there were three major data gaps in the growing season: May (10 days), June (16 days) and August (8 days).

The peak flux in the summer was used to separate the season into green-up and senescence phases in order to avoid possible effects of hysteresis (Flanagan et al. 2015). Considering the date of the airplane flight (17 August 2012), a model of proxy NDVI–NEP in the second half of the growing season was used.

### 3.2.3 Biomass Harvest

To calibrate productivity estimates, standing biomass was measured monthly at both calibration sites (E3 and E5) during the growing season in 2012 (11 measurements for each site from May to August, 44 measurements in total). A 30 cm diameter metal sampling ring was placed around the vegetation to be harvested. All above-ground vegetation was cut to a height of <1 cm above the ground. Forb and graminoid components were separately collected and taken back to the lab for further processing. The biomass was sorted, oven-dried, and weighed ($g/m^2$) as separate categories (green and brown). A "green fraction" factor was calculated based on the biomass ratio between green and total (green and brown) dry mass, and this was subsequently used in APAR calculation.

### 3.2.4 APAR Determination

Fraction of Absorbed Photosynthetically Active Radiation (*f*APAR) measurements were taken at the same time as the biomass harvest in the field using a light bar (Accupar, Decagon Inc.), and were calibrated against proxy NDVI measurements (above) to parameterize the *f*APAR term of the light-use efficiency model. These *f*APAR measurements were multiplied by the green fraction obtained from biomass harvests and calibrated against the proxy NDVI values to derive a continuous $fAPAR_{green}$. This NDVI-derived $fAPAR_{green}$ was subsequently multiplied by the Photosynthetic Photon Flux Density (PPFD) from the phenology stations to estimate radiation absorbed by green canopy material ($APAR_{green}$).

$$APAR_{green} = (fAPAR \times \text{green fraction}) \times PPFD \quad (3.4)$$

### 3.2.5 Ground NDVI

Spectral reflectance was measured with a dual channel spectrometer (Unispec DC, PP Systems, Amesbury, Massachusetts, USA) at biomass and proxy NDVI sampling sites (Figure 3.2). The detectors collected irradiance and radiance from 350 to 1130 nm with an approximate spectral resolution (FWHM) of 10 nm. The upward-looking channel included a fiber optic and a cosine head to record the solar irradiance. The downward-looking channel included a fiber optic and a field-of-view restrictor that limited the field of view to approximately 15 degrees. In this application, the spatial resolution of each sample on the ground was approximately 0.5 $m^2$.

Both upwelling radiance and downwelling irradiance were measured over the vegetation target and a white reference calibration panel (Spectralon, Labsphere, North Sutton, NH, USA), and used to correct for the atmosphere variation and calculate surface reflectance (Gamon et al. 2006). The reflectance (ρ) at wavelength (λ) was calculated as

$$\rho_\lambda = \frac{(L_{target,\lambda}/E_{target,\lambda})}{(L_{panel,\lambda}/E_{panel,\lambda})} \tag{3.5}$$

In this equation, $L_{target,\lambda}$ indicates the radiance measured at each wavelength (λ, in nm) by a downward-pointed detector sampling the surface ("target"), while $E_{target,\lambda}$ indicates the irradiance measured simultaneously by an upward-looking detector sampling the downwelling radiation. $L_{panel,\lambda}$ indicates the radiance measured by a downward-pointed detector sampling the calibration panel, and $E_{panel,\lambda}$ indicates the irradiance measured simultaneously by an upward-pointed detector sampling the downwelling radiation.

Ground NDVI was calculated from spectrometer measurements using Equation (3.4).

$$NDVI_{680,800} = \frac{\rho_{800} - \rho_{680}}{\rho_{800} + \rho_{680}} \tag{3.6}$$

where $\rho_{800}$ and $\rho_{680}$ represent the reflectance at 800 and 680 nm, respectively. Ground spectral reflectance measurements were taken at the same time and over the same 1-ha landscape region as the biomass harvest and proxy NDVI. A linear model between time-series ground NDVI and green biomass was created and later applied to the airborne data for subsequent determination of biomass and $APAR_{green}$ from airborne data (Figure 3.2).

### 3.2.6 Airborne Data

An imaging spectrometer (Headwall A Series, Headwall Photonics Inc., Fitchburg, MA, USA) was used to collect airborne data on 17 August 2012. The instrument was mounted on a fixed-wing aircraft (Piper Navajo, Piper Aircraft, Vero Beach Florida) from a height of 1220 m and a speed of 213–222 km/h. The pixel size on the ground was approximately 1.1 m. The imaging spectrometer provided 400~1000 nm hyperspectral images with 3 nm spectral resolution (Full width at half maximum, FWHM).

Several steps were taken to process the raw digital numbers to reflectance spectra. (1) A flat field correction was done to remove patterns inherent in the detector array; (2) A spectral adjustment was taken using the 760 nm oxygen Fraunhofer line as a reference band to correct for wavelength shifts; (3) Three 9 × 9 meter calibration targets (white, charcoal, and black) made from polyester fabric (Odyssey, J. Ennis, Edmonton, Alberta, Canada) were used in the surface reflectance correction. These targets were placed on the ground during the airplane overflight to calculate coefficients for calculating surface reflectance using the empirical line correction (Conel et al. 1987). Finally, reflectance spectra were degraded to a spectral resolution of 10 nm for better data quality using Equation (3.5).

$$\rho_{\hat{\lambda},FWHMd} = \int_{-\infty}^{\infty} \rho_{\hat{\lambda},FWHMo} K_{\lambda-\hat{\lambda}} d\hat{\lambda}$$

$$\begin{aligned} K_{\lambda-\hat{\lambda}} &= \frac{2\sqrt{2\ln 2}}{\sqrt{2\pi}\sqrt{FWHM_d^2 - FWHM_o^2}} exp\left[-\frac{4(\ln 2)\hat{\lambda}^2}{FWHM_d^2 - FWHM_o^2}\right] \\ &= 2\sqrt{2\ln 2}\ \frac{1}{\sqrt{2\pi}\sqrt{FWHM_d^2 - FWHM_o^2}} \exp\left[-\frac{1}{2}\frac{\left(2\sqrt{2\ln 2}\,\hat{\lambda}\right)^2}{FWHM_d^2 - FWHM_o^2}\right] \end{aligned} \quad (3.7)$$

$FWHM_o$ and $\rho_{\hat{\lambda},FWHMo}$ were the spectral resolution and reflectance of the original spectra, $FWHM_d$ and $\rho_{\hat{\lambda},FWHMd}$ were the spectral resolution and reflectance of the target spectra, $K_{\lambda-\hat{\lambda}}$ was a Gaussian kernel function while $\int_{-\infty}^{\infty} K_{\lambda-\hat{\lambda}} d\hat{\lambda} = 1$ (Damm et al. 2011).

Position and rotational attributes (pitch, roll, and yaw) of the airplane during the flight were recorded by an inflight GPS and inertial measurement unit (IMU). This information

was used to apply the geo-referencing correction. The images were resampled to 1 meter$^2$ spatial resolution when applying the geo-referencing correction. Airborne narrow-band NDVI was calculated using Equation (3.4).

We used a north-south flight line (10 km long × 1.3 km wide) that covered both flux tower sites to estimate the productivity in this region (Figure 3.1). We applied a "space-for-time substitution" strategy by applying an NDVI-green biomass calibration and LUE model (calibrated by data collected from the E3 and E5 calibration sites during the second half of the growing season) to airborne NDVI data (spatially distributed over the landscape) to map the green biomass and NEE distribution in this prairie ecosystem. The airborne NDVI was calibrated using the narrow-band NDVI-green biomass relationship obtained with a ground spectrometer at 11 ground calibration sites located in a 1 ha area at both E3 and E5 sites. The airborne NDVI was calibrated against proxy NDVI to generate the APAR-NEE relationship, which assumed a fixed efficiency (ε) for this prairie ecosystem in the LUE model. Because this NDVI was linearly correlated to both green biomass from harvests ($R^2$ = 0.82) and Net Ecosystem Exchange (NEE) from flux measurements ($R^2$ = 0.77) it provided a proxy metric of productivity for this grassland ecosystem (Table 3.1).

Table 3.1 Equations derived from field calibration and subsequently used to map green biomass and NEE using airborne NDVI. *P* values < 0.01 for both relationships.

| | $R^2$ |
|---|---|
| NEE = −0.0226 × proxy NDVI + 1.3899 | 0.7701 |
| Green biomass = 409.82 × NDVI − 80.57 | 0.8246 |

### 3.2.7 Sensitivity Analysis of Footprint

To help understand the area sampled for $CO_2$ exchange and its influence on the LUE model, flux footprints were calculated for each valid 30 minute period using a parameterization of a Lagrangian stochastic model as described in (Kljun et al. 2004). We ran the footprint model using a fixed boundary layer depth of 1000 m and roughness length and displacement height values derived from canopy height estimates. The cross-wind integrated footprints were summed up into a time-integrated footprint matrix according to wind direction. Aggregation was done in two ways: on a monthly basis at 5

h midday intervals (11:00–16:00) and intervals comprising the entire daytime period (6:00–21:00).

To help design an effective data integration scheme, a sensitivity analysis of the footprint was conducted with the airborne image. We resampled the footprint to the same size (1 × 1 meter) of the airborne image pixel and calculated $NDVI_{weighted}$ according to the footprint using the following equation.

$$NDVI_{weighted} = \sum_{i=1}^{N} NDVI_i * w_i \quad (3.8)$$

N was the total pixel number, $w_i$ was the decimal percent concentration of each grid cell to the cumulative footprint function values that summed up to 1.

To evaluate the sensitivity of the study results to footprint assumptions when comparing optical to flux data, four weighted NDVI results were calculated according to different footprint configurations: (1) midday average footprint calculated using the sampling area calculated from the footprint model; (2) daytime average footprint calculated using the sampling area calculated from the footprint model; (3) 200-m radius circles centered at flux towers; and (4) a 300 × 300 m squares centered on each flux tower; and (5) the 100 × 100 m (1-ha) ground sampling region. The latter three footprints allowed us to consider the possible error associated with arbitrary assumptions of footprint shape on upscaling in the absence of an explicit flux footprint model. The radius (200 m) was calculated based on the assumption of a 100:1 fetch-to-height ratio in flux footprint analysis for simple calculation (Garratt 1990, Leclerc and Thurtell 1990), and the 300 × 300 meter represented a square approximation of the same region, whereas the modeled footprints represented a more realistic sampling footprint depictions based on actual flux data (Figure 3.3).

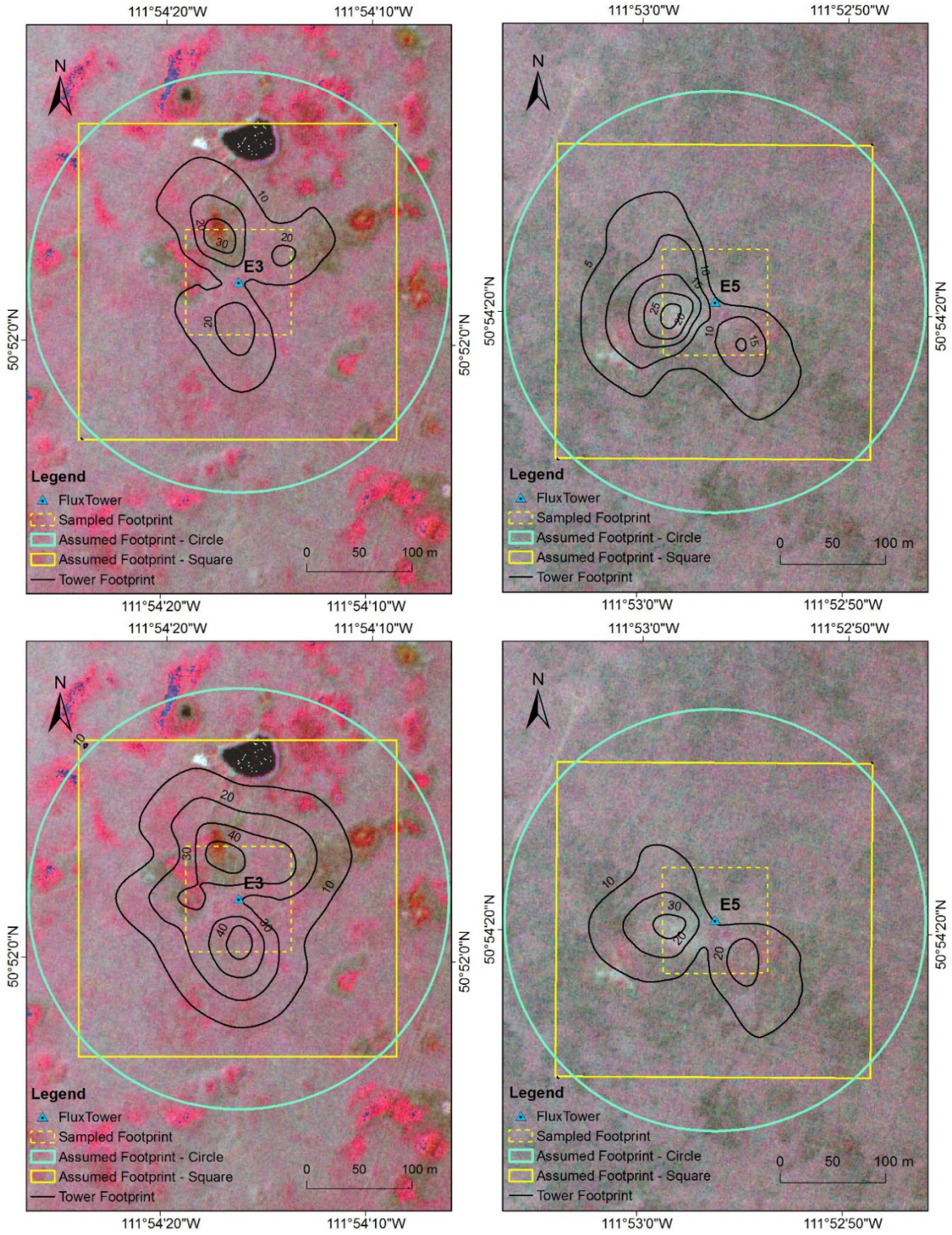


Figure 3.3 Footprints for two flux tower calibration sites (E3 and E5) at Mattheis Ranch in August, 2012 (see "Methods" for details on footprint calculations). Left: Midday (upper) and daytime (lower) flux footprints (black lines) at E3. Right: Midday (upper)

and daytime (lower) flux footprints (black lines) at E5. Also shown for comparison are a square (100 × 100 m) field sampling region used for field biomass and reflectance calibration, and two alternate footprint assumptions: a circular area (200 m radius), and a 300 × 300m square. Sampling methods were overlaid on a false color image from the airborne imaging spectrometer.

### 3.2.8 Vegetation Map Analysis

The vegetation map analysis used a dominant vegetation cover map (1:15,000) at Mattheis Research ranch (Becker 2013). This map was derived from a combination of aerial photos and field sampling begun in 2010 (Becker 2013). For validation of this dominant vegetation cover map, 134 5 × 5 meter plots were selected in the ranch, 66 of which were inventoried by species and percent cover of each species, while only species richness was counted for the other 68 plots (Becker 2013). An inherent assumption of our analysis was that dominant vegetation cover was stable over this study period.

### 3.2.9 Biodiversity Estimation

Biodiversity was evaluated three ways: (1) via optical diversity expressed in the airborne imagery; (2) using the vegetation map depicting vegetation types by dominant species (the vegetation types are shown in Figure S3.1 and Table S3.1 in Appendices); and (3) by independent field measurements of species composition for a subset of two of the calibration sites (E3 and E5) (Figure 3.2). For the first two methods, we used 50 randomly placed circular sampling areas, each having a 200 meters radius, along the flight line (Figure 3.1). Mean reflectance, standard deviation and coefficient of variation of all wavelengths and pixels for each circle were calculated. To provide a metric of optical diversity, we used the average coefficient of variation (CV), calculated as the average CV for all wavelengths from 400 nm to 800 nm (Equation 3.7).

$$\mathrm{CV}_{circle} = \frac{\sum_{\lambda=400}^{800}\left(\frac{std(\rho_\lambda)}{mean(\rho_\lambda)}\right)}{number\ of\ bands} \tag{3.9}$$

In Equation (3.7), $\rho\lambda$ is the reflectance at wavelength $\lambda$, *std*($\rho\lambda$) and *mean* ($\rho\lambda$) are the standard deviation and mean value of reflectance at wavelength $\lambda$ across all the pixels in one circle, respectively. This metric of optical diversity was applied to each of the 50

randomly distributed sampling circles to compare to productivity estimated from the LUE model, as well as to the entire flight line, using a "moving-window" method, to develop an optical diversity map of the entire region. For the moving-window method, we applied a 10-m lag and calculated the CV for both a circular sampling window (200 m radius) and a square sampling window (1 ha), to illustrate the effect of sampling scale on the resulting optical diversity image.

We calculated the number of vegetation types (richness) and Shannon Index of vegetation types (Shannon Index) (Shannon 1948) within each of 50 sampling circles as two metrics of diversity from the vegetation map. Shannon index, which combines the effect of richness and evenness, a commonly used measure of species diversity in ecology, was calculated as:

$$H = -\sum p_i \times \ln(p_i) \quad (3.10)$$

where $p_i$ is the proportion of the number *ith* species. Because this map listed vegetation types according to dominant species (and not all species *per se*), this provided a metric of relative plant species richness by broad community association for each pixel, instead of a full accounting of every species present, which was impractical over such a large region. To confirm that this method correlated with a more complete count of species richness, we also compared the results obtained from the vegetation maps to actual species counts obtained at the two calibration sites in 2015 (assuming a relatively stable species composition between years). Actual species counts were obtained with a subsample of 13 30-cm diameter plots, chosen from a grid covering 1 ha per site.

## 3.3 Results

### 3.3.1 Model Results

In our study, narrow-band NDVI yielded a high correlation with green biomass and NEE (Table 3.1), confirming that NDVI provided a useful metric of productivity for this prairie ecosystem. NDVI correlated better with green biomass than with total biomass (data not shown) due to the presence of the prior year's dead or non-green canopy materials, which intercepted solar radiation but contributed little to NDVI.

The relationship between proxy NDVI and net $CO_2$ flux showed an optimal fit using a 5-h aggregation period around solar noon (data not shown), so this aggregation period was used to develop the NEE model applied here (Table 3.1). The NDVI-flux relationship from the first half season data (greening phase, before peak biomass) was different from the second half season (July–September senescence phase, after peak biomass) (data not shown). Considering the airborne data was collected in mid-August, which was located around the middle of the July–September senescence phase, data from this second half were used to calibrate the linear model, which yielded an $R^2$ value of 0.7701 (Table 3.1). The linear shape of this equation supports the assumption of a constant LUE applied over this time frame for this prairie ecosystem (Gamon et al. 1995, Flanagan et al. 2015) and allowed us to use NDVI as an index of productivity.

### 3.3.2 Sensitivity Analysis of Footprint

The footprint analysis (Figure 3.3) revealed subtle differences between footprint assumptions that had a relatively small effect on the productivity model. In most cases, the primary source areas for flux measurements were concentrated on wind directions from north–northwest and south for E3 and northwest and southeast for E5. The estimated footprint lengths peaked most frequently between 15 m and 60 m and did generally not exceed 125 m in the along-wind direction.

The footprint sensitivity analysis showed that $NDVI_{weighted}$ was less sensitive to the month of footprint (data not shown) than to the differences between the two sites. On the other hand, assumptions about footprint size and shape (commonly used in multi-scale analyses) had a slightly larger effect on the calculated NDVI than the temporal variation in flux footprint (Table 3.2). For example, the 1 hectare measurements matching the calibration site areas overestimated the result compared to the modeled footprint analysis by 4% at the E3 site. Two alternative methods of estimating the footprint (200 radius circles and 300 × 300 m squares) overestimated the weighted NDVI calculated using the actual percentages of the isopleths at the E5 site (by 2% and 1.7% respectively), but the difference was small at the E3 site (0.6% and −0.9%) (Table 3.2). Regardless of the method, E3 had a higher NDVI than E5, showing this site to be more productive.

Table 3.2 Estimated $NDVI_{weighted}$ according to different footprint assumptions. Footprint areas are illustrated in Figure 3.3.

| | E3 | E5 |
|---|---|---|
| 1 hectare square | 0.4931 | 0.3715 |
| 200 meter circle | 0.4746 | 0.3823 |
| 300 m × 300 m Square | 0.4668 | 0.3812 |
| Midday (5 h) | 0.4714 | 0.3745 |
| Monthly | 0.4732 | 0.3771 |

### 3.3.3 Diversity Estimation at Calibration Sites

To evaluate optical diversity, we calculated the coefficient of variation (CV) using spectral data from both calibration sites, E3 and E5 (Figure 3.4). Site E3 revealed a higher overall CV than E5, indicating a higher optical diversity for this site. Similarly, we calculated the CV spectra for each 200-m radius sampling circle indicated in Figure 3.1, and representative values of high and low optical diversity (CV) are shown from this analysis (Figure 3.4). For subsequent analyses, CV values for each spectrum were averaged across all wavelengths to obtain a single metric of optical diversity for each sampling area.

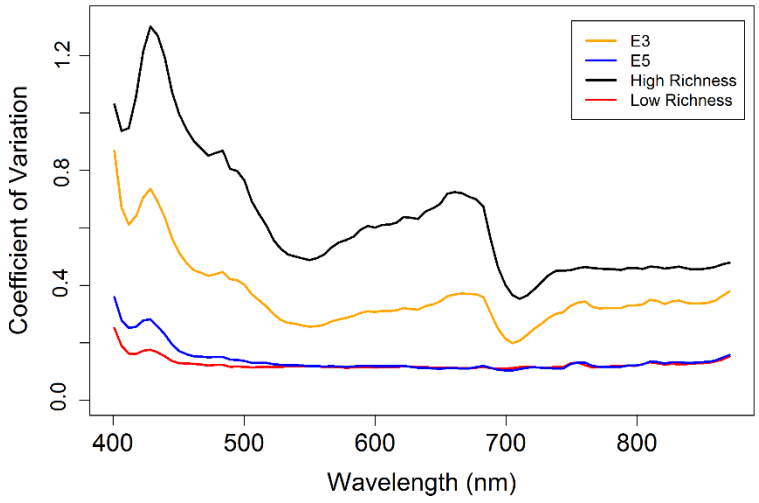


Figure 3.4 Sample coefficient of variation (CV) spectra along the flight line. E3 and E5 indicate the CV spectra of the 200-m radius circle around the two calibration sites. High

and low richness spectra indicate the site with highest and lowest CV values of all the 50 200-m radius circles along the flight line (Figure 3.1). The positions of low and high richness sites are shown in Figure 3.5. The average CV (averaged across wavelengths) provided a metric of optical diversity for subsequent comparison with other metrics of diversity and productivity (Figures 3.6 and 3.7).

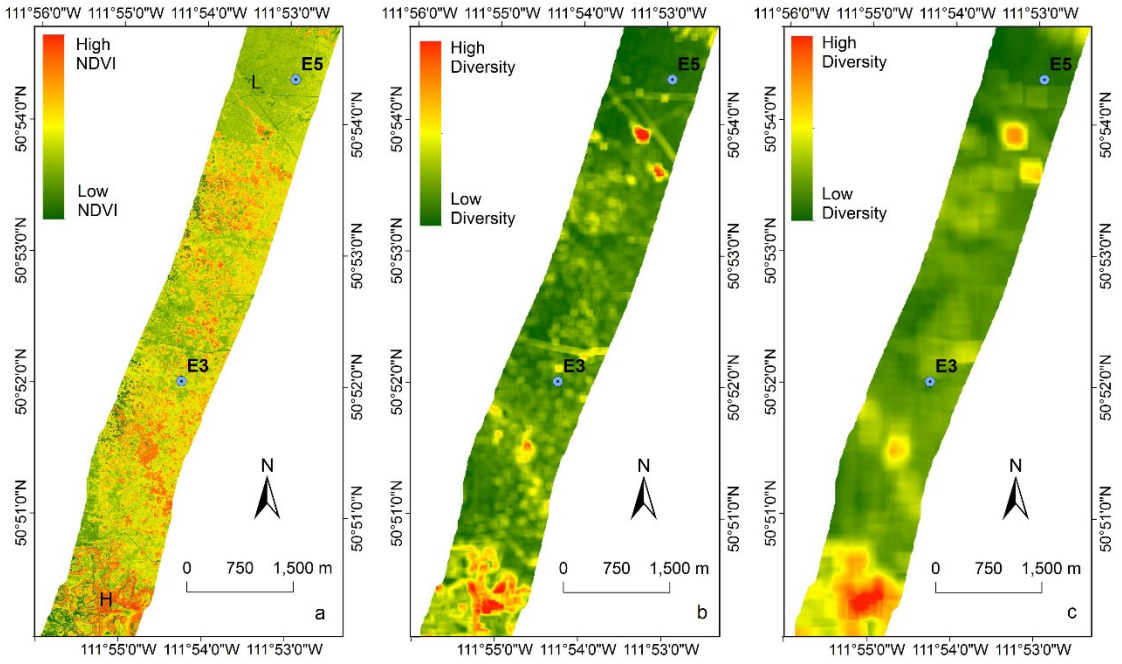


Figure 3.5 Airborne image of NDVI (**a**) and optical diversity (b and c) along the flight line. The letters "H" and "L" in the flight line (a) indicate the position of high and low diversity sites illustrated in Figure 3.4. Calibration sites E3 and E5 are also shown. Since NDVI was linearly related to biomass and NEE, the NDVI maps also indicate relative productivity according to those metrics (Table 3.1). Two different sampling scales, a 1-ha square (**b**) and a 200m circle (**c**), were selected for calculating CV as a metric of optical diversity using a sampling lag of 10 meters.

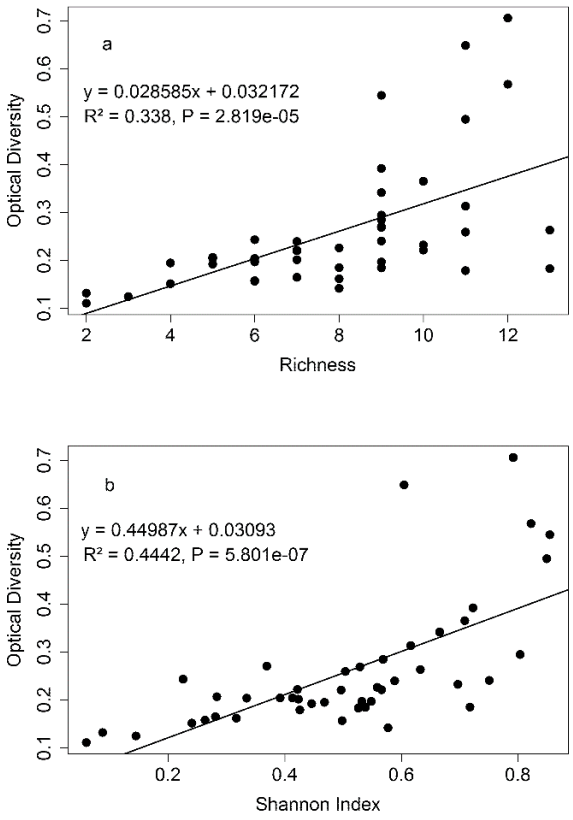


Figure 3.6 Optical diversity (coefficient of variation) *versus* richness (**a**) and Shannon index (**b**) calculated with the vegetation cover map. Richness represents number of dominant vegetation types indicated on the vegetation cover map (the vegetation types are shown in Figure S3.1 and Table S3.1 in Appendices) rather than a full field count of all species. Each data point represents a 200-m radius circular sampling area (Figure 3.1).

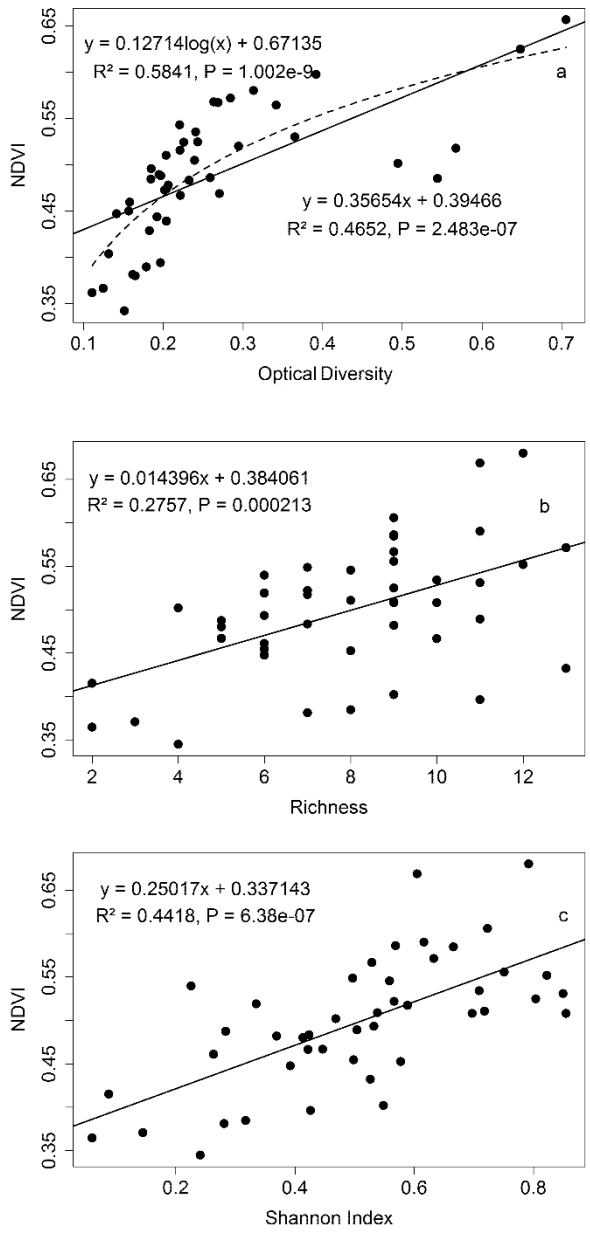


Figure 3.7 Optical diversity (coefficient of variation) *versus* NDVI (**a**), Mean NDVI *versus* relative richness (**b**) and Shannon Index (**c**). Both linear and logarithmic fits are shown for panel (**a**). Each data point represents a 200-m radius circular sampling area (Figure 3.1)

The vegetation diversity analysis revealed differences between the two sites. Tables 3.2 and 3.3 showed the NDVI, vegetation community richness, Shannon index, and field

sampling species richness at the two calibration sites (E3 and E5). Species counts from a subset of plots at the two primary calibration sites (E3 and E5) supported this interpretation of biodiversity based on vegetation types; the relative relationship for species richness between the two sites obtained with field sampling matched that of the vegetation map, with higher species richness occurring at the E3 site (Table 3.3). Similarly, both the mean NDVI and standard deviation of NDVI were higher at the E3 site than at the E5 site, indicating higher productivity and variability in biomass.

Table 3.3 Biodiversity metrics within a 200-m radius from the flux towers. Richness refers to the number of dominant vegetation types sampled within this 200-m radius based on the vegetation map, and the Shannon Index considered both number and evenness of these vegetation types. Field sampling species richness is based on an actual plant species count of a subset of locations (thirteen 30-cm diameter plots) within a 1-ha area surrounding the flux towers, as shown in Figure 3.

| Site | Richness (Vegetation Map) | Shannon Index (Vegetation Map) | Species Richness (Field Sampling) |
|---|---|---|---|
| E3 | 9 | 0.9060 | 26 |
| E5 | 3 | 0.1547 | 20 |

### 3.3.4 Extrapolating to a Larger Region

Using data from a larger region (10 $km^2$) of the flight line allowed us to extend the analysis and explore the diversity-productivity relationship over a much larger area. Over the whole flight line, places with higher optical diversity (higher coefficient of variation) tended to have higher mean NDVI, indicating higher green biomass and productivity (Figure 3.5). The clarity of the diversity images varied with sampling scale, with smaller sampling areas (1-ha square, panel b) providing a sharper image than coarser sampling areas (200-m radius circle, panel c), but both showed similar spatial patterns of optical diversity.

From the analysis of the entire flight line, diversity metrics calculated using the 200-m radius sampling circles (Figure 3.1) applied to the vegetation cover map showed that places with higher richness or Shannon index had higher optical diversity, expressed as coefficient of variation (Figure 3.6), and higher NDVI (Figure 3.7). The Shannon index showed a stronger correlation with both coefficient of variation and NDVI than with

richness in our study (Figures 3.6 and 3.7), suggesting an important influence of evenness on these relationships. The fit of the regression for the NDVI-optical diversity relationship can be improved ($R^2$ increased from 0.46 to 0.58) by applying a logarithmic transformation to the optical diversity data (Figure 3.7a). In all cases, the relationships between diversity metrics (coefficient of variation, relative richness, or Shannon index) and productivity (NDVI) were highly significant ($p < 0.001$), supporting a positive relationship between productivity and biodiversity for this prairie landscape.

## 3.4 Discussion

### 3.4.1 Green Biomass and NDVI

Like other studies of grasslands (Gamon et al. 1995, Flanagan et al. 2015) we found significant correlations between NDVI and biomass. In our study, green biomass showed a clear linear, not exponential, relationship with NDVI, which at first glance seems to contradict results from other grassland studies that have often reported non-linear relationships (Gamon et al. 1995, Wehlage 2012). However, this difference was most likely due to the relatively low green biomass values found in our study. The highest green biomass measured in our study was 135.75 $g/m^2$, which was a small fraction (2%) of the reported biomass from one study spanning several vegetation types (Gamon et al. 1995) and 1/3 of the maximum green biomass of another study from Alberta prairie that included a relatively wet year (Wehlage 2012). The lower green biomass measurement in our study only captured the lower part of the exponential relationship between NDVI and green biomass, which may have appeared linear by missing the rapidly increasing part of what has been described as an exponential function (Gamon et al. 1995). Presumably, if our study spanned many sites and years having higher productivity, a similar non-linear relationship would have emerged between green biomass and NDVI.

### 3.4.2 Sensitivity Analysis of Footprint

The actual flux footprint varied temporally with wind speed and direction, in agreement with previous studies (Schmid 2002). The exact position of the flux tower or other ground sampling is not an issue when the surface is homogeneous (Schmid 2002). In our study, the footprint area was larger than 1 ha and there was little difference in aggregated NDVI between the circular and square footprint estimates (200 m radius and 300 × 300

$m^2$) that were insensitive to atmospheric conditions and the aggregated half hourly footprint model predictions. The footprint analysis allowed us to evaluate potential upscaling errors, and confirmed that, in this case, other approximations of the footprint (e.g., circular or square areas surrounding the flux tower) provide reasonably accurate approximations of the actual flux footprint over a relatively flat and uniform landscape such as the grassland at our site. By contrast, the difference in NDVI values between sites were closer to 20% (Table 3.2) suggesting that our upscaling method can accurately depict relative differences in productivity across this landscape. These results indicate that, depending upon the degree of landscape heterogeneity, the highly dynamic footprint of eddy covariance measurements (Schmid 2002) can add uncertainty to the calibration, but that any resulting error would have been small for this relatively homogenous site.

### 3.4.3 Biodiversity—Ecosystem Function

Productivity represents one of the most important ecosystem metrics, and the species richness-productivity relationship has long been of interest in ecology (Tilman et al. 1996, Tilman 1997). Although productivity cannot assess biodiversity directly, it integrates other major drivers of biodiversity that can include land use, climate, nitrogen decomposition, biotic change and increasing atmospheric $CO_2$ (Sala et al. 2000). Other prairie studies from the US have shown that high biodiversity plots tend to have higher biomass (Isbell et al. 2011), and our results are consistent with this finding. On the other hand, a recent study of 30 grassland sites around the world (19 countries and 6 continents, including samples from this landscape) suggests that the global diversity-productivity relationship may be more "hump-shaped", particularly when intensively managed ecosystems are included (Fraser et al. 2015). This decline in diversity at high productivity was not seen in our study, and may reflect the greater input of water or nutrients and other management practices associated with many highly managed ecosystems. Compared to many other grassland sites, our study site was a low-productivity grassland. The airborne data offered a means of evaluating the productivity–diversity relationships over a much larger area of this natural prairie ecosystem than would be feasible from the ground, and provided an objective means to address the biodiversity–productivity relationship over large landscapes.

The NDVI–diversity relationship can change through time and be affected by environmental variables and phenology. Cool-season grasses usually dominate the productivity in the early season. Both cool-season and warm-season grasses affect the productivity in the peak season (August) but can be easily influenced by precipitation in summer (Bork and Irving 2015). In our study, NDVI was strongly associated with green biomass, which related to diversity, but it can be influenced by other factors, e.g., canopy growth stage, water stress and flowering patterns. A full evaluation of the seasonal effects on the NDVI-diversity relationship was beyond the scope of this study. However, in a parallel study of a manipulated prairie ecosystem, Wang *et al.* (Wang et al. 2016b) explored the dynamics of the NDVI–diversity relationship over a full growing season and found that the optimal NDVI–productivity relationship occurred in early August, similar to the time of the overflight in this study.

"Optical diversity", which indicates the variation in optical signals detected by remote sensing, has been proposed to relate to more conventional metrics of biodiversity (Gamon 2008). Instead of mapping species *per se*, optical diversity presumably detects different functional and structural properties, which vary with species or functional groups ("optical types") (Gamon 2008, Ustin and Gamon 2010). This spectral heterogeneity has been related to variation of species or optical types of forests (Rocchini et al. 2010, Féret and Asner 2014). In our study, the coefficient of variation was applied as a metric of optical diversity based on information content present in the reflectance spectra themselves, and expressed as the coefficient of variation of reflectance calculated over many pixels. This optical diversity metric showed significant correlations with conventional species diversity indices (richness and Shannon index) (Figure 3.6), suggesting that optical diversity metrics from airborne remote sensing can provide useful diversity metrics over large regions. This method, based on a statistical assessment of spectral variability, does not directly identify the cause of the strong links with productivity and other diversity metrics. However, it does provide an objective method that can be readily applied to remotely sensed imagery.

The surrogacy hypothesis is sometimes invoked to relate species richness in one taxon, or diversity at one level, to diversity at another level (Magurran 2004). For example, high

genetic richness is related to high species richness and environmental heterogeneity is related to species richness. Similarly, in this study, we used the number of vegetation types by dominant species as a surrogate for species richness by assuming species richness will be higher in places with more vegetation types. Our current working hypothesis is that optical diversity is influenced by both leaf traits and canopy structure, as further influenced by the seasonal expression of these leaf and canopy features (Ustin and Gamon 2010). Because leaf traits and canopy structure vary between species, optical diversity can provide a surrogate (or proxy metric) for traditional metrics based on species richness and evenness. Both optical diversity and species diversity can be influenced by environmental heterogeneity, such as soil texture and microtopographic variability. In our study, subtle gradients in soil and microtopography could have affected the pattern of diversity across the landscape. Fully understanding the mechanisms underlying the optical diversity–biodiversity relationship should be an objective of future work.

The positive NDVI – diversity relationship (Figure 3.7) is consistent with another recent study using ground NDVI measurement assessing the biodiversity – productivity relationship with a manipulated prairie ecosystem (Cedar Creek Ecosystem Science Reserve, Minnesota, US) (Wang et al. 2016b). Together, these findings support the positive diversity–productivity hypothesis for these two prairie ecosystems, and are consistent with previous studies of prairies using more traditional field sampling methods (Tilman 1997, Isbell et al. 2011).

More work is needed on the scale-dependence of this method, as sampling scale clearly influences the resulting optical diversity patterns (Figure 3.5). The coefficient of variation is influenced by the spatial scale ("grain" or sampling size) that relates to the actual vegetation distribution. In our study, we used different sampling scales both in our footprint analysis (Figure 3.3) and in our depiction of optical diversity (Figure 3.5). The results at two different scales showed a similar pattern of CV along the flight line (Figure 3.5). However, it is not yet clear how to decide the "best" scale that balances a large sampling region with the need for fine spatial detail. Multi-scale analysis is needed to

investigate the correlation between optical diversity and biodiversity, and remote sensing provides one tool for such an investigation.

Both species richness and evenness influence ecosystem services and the optical diversity metrics measured here. Recent studies have shown that both species richness and evenness have positive effects on the diversity – productivity relationship in ecosystems (Nijs and Roy 2000, Wilsey and Potvin 2000, Kirwan et al. 2007). In accordance with another recent study (Oldeland et al. 2010), our measure of optical diversity showed a better correlation with the Shannon index than richness *per se*, suggesting that vegetation evenness (or heterogeneity) influences both optical diversity and the productivity patterns detected by NDVI. Adding evenness can add additional information on community structure, which can apparently affect the variance of the optical signal beyond the effects of species richness alone. Further work is needed to explore the exact impact of richness and evenness on the optical signals detected by spectral reflectance. Similarly, more study is needed to understand the relative importance of factors influencing optical diversity that may include canopy structure, leaf traits, and phenology (Ustin and Gamon 2010).

This study demonstrates a method for integrated analysis of productivity and diversity using a combination of airborne, field sampling and flux measurements. Integrating flux measurements and remote sensing with the LUE model provides a method for assessing ecosystem health and productivity in continuous temporal and spatial dimensions. This can also be a useful approach for evaluating both biodiversity and carbon uptake together, and thus for assessing overall ecosystem health via the provision of goods and services. Airborne campaigns can acquire surface reflectance measurements over large areas without disrupting the flux footprint and can assess ecosystem status over large areas at high spatial resolution. Additionally, airborne imagery can provide help in selecting the ideal position of the flux station to best represent the target ecosystem. However, obtaining high frequency time series of airborne data is still a challenge, largely due to the high cost of airborne acquisition (which can easily run $20–$30K per field campaign). However, these high costs are largely due to the fixed costs of maintaining an aircraft, pilot and flight team over a period of several days. Such costs could be greatly lowered to

end users through subsidizing flight costs or through “volume pricing” if groups of users could share the cost of data acquisition, much in the way that satellite imagery can be provided for “free” or at low cost by volume pricing or via government or corporate support. The Google model of providing “free” global imagery to all via Google Earth, and NASA’s provision of satellite data through the Earth Observing System (EOS) are both examples of cost-effective business models for remote sensing.

### 3.5 Conclusions

Remote sensing provides an efficient approach to estimating prairie production and biodiversity over large regions. Differences of biomass and ecosystem production across a 10-km prairie transect were shown clearly with airborne images. Regardless of the diversity method used, higher biodiversity areas tended to have higher production, in this grassland ecosystem. These relationships were sensitive to both richness and evenness, and the addition of evenness improved the relationship with remotely sensed optical diversity, assessed as the coefficient of variation of reflectance. We propose that optical diversity provides a potent proxy for other more traditional biodiversity metrics (richness and Shannon index). Further work is needed to further understand the proximal drivers and scale-dependence (spectrally, spatially and temporally) of the biodiversity–optical diversity relationships.

This study demonstrates the benefit of coupling traditional field sampling, eddy covariance footprint analysis and airborne remote sensing to estimate rangeland productivity and biodiversity. The CV provides a simple, objective metric of optical diversity that is significantly correlated with other traditional diversity metrics. However, like other commonly used indices in remote sensing of biodiversity studies, we currently lack a full mechanistic understanding of the optical diversity–biodiversity relationship. Future work could also include more extensive airborne campaigns coupled with continuous satellite observation, along with more detailed field studies to detect changing prairie ecosystem function and composition over larger areas and longer time series. At the same time, experimental approaches employing remote sensing methods at multiple spatial, spectral and temporal scales, and across additional ecosystems, are also needed to test the general applicability of the findings reported here. Such experiments are key to

developing a defensible operational approach for wide application in prairies for the purpose of assessing rangeland health, production, biodiversity and carbon sequestration.

**Acknowledgments**:
We thank David Stonehouse and Verimap for help with the airborne acquisition, Adrienne Tastad, Ellen Macdonald and Lori Schroeder for providing information regarding the Mattheis Research Ranch land cover and soil map, and Ed Bork for information on grazing and management regimes. Evan Delancey provided help in using geo-referencing code for airborne data. Chris Wong, Shayna Harris, Saulo Castro, and Kyle Springer provided field assistance. This work was supported by iCORE, AITF, Rangeland Research Institute, CFI, and NSERC funding to J.A.G., and China Scholarship Council fellowship to R.W. We are grateful to Edwin and Ruth Mattheis for providing the University of Alberta with the Mattheis Ranch to support long-term research.

### 3.6 References

Adams, B. W. et al. 2013. Range plant communities and range health assessment guidelines for the dry mixedgrass natural subregion of Alberta.

Becker, S. 2013. Mattheis Ranch Vegetation and Soil Inventory.

Bernhardt-Römermann, M. et al. 2011. Explaining grassland biomass - the contribution of climate, species and functional diversity depends on fertilization and mowing frequency. - J. Appl. Ecol. 48: 1088–1097.

Booth, D. T. and Tueller, P. T. 2003. Rangeland monitoring using remote sensing. - Arid L. Res. Manag. 17: 455–467.

Bork, E. W. and Irving, B. D. 2015. Seasonal availability of cool- and warm-season herbage in the northern mixed prairie. - Rangelands 37: 178–185.

Bork, E. W. et al. 1999. Rangeland cover component quantification using broad (TM) and narrow-band (1.4 NM) spectrometry. - J. Range Manag. 52: 249–257.

Boundary Files, 2011 Census. Statistics Canada. 2011, Catalogue no. 92-16-X.

Clark, M. L. and Roberts, D. A. 2012. Species-level differences in hyperspectral metrics among tropical rainforest trees as determined by a tree-based classifier. - Remote Sens. 4: 1820–1855.

Clark, D. A. et al. 2001. Measuring net primary production in forest : concepts and field methods. - Ecol. Appl. 11: 356–370.

Clark, M. L. et al. 2005. Hyperspectral discrimination of tropical rain forest tree species at leaf to crown scales. - Remote Sens. Environ. 96: 375–398.

Conel, J. E. et al. 1987. AIS-2 radiometry and a comparison of methods for the recovery of ground reflectance. - Proc. 3rd Airborne Imaging Spectrom. Data Anal. Work. shopJPL Publ. 87–30

Connell, J. H. 1978. Diversity in Tropical Rain Forests and Coral Reefs. - Science. 199: 1302–1310.

Damm, A. et al. 2011. Modeling the impact of spectral sensor configurations on the FLD retrieval accuracy of sun-induced chlorophyll fluorescence. - Remote Sens. Environ. 115: 1882–1892.

de Mazancourt, C. et al. 2013. Predicting ecosystem stability from community composition and biodiversity. - Ecol. Lett. 16: 617–625.

DeFries, R. S. and Townshend, J. R. G. 1994. NDVI-derived land cover classifications at a global scale. - Int. J. Remote Sens. 15: 3567–3586.

Féret, J.-B. and Asner, G. P. 2014. Mapping tropical forest canopy diversity using high-fidelity imaging spectroscopy. - Ecol. Appl. 24: 1289–1296.

Flanagan, L. B. et al. 2015. Application of the photosynthetic light-use efficiency model in a northern Great Plains grassland. - Remote Sens. Environ. 168: 239–251.

Fraser, L. H. et al. 2015. Worldwide evidence of a unimodal relationship between productivity and plant species richness. - Science. 349: 302–306.

Gamon, J. A. 2008. Tropical sensing — opportunities and challenges. - In: M, K. and GA, S.-A. (eds), Hyperspectral remote sensing of tropical and subtropical forests. CRC Press Taylor&Francis Group, pp. 297–304.

Gamon, J. A. et al. 1993. Functional patterns in an annual grassland during an AVIRIS overflight *. - Remote Sens. Environ. 44: 239–253.

Gamon, J. A. et al. 1995. Relationships between NDVI, canopy structure, and photosynthesis in three californian vegetation types. - Ecol. Appl. 5: 28–41.

Gamon, J. A. et al. 2006. A mobile tram system for systematic sampling of ecosystem optical properties. - Remote Sens. Environ. 103: 246–254.

Gamon, J. A. et al. 2010. SpecNet revisited: Bridging flux and remote sensing communities. - Can. J. Remote Sens. 36: S376–S390.

Garratt, J. R. 1990. The internal boundary layer - A review. - Boundary-Layer Meteorol. 50: 171–203.

Gitelson, A. A. and Gamon, J. A. 2015. The need for a common basis for defining light-use efficiency: Implications for productivity estimation. - Remote Sens. Environ. 156: 196–201.

Grime, J. P. 1973. Competitive exclusion in herbaceous vegetation. - Nature 242: 344–347.

Hill, M. J. 2013. Vegetation index suites as indicators of vegetation state in grassland and savanna: An analysis with simulated SENTINEL 2 data for a North American transect. - Remote Sens. Environ. 137: 94–111.

Huemmrich, K. F. et al. 1999. High temporal resolution NDVI phenology from micrometeorological radiation sensors. - J. Geophys. Res. 104: 27935.

Hunt, E. R. et al. 2003. Applications and research using remote sensing for rangeland management. - Photogramm. Eng. Remote Sens. 69: 675–693.

Isbell, F. I. et al. 2009. Biodiversity, productivity and the temporal stability of productivity: Patterns and processes. - Ecol. Lett. 12: 443–451.

Isbell, F. et al. 2011. High plant diversity is needed to maintain ecosystem services. - Nature 477: 199–202.

Kirwan, L. et al. 2007. Evenness drives consistent diversity effects in intensive grassland systems across 28 European sites. - J. Ecol. 95: 530–539.

Kljun, N. et al. 2004. A simple parameterisation for flux footprint predictions. - Boundary-Layer Meteorol. 112: 503–523.

Leclerc, M. Y. and Thurtell, G. W. 1990. Footprint prediction of scalar fluxes using a markovian analysis. - Boundary-Layer Meteorol. 52: 247–258.

Lucas, R. et al. 2008. Classification of Australian forest communities using aerial photography, CASI and HyMap data. - Remote Sens. Environ. 112: 2088–2103.

Magurran, A. E. 2004. Measuring biological diversity. - Blackwell Publishing.

Monteith, J. L. 1972. Solar radition and productivity in tropical ecosystems. - J. Appl. Ecol. 9: 747–766.

Monteith, J. L. and Moss, C. J. 1977. Climate and the efficiency of crop production in Britain. - Philos. T. Roy. Soc. B 281: 277–294.

Nijs, I. and Roy, J. 2000. How important are species richness, species evenness and interspecific differences to productivity? A mathematical model. - Oikos 88: 57–66.

Oldeland, J. et al. 2010. Does using species abundance data improve estimates of species diversity from remotely sensed spectral heterogeneity? - Ecol. Indic. 10: 390–396.

Palmer, M. W. et al. 2002. Quantitative tools for perfecting species lists. - Environmetrics 13: 121–137.

Piñeiro, G. et al. 2006. Seasonal variation in aboveground production and radiation-use efficiency of temperate rangelands estimated through remote sensing. - Ecosystems 9: 357–373.

Pottier, J. et al. 2014. Modelling plant species distribution in alpine grasslands using airborne imaging spectroscopy. - Biol. Lett. 10: 1–4.

Roberts, D. A. et al. 1998. Mapping chaparral in the Santa Monica mountains using multiple endmember spectral mixture models. - Remote Sens. Environ. 65: 267–279.

Rocchini, D. 2007. Effects of spatial and spectral resolution in estimating ecosystem α-diversity by satellite imagery. - Remote Sens. Environ. 111: 423–434.

Rocchini, D. et al. 2004. Testing the spectral variation hypothesis by using satellite multispectral images. - Acta Oecologica 26: 117–120.

Rocchini, D. et al. 2010. Remotely sensed spectral heterogeneity as a proxy of species diversity: Recent advances and open challenges. - Ecol. Inform. 5: 318–329.

Sala, O. E. et al. 1996. Biodiversity and ecosystem functioning in grasslands. - In: Mooney, H. A. et al. (eds), Functional Roles of Biodiversity: A Global Perspective. John Wiley and Sons Ltd, pp. 129–149.

Sala, O. E. et al. 2000. Global biodiversity scenarios for the year 2100. - Science. 287: 1770–1774.

Schmid, H. P. 2002. Footprint modeling for vegetation atmosphere exchange studies : a review and perspective. - Agric. For. Meteorol. 113: 159–183.

Shannon, C. E. 1948. A mathematical theory of communication. - Bell Syst. Tech. J. 27: 379–423, 623–656.

Sims, P. L. and Risser, P. G. 2000. Grasslands. - In: Barbour, M. G. and Billings, W. D. (eds), Northern American Terrestrial Vegetation. 2nd ed.n. Cambridge University Press, pp. 323–356.

Tilman, D. 1997. The influence of functional diversity and composition on ecosystem processes. - Science. 277: 1300–1302.

Tilman, D. et al. 1996. Productivity and sustainability influenced by biodiversity in grassland ecosystems. - Nature 379: 718–720.

Tucker, C. J. et al. 1985. African land-cover classification using satellite data. - Science. 227: 369–375.

Ustin, S. L. and Gamon, J. A. 2010. Remote sensing of plant functional types. - New Phytol. 186: 795–816.

Wang, R. et al. 2016. Seasonal variation in the NDVI–species richness relationship in a prairie grassland experiment (Cedar Creek). - Remote Sens. 8: 128.

Wehlage, D. C. 2012. Monitoring year-to-year variability in dry mixed-grass prairie yield using multi-sensor remote sensing.

Wilsey, B. J. and Potvin, C. 2000. Biodiversity and ecosystem functioning: importance of species evenness in an old field. - Ecology 81: 887–892.

Xiao, Q. et al. 2004. Using AVIRIS data and multiple-masking techniques to map urban forest tree species. - Int. J. Remote Sens. 25: 5637–5654.

Yuan, W. et al. 2007. Deriving a light use efficiency model from eddy covariance flux data for predicting daily gross primary production across biomes. - Agric. For. Meteorol. 143: 189–207.

# Chapter 4 The spatial sensitivity of the spectral diversity-biodiversity relationship: an experimental test in a prairie grassland


## Abstract

Remote sensing has been used to detect plant biodiversity in a range of ecosystems based on the varying spectral properties of different species or functional groups. However, the most appropriate spatial resolution necessary to detect diversity remains unclear. At coarse resolution, differences among spectral patterns may be too weak to detect. In contrast, at fine resolution, redundant information may be introduced. To explore the effect of spatial resolution, we studied the scale-dependence of spectral diversity in a prairie ecosystem experiment at Cedar Creek Ecosystem Science Reserve, Minnesota, USA. Our study involved a scaling exercise comparing synthetic pixels resampled from high-resolution images within manipulated diversity treatments. Hyperspectral data were collected using several instruments on both ground and airborne platforms. We used the coefficient of variation (CV) of spectral reflectance in space as the indicator of spectral diversity and then compared CV at different scales ranging from $1mm^2$ to $1m^2$ to conventional biodiversity metrics, including species richness, Shannon's Index, Simpson's Index, phylogenetic species variation, and phylogenetic species evenness. In this study, high species richness plots generally had higher CV. CV showed higher correlations with Shannon's index and Simpson's index than species richness alone, indicating evenness contributed to the spectral diversity. Correlations with species richness and Simpson's index were generally higher than with phylogenetic species variation and evenness measured at comparable spatial scales, indicating weaker relationships between spectral diversity and phylogenetic diversity metrics than with species diversity metrics. High resolution imaging spectrometer data ($1mm^2$ pixels) showed the highest sensitivity to diversity level. With decreasing spatial resolution, the difference in CV between diversity levels decreased and greatly reduced the optical detectability of biodiversity. The optimal pixel size for distinguishing α diversity in these prairie plots appeared to be around 1mm to 10cm, a spatial scale similar to the size of an individual herbaceous plant. These results indicate a strong scale-dependence of the

spectral diversity-biodiversity relationships, with spectral diversity best able to detect a combination of species richness and evenness, and more weakly detecting phylogenetic diversity. These findings can be used to guide airborne studies of biodiversity and develop more effective large-scale biodiversity sampling methods.

## 4.1 Introduction

Biodiversity loss, one of the most crucial challenges of our time, endangers ecosystem services that maintain human wellbeing (Magurran and Dornelas 2010). "Essential biodiversity variables" have been proposed by ecologists to monitor the variation of biodiversity globally (Pereira et al. 2013). Traditional methods of measuring biodiversity require extensive and costly field sampling by biologists with considerable experience in species identification, and the results may vary with sampling effort (Gotelli and Colwell 2001, Bonar et al. 2010). It is impossible to acquire sufficient information about changing species distributions through time from field campaigns alone (Heywood 1995). Remote sensing has the potential to detect plant biodiversity and can provide efficient and cost-effective means to determine plant and ecosystem diversity over large areas (Nagendra, 2001). Consistent and repeatable remote sensing measurement is critical to long term global biodiversity assessment (Turner, 2014).

Diversity can be defined by a large range of indices according to the scale of observation (Whittaker 1960, 1972). Alpha (α) diversity is diversity within a defined place or a habitat at a local scale, typically within a single circumscribed community or field plot; Beta (β) diversity describes the variation among habitats or communities; Gamma (γ) diversity is the total diversity of a large region (landscape, ecoregion or biome). Local-scale (α) diversity can be measured several ways (Gotelli and Colwell 2001, Magurran 2004). Species richness – number of species at a site - is the oldest and among the most widely used measure of α diversity. Unlike species richness, heterogeneity indices measure "evenness," or the apparent number of species taking abundance into account rather than simply the absolute number of species in a given area (Peet 1974). Some metrics (e.g. Simpson or Shannon Indices) combine elements of species richness and evenness into a single metric of α diversity (Peet 1974).

## Remote sensing of biodiversity

Recent technological advances in remote sensing, including imaging spectroscopy and LiDAR, can provide detailed spectral and structural information to characterize diversity (Asner 2013). An increasing number of studies applying airborne or satellite remote sensing in biodiversity assessment in different ecosystems, e.g. tropical rainforest (Asner et al. 2008, Sanchez-Azofeifa et al. 2009, Asner and Martin 2009, Féret and Asner 2014), prairie grassland (John et al. 2008, Wang et al. 2016a), island vascular plants (Lucas and Carter 2008), and arctic regions (Gould 2000). But there is still no single, universally accepted scale or method for remotely sensing biodiversity, and a wide variety of approaches to biodiversity assessment are used, along with multiple definitions of biodiversity (Rocchini 2007, Féret and Asner 2014, Dahlin 2016).

## Spectral diversity hypothesis

'Spectral diversity', sometimes called 'optical diversity' (Ustin and Gamon 2010), refers to variation in remote sensing measurements, typically spectral reflectance, across sets of pixels and has been proposed to relate to conventional metrics of biodiversity. Instead of mapping species *per se*, spectral diversity presumably detects functional and structural properties, which vary among species or functional groups ("optical types") (Gamon 2008, Ustin & Gamon 2010). According to the spectral diversity hypothesis, varying plant leaf traits, canopy structure and phenology can cause wavelength-dependent variations in optical signals (Ustin & Gamon 2010). Since leaf traits (Wright et al. 2004) and canopy structure (Field 1991, Díaz et al. 2015) reflect different evolutionary solutions to resource limitations, spectral diversity can detect different environmental adaptations or resource use strategies. If optical type is regarded as a fundamental vegetation property, resulting from "ecological rules" driven by resource allocation (Field 1991), there should be predictable relationships among plant traits and plant spectral properties.

Recent attempts to assess leaf and canopy functional properties through remote sensing illustrate the promise of optical approaches to biodiversity assessment. Airborne spectra have been successfully related to plant leaf chemical properties in tropical forests (Asner

and Martin 2009, Féret and Asner 2014). Moreover, particular leaf traits can affect canopy level architecture which can accentuate the leaf spectral properties through multiple scattering and contrasting illumination (Ollinger 2011). As a consequence, variation in leaf- and canopy-scale optical properties and their associated traits in time and space might enable us to detect functional diversity and also biodiversity at different scales.

Scale in ecology and remote sensing

Changing scale alters the perceived patterns of reality, thus changing our understanding of the dynamics of an environmental system (Marceau and Hay 1999). Here, we confine our discussion of scale to the spatial domain, and briefly recognize that other domains are also relevant. In ecology, the concept of scale defines the grain size and spatial extent at which a variety of ecological processes may occur in a landscape (Turner, Dale, & Gardner 1989). Scaling up (sampling at coarser scales) changes the level of observed organization and leads to information loss (O'Neill and King 1998). In remote sensing, spatial scale refers to the terms "resolution" (pixel size, determined by sensor technology and flight characteristics) and "spatial extent" (the total area measured). Scale can also relate to spectral scale, the wavelengths (spacing, bandwidth, and spectral range) of spectral bands as measured by a sensor (Marceau and Hay 1999, Rocchini 2007). In addition, temporal scale (frequency and timespan of observation) is important in both ecology and remote sensing, affecting our ability to detect the important processes at the appropriate times.

Meaningful scaling studies in remote sensing are challenging because most campaigns collect data at a single resolution and extent determined by the instrument and sampling platform. Similarly, most ecological sampling methods and the associated definitions are restricted to a particular spatial scale, usually determined by what is possible to sample in a field campaign. Although studies have evaluated sampling effects at large scales (several meters to hundreds meters) (Rocchini 2007, Oldeland et al. 2010), few, if any, experimental studies have been done to systematically explore the scale dependence of the spectral diversity-biodiversity relationship. Consequently we do not know the "correct" or "ideal" spatial scale for detecting a specific type of diversity (e.g. $\alpha$ or $\beta$

diversity, species richness or heterogeneity indices). In remote sensing, practical limitations (tradeoffs between sampling resolution and signal-to-noise) result in operational decisions that are largely based on engineering choices in the design of sensors, and these rarely consider the "optimal" design for a biological objective such as assessing biodiversity. The application of current (Turner et al. 2015) or future (Jetz et al. 2016) satellite data to global biodiversity conservation has been proposed, yet these studies lack a clear discussion of the appropriate or optimal spatial scales for this task. A meaningful evaluation and definition of scale is essential to implementing a biodiversity assessment campaign using remote sensing.

To address these issues, we studied the scale-dependence of spectral diversity in a prairie ecosystem experiment at Cedar Creek Ecosystem Science Reserve (CCESR), Minnesota, USA. We conducted a scaling experiment comparing airborne imagery with ground-based data collected along transects within manipulated plant diversity treatments. Hyperspectral data were collected using several instruments on both ground and airborne platforms, and ground-based images were resampled at several spatial scales to simulate progressively coarse pixel sizes. We used the coefficient of variation (CV) of spectral reflectance in space, which in this case means CV calculated across all pixels in a plot, as the indicator of spectral diversity. We then compared the spectral diversity measured at different scales (pixels) ranging from 1 $mm^2$ to 1 $m^2$ to various standard metrics of α diversity to investigate how those conventional diversity metrics relate to remote sensing and to explore the scale dependence of spectral diversity.

## 4.2 Methods

### 4.2.1 Field site and study design

This study was conducted within the BioDIV experiment at the Cedar Creek Ecosystem Science Reserve, Minnesota, US (45.4086° N, 93.2008° W). The BioDIV experiment has maintained 168 planted prairie plots (9 m × 9 m) since 1994 with species richness of vascular plants ranging from 1 to 16 (Tilman et al 1996, Mittelbach 2012). The species planted in each plot were originally randomly selected from a pool of 18 species typical of Midwestern prairie, including $C_3$ and $C_4$ grasses, legumes, forbs and trees. Of the original 168 plots, 33 plots with species richness ranging from 1 to 16 were selected for

this study. These 33 plots included nine monocultures and six replicates of every other richness level (2, 4, 8, and 16) but with differing species combinations (see section 4.1 in Appendices).

### 4.2.2 Imaging spectrometry at fine scale

In the 33 selected plots, an imaging spectrometer (Headwall E Series, Headwall Photonics Inc., Fitchburg, Massachusetts, USA) was mounted on a tram system (Gamon et al. 2006) to collect fine-scale images of the northern-most row of each sampling plot at peak season, both in 2014 (14 plots were sampled from July 23 to July 31) and 2015 (19 plots were sampled from July 17 to July 26) (Figure 4.1 a). A speed control circuit was added to the tram cart to maintain a slow and constant moving speed, creating high-fidelity images. The cart speed (0.0256 m/s) allowed us to build clear, high signal-to-noise ratio (SNR) hyperspectral images under low wind-speed conditions. Typically, wind can affect the field reflectance measurements, especially in canopies with a high vertical structure (Lord et al. 1985). Excessive plant sway caused by strong wind can blur the image, which will degrade the spatial resolution in subsequent analysis. To reduce wind artifacts on windy days, a wind screen consisting of black cloth was placed on 2-3 sides of the sampling plot, at least 1 meter from the sampling area. Data were manually evaluated to further remove any windy (blurred) images.

The imaging spectrometer provided hyperspectral images with a 3 nm spectral resolution (Full Width at Half Maximum, FWHM) and a 0.65 nm spectral sampling interval over the 400 ~ 1000 nm range. The focal length of the lens was 17 mm with a field of view (FOV) of ~34°. The spectrometer was mounted 3 meters above ground surface, obtaining a ground pixel size of approximately 1 $mm^2$ (Figure 4.1 a). The dimension of the raw image was 1600 x 1000 pixels (Figure 4.1 b). Subsequent image processing avoided 1 m from either end of the plot, and removed 600 pixels from the north side to minimize edge effects, yielding a final image size of 1 x 1 m (Figure 4.1 b). Reflectance spectra (Figure 4.1 c) were then extracted from each 1 x 1m image and used for spectral diversity calculations.

A dark file ($DN_{dark,\lambda}$) was obtained before each measurement by covering the lens of the spectrometer with a black lens cap. Scans of a white reference calibration panel

(Spectralon, Labsphere, North Sutton, NH, USA) were taken before and after ground target measurements to calculate surface reflectance. The relative reflectance (ρ) at each wavelength (λ) was calculated as:

$$\rho_\lambda = \frac{(DN_{target,\lambda} - DN_{dark,\lambda})}{(DN_{panel,\lambda} - DN_{dark,\lambda})} \quad (4.1)$$

In this equation, $DN_{target,\lambda}$ and $DN_{panel,\lambda}$ indicate the digital number measured at each wavelength (λ, in nm) over the ground target and white reference panel, respectively. All the images were collected under sunny conditions, and reference panel data were collected under similar sky conditions as the target data.

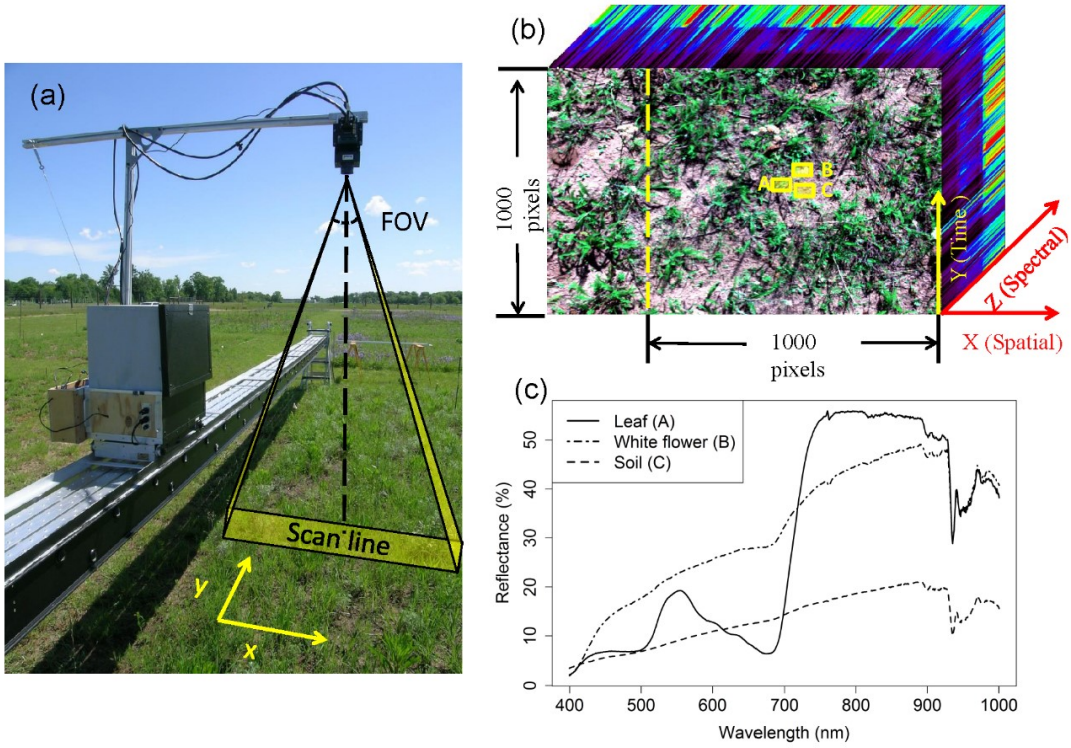


Figure 4.1. (a) Headwall imaging spectrometer on the tram. Cart motion along the Y axis produced an image cube. (b) Sample image cube from Plot 11, richness = 1 (*Achillea millefolium*). (c) Sample spectra. For each image, 600 pixels of each scan line to the left of the dashed line (b) were removed from the original image, leaving a 1000x1000mm square image cube for further analysis. Three yellow squares (A, B, and C) in panel b indicated the positions of the different sunlit targets (leaves, white flowers, and soil) in panel c. Approximately 100 pixels were used to generate each spectrum in panel c.

### 4.2.3 Image resampling

To simulate different spatial scales, a resampling strategy was used to increase the 1x1 mm pixels to successively larger spatial scales: 1x1 cm, 10x10 cm, 25x25 cm, 50x50 cm and 1x1m by averaging all the small pixel reflectance values in each "large" pixel. This method assumes an idealized square-wave response on the part of the sensor, ignoring effects from neighboring pixels (Woodcock and Strahler 1987). This scaling up process can also smooth the data, which increases the signal to noise ratio (SNR) of the image, but this effect was ultimately found to be small compared to the treatment effects driven by different diversity levels (see section 4.2 in Appendices). To validate this approach, we also compared these simulated data to independent samples collected both from the ground and from aircraft at larger (1x1m) spatial scales.

### 4.2.4 Whole plot canopy reflectance sampling

To sample entire plots, we measured canopy reflectance of the 33 plots using a non-imaging spectrometer (Unispec DC, PP Systems, Amesbury, Massachusetts, USA) on a tram system (Gamon et al. 2006) at peak season (July 23 to August 3) 2014. This system allowed a systematic measurement of each 1 $m^2$ portion of each plot (Wang et al. 2016b). This resulted in a total of 81 measurements (9x9 m) for each plot with approximately 1 $m^2$ spatial resolution, creating a synthetic image that provided a full sample of each of the 31 plots, and providing one set of independent samples for comparison with the data from the imaging spectrometer on the tram. Edge pixels were discarded to avoid possible edge effects, resulting in a final analysis based on a 7x7 m pixel array. All measurements were made ±2 hours of solar noon to reduce the effects of sun position.

In this whole-plot sampling, both upwelling radiance and down-welling irradiance were measured over the vegetation target and a white reference calibration panel (Spectralon, Labsphere, North Sutton, NH, USA) that was used to correct for the atmospheric variation and calculate surface reflectance. The relative reflectance ($\rho$) at wavelength ($\lambda$) was calculated as:

$$\rho_\lambda = \frac{(L_{target,\lambda}/E_{target,\lambda})}{(L_{panel,\lambda}/E_{panel,\lambda})} \quad (4.2)$$

In this equation, $L_{target,\lambda}$ indicates the radiance measured at each wavelength (λ , in nm) by a downward-pointed detector sampling the surface ("target"), while $E_{target,\lambda}$ indicates the irradiance measured simultaneously by an upward-looking detector sampling the downwelling radiation. $L_{panel,\lambda}$ indicates the radiance measured by a downward-pointed detector sampling the calibration panel (Spectralon, Labsphere, North Sutton, NH, USA), and $E_{panel,\lambda}$ indicates the irradiance measured simultaneously by an upward-pointed detector sampling the downwelling radiation.

### 4.2.5 Airborne reflectance sampling

Airborne data for the Cedar Creek region were collected on August 2, 2014 using an imaging spectrometer (AISA Eagle, Specim, Oulu, Finland) mounted on a fixed-wing aircraft (Piper Saratoga, Piper Aircraft, Vero Beach, Florida, USA) operated by the University of Nebraska Center for Advanced Land Management Information Technologies (CALMIT) Hyperspectral Airborne Monitoring Program (CHAMP). Images were collected from a height of 1540 m and a speed of 196 km/h. The ground pixel size was approximately 1 $m^2$. The imaging spectrometer provided 400 ~ 970 nm hyperspectral images with 3.3 nm spectral resolution (FWHM). Spectral binning (approximately 10nm) was used to increase signal-to-noise ratio (SNR) of the data. Imagery acquired with this band configuration has 63 bands across the 400~970 nm continuum. Airborne data covered 125 prairie plots in the BioDIV experiment and data for the 33 ground sampling plots were extracted. This method yielded an image from each plot comparable in scale to the whole-plot canopy reflectance sampling described above.

To extract reflectance from airborne data, lab-measured calibration coefficients were used to radiometrically convert DN to radiance ($Wm^{-2}Sr^{-1}$ $nm^{-1}$). Geometric correction utilized the position and rotational attributes (pitch, roll, and yaw) of the airplane collected by an inflight GPS and inertial measurement unit (IMU) (C-Migits III, Systron Donner Inertial, Concord, California, USA) during the flight. Fast Line-of-sight

Atmospheric Analysis of Hypercubes (FLAASH) embedded in ENVI version 4.8 (Exelis Visual Information Solutions, Boulder, Colorado) was used for atmospheric correction to convert radiance to reflectance. To obtain a corrected surface reflectance, we used field spectrometer (ASD Field Spec, Analytical Spectral Devices, Inc., Boulder, Colorado, USA) measurements from three 9x9 meter calibration targets (white, charcoal, and black) made from polyester fabric (Odyssey, J. Ennis, Edmonton, Alberta, Canada) located in the scene to compute coefficients and apply an empirical line correction (Conel et al 1987) to remove remaining errors in the atmospheric correction.

### 4.2.6 Comparisons of spectral range

To evaluate the effect of spectral range on the assessment of spectral diversity, we also made measurements with a full-range spectrometer (PSR 3500, Spectral Evolution, Lawrence, MA, USA). Since these tests found no added benefit of a full-range spectrometer to the method described here, and since they covered a different spectral range from all other instruments, the results of these full-range tests are briefly summarized in section 4.3 in Appendices.

### 4.2.7 Spectral diversity

As an indicator of spectral diversity of each plot, we used the average coefficient of variation (CV) (Wang et al. 2016a), calculated as the average CV for each wavelength from 430 nm to 925 nm (758 bands in total).

$$\mathrm{CV}_{image} = \frac{\sum_{\lambda=430}^{925}\left(\frac{\sigma(\rho_\lambda)}{\mu(\rho_\lambda)}\right)}{number\ of\ bands} \tag{4.3}$$

*where* $\rho_\lambda$ denotes the reflectance at wavelength λ, and $\sigma(\rho_\lambda)$ and $\mu(\rho_\lambda)$ indicate the standard deviation and mean value of reflectance at wavelength λ across all the pixels in one plot, respectively. We calculated CV for all reflectance data, including the tram images, synthetic images, ground canopy reflectance and airborne images. In this case, CV expresses the spectral heterogeneity among pixels with one single value per plot. Sample CV spectra and the spectral averaging method are illustrated in Figure 4.2 for two

plots of contrasting diversity. [Note that for spectral range tests, CV was calculated over different spectral ranges, as described in results and section 4.3 in Appendices].

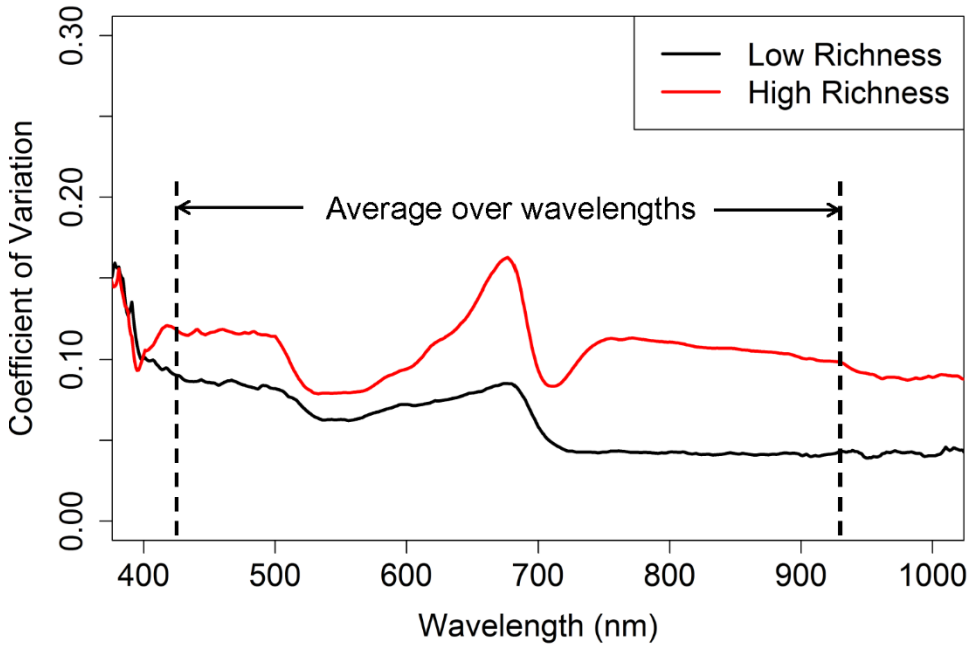


Figure 4.2. Sample coefficient of variation (CV) spectra of plots with different species richness levels (1 and 16). As a summary metric, an average CV was calculated over 430-925 nm as indicated in Equation 4.3 and the Figure above. Data were derived from the Headwall E Series imaging spectrometer sampling at 1 mm pixels for plots 11 and 34 (See section 4.1 in Appendices for detailed descriptions of sampling plots).

### 4.2.8 Conventional diversity metrics

To calculate diversity metrics based on richness and evenness, biomass data were collected from all plots. Above-ground living plant biomass of the selected 33 plots was measured in late July to early August (August 4, 2014 and July 27 to August 3, 2015). Plots were sampled by clipping, drying and weighing four parallel and evenly spaced 0.1 m × 6 m strips per plot. The biomass of each strip was sorted to species. Planted species richness was the number of species originally planted and maintained in each plot, providing a nominal metric of biodiversity. In most cases the observed species number

and richness derived from harvested vegetation varied from the planted due to missing species or other species present in the plot besides the ones maintained. As a result of the periodic weeding, the abundance of these non-maintained species was typically much less than the maintained species, allowing us to assume that the planted plant species richness provided a reasonable approximation of the observed species richness.

Previous results (Wang et al. 2016) have suggested that spectral diversity may be affected by evenness as well as species richness. Consequently, we also calculated three indices that weighted species abundance by proportional biomass, thus accounting for the effects of rare or common occurrences: Shannon's index (Shannon 1948), reciprocal of Simpson's index (Simpson 1949, Williams 1964), and species evenness (Pielou, 1966) (Table 4.1) and related these metrics to spectral diversity (CV) at different scales. Shannon's Index expresses the equitability of all the species while Simpson's Index focuses on a few dominant species (Whittaker 1972).

Phylogenetic diversity is recognized as representing an integrated measure of functional differences among species and often helps explain ecological variation among species beyond what can be explained by richness alone (Cadotte et al. 2008, 2009, Cavender-Bares et al. 2009, Srivastava et al. 2012). However, metrics of phylogenetic diversity that rely on total evolutionary distances among species in an assemblage are strongly associated with species richness. We intentionally chose metrics of phylogenetic diversity independent of species richness to separate variation associated with species richness and that associated with evolutionary distinctiveness of species in assemblages. Phylogenetic data was based on the phylogeny from Zanne et al. (2014) and pruned to include only the species observed in BioDIV. To study the influence of phylogenic diversity on spectral diversity, two indices independent of species richness, phylogenetic species variability (PSV) and phylogenetic species evenness (PSE) (Helmus et al. 2007), were calculated with the picante R package (Kembel et al. 2010). PSV quantifies how phylogenetic relatedness decreases the variance of a hypothetical neutral trait shared by all species in a community. PSV is directly related to mean phylogenetic distance and ranges from 0 (low) to 1 (high) and compares observed phylogenetic distinctness to null communities. PSE is PSV modified to incorporate relative species abundance. The maximum attainable

value of PSE (i.e., 1) occurs when each species has the same abundance and evolves independently from a common starting point (Helmus et al. 2007). In this case, PSE was weighted by biomass at the plot level.

Table 4.1 Summary of diversity metrics used in this study

| Diversity Metric | Description / Equation |
|---|---|
| Planted species richness ($S_0$) | Number of species originally planted and subsequently maintained in each plot |
| Observed species richness ($S$) | Number of harvested species in each plot (includes rare species) |
| Shannon's Index ($H'$) | $H' = -\sum p_i * \ln(p_i)$ |
| Simpson's Index ($D$) | $D = 1/\sum {p_i}^2$ |
| Evenness ($J'$) | $J' = H'/\ln(S)$ |
| Phylogenetic species variability (PSV) | PSV varies between 0 and 1. Values close to 1 have higher phylogenetic diversity. |
| Phylogenetic species evenness (PSE) | PSE varies between 0 and 1. Values closer to 1 have higher phylogenetic diversity and evenness. |

where $p_i$ is biomass proportion of the number $i^{th}$ species.

## 4.3 Results

### 4.3.1 Effect of spatial scale

The mean reflectance of each image was the same across spatial scales, but the variation around this mean (expressed as SD and max/min in Figure 4.3, and as the CV in subsequent figures) decreased with increasing pixel size, revealing the sensitivity of the spectral diversity - species richness (SR) relationship to pixel size.

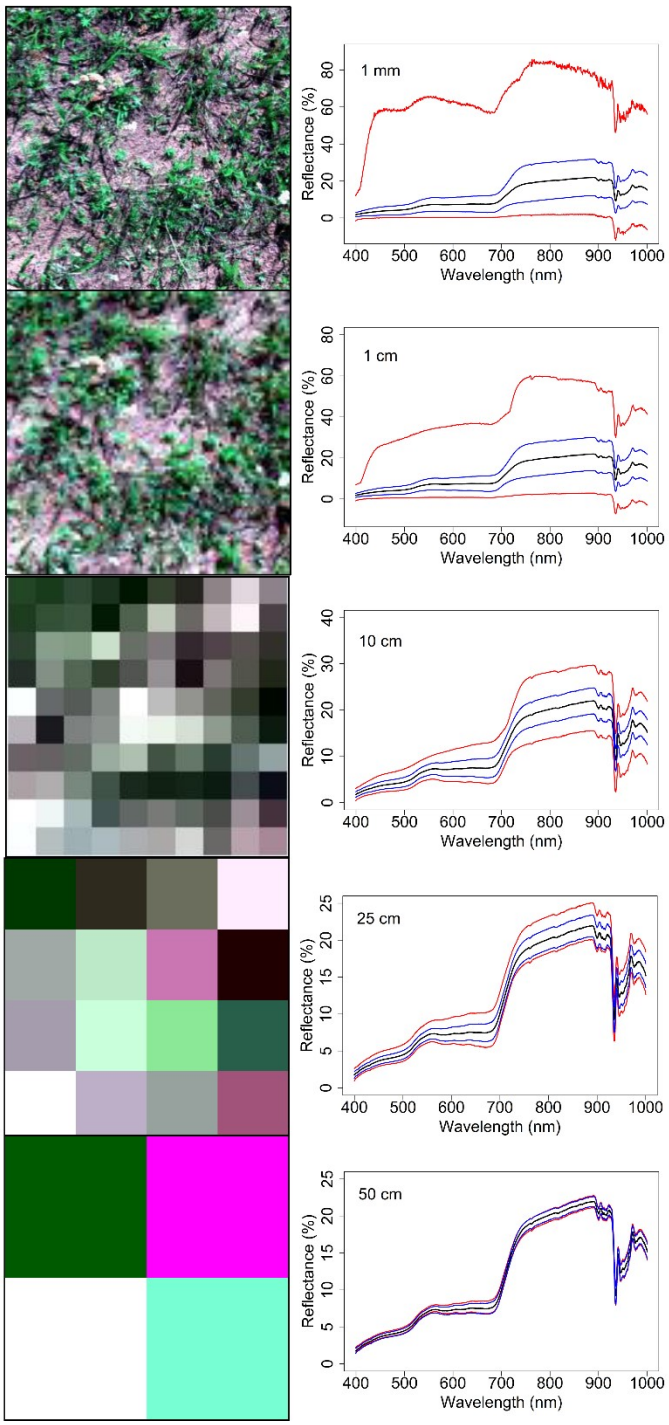


Figure 4.3. Sample images and reflectance spectra at different sampling pixel sizes (1 mm to 50 cm diameter, as indicated in the spectral plots). The image shown here was the second meter from the west of Plot 11 (planted species richness = 1) (See section 4.1 in Appendices for detailed descriptions of sampling plots). The dimension of the original image in the top panel was 1000 x 1000mm pixels (approx. 1 x 1 m), which was

successively degraded by resampling to progressively larger sizes (up to 50 x 50 cm in the bottom panel). Colored lines indicate mean (black), standard deviation (blue) and min/max (red) reflectance. The images on the left were stretched to maintain contrast and the plots on the right showed the true contrast.

Spectral diversity (measured by CV) increased with planted species richness. Increasing pixel size reduced the sensitivity of spectral diversity to planted species richness (Figure 4.4 a). By 10x10 cm and above, the linear relationship between CV and planted species richness started to disappear, and the relationships were no longer significant at $p = 0.05$ for pixel sizes above 10x10 cm. By applying an analysis of covariance (ANCOVA) test to see whether the regression slopes varied with scales, there was no significant difference between slopes of regression at 1 mm and 1 cm scales. But the difference of slopes between 1 cm and 10 cm was significant ($p = 0.009$).

There was no significant relationship found between observed species richness and spectral diversity (Figure 4.4 b). The relationship between CV and Shannon's index (Figure 4.4 c) was similar to the CV-planted species richness relationship (Figure 4.4 a). Simpson's index (Figure 4.4 d) showed stronger relationships with spectral diversity than species richness and Shannon's index. The relationships between CV and Shannon's index and Simpson's index also weakened with increasing pixel size. The CV-Simpson's index relationship was still maintained even at coarse spatial scales (at least better than the other comparisons with observed species richness, planted species richness and Shannon's index). For both Shannon's index and Simpson's index, the difference between regression slopes at 1 mm and 1 cm scales were not significant. There were significant differences between slopes at larger scales ($p < 0.001$).

Evenness (Figure 4.4 e) showed similar but slightly weaker relationship with spectral diversity than Shannon's index. A linear relationship was found between phylogenetic evenness (Figure 4.4 f) and spectral diversity at fine scales (1 mm). The relationship was not as strong as the species evenness – spectral diversity relationship but still significant at smaller spatial scales. Similar to the CV-plant species richness relationships,

ANCOVA tests suggested no significant difference between 1 mm and 1 cm regression slopes for CV-species evenness and CV-phylogenetic evenness relationships.

Key results from figures 4.4 were summarized in Table 4.2. For all diversity metrics, the difference in CV between diversity levels tended to decrease with increasing pixel size. For most biodiversity metrics, at a resolution of 10x10 cm or higher, much of the power to assess biodiversity was lost. At 1 m resolution, there was very little power to distinguish diversity levels for most metrics of biodiversity. Only CV-Simpson's Index maintained significant relationships at all spatial scales (Table 4.2).

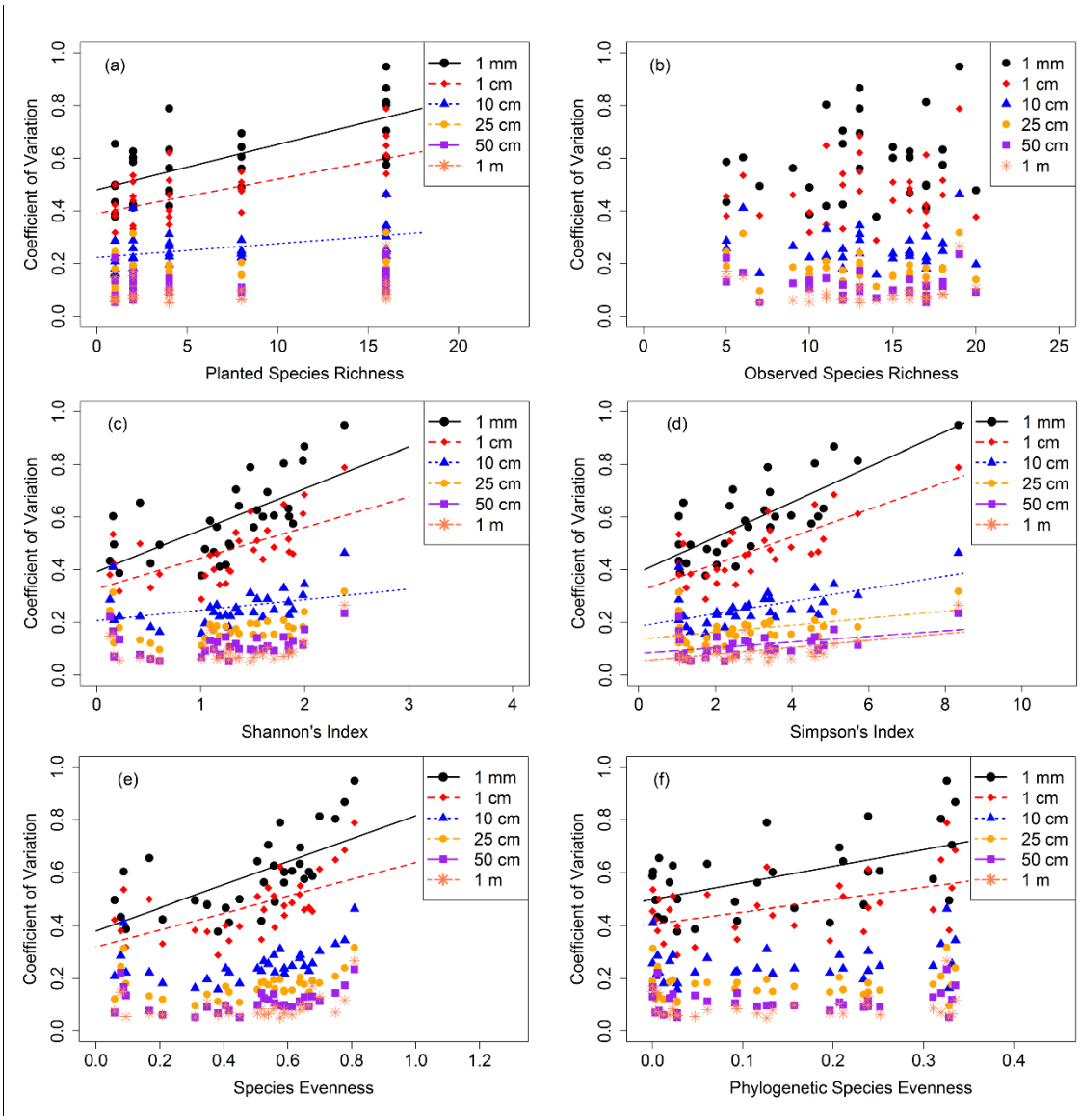


Figure 4.4 Spectral diversity (coefficient of variation) versus conventional biodiversity metrics ((a)planted species richness, (b) observed species richness, (c) Shannon's index, (d) Simpson's index, (e) species evenness, (f) phylogenetic species evenness) for varying pixel sizes (diameters). The definitions of conventional biodiversity metrics are in Table 4.1. Fit lines are not shown for $p > 0.05$.

Table 4.2 Slopes (and coefficient of determination, $R^2$) of regressions between coefficient of variation (CV) and conventional diversity metrics (see table1) at different scales (pixel diameter values). PSV and PSE indicate the phylogenetic species variability and phylogenetic species evenness, respectively. Significant codes: NS, $0.05 < p$, *, $0.01 < p < 0.05$, **, $0.001 < p < 0.01$ and ***, $p < 0.001$. Slopes were shown only for significant relationships ($p < 0.05$).

| Pixel diam. | Planted richness | Observed richness | Shannon's index | Simpson's index | Evenness | PSV | PSE |
|---|---|---|---|---|---|---|---|
| 1 mm | 0.017 | - | 0.158 | 0.067 | 0.435 | - | 0.629 |
| | ($0.467^{***}$) | ($0.036^{NS}$) | ($0.427^{***}$) | ($0.583^{***}$) | ($0.421^{***)}$ | (6e-$4^{NS}$) | ($0.273^{**}$) |
| 1 cm | 0.013 | - | 0.116 | 0.052 | 0.317 | - | 0.459 |
| | ($0.44^{***}$) | ($0.027^{NS}$) | ($0.378^{***}$) | ($0.571^{***}$) | ($0.364^{***}$) | (8e-$5^{NS}$) | ($0.237^{**}$) |
| 10 cm | 0.005 | - | 0.040 | 0.024 | - | - | - |
| | ($0.21^{***}$) | ($0.003^{NS}$) | (0.131*) | ($0.357^{***}$) | ($0.127^{NS}$) | ($0.082^{NS}$) | ($0.056^{NS}$) |
| 25 cm | - | - | - | 0.013 | - | -8.64e-5 | - |
| | ($0.11^{NS}$) | ($0.046^{NS}$) | ($0.041^{NS}$) | ($0.185^{*}$) | ($0.045^{NS}$) | ($0.176^{*}$) | ($0.126^{NS}$) |
| 50 cm | - | - | - | 0.011 | - | -6.34e-5 | - |
| | ($0.123^{NS}$) | ($0.055^{NS}$) | ($0.035^{NS}$) | ($0.174^{*}$) | ($0.041^{NS}$) | ($0.134^{*}$) | ($0.017^{NS}$) |
| 1 m | - | - | - | 0.013 | - | - | - |
| | ($0.086^{NS}$) | (9e-$4^{NS}$) | ($0.048^{NS}$) | ($0.239^{**}$) | ($0.054^{NS}$) | ($0.078^{NS}$) | ($0.016^{NS}$) |

### 4.3.2 Effect of Wavelength Regions

To investigate spectral scale, we examined the CV from different spectral regions. The relative contribution to CV varied by wavelength region. CV spectra at different pixel sizes showed that at a fine scale (pixel size < 25 cm), high richness plots had a higher average CV than low richness plots. This pattern was apparent for all wavelengths but was especially strong for the visible region (Figure 4.5). By contrast, the relative importance of the NIR increased as spatial scale increased. At scales of 10 and 25 cm, it was hard to distinguish richness levels from the visible spectra but the NIR region was still distinguishable. At coarser scales (pixel size > 25 cm), all the CV spectra overlapped,

except for the highest richness level (richness = 16), illustrating the declining power to distinguish richness at coarser spatial scales.

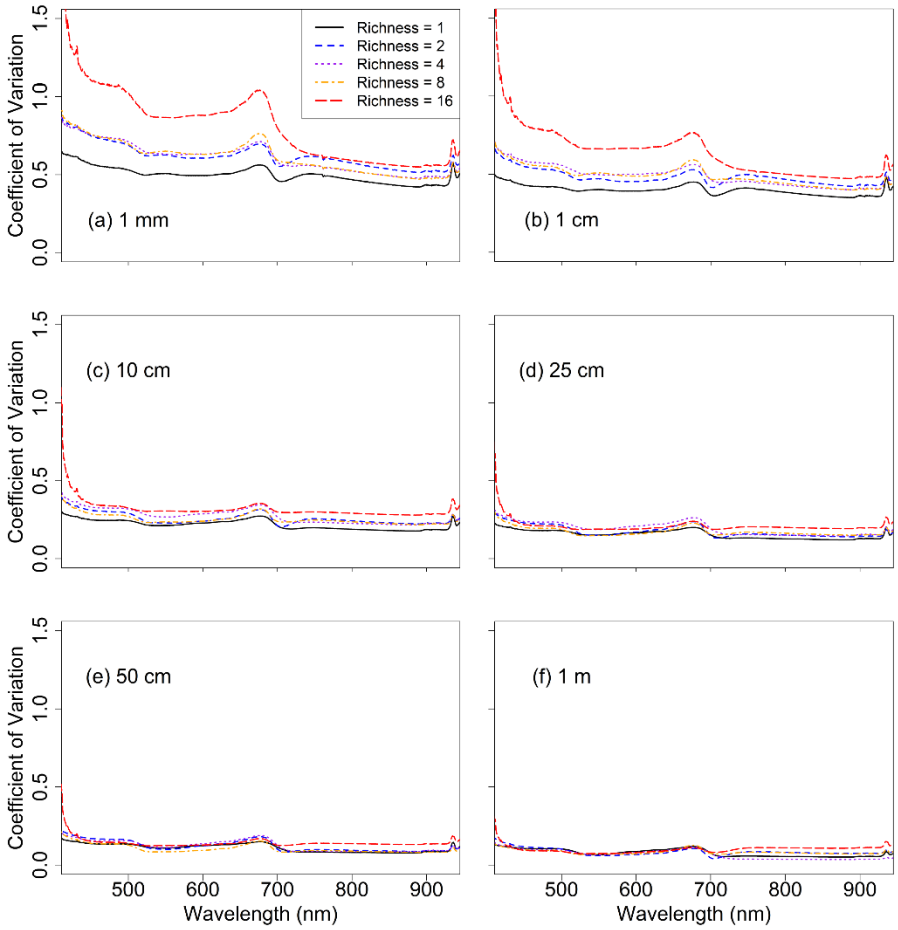


Figure 4.5 Coefficient of variation spectra at different pixel sizes resampled from ground-sampled image cubes (imaging spectrometer on the tram) for pixel sizes 1 mm to 1 m. Line color indicates different planted species richness levels.

To provide further insight into the spectral regions contributing to spectral diversity information (Figure 4.5), we compared the CV calculated over different spectral ranges (430-900 nm), and compared these results to the Simpson's Index, which displayed the strongest correlation with CV (Table 4.2). We also conducted independent tests over a larger spectral range using a full-range spectrometer. The full range spectrometer did not indicate improved results over the VIS-NIR range (section 4.3 in Appendices).

Consequently, in this study, we confined our primary analyses to the VIS-NIR range (the range covered by our imaging spectrometer).

At a fine scale (<=25 cm diam.), the CV values in visible wavelengths (430-700 nm, $CV_{visible}$) were larger than the CV of visible+NIR (430-900 nm, $CV_{VN}$) and the CV of NIR (700-900 nm, $CV_{NIR}$) (Figure 4.6 and Table 4.3). Similarly, the $R^2$ of $CV_{visible}$-Simpson's index was similar to the $CV_{VN}$-Simpson index and larger than $CV_{NIR}$-Simpson's index at fine scales. These relationships changed at larger pixel sizes. With increasing pixel size, $R^2$ of all three regressions decreased, but the $R^2$ of the $CV_{NIR}$-Simpson's index relationship decreased with resolution less than the other two. Consequently, at the 25 cm and 50 cm pixel sizes, $R^2$ of the $CV_{NIR}$-Simpson's index became the largest among the three CV formulations derived from different spectral ranges, and still retained significant correlations ($p$<0.01). The ANCOVA test indicated significant difference between slopes of CV-Simpson's Index relationships at different scales ($p < 0.01$ for all of the three spectral regions).

Table 4.3 Spectral diversity (coefficient of variation) of different wavelength versus Simpson's Index. Significant codes: NS, $0.05 < p$, *, $0.01 < p < 0.05$, **, $0.001 < p < 0.01$ and ***, $p < 0.001$.

| Pixel size | $CV_{VN}$ | | $CV_{visible}$ | | $CV_{NIR}$ | |
|---|---|---|---|---|---|---|
| | Slope | $R^2$ | Slope | $R^2$ | Slope | $R^2$ |
| 1 mm | 0.067 | 0.583*** | 0.091 | 0.567*** | 0.037 | 0.437*** |
| 1 cm | 0.052 | 0.571*** | 0.067 | 0.567*** | 0.034 | 0.434*** |
| 10 cm | 0.024 | 0.356*** | 0.027 | 0.310*** | 0.020 | 0.343*** |
| 25 cm | 0.013 | 0.185* | 0.013 | 0.129* | 0.013 | 0.229** |
| 50 cm | 0.011 | 0.173* | 0.010 | $0.107^{NS}$ | 0.012 | 0.244** |
| 1 m | 0.013 | 0.239** | 0.018 | 0.180* | 0.007 | $0.109^{NS}$ |

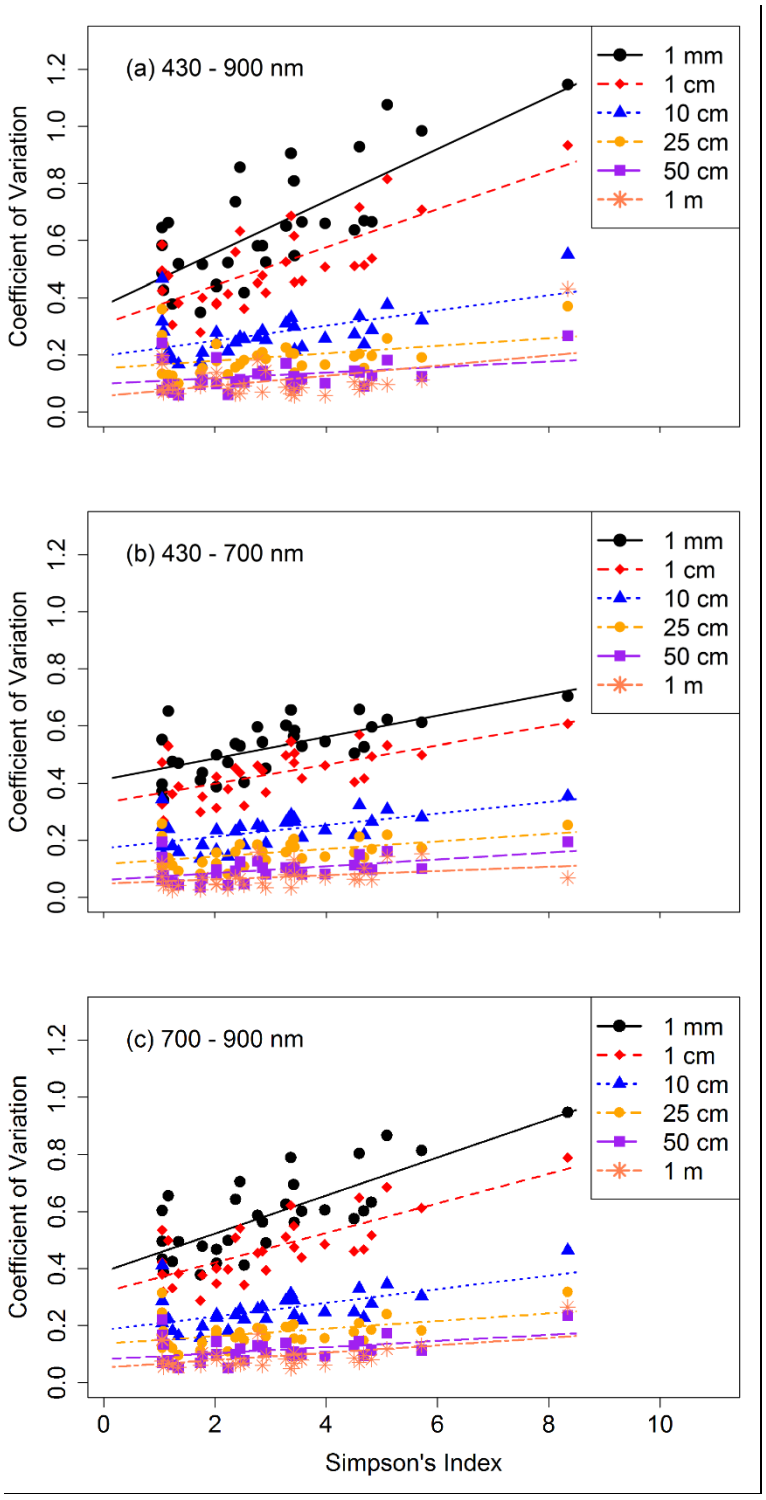


Figure 4.6 Spectral diversity (coefficient of variation) versus Simpson's Index for different wavelength regions (a: 430 – 900 nm; b: 430 – 700 nm; c: 700 – 900 nm) and different pixel sizes (1x1 mm to 1x1 m). Slopes and $R^2$ of the regressions were listed in Table 4.2.

### 4.3.3 Comparison of Instruments

A comparison of different methods yielded good agreement between instruments and sampling methods. The CV-planted species richness relationship in the synthetic images ($1m^2$ pixels) fit the trend found in the resampled images (spanning $1mm^2$ to $1m^2$ pixels) (Figure 4.7). CV values for the different diversity levels were slightly more variable when calculated from the imaging spectrometer on the ground than when calculated from the non-imaging spectrometer or the airborne spectrometer (Figure 4.7 a). Airborne CV values were slightly smaller than synthetic and ground measurements at all planted species richness levels. Regardless of method, by 1x1m there was very little power to distinguish planted richness levels (except at the most extreme levels of 1 vs. 16).

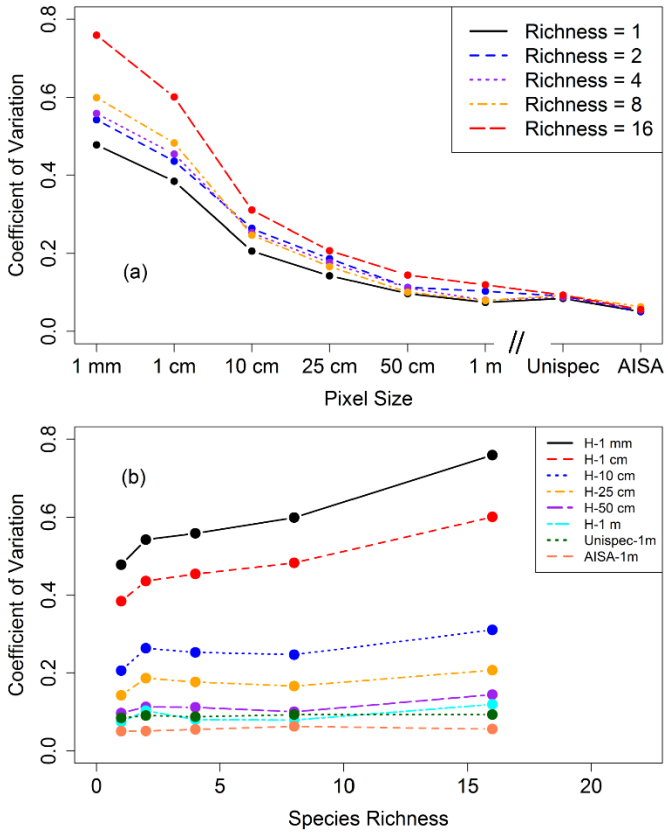


Figure 4.7 (a) Coefficient of variation as a function of pixel size for the resampled Headwall images and AISA Eagle airborne data for 125 plots. (b) Comparison of coefficient of variation-planted species richness relationship at different scales obtained from different instruments (Headwall (H), UnispecDC (Unispec), and AISA Eagle (AISA)) and platforms (tram and aircraft).

## 4.4 Discussion

### 4.4.1 Scale dependence of spectral diversity

Applying the imaging spectrometer using the tram system on the experimental biodiversity plots allowed us to collect very high resolution (1 $mm^2$ pixel size) images and test the scale dependence of the spectral diversity-biodiversity relationship. Instead of enumerating plant species, CV is an abstract expression that represents the information content (variability) of the reflectance spectra among pixels. Using this method, the detectability of biodiversity with remote sensing declined dramatically when scaling up from 1 $mm^2$ to 1 $m^2$ in this plot level experiment. The slightly smaller CV value calculated from the airborne image compared to synthetic images (created from the Unispec spectrometer) may be due to a blurring result caused by the point spread function of the airborne imaging spectrometer, which reduced the variation between neighboring pixels. The overall consistency of the patterns across spatial scale for the different methods indicated a strong effect of spatial scale on the ability to detect alpha biodiversity with optical remote sensing methods.

### 4.4.2 OD-Richness-Evenness

The stronger relationship between spectral diversity and Simpson's index than between spectral diversity and observed species richness agrees with recent studies (Oldeland et al. 2010, Wang et al. 2016a) that measures of evenness can improve the correlation between spectral diversity and conventional diversity metrics. Integrating species evenness adds additional information on community structure beyond species richness *per se*. These findings suggest that spectral diversity relates to the heterogeneity within a small region that is determined by a combination of species composition, richness and evenness.

Both Shannon's index and Simpson's index are commonly used metrics in quantifying biodiversity, but the two metrics show variable responses to different combinations of richness and evenness (Nagendra, 2002). In our study, spectral diversity showed a stronger relationship with Simpson's index than Shannon's index, which agrees with findings from a study in tropical forests (Schäfer et al. 2016). This may be because Simpson's index is more sensitive to dominant or common species than Shannon's index, which assumes all species are present and randomly sampled (Peet 1974). This BioDIV

experiment is a highly manipulated experimental landscape, weeded in summer to maintain species richness so that the percentage of rare species is small and the evenness of low richness plots tends to be low. It is also reasonable that planted species richness, which implicitly includes a degree of evenness by ignoring "rare," unintended species (which likely do not contribute much or at all to the optical signals measured here), leads to a better correlation to spectral diversity than observed species richness (which includes more "rare" species that are not an intended part of the experiment).

### 4.4.3 Species evenness-phylogenetic evenness

In principle, if phylogenetic diversity reflects functional properties that are detectable with remote sensing, spectral diversity should increase with phylogenetic diversity. Two indices we used, PSV and PSE. The latter metric incorporates abundance, but both are independent of species richness. Both metrics showed significant relationships with CV (Table 4.2). Similar to the indices at the species level, the significant relationship between CV and PSE at fine spatial scale (1mm) disappeared rapidly at coarser scales (pixel size > 1cm). These results indicate that species richness measures, particularly when they account for abundance, capture more detectable variation than phylogenetic distinctiveness measures that are independent of species richness. These findings are consistent with recent studies indicating that species richness and evenness are often the most critical factors explaining relationships between biodiversity and ecosystem function (Zhang et al. 2012).

### 4.4.4 Optimal pixel size

The predictability of a phenomenon is scale-dependent both in ecology (Costanza and Maxwell 1994) and remote sensing (Woodcock and Strahler 1987). In ecology, grain size is the extent of the elementary sampling units and the minimum size of measure (Costanza and Maxwell 1994, Legendre and Legendre 1998). Fine-scale sampling provides more information about detailed patterns that will be lost at coarse scales. In this study, considerable information on fine-scale variability decreased with increasing pixel size, and this result is in accordance with the finding that significant information may be lost when the sampling elements are scattered and small compared to the pixel size (O'Neill et al. 1986). From a remote sensing perspective, the spatial structure of an image

relates to the size of the objects in the scene and the spatial resolution (pixel size). Woodcock and Strahler (1987) noted local variance peaked when the size of the object equaled (or was close to) the spatial resolution of the image, which may help explain our results. In our study, the optimal pixel size for distinguishing diversity levels in these prairie plots, particularly for the visible spectral region (sensitive to leaf pigments) appears to be in the range of 1mm to 10 cm, a range of spatial scales similar to those of a single leaf or herbaceous plant species in this experimental prairie landscape.

In another study of prairie grassland in southern Alberta, Canada, CV calculated with airborne imagery correlated well with biodiversity metrics, e.g., richness and Shannon's index even at 1 $m^2$ scale (Wang et al. 2016a), yet in our study of experimental plots, this correlation was largely lost by 1 $m^2$. In experimental plots of constant size with long-term maintenance, grain and extent are determined and perhaps maintained artificially but these properties may be different or exhibit inconstant temporal behavior in real landscapes. The larger extent captured in airborne sampling in a natural landscape can introduce higher-level diversity effects (e.g. beta diversity), which may explain contrasting results across studies at different spatial scales or settings. As well, the discontinuity measured on a real landscape may appear continuous when broken into finer grained observations, especially at a small extent (9x9 m) as in this study. When considering other applications of airborne and satellite remote sensing in biodiversity detection in natural landscapes, spectral diversity may reveal variation between species, between dominant species, or even the transition from α diversity to β diversity with increasing grain size and spatial extent. These factors of scale are generally not considered explicitly in remote sensing campaigns addressing biodiversity, most of which do not use experimental approaches, but are restricted to a single grain size and extent.

Considering the surrogacy hypothesis (Magurran 2004), high species richness in one taxon may be related to high richness in other, particularly at higher trophic levels, as has been demonstrated in insect herbivore communities (Siemann et al. 1998, Haddad et al. 2009). High environmental variation, e.g., temperature or topographical, diversity is frequently related to high species richness (environmental surrogacy), such as in the case of habitat heterogeneity and butterfly diversity (Kerr et al. 2001). It is possible that the

relationship between spectral diversity and species richness at certain scales is fortuitous and often remains significant at even coarse spatial scales because we actually see something indirectly related to species richness rather than species richness *per se*. Presumably, species richness is also related to functional diversity to some extent (e.g., (Petchey and Gaston 2002, Flynn et al. 2011)) despite well-understood complexities (Cadotte et al. 2011, Violle et al. 2012). A more diverse ecosystem is thus likely to include a greater variety of functional behaviours as indicated by plant traits relate to different leaf biochemical content and canopy structure. The variation in plant traits among species can affect the optical properties of plants and lead to spectrally detectable features (spectral diversity). Our findings suggest that, for pixels much larger than the individual plant size, a direct detection of alpha diversity is not feasible, although other measures of diversity at larger scales may apply. The results suggest that further assessment of the scale dependence of the spectral diversity-biodiversity relationships for different vegetation types (e.g. different crown sizes) is warranted, particularly if the goal is to develop reliable and repeatable remote methods of assessing biodiversity. We recommend that similar scaling studies be conducted in natural landscapes to better reveal both the underlying causes and larger significance of the scale-dependent relationships reported in this study. Such studies should also address much larger pixel sizes, such as are proposed for spaceborne sensors, and should enable fully testing the degree to which regional α and β diversity are detectable for grain sizes that are relatively coarse when compared to those used in this study.

The ecological concept of patch size is clearly relevant to the remote sensing of spectral diversity. Broadly, a patch can be defined as a relatively homogeneous spatial unit that is different from its neighbors in nature or appearance (Wu and Loucks 1995, Bazzaz 1996). Variation within a patch is influenced by the minimum size of all of the patches that will be mapped as well as which components of the system are ecologically relevant to the organism or process of interest. In this study, we used visible to near-infrared waveband regions to calculate the coefficient of variation and the optical "patch size" appeared to vary slightly with spectral region. The different responses of visible and near-infrared spectral regions to pixel size suggested possible changes in the relative contribution to spectral diversity from leaf traits to canopy structure with increasing pixel size. Some leaf

traits (e.g. pigment levels) are detectable in the visible region (Ollinger 2011, Ustin 2013), and the sensitivity of $CV_{vis}$ to planted species richness or Simpson's Index was quickly lost at pixel sizes above that of the individual leaves and plants. In this case, the relevant "patch size" seems close to that of an individual leaf or plant. On the other hand, the NIR region is sensitive to canopy structure (Ollinger 2011, Ustin 2013), and the $CV_{NIR}$-Simpson's index retained a significant correlation at relatively large spatial scales (25-50 cm), suggesting the relevant "patch size" of canopy structure is larger than that of leaf traits.

Spectral resolution and range also affect the spectral diversity-biodiversity relationship. When compared to multispectral data, adding spectral information has been shown to increase the accuracy of biodiversity estimation (Rocchini 2007). Using full range spectra including the shortwave infrared (400-2500 nm) could add information on other biochemical properties, e.g. leaf water content, pigment, nitrogen content, and lignin (Asner and Martin 2009). While not easily possible in this study due to the limited range of our primary instruments, future studies should consider the effects of the full spectral range on the scale dependence of the spectral diversity-biodiversity relationship. In our initial tests (section 4.3 in Appendices), sampling the full spectral range did not enhance the CV-Simpson's Index relationships over the VIS-NIR range, but given the wide range of vegetation types and possible analytical approaches not considered here, these negative findings should not be viewed as conclusive. We note that many of the promising applications of full-range spectroscopy to biodiversity have been developed for tropical forests, which are functionally (and spectrally) distinct from the prairie species studied here. Full-range spectroscopy can be very useful in assessing leaf and plant traits (Asner and Martin 2009), and presumably would be useful in studying other aspects of diversity (e.g. functional diversity) not considered here. Consequently, further studies of spectral range for biodiversity assessment are needed, and these studies should consider more than one biome type, and additional aspects of diversity in addition to the ones considered here.

Finally, hierarchy theory suggests that the scale of measurement limits the scope of what can be captured in an observation (Ahl and Allen 1996). The scaling effect of observation

relies on the observer's choice of measurement. Here, we would expect that the "best" pixel size may vary among biomes and communities having different dominant species, e.g. prairie (with small plant sizes) versus forests (where tree crown size is typically several meters in diameter). As well, for natural landscapes, there may be higher-level effects at coarser spatial scales that reflect other aspects of diversity besides α diversity, e.g. β diversity as driven by environmental gradients or disturbance.

### 4.4.5 Confounding effects

The CV-diversity relationship may depend on the stand structure, including plant density and spacing, homogeneity of distribution among the species, and the presence of non-vegetated cover (e.g. bare soil). In this system, plant density is known to depend on diversity, which is maintained by weeding; as a consequence, lower diversity plots are less densely vegetated, have more bare ground, and have been shown to be more invasible (Naeem et al. 2000). As diversity declines and plant density in the plot decreases, spectral diversity is impacted (revealed as increased CV values for low diversity plots) and the degree of cover and bare soil affected the ability to detect alpha diversity. In a separate modeling analysis (data not shown), adding soil spectra to pure plant pixels increased plot-level CV and weakened the spectral diversity-biodiversity relationships but the spectral diversity-biodiversity relationships stayed significant. Clearly, more work on the effects of stand structure including the influence of bare soil and other non-vegetated cover types on the CV-diversity relationship is needed, and this is the focus of current studies (in preparation). Forest diversity experiments in which plant stem density is held constant while species richness and phylogenetic diversity vary are a means to uncouple density and diversity in manipulated experimental systems and could be considered in future experimental studies of biodiversity from remote sensing.

CV shows potential in estimating biodiversity using remote sensing, and is not very sensitive to the sample size (section 4.4 in Appendices). But CV condensed the information contained in a full spectrum into a single value, which may not fully use the entire spectral information available with other methods. Particularly for assessing functional diversity tied to plant traits or biochemical composition, full spectral information can be critical. Other spectral diversity methods have been proposed to

calculate diversity metrics in the principal components (PC) space, e.g. mean distance from the centroid of all PCs (Rocchini 2007, Oldeland et al. 2010), or to sum of the variance and convex hull volume for the first three PCs (Dahlin 2016). Future studies should compare the performance of different spectral diversity metrics across spatial, temporal and spectral scales.

### 4.5 Conclusion

The scale dependence of processes and patterns are central topics in both ecology and remote sensing. Few studies have considered the scale-dependence of spectral diversity due to the difficulty of obtaining comparable remote sensing data at different scales. To address this challenge, we developed a method to apply imaging spectrometry at multiple spatial resolutions using an imaging spectrometer mounted on a ground-based tram system in a manipulated experiment and compared these results to other ground sampling and airborne methods to investigate how the spectral diversity-biodiversity relationship worked at different grain sizes (pixel sizes). Among all the tested conventional biodiversity indices, spectral diversity showed the strongest relationship with Simpson's index, likely because Simpson's Index combined species richness and evenness and was sensitive to dominant species. Our fine-scale study also showed rapid information loss with increasing pixel size; the best resolution to detect α diversity using spectral diversity was the size close to a typical herbaceous plant leaf or single canopy. Although it will become more complicated as the dimensionality of number of species, and their identity increases, most likely, the "optimal" pixel size for detecting plant biodiversity with this method would vary depending upon the size of the individual organisms in question, and more work across a variety of ecosystems is needed to test this hypothesis.

While restricted to ground and airborne sampling, our study provides insights for the design and application of future spaceborne and airborne sensors, and suggests that direct assessment of α diversity, at least for prairie regions, may require spatial resolution higher than most existing satellite sensors. These findings can be exploited in future airborne remote sensing campaigns to determine the most appropriate pixel size for spatially extensive assessment of α diversity. It is also critical to understand the scale

dependence of the spectral diversity-biodiversity relationship as we transit from manipulated experiments to natural landscapes; natural landscapes may differ in their spectral patterns due to contrasting patch sizes, as a result of vegetation clumping (e.g., due to vegetative reproduction, clonality or dispersal limitation), which influence the grain size and spatial extent optimal for detection of biodiversity. Further studies in natural landscapes are also needed to explore higher-level (e.g. beta diversity) effects on spectral diversity, which may be more amenable to remote sensing. Data from multiple ecosystems and vegetation types, e.g. prairie and forest, should be included in future studies, with attention to the consequences of canopy and patch size on the scale dependence of the biodiversity-spectral diversity relationship.

**Acknowledgements**

We thank staff at the Cedar Creek Ecosystem Science Reserve, particularly Troy Mielke and Kally Worm. We thank Rick Perk and Abby Stilwell from CALMIT, University of Nebraska-Lincoln for acquiring and processing airborne data. We also thank Aidan Mazur and Melanie Sinnen from University of Wisconsin-Madison for helping collect the whole plot reflectance data. We appreciate Anna Schweiger from University of Minnesota for her coordination in data collection in 2015. This study was supported by a NASA and NSF grant (DEB-1342872) to J. Cavender-Bares, a NSF-LTER grant (DEB-1234162) to J. Cavender-Bares, and by iCORE/AITF (G224150012 & 200700172), NSERC (RGPIN-2015-05129), and CFI (26793) grants to J. Gamon, and a China Scholarship Council fellowship to R. Wang.

## 4.6 References

Ahl, V. and Allen, T. F. H. 1996. Hierarchy theory: A vision, vocabulary, and epistemology. - Columbia University Press.

Asner, G. P. 2013. Biological diversity mapping comes of age. - Remote Sens. 5: 374–376.

Asner, G. P. and Martin, R. E. 2009. Airborne spectranomics: mapping canopy chemical and taxonomic diversity in tropical forests. - Front. Ecol. Environ. 7: 269–276.

Asner, G. P. et al. 2008. Remote sensing of native and invasive species in Hawaiian forests. - Remote Sens. Environ. 112: 1912–1926.

Bonar, S. et al. 2010. An overview of sampling issues in species diversity and abundance surveys. - In: Magurran, A. E. and McGill, B. J. (eds), Biological Diversity: frontiers in measurement and assessment. Oxford University Press, pp. 376.

Cadotte, M. W. et al. 2008. Evolutionary history and the effect of biodiversity on plant productivity. - Proc. Natl. Acad. Sci. USA 105: 17012–17017.

Cadotte, M. W. et al. 2009. Using phylogenetic, functional and trait diversity to understand patterns of plant community productivity. - PLoS One 4: 1–9.

Cavender-Bares, J. et al. 2009. The merging of community ecology and phylogenetic biology. - Ecol. Lett. 12: 693–715.

Costanza, R. and Maxwell, T. 1994. Resolution and predictability: An approach to the scaling problem. - Landsc. Ecol. 9: 47–57.

Dahlin, K. M. 2016. Spectral diversity area relationships for assessing biodiversity in a wildland-agriculture matrix. - Ecol. Appl. 26: 2756–2766.

Díaz, S. et al. 2015. The global spectrum of plant form and function. - Nature 529: 167–171.

Féret, J.-B. and Asner, G. P. 2014. Mapping tropical forest canopy diversity using high-fidelity imaging spectroscopy. - Ecol. Appl. 24: 1289–1296.

Field, C. B. 1991. Ecological Scaling of Carbon Gain to Stress and Resource Availability.

Gamon, J. A. 2008. Tropical sensing — opportunities and challenges. - In: M, K. and GA, S.-A. (eds), Hyperspectral remote sensing of tropical and subtropical forests. CRC Press Taylor&Francis Group, pp. 297–304.

Gamon, J. A. et al. 2006. A mobile tram system for systematic sampling of ecosystem optical properties. - Remote Sens. Environ. 103: 246–254.

Gotelli, N. J. and Colwell, R. K. 2001. Quantifyinf biodiversity: procedures and pitfalls in the measurement and comparison of species richness. - Ecol. Lett. 4: 379–391.

Gould, W. 2000. Remote sensing of vegetation , plant species richness , and regional biodiversity hotspots. - Ecol. Appl. 10: 1861–1870.

Gustafson, E. J. 1998. Pattern : What is the state of the art? - Ecosystems 1: 143–156.

Helmus, M. R. et al. 2007. Phylogenetic measures of biodiversity. - Am. Nat. 169: E68-83.

Heywood, V. H. 1995. Global biodiversity assessment. - Cambridge University Press.

Jetz, W. et al. 2016. Monitoring plant functional diversity from space. - Nat. Plants 2: 16024.

John, R. et al. 2008. Predicting plant diversity based on remote sensing products in the semi-arid region of Inner Mongolia. - Remote Sens. Environ. 112: 2018–2032.

Kembel, S. W. et al. 2010. Picante: R tools for integrating phylogenies and ecology. - Bioinformatics 26: 1463–1464.

Legendre, P. and Legendre, L. 1998. Numerical Ecology. - Elsevier.

Lord, D. et al. 1985. Influence of wind on crop canopy reflectance measurements. - Remote Sens. Environ. 18: 113–123.

Lucas, K. and Carter, G. 2008. The use of hyperspectral remote sensing to assess vascular plant species richness on Horn Island, Mississippi. - Remote Sens. Environ. 112: 3908–3915.

Magurran, A. E. 2004. Measuring biological diversity. - Blackwell Publishing.

Magurran, A. E. and Dornelas, M. 2010. Biological diversity in a changing world. - Philos. Trans. R. Soc. Lond. B. Biol. Sci. 365: 3593–3597.

Marceau, D. J. and Hay, G. J. 1999. Contributions of remote sensing to the scale issue. - Can. J. Remote Sens. 25: 357–366.

Mittelbach, G. G. 2012. Biodiversity and ecosystem functioning. - In: Community Ecology. 1st ed.n. Sinauer Associates, Inc., pp. 41–62.

Naeem, S. et al. 2000. Plant diversity increases resistance to invasion in the absence of covarying extrinsic factors. - Oikos 91: 97–108.

Nagendra, H. 2001. Using remote sensing to assess biodiversity. - Int. J. Remote Sens. 22: 2377–2400.

Nagendra, H. 2002. Opposite trends in response for the Shannon and Simpson indices of landscape diversity. - Appl. Geogr. 22: 175–186.

O'Neill, R. V. and King, A. W. 1998. Homage to ST. Michael; Or, Why are there so many books on scale? - In: Peterson, D. L. and Parker, V. T. (eds), Ecological scale: Theory and applications. Columbia University Press, pp. 615.

O'Neill, R. V. et al. 1986. A Hierarchical concept of ecosystems. - Princeton University Press.

Oldeland, J. et al. 2010. Does using species abundance data improve estimates of species diversity from remotely sensed spectral heterogeneity? - Ecol. Indic. 10: 390–396.

Ollinger, S. V 2011. Sources of variability in canopy reflectance and the convergent properties of plants. - New Phytol. 189: 375–394.

Peet, R. K. 1974. The measurement of species diversity. - Annu. Rev. Ecol. Syst. 5: 285–307.

Pereira, H. M. et al. 2013. Essential biodiversity variables. - Science. 339: 277–278.

Rocchini, D. 2007. Effects of spatial and spectral resolution in estimating ecosystem α-diversity by satellite imagery. - Remote Sens. Environ. 111: 423–434.

Sanchez-Azofeifa, G. A. et al. 2009. Differences in leaf traits, leaf internal structure, and spectral reflectance between two communities of lianas and trees: Implications for remote sensing in tropical environments. - Remote Sens. Environ. 113: 2076–2088.

Schäfer, E. et al. 2016. Mapping tree species diversity of a tropical montane forest by unsupervised clustering of airborne imaging spectroscopy data. - Ecol. Indic. 64: 49–58.

Shannon, C. E. 1948. A mathematical theory of communication. - Bell Syst. Tech. J. 27: 379–423, 623–656.

Simpson, E. H. 1949. Measurement of diversity. - Nature 163: 688–688.

Srivastava, D. S. et al. 2012. Phylogenetic diversity and the functioning of ecosystems. - Ecol. Lett. 15: 637–648.

Tilman, D. et al. 2001. Diversity and productivity in a long-term grassland experiment. - Science. 294: 843–845.

Turner, W. 2014. Sensing biodiversity. - Science. 346: 301–303.

Turner, M. G. et al. 1989. Predicting across scales: Theory development and testing. - Landsc. Ecol. 3: 245–252.

Turner, W. et al. 2015. Free and open-access satellite data are key to biodiversity conservation. - Biol. Conserv. 182: 173–176.

Ustin, S. L. 2013. Remote sensing of canopy chemistry. - Proc. Natl. Acad. Sci. U. S. A. 110: 804–805.

Ustin, S. L. and Gamon, J. A. 2010. Remote sensing of plant functional types. - New Phytol. 186: 795–816.

Wang, R. et al. 2016a. Integrated analysis of productivity and biodiversity in a southern Alberta prairie. - Remote Sens. 8: 214.

Wang, R. et al. 2016b. Seasonal variation in the NDVI–species richness relationship in a prairie grassland experiment (Cedar Creek). - Remote Sens. 8: 128.

Whittaker, R. H. 1960. Vegetation of the Sisiyou Mountains, Orgeon and California. - Ecol. Monogr. 30: 279–338.

Whittaker, R. H. 1972. Evolution and measurement of species diversity. - Taxon 21: 213–251.

Williams, C. B. 1964. Patterns in the balance of nature and related problems in quantitative ecology. - Academic Press.

Woodcock, C. E. and Strahler, A. H. 1987. The factor of scale in remote sensing. - Remote Sens. Environ. 21: 311–332.

Wu, J. and Loucks, O. L. . 1995. From balance of nature to hierarchical patch dynamics : A paradigm shift in ecology. - Q. Rev. Biol. 70: 439–466.

Zanne, A. E. et al. 2014. Three keys to the radiation of angiosperms into freezing environments. - Nature 506: 89–92.

Zhang, Y. et al. 2012. Forest productivity increases with evenness, species richness and trait variation: A global meta-analysis. - J. Ecol. 100: 742–749.

# Chapter 5 Investigating the effect of species richness, evenness and composition on spectral diversity using simulated hyperspectral images


## Abstract

Biodiversity loss endangers ecosystem services that maintain human wellbeing. Many remote sensing metrics have been applied to estimate α biodiversity directly through spectral diversity. However, a better understanding of the mechanisms behind the spectral diversity-biodiversity relationship is needed, with a particular focus on the relative contributions of species composition, richness, and evenness. We studied how these three factors (species composition, richness, and evenness), affect the optical signals in a prairie ecosystem experiment at Cedar Creek Ecosystem Science Reserve, Minnesota. To achieve this, we used hyperspectral reflectance of 16 prairie species (collected using both a full-range field spectrometer fitted with a leaf clip, and an imaging spectrometer carried by a tram system) to simulate plot-level images with different species composition, richness and evenness. The coefficient of variation (CV) of spectral reflectance in space and spectral species obtained using a Partial Least Squares Discriminant Analysis (PLSDA) classification method were calculated as indicators of spectral diversity. Spectral diversity metrics (CV and spectral species indices) scaled with α diversity and were affected by species richness and evenness. At fine scales, species composition had a substantial influence on both CV and spectral species indices. These findings can be used to understand the effects of species richness, evenness, and composition on spectral diversity and to guide regional studies of biodiversity estimation using high spatial and spectral resolution remote sensing.


## 5.1 Introduction

The use of remote sensing to estimate biodiversity can be dated back to the late 1980s. The early applications of remote sensing in biodiversity estimation focused on mapping landscape or habitat through landcover classification. At that time little had been accomplished to understand or verify the statistical or ecological significance of the relationship between remotely sensed indices and biodiversity (Stoms and Estes 1993).

This was partly due to the limited understanding of the effects of biodiversity on ecosystem function and partly due to the limitation of remote sensing techniques (achievable spatial, spectral, and temporal resolution of remote sensing products) at the time.

Imaging spectrometry can now cover the whole range of the visible and short-wave infrared reflectance spectrum (400 – 2500 nm) at high spectral resolution (Ustin et al. 2004). This technology enables us to detect the absorption features of leaves in specific tiny bands and has been widely used in vegetation remote sensing in the past decades. Imaging spectrometry is expanding the range of detectable plant physiological and structural properties that can contribute to an assessment of functional diversity (Ustin and Gamon 2010). A key question remains the spatial resolution necessary for effective remote detection of biodiversity, which is a particularly complex question given the range of definitions, methods, and instruments used.

'Spectral diversity' (Palmer et al. 2002), sometimes called "optical diversity" (Ustin and Gamon 2010), indicates the variation in spectral reflectance detected by remote sensing. Vegetation optical properties are affected by both leaf biochemical traits and canopy structure (Ustin and Gamon 2010) that vary with evolutionary history and environment conditions. This variation of plant leaf traits and canopy structures across environmental gradients can lead to high spectral variability within species (Asner 1998). Therefore, instead of mapping species *per se*, spectral diversity detects functional and structural properties, which vary with species or functional groups ("optical types") (Ustin and Gamon 2010). If optical type is regarded not only as an indicator of plant physiological and biochemical properties but also of fundamental vegetation properties resulting from "ecological rules" driven by resource allocation, there should be predictable interrelationships among the plant traits and optical properties. As a consequence, variation in these optical properties and their associated traits in time and space might enable us to detect biodiversity through spectral diversity, particularly if appropriate spatial, temporal and spectral scales are used.

Many remote sensing metrics have been applied to assess α diversity using spectral diversity. These metrics can be divided into two major categories: 1) metrics based on

information theory (e.g., entropy) and 2) metrics based on classification results (e.g. spectral species). The information theory based metrics extract information from the spectral space in number of ways, for example by calculating the variance of vegetation reflectance indices (e.g., NDVI) (Gould 2000, Carlson et al. 2007), the coefficient of variation of the reflectance across space (Wang et al. 2016a), or the distance from the spectral centroid (Palmer et al. 2002). Alternatively, information theory metrics can be obtained from patterns in principal component space, such as the distance from the centroid in principal component space (Rocchini 2007), that compact spectral information and removes noise and band collinearity. In contrast to information theory, classification based metrics typically apply an unsupervised classification (Féret and Asner 2014) or object-based classification (Schäfer et al. 2016), to the remotely sensed images and relate the metrics calculated based on the resulting "spectral species" to actual biodiversity metrics. In this case, spectral types (optical types) are considered proxies for biological species, and spatial variation in these types can be used to infer species richness or other similar metrics of α diversity.

When comparing optical diversity to α diversity, stronger relationships emerge when considering both species richness and evenness (e.g., Shannon's index) (Oldeland et al. 2010, Wang et al. 2016a). These results indicate that incorporating measures of evenness can improve the correlation between spectral diversity and conventional diversity metrics, presumably because species evenness adds additional information on stand composition beyond species richness *per se*., and this information is also detected by spectral variation. Consequently, spectral diversity relates to the heterogeneity within a small region that is determined by a combination of species composition, richness and evenness, and often provides a measure of α diversity. However, it is still not clear exactly how or to what degree species composition, richness, and evenness, affect the overall optical signals, in part because experimental approaches are difficult to apply in remote sensing studies due to the large spatial scales involved.

In this study, we applied a modeling framework to investigate the effect of species richness, evenness and composition on spectral diversity using simulated hyperspectral images. Leaf reflectance measurements collected from the Cedar Creek BioDIV

experimental prairie plots were used to simulated synthetic plot-level images with different combinations of species richness, evenness, and composition. In this modeling experiment, leaf spectra were collected two ways: 1) using a leaf clip that normalized sampling geometry and illumination and 2) using an imaging spectrometer that allowed for natural variation in leaf orientation and illumination. Two types of spectral diversity metrics, coefficient of variation (CV) and metrics calculated based on a Partial Least Squares Discriminant Analysis (PLSDA) classification method, were used to compare to the conventional diversity metrics. This simulation approach applied the field reflectance as input data and allowed us to investigate the spectral diversity-biodiversity relationship by isolating factors contributing to the overall optical signal that was not possible from empirical measurements alone.

## 5.2 Methods

### 5.2.1 Study site

The field data used in this study were collected at the Cedar Creek Ecosystem Science Reserve, Minnesota, US (45.4086° N, 93.2008° W). The BioDIV experiment has maintained 168 prairie plots (9 m × 9 m) with nominal plant species richness ranging from 1 to 16 since 1994 (Mittelbach 2012). The species planted in each plot were originally randomly selected from a pool of 18 species typical of Midwestern prairie, including $C_3$ and $C_4$ grasses, legumes, forbs and trees. Weeding is done 3 to 4 times each year for all the plots to maintain the planted species richness (Tilman et al. 2001, Reich et al. 2012).

### 5.2.2 Spectral data

Leaf-clip derived reflectance

A full range spectrometer (HR-1024i, Spectral Vista Corporation, Poughkeepsie, NY, USA) coupled with a leaf clip with internal light source (LC-RP PRO; Spectra Vista Corporation, Poughkeepsie, NY, USA) was used to collect leaf reflectance spectra for 16 prairie species in Cedar Creek BioDIV plots in the summer, 2015. The spectral range of the spectrometer was from 400 to 2400 nm. Scans were referenced to the white calibration disc (Spectralon, LabSphere, North Sutton, NH) before the target

measurements to calculate surface reflectance. The reflectance at each wavelength was calculated as:

$$\rho_\lambda = \frac{(DN_{leaf,\lambda} - DN_{dark,\lambda})}{(DN_{white\ reference,\lambda} - DN_{dark,\lambda})} \quad (5.1)$$

where $DN_{leaf,\lambda}$ and $DN_{white\ reference,\lambda}$ indicate the reflected energy of leaf and white reference measured at wavelength ($\lambda$, in nm), respectively. $DN_{dark,\lambda}$ indicates the measured energy when the shutter was closed (dark-current and noise). Spectral data processing also included correcting artifacts at the sensor overlap regions between the Si and first InGaAs sensors (around 1000 nm), and the first InGaAs and second InGaAs sensors (around 1890 nm), respectively, interpolating the data to 1 nm spectral resolution. Noisy regions at the beginning and end of the spectrum, i.e. wavelengths smaller than 400 nm and greater than 2400 nm, were excluded from analysis. All processing was done using the R package spectrolab (https://github.com/annakat/spectrolab) and all the processed spectral data can be found on EcoSIS (http://data.ecosis.org).

24 9 x 9 m plots were selected to obtain leaf reflectance measurements. Within each plot, between 4 and 8 quadrats were sampled based on the expected diversity of the plot. Within each quadrat, four individuals were sampled, but some of those individuals could be of the same species if there were fewer than four species in the quadrat. For those quadrats that had less than 4 species, the choice of which species to 'duplicate' was dependent on relative dominance. Consequently, the number of individuals of each species measured was dependent on the number of plots in which that species was found, the number of other species in those plots, and the relative dominance of that species in those plots. Generally, the sample size of one species correlated with commonness of that species. A pool of leaf clip-derived spectra of the 16-species (Table 5.1) was created using all the measurements and prepared for further analysis. Soil radiance spectra were collected using a full range spectrometer (PSR 3500, Spectral Evolution, Lawrence, MA, USA) in BigDIV bare ground plots in July 2016. A white reference panel (Spectralon, Labsphere, North Sutton, NH, USA) was used to calculate the soil reflectance.

Table 5.1 Species, abbreviations, and sample size per species of leaf reflectance spectra

| Species | Abbrev | No. of samples |
|---|---|---|
| *Achillea millefolium* | ACHMI | 134 |
| *Amorpha canescens* | AMOCA | 88 |
| *Andropogon gerardii* | ANDGE | 577 |
| *Asclepias tuberosa* | ASCTU | 249 |
| *Koeleria cristata* | KOECR | 44 |
| *Lespedeza capitata* | LESCA | 370 |
| *Liatris aspera* | LIAAS | 195 |
| *Lupinus perennis* | LUPPE | 380 |
| *Monarda fistulosa* | MONFI | 74 |
| *Panicum virgatum* | PANVI | 169 |
| *Petelostemum candidum* | PETCA | 88 |
| *Petalostemum purpureum* | PETPU | 157 |
| *Petalostemum villosum* | PETVI | 137 |
| *Poa pratensis* | POAPR | 49 |
| *Schizachyrium scoparium* | SCHSC | 260 |
| *Solidago rigida* | SOLRI | 173 |

Image-derived reflectance

A push broom imaging spectrometer (E Series, Headwall Photonics Inc., Fitchburg, MA, USA) mounted on a tram system (Gamon et al. 2006) was used to collect fine-scale images of the northern-most row of each sampling plot at peak season, 2015 (Figure 5.1a). A speed control circuit was added to the tram cart to maintain a slow and constant moving speed, creating high-fidelity images. The cart speed (0.0256 m/s) allowed us to build clear, high signal-to-noise ratio (SNR) hyperspectral images under low wind-speed

conditions. Typically, wind can affect the field reflectance measurements, especially in canopies with a high vertical structure (Lord et al. 1985). Excessive plant sway caused by strong wind can blur the image, which will alter the vegetation optical properties and degrade the spatial resolution in subsequent analysis, possibly affecting the study results. Consequently, only low-wind conditions were used in our analyses. To reduce wind artifacts on windy days, a wind screen consisting of black cloth was placed on 2-3 sides of the sampling plot, at least 1 meter from the sampling area. Data were manually evaluated to further remove any windy (blurred) images.

The imaging spectrometer provided hyperspectral images with a 3-nm spectral resolution (Full Width at Half Maximum, FWHM) and a 0.65 nm spectral sampling interval over the 400 ~ 1000 nm range. The focal length of the lens was 17 mm with a field of view (FOV) of ~34°. The spectrometer was mounted 3 meters above ground surface, obtaining a ground pixel size of approximately 1 $mm^2$ (Figure 5.1b). The dimension of the raw image was 1600 x 1000 pixels (Figure 5.1b). Subsequent image processing avoided 1 m from either end of the plot, and removed 600 x 1000 pixels from the north side to minimize edge effects, yielding a final image size of 1 x 1 m (Figure 5.1b).

A dark file ($DN_{dark,\lambda}$) was obtained before each measurement by covering the lens of the spectrometer with a black lens cap. Scans of a white reference calibration panel (Spectralon, Labsphere, North Sutton, NH, USA) were taken before and after ground target measurements to calculate surface reflectance.

The same 16 species with the SVC field spectrometer measurements were identified from the Headwall images and a sample of 1000 leaf pixels of each species was taken to create a pool of image-derived reflectance spectra. Unlike the pool of leaf clip-derived measurements, where leaf spectra were collected with normalized geometry and illumination the pool of image-derived spectra provided a sample of leaves in their natural orientation and illumination, collectively comprising a “canopy” spectrum for each species. This set of image-derived leaf spectra allowed us to explore the effect of including natural variation in leaf reflectance due to illumination and geometry for comparison with leaf clip-derived spectra. Soil reflectance spectra were extracted from the bare ground images of low richness plots.

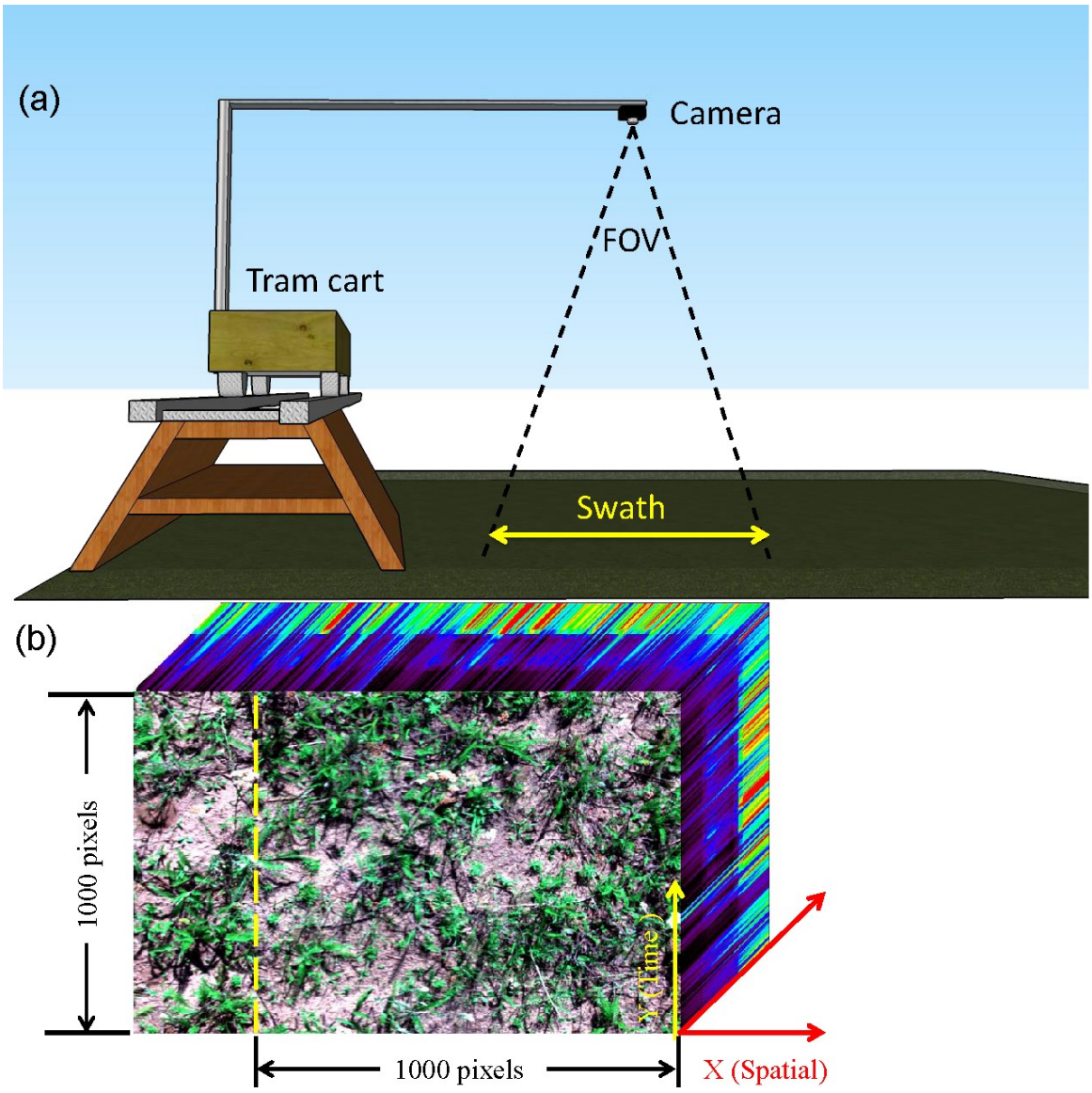


Figure 5.1. Schematic picture of Headwall imaging spectrometer on the tram (a) and sample image (b) showing spatial and spectral dimensions (arrows). Yellow vector in panel b indicates direction of cart motion

### 5.2.3 Spectral variability

Two metrics were calculated to test the spectral separability among species. First, species spectral variation was estimated using the Euclidean distance between each spectrum and was tested based on the null hypothesis that the within- and among- species variation are

equal with a nonparametric multivariate analysis of variance technique (NPMANOVA), which was first developed for use with ecological distance matrices (Anderson 2001). A pseudo ratio of *F*-statistics was calculated as the ratio of among species and within species sum of squares (Anderson 2001). The larger the *F* value, the more likely that the null hypothesis ($H_0$, of no difference between species) is false. The Euclidean distance between two spectra ($S_1$ and $S_2$), is simply the root mean square difference between them, averaged over the whole spectral range:

$$d = \left[\frac{1}{N}\sum_{i=1}^{N}[S_1(\lambda_i) - S_2(\lambda_i)\,]^2\right]^{1/2} \tag{5.2}$$

where $N$ is the number of wavelength and $\lambda_i$ indicates the $i^{th}$ wavelength.

Second, a Partial Least Squares Discriminant Analysis (PLSDA) classification method (Karlsson 2006) was applied to the two spectral pools. PLS has been gaining attention for its ability to accommodate high-dimensional classification problems because it can handle large dataset and high collinearity among predictors (Nguyen and Rocke 2002, Chung and Keles 2010). In this study, the PLSDA classification was calculated with the caret R package (Kuhn 2016). Each dataset was randomly split into 2/3 training and 1/3 testing sets. The training set was used to train and optimize the classification model, while the testing set was used to validate the optimized classification model. The confusion matrix for the actual and predicted species identities was calculated to assess the overall accuracy of the classifier.

### 5.2.4 Generation of plot-level synthetic images

The species-abundance relationship was calculated on a vegetation percent cover base using plot-level vegetation percent cover data of the 168 prairie plots that had been collected in July 2007. In these analyses, percent cover of each species within 2 marked quadrats (0.5 x 0.5 m) inside each larger 9 x 9 m plot was recorded, and assumed to represent plot-level cover values. We calculated the mean and standard deviation of

vegetation cover at each planted species richness level. Linear relationships between mean and standard deviation of vegetation percent cover and planted species richness were created and applied to parameterize a Gaussian function to simulate plot-level vegetation percent cover at each richness levels. These richness-vegetation cover relationships were then used to generate the vegetation cover of each simulated plot according to its assigned species richness.

We simulated 1000 plots by following three steps: a) assign a species richness number for each plot randomly; b) calculate the vegetation percent cover of each simulated plot according to the estimated Gaussian distributed species richness-percent cover relationship at each richness level; c) generate the percent cover of each species randomly with the total percent cover equal to the percent cover of this plot. Two synthetic images were created for each plot: first, using the mean reflectance of each species, which ignored the within-species variation and second, using all the sampled reflectance. Both leaf clip- and image-derived reflectance were used to generate synthetic images, allowing us to explore the effect of within-species spectral variability due to varying leaf orientation and illumination. The total pixel number of each synthetic image was 10, 000. Soil reflectance spectra were used to fill the rest of each image other than reflectance of prairie plants according to the relative vegetation percent cover. The effects of soil spectra on the plot-level spectral diversity were tested separately.

### 5.2.5 Spectral diversity and conventional metrics

We calculated two categories of spectral diversity metrics for each simulated plot-level image: (a) CV that relates to the information content or "complexity" of each plot (Rocchini et al. 2010, Wang et al. 2016a). (b) spectral diversity calculated based on the classified spectral types using the PLSDA classification. For all the simulated plots, spectral species richness, Shannon's index and Simpson's index were also calculated based on the classification results.

Three conventional diversity indices that weighted species abundance by relative vegetation percentage cover were calculated and related to the spectral diversity metrics:

Shannon's index (Shannon 1948), reciprocal of Simpson's index (Simpson 1949, Williams 1964), and species evenness (Pielou 1966) (Table 5.2). Shannon's Index expresses the equitability of all the species while Simpson's Index focuses on a few dominant species (Whittaker 1972).

Table 5.2 Summary of conventional diversity metrics used in this study

| Diversity Metric | Description / Equation |
|---|---|
| Species richness (*S*) | Number of species in each simulated plot |
| Shannon's Index (*H'*) | $H' = -\sum p_i * \ln(p_i)$ |
| Simpson's Index (*D*) | $D = 1/\sum {p_i}^2$ |
| Evenness (*J'*) | $J' = H'/\ln(S)$ |

where $p_i$ is percent cover proportion of the number $i^{th}$ species.

Figure 5.2 summarizes the methods used in this study, CV and PLSDA represent two categories of spectral diversity metrics (information-based and classification-based). Leaf clip-derived reflectance focused on the spectral variations mainly driven by the physical and chemical properties under normalized illumination, while image-derived reflectance also considered the illumination conditions and orientations of different leaves.

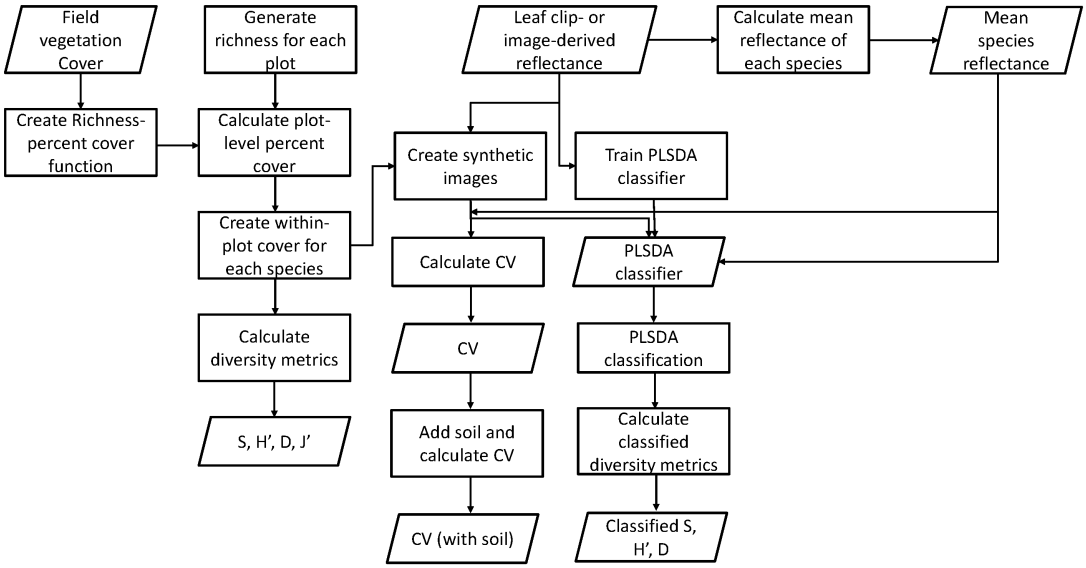


Figure 5.2 Experimental design and data used in this study. The two categories of spectral diversity metrics, coefficient of variation (CV) of spectral reflectance in space and spectral species obtained using partial least square discriminant analysis (PLSDA) classification, were used to relate to the biodiversity metrics, including species richness (*S*), Shannon's Index (*H'*), Simpson's Index (*D*), and evenness (*J'*).

## 5.3 Results

### 5.3.1 Reflectance and spectral variability

5.3.1.1 Reflectance

Leaf clip-derived reflectance of the 16 prairie species showed typical properties of vegetation spectra (Figure 5.3): absorption of blue and red light by chlorophyll and other pigments, high reflectance in the near infrared due to the multiple scattering, weak NIR water absorption features near 980 and 1200 nm, and strong water absorption near 1400 and 1900 nm (Roberts et al. 2004, Ustin et al. 2009). Image-derived reflectance covered the visible-NIR region with higher spectral sampling intervals and showed similar patterns to the leaf clip-derived measurements in the visible region but had larger variations in the NIR region resulting from varying leaf angles and illumination (Figure 5.3).

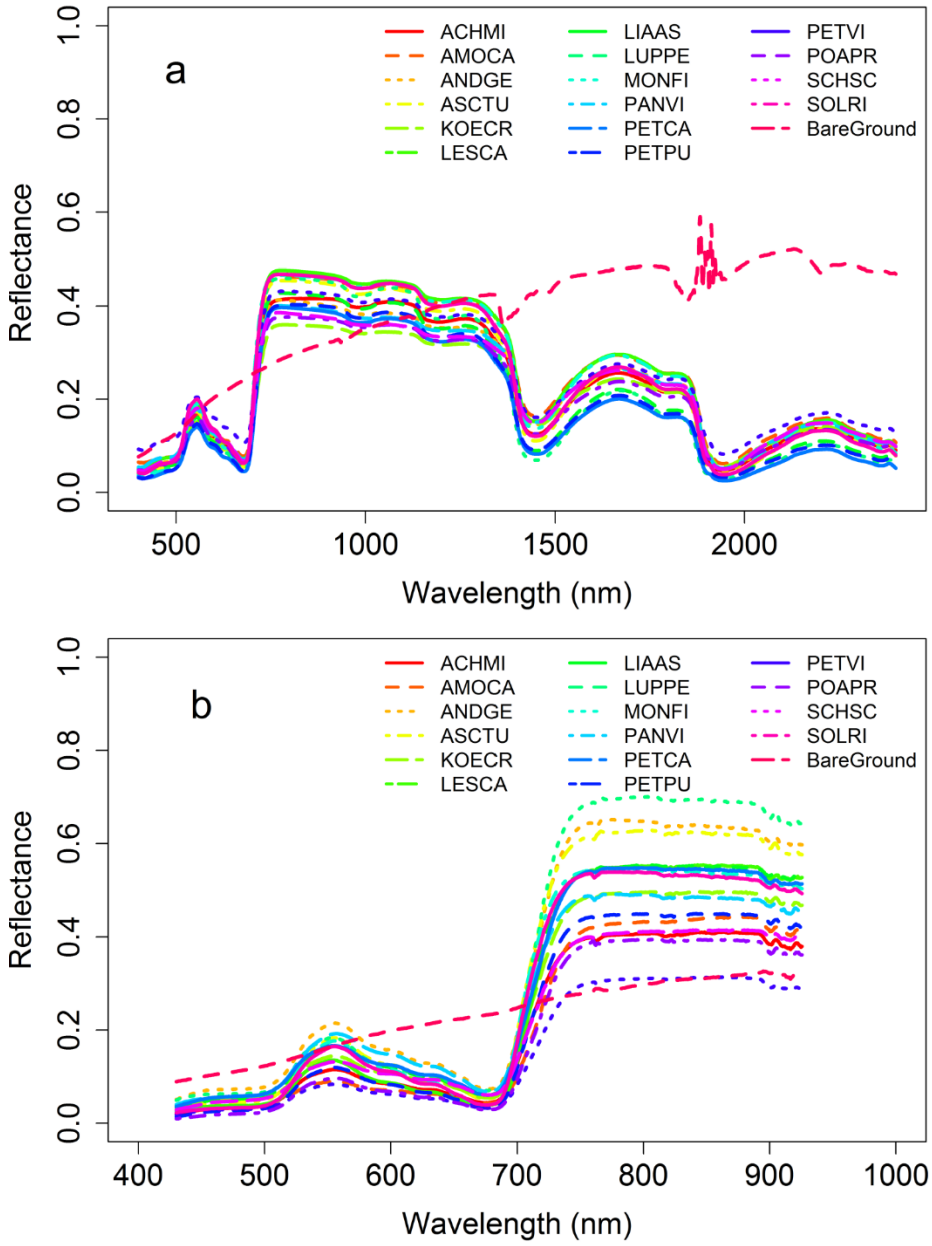


Figure 5.3 Mean reflectance spectra of prairie species used in this study. a: Leaf clip-derived reflectance: leaf reflectance obtained with a portable spectrometer (HR-1024i, Spectral Vista Corp., Poughkeepsie, NY) (400 – 2400 nm) and leaf clip (LC-RP PRO; Spectra Vista Corp., Poughkeepsie, NY); b: Image-derived leaf reflectance: leaf reflectance extracted from images measured with an imaging spectrometer mounted on a tram (E Series, Headwall Photonics Inc., Fitchburg, MA) (400 – 1000 nm).

Considerable variation within each species was found by both reflectance sampling methods. The leaf clip-derived measurements (Figure 5.4a) normalized illumination and sampling geometry, and were restricted to large and mature leaves since smaller leaves could not cover the clip's fiber probe. The image-derived measurements (Figure 5.4b) incorporated canopy structure to some extent by including leaves with different angles under different illumination conditions. Therefore, the image-derived measurements led to larger reflectance variations that were largely due to the variation in illumination and sampling geometry both among different species and among individuals within the same species (see Table S5.1 in *Appendices* for the within-species variations of each species).

Within-species variation varied between leaf clip-derived and image-derived reflectance (Table S5.1 in *Appendices*). *Amorpha canescens* had the largest within-species variation for the leaf clip-derived data, while *Petalostemum villosum* had the largest within-species distance for the image-derived data. The large within-species variation for *Petalostemum villosum* captured by image-derived reflectance presumably reflected both leaf properties and canopy architecture, incorporating complex scattering properties of adjacent plant tissues (e.g., branches and flowers).

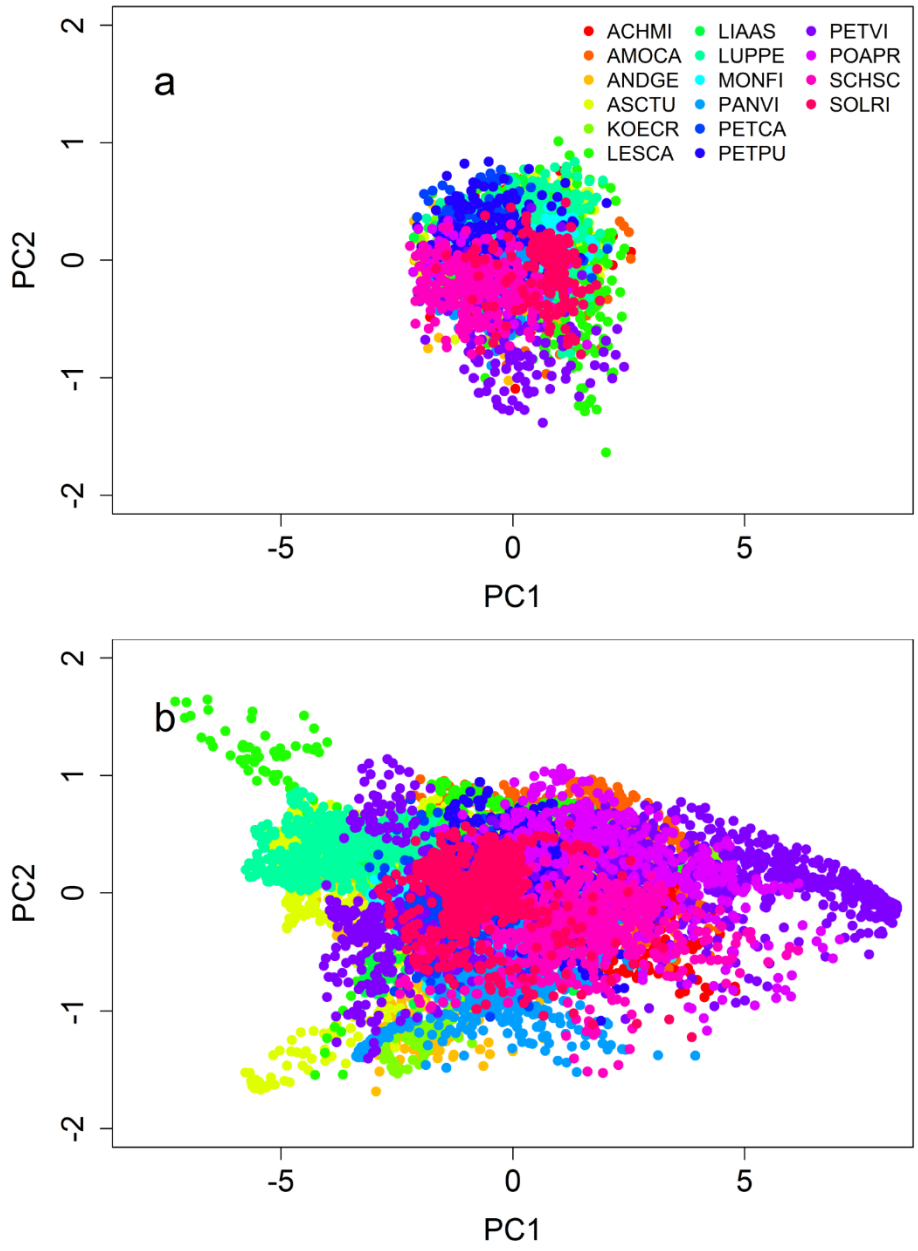


Figure 5.4 The distribution of different species within a principal component space: (a) leaf clip-derived reflectance and (b) Image-derived reflectance. Axes are the first and second principal components.

5.3.1.2 Spectral distance

Spectral separability of species can be successful if a high statistical distance exists between different species in the feature space and if the within- species variation is less

than among- species variation (Clark et al. 2005). In this study, among-species variability was greater than within-species variability for both leaf clip-derived and image-derived measurements (Table 5.3) when using Euclidean distance as the spectral variability metric. A slightly larger *F*-ratio was achieved when using the full range spectra than visible-NIR spectra with leaf clip-derived measurements, indicating that full range spectra increased the species spectral separability, presumably by adding additional information on leaf structure, water, and biochemical content. The greater separation of species with image-derived spectra was presumably due to the standardized illumination and geometry of the leaf clip-derived measurements among individuals, which removed spectral variation contributed by canopy structure and illumination. This result indicated that including the variations in canopy structure, e.g. LAI, and leaf-angle distributions can increase species separability.

#### 5.3.1.3 Classification of prairie species

Most of the prairie species could be classified with the PLSDA classification and the classification accuracy varied with method and spectral range. Generally, a higher accuracy was achieved with leaf clip-derived measurements than with image-derived measurements (Table 5.3). When all spectra were included, the overall accuracy of classification using leaf clip-derived data was 0.77 for using visible and NIR wavelengths and 0.80 for using all the bands (400 to 2400 nm). The major classification errors occurred with the several graminoid species (*Poa pratensis, Andropogon gerardi* and *Panicum virgatum*; data not shown). For the leaf clip-derived reflectance, using full range spectra increased the classification accuracy, indicating that including information in the SWIR wavelengths increased the species separability. When the mean reflectance of each species was used instead of all individual spectra to test the PLSDA classifier, the classification accuracy of leaf clip-derived measurements declined to 0.69 using either visible-NIR wavelengths or full spectra. The overall classification accuracy for image-derived measurements was 100% (1) when using mean spectra only, and 0.73 when using all spectra. When using leaf clip data, all samples improved results over mean spectra

alone, but this was not true for the image-derived data, where mean spectra yielded 100% classification accuracy.

Table 5.3 Non-parametric multivariate analysis of variance (NPMANOVA), comparing between- and within-species spectral variation using Euclidean distance and overall accuracy of PLSDA classification

| Spectral region | Bands | *F* ratios | PLSDA Accuracy |
|---|---|---|---|
| Leaf clip-derived Visible-NIR (mean Ref) | 601 | - | 0.69 |
| Leaf clip-derived Visible-NIR (all samples) | | 133.06 | 0.77 |
| Leaf clip-derived full spectra (mean Ref) | 2001 | - | 0.69 |
| Leaf clip-derived full spectra (all samples) | | 188.94 | 0.80 |
| Image-derived Visible-NIR (mean Ref) | 762 | - | 1 |
| Image-derived Visible-NIR (all samples) | | 694.94 | 0.73 |

### 5.3.2 Plot-level percent cover

This modeling scheme allowed us to simulate any species richness from 1 to 16 by interpolation between the planted richness values (1, 2, 4, 8, and 16) and by simulating the field vegetation percent cover measurements. In our study, plots with higher species richness levels generally had higher vegetation percent cover (Figure 5.5 a), as has previously been noted (Wang et al. 2016b). Species composition had a large effect on the vegetation percent cover, especially in the plots of medium richness levels (Figure 5.5 b). For example, some species led to a relative high vegetation percent cover when the number of individuals was high, e.g., *Amorpha canescens* and *Petalostemum purpureum*, while some graminoid species, e.g., *Asclepias tuberosa*, *Koeleria cristata*, and *Andropogon gerardii* had a low vegetation percent cover (data not shown).

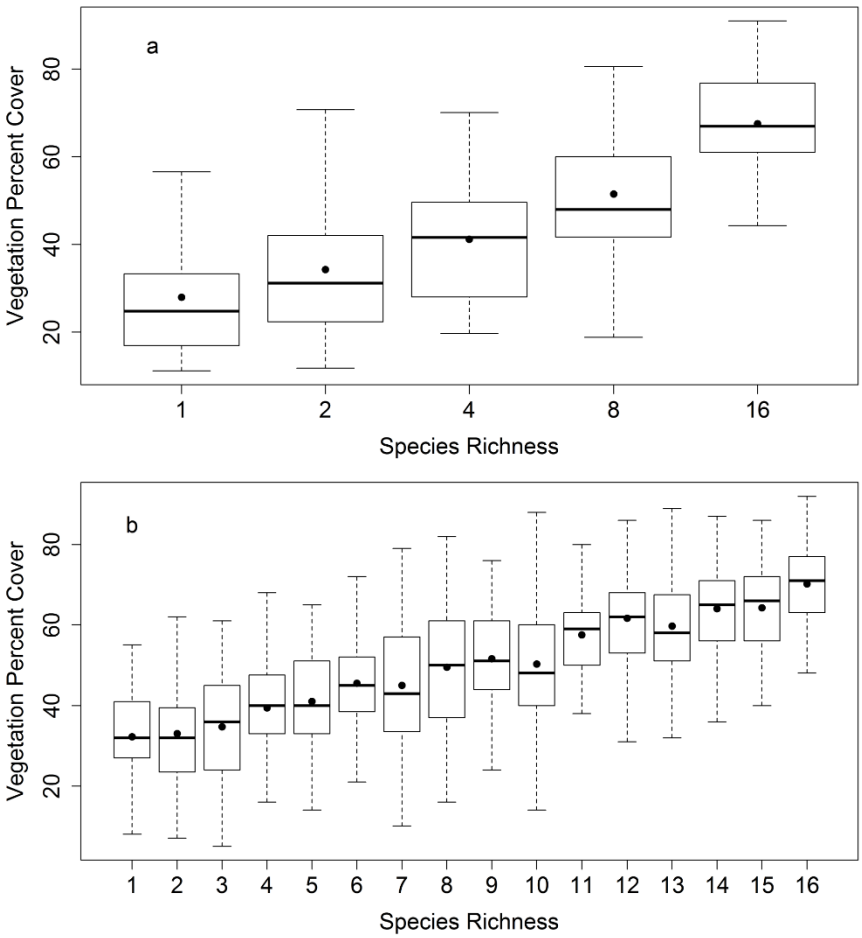


Figure 5.5 Measured (a) and simulated (b) vegetation percent cover at different species richness levels in the prairie plots. Linear relationships of mean and standard deviation of vegetation percent cover and species richness were created with the field measurements in 2007 (illustrated in panel a) and applied to parameterize a Gaussian function to simulate plot-level vegetation percent cover at each richness levels (illustrated in panel b).

### 5.3.3 Spectral diversity

5.3.3.1 CV

In accordance with larger spectral distance captured by image-derived reflectance (relative to leaf-clip-derived reflectance), the plot-level CV values calculated with image-derived reflectance had a larger range than CV calculated with leaf clip-derived

reflectance. When the mean reflectance spectrum of each species was used to simulate the plots, a weak but significant relationship was found between plot level CV and species richness (Table 5.4). The linear relationship between CV and diversity metric was improved by including species evenness (Shannon's Index and Simpson's Index) rather than calculating species richness alone, and CV showed the strongest linear relationship with Shannon's Index (Table 5.4).

Table 5.4 Slopes (and coefficient of determination, $R^2$) of regressions between coefficient of variation (CV) and conventional diversity metrics (species richness (*S*), Shannon's Index (*H'*), Simpson's Index (*D*), and evenness (*J'*)) for different sampling methods and spectral ranges. Significant codes: NS, $0.05 < p$, *, $0.01 < p < 0.05$, **, $0.001 < p < 0.01$ and ***, $P < 0.001$. Parameters were not shown for non-significant relationships.

| | Mean Reflectance (No Soil) | | | Full Sample (No Soil) | | | Full Sample (with Soil) | | |
|---|---|---|---|---|---|---|---|---|---|
| | Leaf clip-derived (visible-NIR) | Leaf clip-derived (full range) | Image-derived (Visible-NIR) | Leaf clip-derived (visible-NIR) | Leaf clip-derived (full range) | Image-derived Visible-NIR) | Leaf clip-derived (visible-NIR) | Leaf clip-derived (full range) | Image-derived (Visible-NIR) |
| *S* | 0.0041 | 0.0044 | 0.0067 | 0.002 | 0.0023 | 0.003 | -0.001 | 0.0039 | 0.006 |
| | (0.27***) | (0.25***) | (0.18***) | (0.11***) | (0.14***) | (0.01***) | (0.06***) | (0.25***) | (0.18***) |
| *H'* | 0.031 | 0.055 | 0.082 | 0.022 | 0.029 | 0.03 | NS | 0.025 | 0.038 |
| | (0.52***) | (0.51***) | (0.37***) | (0.23***) | (0.30***) | (0.03***) | | (0.15***) | (0.09***) |
| *D* | 0.05 | 0.016 | 0.024 | 0.007 | 0.0094 | 0.01 | NS | 0.0057 | 0.007 |
| | (0.51***) | (0.31***) | (0.22***) | (0.16***) | (0.21***) | (0.02***) | | (0.05***) | (0.02***) |
| *J'* | 0.11 | 0.12 | 0.19 | 0.05 | 0.064 | 0.1 | 0.009 | NS | NS |
| | (0.37***) | (0.37***) | (0.32***) | (0.18***) | (0.22***) | (0.04***) | (0.01**) | | |

When estimating optical diversity via CV, adding within-species variation by using the full set of sample spectra instead of the mean spectrum for each species increased the CV values and weakened the relationships between CV and conventional diversity metrics (Table 5.4 and Figure 5.6). For the image-derived reflectance, the linear relationships between CV and diversity metrics almost disappeared. An analysis of covariance (ANCOVA) showed that the shapes of CV-Shannon's Index relationships were changed by including within-species variation ($p < 0.001$).

Leaf clip derived CV showed stronger relationships with diversity metrics than image-derived CV (Table 5.4). When the full set of sample reflectance were used, using full range leaf clip reflectance led to stronger CV-biodiversity relationships than using visible-NIR wavelength leaf clip reflectance. The slope of the CV-diversity relationship increased with increasing spectral distance captured by different sampling methods and spectral ranges (leaf clip derived visible-NIR < leaf clip-derived full range < image-derived) (Figure 5.6).

Adding soil spectra in the simulation had substantial effects on the plot level CV (Figure 5.6), and greatly reduced the correlation with conventional biodiversity metrics (S, H', D, and J'). When using the mean reflectance of each species, including soil in the simulation increased the plot level CV dramatically (approx. 500 times) and eliminated all the CV-biodiversity relationships, indicating a confounding effect of soil on the ability to detect alpha diversity. When using the full set of spectral samples rather than the mean spectra alone, adding soil increased CV values and weakened the CV-biodiversity relationships (although relationships with S, H' and D were still significant when using full-range leaf clip spectra or image-derived spectra). No significant relationships were found between Shannon's index, Simpson's index and CV calculated using the visible-NIR wavelengths of leaf clip-derived reflectance after including soil spectra. Image-derived CV was less sensitive to the inclusion of soil than the leaf clip-derived CV (Table 5.4, Figure 5.6). The effect of including soil on degrading the CV-biodiversity relationships is clearly visible in Figure 5.6. These results revealed that the degree of cover and bare soil also affected the information based spectral diversity metrics and their ability to detect alpha diversity.

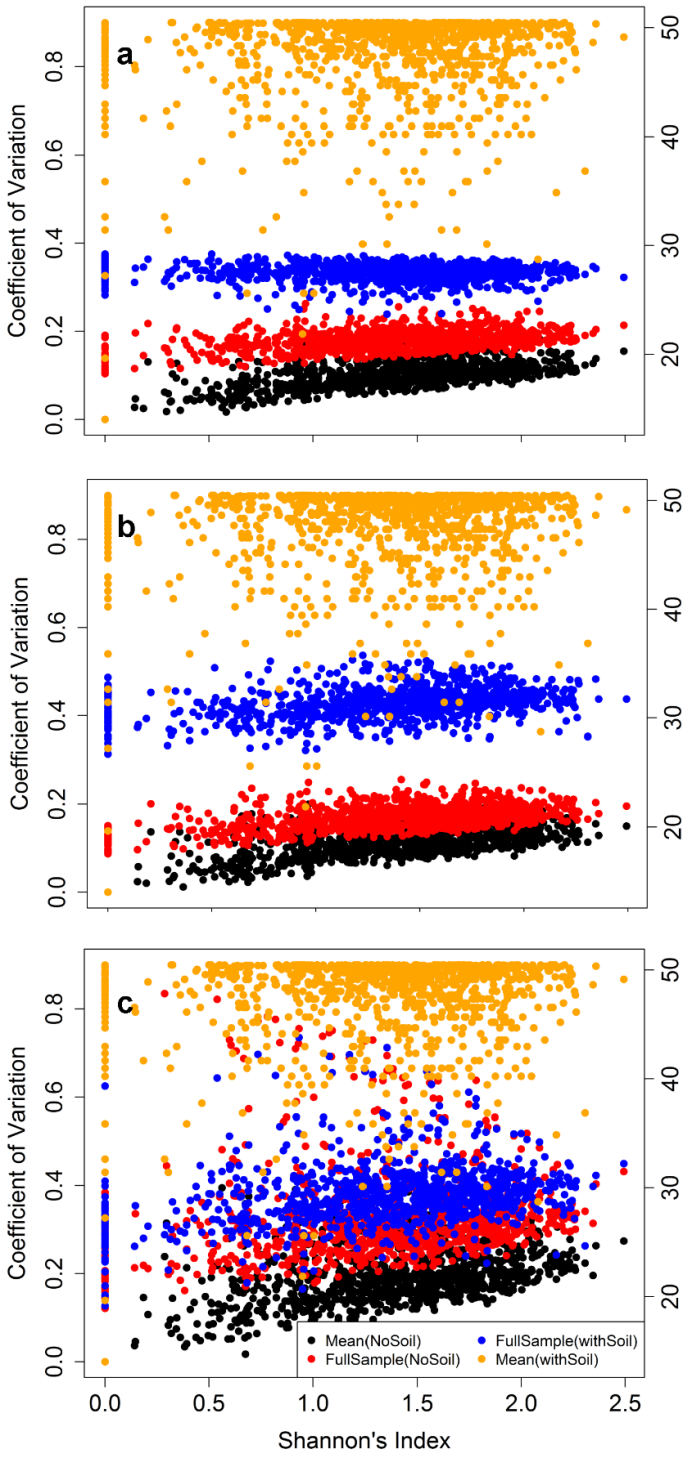


Figure 5.6 Coefficient of variation-Shannon's index relationships from the simulated plots. a: Leaf clip-derived (visible-NIR); b: Leaf clip-derived (full range); c: Image-derived. The mean reflectance spectra (with soil) CV (Orange points) were drawn on the right Y-axis.

To test the separate contributions of richness and evenness to CV, we plotted CV as a function of both species richness and evenness (Table 5.5 and Figure 5.7). Generally, CV scaled with increasing species richness and evenness (Figure 5.7). The shape of the full sample CV-richness-evenness surfaces confirmed that both species richness and evenness affected the optical signal (Figure 5.7). No statistically significant interaction between richness and evenness was found with leaf clip-derived CV. On the other hand, a weak interaction between richness and evenness was found with image-derived CV, indicating that the effect of species richness on CV varied slightly with evenness. (Table 5.5).

Leaf clip-derived CV and image-derived CV showed different patterns at the low richness but high evenness region (Figure 5.7). For the leaf clip-derived reflectance, CV values were lower at low richness than high richness at a given evenness. For the image-derived reflectance, however, large CV values were often found at the low richness plots and the largest CV values occurred at one of the low richness plot (richness = 2). The large CV values obtained by the image-derived reflectance indicated that the species identities also affected the spectral diversity.

Table 5.5 ANOVA results of CV-richness and evenness relationships. The CV-richness and evenness relationships were plotted in Figure 5.7.

| Measurement | Diversity Metric | Mean Sum of Qquares | *F* Value |
|---|---|---|---|
| Leaf clip-derived VISNIR Mean Reflectance | Richness | 0.372 | $598.453^{***}$ |
| | Evenness | 0.389 | $626.353^{***}$ |
| | Richness:Evenness | 0.00091 | $1.464^{NS}$ |
| Leaf clip-derived VISNIR Full Sample | Richness | 0.0680 | $146.708^{***}$ |
| | Evenness | 0.0833 | $179.720^{***}$ |
| | Richness:Evenness | 0.000371 | $0.800^{NS}$ |
| Leaf clip-derived Full Spec Mean Reflectance | Richness | 0.435 | $531.219^{***}$ |
| | Evenness | 0.48 | $585.919^{***}$ |
| | Richness:Evenness | 0.00042 | $0.514^{NS}$ |
| Leaf clip-derived Full Spec Full Sample | Richness | 0.114 | $198.089^{***}$ |
| | Evenness | 0.145 | $250.608^{***}$ |
| | Richness:Evenness | 0.0018 | $3.1163^{NS}$ |
| Image-derived Mean Reflectance | Richness | 0.976 | $323.54^{***}$ |
| | Evenness | 1.365 | $452.47^{***}$ |
| | Richness:Evenness | 0.0405 | $13.44^{***}$ |
| Image-derived Full Sample | Richness | 0.143 | $13.529^{***}$ |
| | Evenness | 0.376 | $35.501^{***}$ |
| | Richness:Evenness | 0.0881 | $8.319^{**}$ |

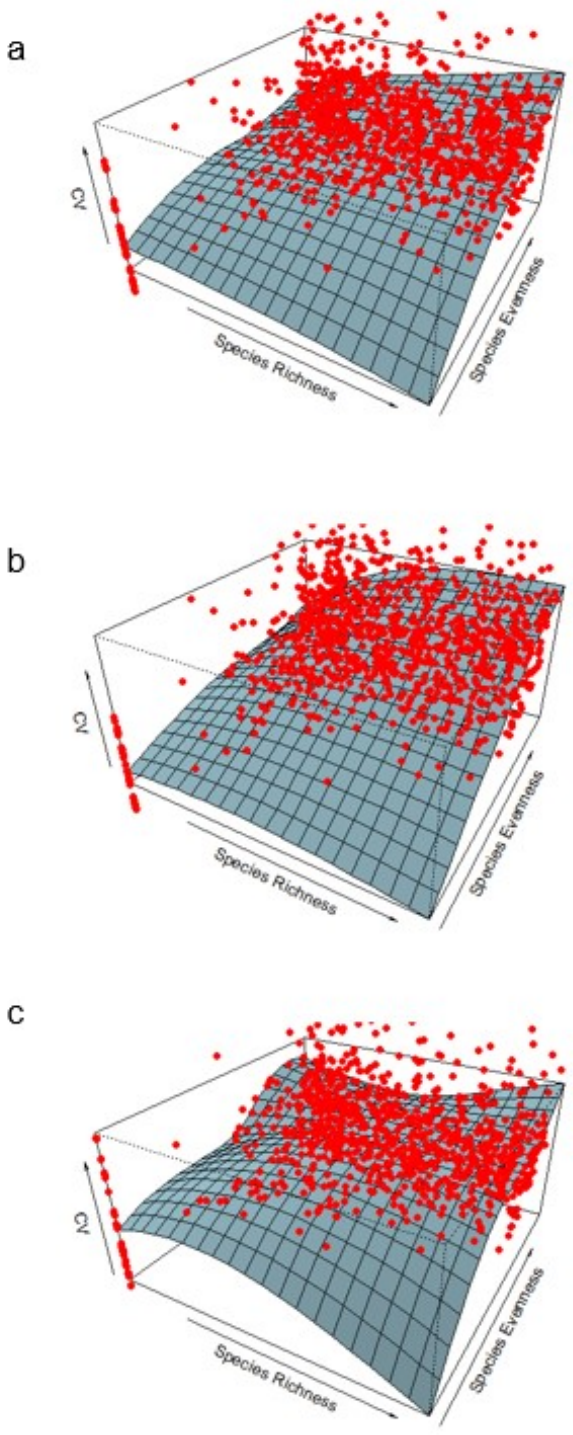


Figure 5.7 CV calculated using full set of sample reflectance spectra as a function of species richness and evenness. A Local Polynomial Regression Fitting method was used to fit the 3D surface. a: Leaf clip-derived (visible-NIR); b: Leaf clip-derived (full spectral range); c: Image-derived. The ANOVA results of CV-richness and evenness relationships were summarized in Table 5.5.

To understand why low richness plots sometimes had high CV with the image-derived measurements, we separated the image-derived CV into two categories (CV larger and less than 0.5) presuming that another mechanism besides species richness and evenness affected the spectral diversity. There was no clear relationship between CV and Shannon's index when all the image-derived data were used. However, two contrasting and significant relationships emerged between CV and Shannon's index for the two categories after the data division (Table 5.6 and Figure 5.8). For most the data, CV increased with increasing Shannon's index, while a small portion of data showed decreasing CV with increasing Shannon's index. Further exploration revealed that *Petalostemum villosum* that has the largest within-species variation among all the species was largely responsible for this effect. The deceasing CV-Shannon's index relationship indicated that a high percentage of species with large within-species variation (*Petalostemum villosum*) or a mixture of a couple particular species (e.g., *Lupinus perennis* and *Petalostemum villosum*) led to high CV; increasing diversity level could decrease the CV value for these cases. This result revealed that besides the species richness and evenness, species composition and spectral properties of specific species identities affect CV values.

Table 5.6 Dependence of CV on Shannon's index for different measurements (sampling methods and spectral ranges). Values shown are multiple linear regression parameters, including intercepts, Slopes, $R^2$, and P values.

| Measurements | Regression Parameters | | | |
|---|---|---|---|---|
| | Intercept | Slope | $R^2$ | P value |
| Leaf Clip Visible-NIR | 0.149 | 0.022 | 0.23 | 2.2e-16 |
| Leaf Clip Full Range | 0.129 | 0.029 | 0.30 | 2.2e-16 |
| Image-derived (CV<0.5) | 0.246 | 0.047 | 0.15 | 2.2e-16 |
| Image-derived (CV>0.5) | 0.837 | -0.15 | 0.58 | 1.9e-12 |

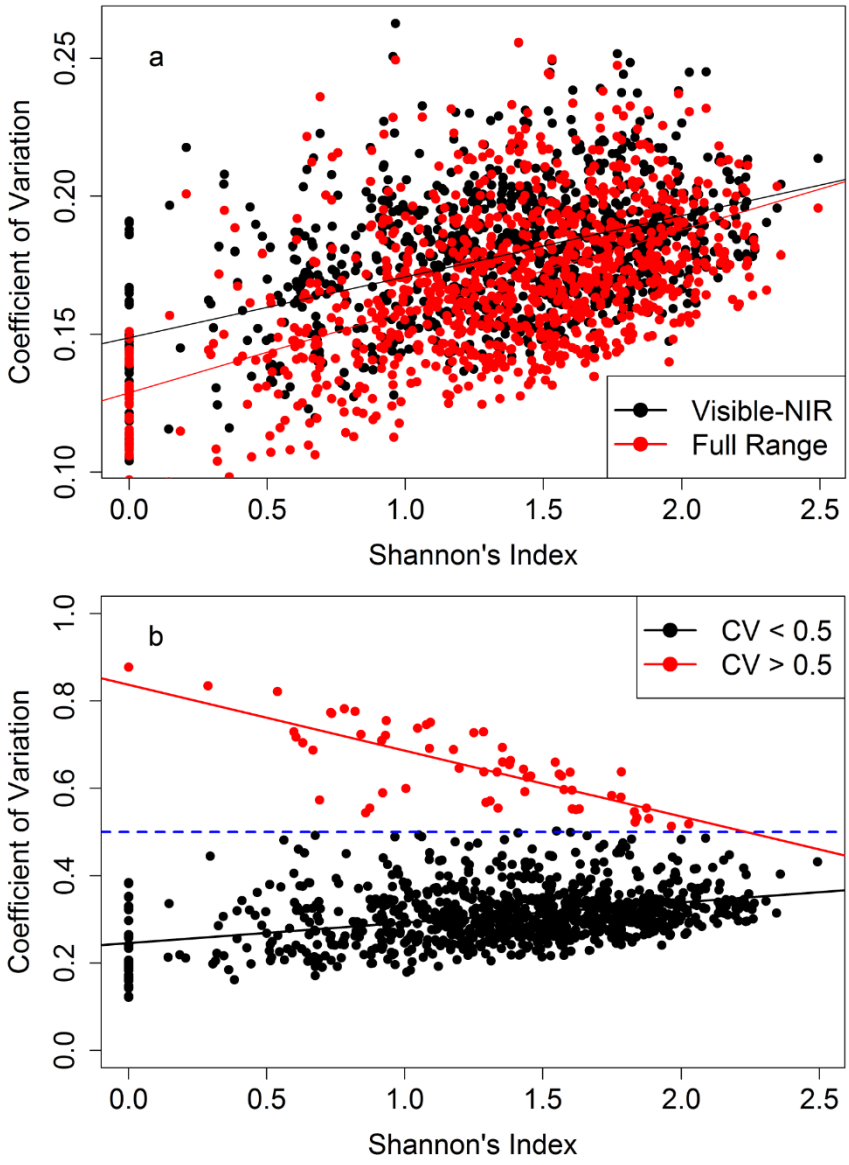


Figure 5.8 Coefficient of variation-Shannon's index relationships from the simulated plots. a: Leaf clip-derived reflectance; b: Image-derived reflectance. The regression parameters were shown in Table 5.6. Only reflectance spectra of prairie plants were used to calculate CV.

5.3.3.2 PLSDA classification

The classification accuracy for simulated plots using mean reflectance depended only on the species composition of the plot. When using the mean reflectance of leaf clip-derived

reflectance, the classified species richness was equal to or less than the real species richness depending on which species was included because only 12 of 16 species could be recognized accurately. On the other hand, when using the mean reflectance of image-derived reflectance, the classified diversity metrics perfectly predicted the conventional diversity metrics because all the species could be separated correctly using the mean reflectance of each species for the image-derived measurements (Table 5.3).

When the full sample of reflectance spectra were used, the modeled species richness, Shannon's index and Simpson's index calculated with classified species overestimated the comparative real conventional diversity metrics (Figure 5.9). The larger overestimation obtained with image-derived reflectance than leaf clip-derived reflectance was due to the lower classification accuracy that presumably was caused by the larger within-species variation captured by the image-derived reflectance than leaf clip-derived reflectance. Additionally, the overestimation was larger in the low richness end than in the high richness end for both leaf clip-derived reflectance and image-derived reflectance.

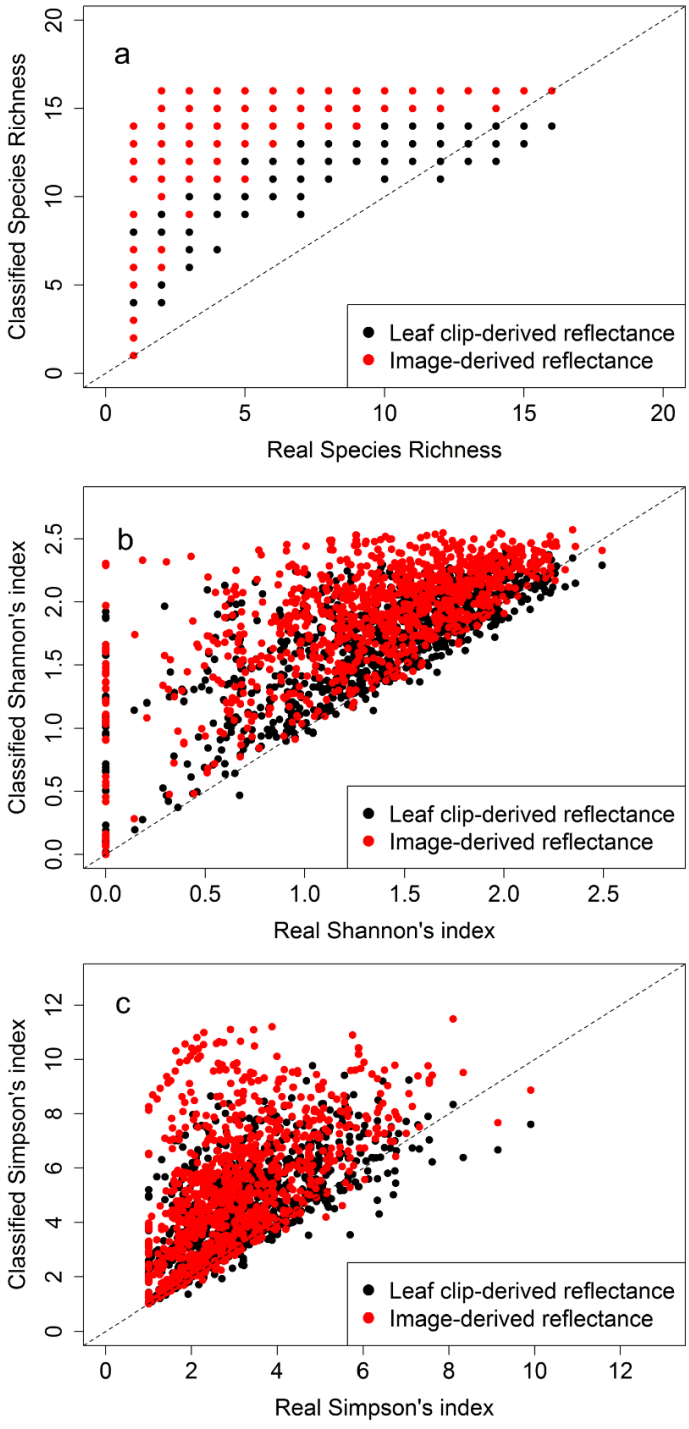


Figure 5.9 Spectral diversity metrics, including richness (a), Shannon's index (b), and Simpson's index (c), calculated based on the PLSDA classification for the full sample reflectance spectra (Y-axis) versus comparative conventional diversity metrics (X-axis) for all the simulated plots. The dotted line in each panel represented the 1:1 line.

## 5.4. Discussion

### 5.4.1 Advantages of image-derived reflectance

The reflectance spectra of one species are determined by both biochemical and structural properties, and can be affected by many factors, including leaf pigments, water content, and structure properties (Pielou 1966, Ustin et al. 2004, Clark et al. 2005, Ustin and Gamon 2010, Ollinger 2011). Besides the spectral variation among different species, there is also considerable reflectance variation among individuals within the same species associated with leaf age and environmental conditions. In addition to internal features, leaf surface properties, such as wax and leaf hairs, can have large effects on leaf reflectance for leaves under different illumination conditions, especially for leaves with large incident or observation angles (Clark et al. 2005).

Our study revealed that optical sampling methods can have important effects on biodiversity detection. Compared to the leaf clip measurements that presumably emphasized certain leaf trait differences, the image-derived reflectance obtained from the imaging spectrometer on the tram expanded the scope of field leaf reflectance collection by providing a large number of reflectance spectra for leaves under different natural illumination conditions. Although Unmanned Aerial Vehicle (UAV) have been proposed to be useful in obtaining high resolution data, in this case, small and low-cost drones are limited by the payload size and stability while the operational costs for large drones (e.g., NASA *Ikhana*) are very expensive (Anderson and Gaston 2013). With this unique dataset, we were able to explore the spectral diversity-biodiversity relationship with a leaf reflectance sample that covered larger and more realistic variations than possible with the leaf clip measurements. By experimentally varying the pool of leaf reflectance samples, we found a large effect of sample variability on the ability to detect alpha diversity with remote sensing.

This finding has implications for studies that "scale up" from leaf to canopy or stand-scale samples. One way would be to try to replicate these effects using radiative transfer models. Instead, we were able to simulate plot scale results by using a realistic set of leaf spectra that captured the range of leaf traits and canopy-level effects of geometry and

illumination, presumably attaining a more realistic result because of the intrinsic limitations of many radiative transfer models (e.g., SAIL model) in dealing with complex canopy architecture, such as leaf clumping (Jacquemoud et al. 2009). The spatial structure of a remote sensing image relates to the size of the objects in the scene and the spatial resolution (pixel size). It has been found that the fine-scales spectral diversity-biodiversity relationships can be weakened or lost with increasing pixel size (*Wang et al. in review*) presumably due to significant information lost when the sampling elements are small compared to the pixel size (O'Neill et al. 1986).

### 5.4.2 Spectral diversity indices

CV

Previous studies have indicated that spectral diversity (CV) reflects a combination of species richness and evenness rather than species richness alone (Wang et al. 2016a), and this study supported that conclusion. CV might not be a good indicator for species richness only, because when species richness increases but evenness stays low, which meant that single species dominates the plot, the plot-level CV also remains low. This study also illustrated two different scenarios where the plot-level CV achieved large values (Figure 5.8): first, the diversity level of the simulated plot was high (high species richness and species evenness); second, the simulated plot had low species richness but there were large dissimilarities among simulated plots having different species and, at the same time, each species had a similar number of individuals (species evenness of the plot was high).

This first scenario that CV increased with increasing diversity levels (Shannon's index) was straightforward and in accordance with most the spectral diversity studies (Rocchini et al. 2010). However, our study revealed that it was possible for low diversity (richness or Shannon's index, because value of Shannon's index is limited by the species richness ($0 < H' < \log(S)$)) plots to have high CV values. In this particular case, if a plot had low species richness but was dominated by *Petalostemum villosum* that has the largest within-species variation in the image-derived measurements (Table S5.1 and largest ranges when plotted in PC space in Figure 5.4), or composed of *Lupinus perennis* and *Petalostemum villosum* with similar number of individuals, the CV of the plot could be even larger than

plots with high diversity levels (Figure 5.4). The large within-species variation of *Petalostemum villosum* captured by image-derived reflectance was presumably due to the tiny but dense and multi-layer leaves that led to large variations of illumination within canopies and the scattering light from flowers that was totally ignored by the leaf clip-derived measurements. These results indicated that an idiosyncratic, species-specific affect on canopy architecture influenced optical diversity, suggesting that the presence or absence of key individual species could alter the CV-biodiversity relationship. In situations having this strong-single species effect, increasing diversity levels by adding more species to the plot could more likely decrease the plot-level CV.

Classified species

The accuracy of assessing spectral diversity metrics using classified species (spectral species or optical types) to estimate biodiversity depends on the spectral training sample and the accuracy of the classifier. In this study, the larger range of reflectance and lower classification accuracy obtained with image-derived measurements reflected the higher possibility of including individuals that cannot be identified correctly when generating the plots with random sampling strategies than with systematic leaf clip-derived reflectance. Some of the graminoid species were too similar to each other to be distinguished using their spectral traits. Consequentially, the overall classification accuracy for prairie ecosystems might decrease when many graminoid and fewer broadleaf species were included in a plot. This decreased accuracy of the classification for the simulated plots might lead to incorrectly estimating the true species richness and other diversity metrics (e.g., Shannon's index).

Background effects

The scattering and reflectance properties of background (e.g., soil and litter) affect the vegetation canopy reflectance (Huete 1988, van Leeuwen and Huete 1996). An intermediate level (50%) of background cover has the greatest influence on the overall vegetation canopy reflectance and vegetation indices (Huete 1988). Our study indicated that the effects of background on detecting biodiversity through spectral diversity varied with the selected indices. The classification-based metric (PLSDA) was less sensitive to

background (e.g., soil) than the information-based metric (CV in this case) because, at the fine scales, the backgrounds, which are usually spectrally unique types, can be mapped accurately (Roth et al. 2015). Therefore, the selection of different spectral diversity metrics could have different performances under different conditions, depending upon the vegetation percent cover, species composition, and the properties of the sensor (spatial and spectral scale).

Information-based indices versus classification-based spectral diversity metrics

Our results reveal that selecting the right spectral diversity metrics for different situations may be critical for accurate biodiversity estimation. It is difficult to have a one-size-fits-all criterion for assessing spectral diversity because it appears that the results would be based on the properties of the available data and the particular goals in mind. Here, we discuss some suggestions to consider.

The effectiveness of information content indices (CV in this case) can be related to surrogacy. In biodiversity studies, the surrogacy hypothesis states that high species richness in one taxon is related to high richness in others (Magurran 2004). Similarly, species richness is also likely to be related to functional biodiversity to some degree. For example, a more diverse ecosystem can have a greater variety of functional behaviors as shown by plant traits that reflect different biochemical content, leaf structure, and physiological function. Therefore, information content indices might work better when medium to large pixel-size satellite images were used to estimate species or diversity at higher taxonomic levels (metacommunities or β diversity) (Rocchini et al. 2004, Rocchini 2007). Presumably, information-based indices would be sensitive to the plant percentage cover because the optical properties of the background (e.g., soil and litter) also contributed to the indices (Figure 5.6).

Classification metrics might work better under the circumstance that each species has a dense distribution and the distance between different species was large enough in spectral space to distinguish one from another (Figure 5.4). An example in this study is the 100% classification accuracy achieved by using the average spectra of each species from the image-derived reflectance (Table 5.3). It has been reported that the use of classification

methods to identify optical diversity (and thus biodiversity) becomes possible with high-resolution imaging spectrometry (Féret and Asner 2014). However, the classification methods fail when it is impossible to find end spectral members or pure pixels rather than mixed pixels in the image or the species are too similar to be separated (e.g., 69% classification accuracy with average species reflectance from leaf clip-derived reflectance), and the classification accuracy decreases when scaling up due to information loss (Clark et al. 2005).

Both high within- and among- species variation in reflectance properties influence the ability of spectral diversity indices to assess biodiversity. Generally, increasing within-species variation weakens the ability of detecting biodiversity using information-based spectral diversity indices, as indicated in this study by the stronger relationships between CV calculated with average reflectance and diversity metrics than between CV calculated with full sample of reflectance and diversity metrics (Table 5.4). Having a larger within-species variation than among-species variation clearly complicates detection of biodiversity (Roth et al. 2015) especially at low richness communities (Figure 5.9). Meanwhile, it might become less practical for either of these methods to assess distribution of rare species even from remarkably accurate and detailed datasets (Kerr 2003).

### 5.4.3 Spectral diversity across space and time

Phenotypic plasticity means that one single species (or individual genotype) can develop different phenotypes under different environmental conditions (Pigliucci et al. 2006). In terms of space, this means an individual organism has the ability to change its phenotypic state or activity in response to changing environmental conditions (Garland and Kelly 2006). As a result, an individual organism's phenotype is the combination of interaction between its genome, the environment, and random events (Fusco and Minelli 2010) as modified in time. Over time, a single individual's optical properties will vary with leaf and canopy development and this variation of plant leaf traits and canopy structures across environmental gradients can lead to high spectral variability among and within species (Asner 1998).

Understanding temporal changes in the expression of biodiversity is fundamental to understanding communities because sampling duration can have a profound influence on the perceived shape of distribution so it is hardly possible to have a good understanding of the community from one point measurement in time (Magurran 2007). Additionally, diversity changes can reflect changing environmental conditions in the short term and ecological and evolutionary processes in the long run (Magurran and Dornelas 2010). In terms of spectral diversity, including information about vegetation phenology might be able to decrease inter-species spectral similarity (Clark and Roberts 2012). Therefore, including optical measurements across the whole growing season could increase the classification accuracy for species having different phenological properties, such as leaf aging, leaf drop, flowering and fruiting (Jiménez and Díaz-Delgado 2015). For example, leaf aging could cause variations within individual canopy trees as large as intra- and interspecific variations in leaf morphological, biochemical and spectral traits in tropical species (Chavana-Bryant et al. 2016). Studies have also showed that the productivity-biodiversity relationship can vary across the growing season (Wang et al. 2016b). This current study focused on the spectral properties of prairie plants in the peak season; in future work, more attention will be needed to understand temporal changes of spectral diversity.

### 5.5 Conclusions

The images used in this study, which were obtained with an imaging spectrometer mounted on a tram system, provided detailed information about spectral properties of plant leaves under different illumination conditions. With this technique, we obtained hyperspectral field images with among the finest spatial resolution (1 mm pixels) ever used in remote sensing. Our simulation framework allowed us to understand the spectral diversity-diversity relationship in ways that cannot be easily achieved with traditional leaf spectral sampling methods (e.g. leaf clips) alone. Our results revealed that the success of assessing biodiversity through spectral diversity can be influenced by species richness, evenness, composition, spectral properties of the species, the properties of the sensor (spatial and spectral scale) and the selected spectral diversity metrics.

This study related two categories of spectral diversity metrics, either based on information content (CV) or on classification results (PLSDA classification), to better understand how species richness, evenness and composition affect the spectral diversity using simulated synthetic hyperspectral images of prairie plants. Our results indicated that both species richness and evenness influenced spectral diversity metrics. Species identities showed substantial effects on both categories of spectral diversity metrics at this fine scale. Meanwhile, background (e.g., soil) effects on spectral diversity varied with the metric. Information theory-based spectral diversity metrics were sensitive to the background, while background had no effects on classification-based indices at this fine scale. Our findings can be used to understand the effects of species richness, evenness and composition on spectral diversity and guide the future regional studies of biodiversity estimation using remote sensing.

**Acknowledgements**

We thank staff at the Cedar Creek Ecosystem Science Reserve, particularly Troy Mielke and Kally Worm. This study was supported by a NASA and NSF grant (DEB-1342872) and a NSF-LTER grant (DEB-1234162) to J. Cavender-Bares, and by iCORE/AITF (G224150012 & 200700172), NSERC (RGPIN-2015-05129), and CFI (26793) grants to J. Gamon, and a China Scholarship Council fellowship to R. Wang.

## 5.6 References

Anderson, M. J. 2001. A new method for non parametric multivariate analysis of variance. - Austral Ecol. 26: 32–46.

Anderson, K. and Gaston, K. J. 2013. Lightweight unmanned aerial vehicles will revolutionize spatial ecology. - Front. Ecol. Environ. 11: 138–146.

Asner, G. P. 1998. Biophysical and biochemical sources of variability in canopy reflectance. - Remote Sens. Environ. 64: 234–253.

Barbier, N. et al. 2010. The variation of apparent crown size and canopy heterogeneity across lowland Amazonian forests. - Glob. Ecol. Biogeogr. 19: 72–84.

Carlson, K. M. et al. 2007. Hyperspectral remote sensing of canopy biodiversity in Hawaiian lowland rainforests. - Ecosystems 10: 536–549.

Chavana-Bryant, C. et al. 2016. Leaf aging of Amazonian canopy trees as revealed by spectral and physiochemical measurements. - New Phytol. in press.

Chiarucci, A. et al. 1999. Cover versus biomass as an estimate of species abundance: does it make a difference to the conclusions? - J. Veg. Sci. 10: 35–42.

Chung, D. and Keles, S. 2010. Sparse partial least squares classification for high dimensional data. - Stat. Appl. Genet. Mol. Biol. 9: 17.

Clark, M. L. and Roberts, D. A. 2012. Species-level differences in hyperspectral metrics among tropical rainforest trees as determined by a tree-based classifier. - Remote Sens. 4: 1820–1855.

Clark, M. L. et al. 2005. Hyperspectral discrimination of tropical rain forest tree species at leaf to crown scales. - Remote Sens. Environ. 96: 375–398.

Féret, J.-B. and Asner, G. P. 2014. Mapping tropical forest canopy diversity using high-fidelity imaging spectroscopy. - Ecol. Appl. 24: 1289–1296.

Fusco, G. and Minelli, A. 2010. Phenotypic plasticity in development and evolution: facts and concepts. Introduction. - Philos. Trans. R. Soc. Lond. B. Biol. Sci. 365: 547–556.

Gamon, J. A. 2008. Tropical sensing — opportunities and challenges. - In: M, K. and GA, S.-A. (eds), Hyperspectral remote sensing of tropical and subtropical forests. CRC Press Taylor&Francis Group, pp. 297–304.

Gamon, J. A. et al. 2006. A mobile tram system for systematic sampling of ecosystem optical properties. - Remote Sens. Environ. 103: 246–254.

Garland, T. and Kelly, S. A. 2006. Phenotypic plasticity and experimental evolution. - J. Exp. Biol. 209: 2344–2361.

Gotelli, N. J. and Colwell, R. K. 2010. Estimating species richness. - In: Magurran, A. E. and McGill, B. J. (eds), Biological Diversity: Frontiers In Measurement And Assessment. pp. 39–54.

Gould, W. 2000. Remote sensing of vegetation , plant species richness , and regional biodiversity hotspots. - Ecol. Appl. 10: 1861–1870.

Huete, A. R. 1988. A soil-adjusted vegetation index (SAVI). - Remote Sens. Environ. 25: 295–309.

Jacquemoud, S. et al. 2009. PROSPECT+SAIL models: A review of use for vegetation characterization. - Remote Sens. Environ. 113: S56–S66.

Jiménez, M. and Díaz-Delgado, R. 2015. Towards a Standard Plant Species Spectral Library Protocol for Vegetation Mapping: A Case Study in the Shrubland of Doñana National Park. - ISPRS Int. J. Geo-Information 4: 2472–2495.

Karlsson, A. 2006. The pls package: Principal component and partial least squares regression in R. - J. Stat. Softw. 17: 1–11.

Kuhn, M. 2016. caret: Classficication and regression training. in press.

Lord, D. et al. 1985. Influence of wind on crop canopy reflectance measurements. - Remote Sens. Environ. 18: 113–123.

Magurran, A. E. 2004. Measuring Biological Diversity. - Blackwell Publishing.

Magurran, A. E. 2007. Species abundance distributions over time. - Ecol. Lett. 10: 347–354.

Magurran, A. E. and Dornelas, M. 2010. Biological diversity in a changing world. - Philos. Trans. R. Soc. Lond. B. Biol. Sci. 365: 3593–3597.

Mittelbach, G. G. 2012. Biodiversity and ecosystem functioning. - In: Community Ecology. 1st ed.n. Sinauer Associates, Inc., pp. 41–62.

Nguyen, D. V and Rocke, D. M. 2002. Multi-class cancer classification via partial least squares with gene expression profiles. - Bioinformatics 18: 1216–1226.

O'Neill, R. V. et al. 1986. A Hierarchical concept of ecosystems. - Princeton University Press.

Oldeland, J. et al. 2010. Does using species abundance data improve estimates of species diversity from remotely sensed spectral heterogeneity? - Ecol. Indic. 10: 390–396.

Ollinger, S. V 2011. Sources of variability in canopy reflectance and the convergent properties of plants. - New Phytol. 189: 375–394.

Palmer, M. W. et al. 2002. Quantitative tools for perfecting species lists. - Environmetrics 13: 121–137.

Pielou, E. C. 1966. The measurement of diversity in different types of biological collections. - J. Theor. Biol. 13: 131–144.

Pigliucci, M. et al. 2006. Phenotypic plasticity and evolution by genetic assimilation. - J. Exp. Biol. 209: 2362–2367.

Price, J. C. 1994. How unique are spectral signatures? - Remote Sens. Environ. 49: 181–186.

Reich, P. B. et al. 2012. Impacts of biodiversity loss escalate through time as redundancy fades. - Science. 336: 589–592.

Roberts, D. A. et al. 2004. Spectral and structural measures of Northwest forest vegetation at leaf to landscape scales. - Ecosystems 7: 545–562.

Rocchini, D. 2007. Effects of spatial and spectral resolution in estimating ecosystem α-diversity by satellite imagery. - Remote Sens. Environ. 111: 423–434.

Rocchini, D. et al. 2004. Testing the spectral variation hypothesis by using satellite multispectral images. - Acta Oecologica 26: 117–120.

Rocchini, D. et al. 2010. Remotely sensed spectral heterogeneity as a proxy of species diversity: Recent advances and open challenges. - Ecol. Inform. 5: 318–329.

Roth, K. L. et al. 2015. Differentiating plant species within and across diverse ecosystems with imaging spectroscopy. - Remote Sens. Environ. 167: 135–151.

Schäfer, E. et al. 2016. Mapping tree species diversity of a tropical montane forest by unsupervised clustering of airborne imaging spectroscopy data. - Ecol. Indic. 64: 49–58.

Shannon, C. E. 1948. A mathematical theory of communication. - Bell Syst. Tech. J. 27: 379–423, 623–656.

Simpson, E. H. 1949. Measurement of Diversity. - Nature 163: 688–688.

Stoms, D. M. and Estes, J. E. 1993. A remote sensing research agenda for mapping and monitoring biodiversity. - Int. J. Remote Sens. 14: 1839–1860.

Tilman, D. et al. 2001. Diversity and productivity in a long-term grassland experiment. - Science. 294: 843–845.

Ustin, S. L. and Gamon, J. A. 2010. Remote sensing of plant functional types. - New Phytol. 186: 795–816.

Ustin, S. L. et al. 2004. Using imaging spectroscopy to study ecosystem processes and properties. - Bioscience 54: 523–534.

Ustin, S. L. et al. 2009. Retrieval of foliar information about plant pigment systems from high resolution spectroscopy. - Remote Sens. Environ. 113: S67–S77.

van Leeuwen, W. J. D. and Huete, A. R. 1996. Effects of standing litter on the biophysical interpretation of plant canopies with spectral indices. - Remote Sens. Environ. 55: 123–138.

Wang, R. et al. 2016a. Integrated analysis of productivity and biodiversity in a southern Alberta prairie. - Remote Sens. 8: 214.

Wang, R. et al. 2016b. Seasonal variation in the NDVI–species richness relationship in a prairie grassland experiment (Cedar Creek). - Remote Sens. 8: 128.

Whittaker, R. H. 1972. Evolution and Measurement of Species Diversity. - Taxon 21: 213–251.

Williams, C. B. 1964. Patterns in the balance of nature and related problems in quantitative ecology. - Academic Press.

# Chapter 6 Discussion and Conclusion

## 6.1 Summary and Contributions

This work has attempted to understand the spectral diversity – biodiversity relationship at a local scale using both empirical and theoretical methods. First, the biodiversity-productivity relationship was tested though remote sensing in both experimental and natural prairie ecosystems, which indicated that it was feasible to use remote sensing to assess biodiversity. Further studies were conducted within the BioDIV experiment at the Cedar Creek Ecosystem Science Reserve that provides well maintained prairie plots with different diversity levels. In the ground-based experiments, an imaging spectrometer on a tram system was applied to obtain high-resolution (pixel size = 1 $mm^2$) images that are not typically accessible in remote sensing. These images provided detailed information about spectral properties of each plant. Incorporating strategies of image resampling and a simulation framework allowed us to investigate the scale dependence of the spectral diversity-diversity relationship and how the species richness, evenness and composition affected the spectral diversity – biodiversity relationship, which cannot be easily achieved with empirical experiments alone. Moreover, the effects of spectral bands on spectral diversity were compared, and the influence of soil background was considered.

The major findings of this study were:

(1) NDVI, a common remote sensing measure of plant productivity, can be related to species richness, but it was also strongly affected by other factors, including canopy structure (cover or biomass), short-term water stress, and shifting flowering patterns that can confound the NDVI-richness relationship. The relationship between NDVI and biodiversity was sensitive to the vegetation phenology conditions and the strongest NDVI–biodiversity relationship was found in mid-summer, when NDVI showed a temporary decline associated with warm, dry conditions and anthesis.

(2) Differences of biomass and ecosystem production across a 10-km prairie transect in Mattheis Research Ranch, Alberta, Canada were shown clearly with airborne images. Regardless of the diversity method used, high biodiversity areas tended to have higher production in this grassland ecosystem. The optical diversity (CV) - biodiversity relationships were sensitive to both richness and evenness, and the addition of evenness improved the relationship between optical diversity and biodiversity.

(3) Among all the tested conventional biodiversity indices, spectral diversity showed the strongest relationship with species diversity indices combining species richness and evenness. The fine-scale study also showed rapid information loss with increasing pixel size and the best resolution to detect α diversity using spectral diversity at this prairie ecosystem was at a size close to a typical herbaceous plant leaf or single canopy.

(4) Both species richness and evenness influenced spectral diversity metrics. Species identities also showed substantial effects on spectral diversity metrics at the fine scale. Meanwhile, background (e.g., soil) effects on spectral diversity varied with metrics: spectral diversity metrics based on information theory were sensitive to the background, while background had no effects on classification-based indices at this fine scale.

(5) Compared to the leaf clip measurements that presumably emphasized leaf trait differences, the image-derived reflectance obtained from imaging spectrometer on the tram expanded the scope of field leaf reflectance collection by allowing us to obtain a large number of reflectance spectra for leaves under their natural

illumination conditions. The results revealed that spectral diversity was influenced by both leaf traits and canopy structure and including information on canopy structure can increase species separability. This finding has implications for studies that "scale up" from leaf to canopy or stand-scale samples.

(6) Despite the scaling challenges, the airborne study suggested that effective, operational remote sensing methods could be developed and applied to detect biodiversity, even at the relatively coarse 1-m scale, and that optical diversity metrics could be related to other metrics of ecosystem productivity, providing exciting opportunities for combined assessment from remote sensing.

## 6.2 Limitations and future work

### 6.2.1 Expanding the findings to a larger extent

Most of this study focused on the spectral properties of prairie plants at local scales. The Cedar Creek BioDIV experiment is a human maintained biodiversity experiment that might lack the full complexity of a natural landscape (Hillebrand and Matthiessen 2009). In this system, plant density is known to depend on diversity, which is maintained by weeding; therefore, lower diversity plots are less densely vegetated, have more bare ground. As diversity declines and plant density in the plot decreases, the degree of cover and bare soil affected spectral diversity. Moreover, the maintained species richness and biomass of the Cedar Creek plots are low comparing to most natural prairie ecosystems. So, the performance of CV at high diversity is unclear. Therefore, a better sampling approach that includes different ecosystems or biomes is needed to test the optical diversity – biodiversity relationship in the future.

Calculations biodiversity metrics over large landscapes (e.g., Mattheis ranch) necessarily involves a degree of abstraction. At large scales, detailed species counts are not possible and the quality of field biodiversity sampling decreases with increasing grain size, so other methods (e.g., abstraction to dominant species or vegetation types) are necessary,

analogous to the information loss occurring when transitioning from fine- to coarse scales in remote sensing analyses.

The temporal changes of biodiversity have not received as much attention as the spatial distribution of biodiversity (Magurran 2008). Satellite remote sensing provides images as a snapshot in time. In terms of spectral diversity, additional information about the vegetation phenology might be able to improve the performance of spectral diversity metrics because changing phenological state, for example due to leaf aging, can lead to variations within individual canopy trees as large as intra- and interspecific variations in leaf morphological, biochemical and spectral traits in tropical species (Clark and Roberts 2012, Chavana-Bryant et al. 2016). Understanding the temporal changes of spectral diversity is also critical to remote sensing of biodiversity. While this study considered the biodiversity-productivity linkage through time, further studies should also explore the relative influence of leaf traits and canopy structure on optical diversity through time.

### 6.2.2 Concept of surrogacy – where one measure provides a proxy of another

The classical surrogacy hypothesis has three main aspects: 1) high species richness in one taxon is related to high richness in others (cross-taxon surrogacy), 2) high genetic or family richness is related to high species richness (within-taxon surrogacy), and 3) high environmental e.g., temperature or topographical, diversity is related to high species richness (environmental surrogacy) (Magurran 2004). For example, macrolichens served as a good indicator of species richness of mosses, liverworts, and woody plants in the Indian Garwhal Himalaya (Negi and Gadgil 2002) and family and genus-level diversity metrics were reported to be very good indicators of species diversities (Lee 1997). Presumably, species richness is also related to functional biodiversity to some extent. Then, a more diverse ecosystem can have a greater variety of functional behaviours as shown by plant traits that reflect different biochemical content, leaf structure, and physiological function. This variation of plant traits can affect the optical properties of plants and lead to spectral detectable features (spectral diversity). This extension of the surrogacy concept may be a productive direction for future research in this multidisciplinary subject. While this is a goal of the overall project that funded much of this thesis research (*"Linking remotely sensed optical diversity to genetic, phylogenetic*

*and functional diversity to predict ecosystem processes"*), a full analysis of surrogacy was beyond the scope of this thesis. Assessment of other aspects of diversity (e.g. below-ground or phylogenetic diversity), and linking these to remote sensing, remains work in progress.

### 6.2.3 New remote sensing technologies

Over the past hundred years, Earth observation techniques have evolved from aerial photograph, coarse resolution satellite images to products generated by digital imaging spectroscopy, LiDAR and radar systems. Besides of the increasing number of all purpose Earth observation satellites, novel ground-level remote sensing platforms have been introduced to ecological studies and have transformed ecological research (Kerr and Ostrovsky 2003). For example, newly automated sensors, e.g., the two wavelengths NDVI and PRI sensors, allow great flexibility to accomplish continuously sampling (Gamon et al. 2015). And the remote sensors carried by unmanned aerial vehicles (UAVs) can deliver fine spatial scale data at suitable repeat times with reasonable cost (Anderson and Gaston 2013). Although there is still a challenge to applying UAVs to obtain hyperspectral or LiDAR data due to issues like safety and carrying capacity, these new technologies are beginning to provide quantitative and detailed information about our Earth and expanding our abilities to detect the changes in Earth properties and processes. In this context, drones might be particularly useful in "filling the gap" between airborne and proximal studies, i.e. the range of spatial scales where much information on optical diversity appears to be lost.

Deep-learning algorithms, which are branches of machine learning, try to find the representative and discriminative features in a hierarchical manner from the data. Deep learning algorithms have been widely used in remote sensing data analyses, including imaging processing, classification, and pattern recognition (Zhang et al. 2016). The development of new algorithms along with increasing computing power might be helpful in extracting information from large remote sensing datasets. Comparing to the widely-used algorithms, e.g., support vector machines (SVM) and artificial neural networks (ANN), genetic programming (GP) that is generally defined as a specialization of genetic algorithm is quite new in geoscience and remote sensing (Lary et al. 2016). GP has been

used to map coffee crops by combining textural and spectral information with SPOT images (dos Santos et al. 2010). In terms of biodiversity assessment using remote sensing, a clear and solid understanding of the spectral diversity-biodiversity relationship is needed when using these new algorithms because the machine learning algorithms are highly affected by the training or sampling data and we don't want to be lost in the "black box" (Castelvecchi 2016).

### 6.3 Conclusion

There is little doubt that remote sensing can contribute to biodiversity monitoring, but we need to develop effective collaborations between experts in remote sensing and experts in biodiversity monitoring and conservation to make full use of this potential (Pettorelli et al. 2014). Also, a global network to gather biodiversity observations and broader ecosystem-level observations is needed (Turner 2014, Jetz et al. 2016). In the United States, the National Ecological Observatory Network (NEON) has been created. NEON proposes to link in situ sampling around the country with airborne and satellite remote sensing and provides open source data to understand the impacts of climate change, land use change and invasive species on continental-scale ecology (http://www.neonscience.org). The international Group on Earth Observations (GEO) partnership, particularly the global Biodiversity Observation Network (GEO BON), serves as the first attempt by national governments to combine remote sensing biodiversity measurements with genetic-, species- and ecosystem-level observations globally (Scholes et al. 2012). By connecting local and regional biodiversity observation networks, the international network can connect experts in different fields and gather data at multiple scales (e.g., in situ, airborne and satellite data) to fill gaps in the current biodiversity observation, provide a deeper understanding of the relationship between biodiversity and ecosystem services and ultimately, conserve the Earth's biodiversity.

A paradigm is the set of background assumptions that a discipline makes and it is the worldview that the scientists in one discipline hold. Paradigms mold subject area, approaches and models of problems solving (Kuhn 1970). The criteria of observation often vary with the paradigm, including the perspectives taken, the processes involved, and of the interactions included (Pickett et al. 2007). It might be still early to say that

remote sensing has started a new paradigm of biodiversity research, but it does offer a novel perspective on global diversity monitoring and conservation. As Stoms & Estes demonstrated in an early paper that discussed estimating biodiversity though remote sensing (Stoms and Estes 1993): “with remote sensing technology, we may be able to make real progress in understanding why more species occur in some places than in others and in identifying the most critical places that must be protected to preserve the maximum number of species into the 22nd century and beyond.” Optimistically, this process might be advanced because the development of new technologies is far beyond people imagined decades ago. By enhancing cooperation from multidisciplinary scientists, policy makers and others, we can improve global biodiversity estimation and conservation.

To end this discussion, I would like to reverse and modify the famous opening phrases in the novel of *A tale of two cities*:

*It is the worst of time, it is the best of time.*

### 6.4 References

Anderson, K. and Gaston, K. J. 2013. Lightweight unmanned aerial vehicles will revolutionize spatial ecology. - Front. Ecol. Environ. 11: 138–146.

Castelvecchi, D. 2016. Can we open the black box of AI? - Nature 538: 20–23.

Chavana-Bryant, C. et al. 2016. Leaf aging of Amazonian canopy trees as revealed by spectral and physiochemical measurements. - New Phytol. in press.

Clark, M. L. and Roberts, D. A. 2012. Species-level differences in hyperspectral metrics among tropical rainforest trees as determined by a tree-based classifier. - Remote Sens. 4: 1820–1855.

dos Santos, J. A. et al. 2010. A genetic programming approach for coffee crop recognition. University of Campinas Center for Research in Agriculture University of Campinas Campinas , SP , Brazil. - IGARSS 2010: 3418–3421.

Gamon, J. A. et al. 2015. Monitoring seasonal and diurnal changes in photosynthetic pigments with automated PRI and NDVI sensors. - Biogeosciences 12: 4149–4159.

Hillebrand, H. and Matthiessen, B. 2009. Biodiversity in a complex world: Consolidation and progress in functional biodiversity research. - Ecol. Lett. 12: 1405–1419.

Jetz, W. et al. 2016. Monitoring plant functional diversity from space. - Nat. Plants 2: 16024.

Kerr, J. T. and Ostrovsky, M. 2003. From space to species: Ecological applications for remote sensing. - Trends Ecol. Evol. 18: 299–305.

Kuhn, T. S. 1970. The structure of scientific revolutions. - University of Chicago.

Lary, D. J. et al. 2016. Machine learning in geosciences and remote sensing. - Geosci. Front. 7: 3–10.

Lee, M. S. Y. 1997. Documenting present and past biodiversity: conservation biology meets palaeontology. - Trends Ecol. Evol. 12: 132–133.

Magurran, A. E. 2004. Measuring biological diversity. - Blackwell Publishing.

Magurran, A. E. 2008. Diversity over time. - Folia Geobot. 43: 319–327.

Negi, H. R. and Gadgil, M. 2002. Cross-taxon surrogacy of biodiversity in the Indian Garhwal Himalaya. - Biol. Conserv. 105: 143–155.

Pettorelli, N. et al. 2014. Satellite remote sensing, biodiversity research and conservation of the future. - Philos. Trans. R. Soc. B Biol. Sci. 369: 1–5.

Pickett, S. T. A. et al. 2007. Ecological understnding: The nature of theory and the theory of nature. - Academic Press.

Scholes, R. J. et al. 2012. Building a global observing system for biodiversity. - Curr. Opin. Environ. Sustain. 4: 139–146.

Stoms, D. M. and Estes, J. E. 1993. A remote sensing research agenda for mapping and monitoring biodiversity. - Int. J. Remote Sens. 14: 1839–1860.

Turner, W. 2014. Sensing biodiversity. - Science. 346: 301–303.

Zhang, L. et al. 2016. Deep learning for remote sensing data. - IEEE Geosci. Remote Sens. Mag. 4: 22–40.

# Bibliography

Adams, B. W. et al. 2013. Range plant communities and range health assessment guidelines for the dry mixedgrass natural subregion of Alberta.

Adler, P. B. et al. 2011. Productivity is a poor predictor of plant species richness. - Science. 1750: 1750–1754.

Ahl, V. and Allen, T. F. H. 1996. Hierarchy theory: A vision, vocabulary, and epistemology. - Columbia University Press.

Anderson, M. J. 2001. A new method for non parametric multivariate analysis of variance. - Austral Ecol. 26: 32–46.

Anderson, K. and Gaston, K. J. 2013. Lightweight unmanned aerial vehicles will revolutionize spatial ecology. - Front. Ecol. Environ. 11: 138–146.

Anderson, M. J. et al. 2011. Navigating the multiple meanings of β diversity: a roadmap for the practicing ecologist. - Ecol. Lett. 14: 19–28.

Asner, G. P. 1998. Biophysical and biochemical sources of variability in canopy reflectance. - Remote Sens. Environ. 64: 234–253.

Asner, G. P. 2013. Biological diversity mapping comes of age. - Remote Sens. 5: 374–376.

Asner, G. P. and Martin, R. E. 2009. Airborne spectranomics: mapping canopy chemical and taxonomic diversity in tropical forests. - Front. Ecol. Environ. 7: 269–276.

Asner, G. P. et al. 2008. Remote sensing of native and invasive species in Hawaiian forests. - Remote Sens. Environ. 112: 1912–1926.

Austin, G. E. et al. 1996. Predicting the spatial distribution of buzzard Buteo buteo nesting areas using a geographical information system and remote sensing. - J. Appl. Ecol. 33: 1541–1550.

Bailey, S. and Bailey, S. 2004. Primary productivity and species richness: relationships among functional guilds, residency groups and vagility classes at multiple spatial scales. - Ecography (Cop.). 27: 207–217.

Balvanera, P. et al. 2006. Quantifying the evidence for biodiversity effects on ecosystem functioning and services. - Ecol. Lett. 9: 1146–1156.

Barnosky, A. D. et al. 2011. Has the Earth's sixth mass extinction already arrived? - Nature 471: 51–57.

Bazzaz, F. A. 1996. Plants in changing environments: linking physiological, population, and community ecology. - Cambridge University Press.

Becker, S. 2013. Mattheis ranch vegetation and soil inventory.

Bernhardt-Römermann, M. et al. 2011. Explaining grassland biomass - the contribution of climate, species and functional diversity depends on fertilization and mowing frequency. - J. Appl. Ecol. 48: 1088–1097.

Bonar, S. et al. 2010. An overview of sampling issues in species diversity and abundance surveys. - In: Magurran, A. E. and McGill, B. J. (eds), Biological Diversity: frontiers in measurement and assessment. Oxford University Press, pp. 376.

Booth, D. T. and Tueller, P. T. 2003. Rangeland monitoring using remote sensing. - Arid L. Res. Manag. 17: 455–467.

Bork, E. W. and Irving, B. D. 2015. Seasonal availability of cool- and warm-season herbage in the northern mixed prairie. - Rangelands 37: 178–185.

Bork, E. W. et al. 1999. Rangeland cover component quantification using broad (TM) and narrow-band (1.4 NM) spectrometry. - J. Range Manag. 52: 249–257.

Boundary Files, 2011 Census. Statistics Canada. 2011, Catalogue no. 92-16-X.

Cadotte, M. W. et al. 2008. Evolutionary history and the effect of biodiversity on plant productivity. - Proc. Natl. Acad. Sci. USA 105: 17012–17017.

Cadotte, M. W. et al. 2009. Using phylogenetic, functional and trait diversity to understand patterns of plant community productivity. - PLoS One 4: 1–9.

Cadotte, M. W. et al. 2011. Beyond species: Functional diversity and the maintenance of ecological processes and services. - J. Appl. Ecol. 48: 1079–1087.

Cardinale, B. J. et al. 2007. Impacts of plant diversity on biomass production increase through time because of species complementarity. - Proc. Natl. Acad. Sci. U. S. A. 104: 18123–18128.

Carlson, K. M. et al. 2007. Hyperspectral remote sensing of canopy biodiversity in Hawaiian lowland rainforests. - Ecosystems 10: 536–549.

Castelvecchi, D. 2016. Can we open the black box of AI? - Nature 538: 20–23.

Cavender-Bares, J. et al. 2009. The merging of community ecology and phylogenetic biology. - Ecol. Lett. 12: 693–715.

Ceballos, A. et al. 2015. Comparison of airborne LiDAR and satellite hyperspectral remote sensing to estimate vascular plant richness in deciduous mediterranean forests of central Chile. - Remote Sens. 7: v.

Chance, C. M. et al. 2016. Spectral wavelength selection and detection of two invasive plant species in an urban area. - Can. J. Remote Sens. 42: 1–14.

Chavana-Bryant, C. et al. 2016. Leaf aging of Amazonian canopy trees as revealed by spectral and physiochemical measurements. - New Phytol. in press.

Chung, D. and Keles, S. 2010. Sparse partial least squares classification for high dimensional data. - Stat. Appl. Genet. Mol. Biol. 9: 17.

Clark, M. L. and Roberts, D. A. 2012. Species-level differences in hyperspectral metrics among tropical rainforest trees as determined by a tree-based classifier. - Remote Sens. 4: 1820–1855.

Clark, D. A. et al. 2001. Measuring net primary production in forest : concepts and field methods. - Ecol. Appl. 11: 356–370.

Clark, M. L. et al. 2005. Hyperspectral discrimination of tropical rain forest tree species at leaf to crown scales. - Remote Sens. Environ. 96: 375–398.

Clawges, R. et al. 2008. The use of airborne lidar to assess avian species diversity, density, and occurrence in a pine/aspen forest. - Remote Sens. Environ. 112: 2064–2073.

Conel, J. E. et al. 1987. AIS-2 radiometry and a comparison of methods for the recovery of ground reflectance. - Proc. 3rd Airborne Imaging Spectrom. Data Anal. Work. shopJPL Publ. 87–30

Connell, J. H. 1978. Diversity in tropical rain forests and coral reefs. - Science. 199: 1302–1310.

Corbane, C. et al. 2015. Remote sensing for mapping natural habitats and their conservation status - New opportunities and challenges. - Int. J. Appl. Earth Obs. Geoinf. 37: 7–16.

Costanza, R. and Maxwell, T. 1994. Resolution and predictability: An approach to the scaling problem. - Landsc. Ecol. 9: 47–57.

Costanza, J. K. et al. 2011. Multi-scale environmental heterogeneity as a predictor of plant species richness. - Landsc. Ecol. 26: 851–864.

Crutzen, P. J. 2002. Geology of mankind. - Nature 415: 2002.

Dahlin, K. M. 2016. Spectral diversity area relationships for assessing biodiversity in a wildland-agriculture matrix. - Ecol. Appl. 26: 2756–2766.

Damm, A. et al. 2011. Modeling the impact of spectral sensor configurations on the FLD retrieval accuracy of sun-induced chlorophyll fluorescence. - Remote Sens. Environ. 115: 1882–1892.

de Araujo Barbosa, C. C. et al. 2015. Remote sensing of ecosystem services: A systematic review. - Ecol. Indic. 52: 430–443.

de Mazancourt, C. et al. 2013. Predicting ecosystem stability from community composition and biodiversity. - Ecol. Lett. 16: 617–625.

DeFries, R. S. and Townshend, J. R. G. 1994. NDVI-derived land cover classifications at a global scale. - Int. J. Remote Sens. 15: 3567–3586.

Díaz, S. et al. 2015. The global spectrum of plant form and function. - Nature 529: 167–171.

dos Santos, J. A. et al. 2010. A genetic programming approach for coffee crop recognition J . A . Santos , F . Faria , R . Calumby , R . da S . Torres University of Campinas Center for Research in Agriculture University of Campinas Campinas , SP , Brazil. - IGARSS 2010: 3418–3421.

Fairbanks, D. H. K. and McGwire, K. C. 2004. Patterns of floristic richness in vegetation communities of California: regional scale analysis with multi-temporal NDVI. - Glob. Ecol. Biogeogr. 13: 221–235.

Fargione, J. et al. 2007. From selection to complementarity: shifts in the causes of biodiversity-productivity relationships in a long-term biodiversity experiment. - Proc. Biol. Sci. 274: 871–876.

Fava, F. et al. 2010. Fine-scale assessment of hay meadow productivity and plant diversity in the European Alps using field spectrometric data. - Agric. Ecosyst. Environ. 137: 151–157.

Féret, J.-B. and Asner, G. P. 2014. Mapping tropical forest canopy diversity using high-fidelity imaging spectroscopy. - Ecol. Appl. 24: 1289–1296.

Field, C. B. 1991. Ecological scaling of carbon gain to stress and resource availability.

Flanagan, L. B. et al. 2015. Application of the photosynthetic light-use efficiency model in a northern Great Plains grassland. - Remote Sens. Environ. 168: 239–251.

Flynn, D. F. B. et al. 2011. Functional and phylogenetic diversity as predictors of biodiversity--ecosystem-function relationships. - Ecology 92: 1573–1581.

Foody, G. M. 2005. Mapping the richness and composition of British breeding birds from coarse spatial resolution satellite sensor imagery. - Int. J. Remote Sens. 26: 3943–3956.

Fraser, L. H. et al. 2015. Worldwide evidence of a unimodal relationship between productivity and plant species richness. - Science. 349: 302–306.

Friedl, M. A. et al. 2010. MODIS Collection 5 global land cover: Algorithm refinements and characterization of new datasets. - Remote Sens. Environ. 114: 168–182.

Fusco, G. and Minelli, A. 2010. Phenotypic plasticity in development and evolution: facts and concepts. Introduction. - Philos. Trans. R. Soc. Lond. B. Biol. Sci. 365: 547–556.

Gamon, J. A. 2008. Tropical sensing — opportunities and challenges. - In: M, K. and GA, S.-A. (eds), Hyperspectral remote sensing of tropical and subtropical forests. CRC Press Taylor&Francis Group, pp. 297–304.

Gamon, J. A. et al. 1993. Functional patterns in an annual grassland during an AVIRIS overflight *. - Remote Sens. Environ. 44: 239–253.

Gamon, J. A. et al. 1995. Relationships between NDVI, canopy structure, and photosynthesis in three californian vegetation types. - Ecol. Appl. 5: 28–41.

Gamon, J. A. et al. 2006. A mobile tram system for systematic sampling of ecosystem optical properties. - Remote Sens. Environ. 103: 246–254.

Gamon, J. A. et al. 2010. SpecNet revisited: Bridging flux and remote sensing communities. - Can. J. Remote Sens. 36: S376–S390.

Gamon, J. A. et al. 2015. Monitoring seasonal and diurnal changes in photosynthetic pigments with automated PRI and NDVI sensors. - Biogeosciences 12: 4149–4159.

Garland, T. and Kelly, S. A. 2006. Phenotypic plasticity and experimental evolution. - J. Exp. Biol. 209: 2344–2361.

Garratt, J. R. 1990. The internal boundary layer - A review. - Boundary-Layer Meteorol. 50: 171–203.

Gillespie, T. W. 2005. Predicting woody-plant species richness in tropical dry forests: A case study from south Florida, USA. - Ecol. Appl. 15: 27–37.

Gillespie, T. W. et al. 2009. Towards quantifying tropical tree species richness in tropical forests. - Int. J. Remote Sens. 30: 1629–1634.

Gitelson, A. A. and Gamon, J. A. 2015. The need for a common basis for defining light-use efficiency: Implications for productivity estimation. - Remote Sens. Environ. 156: 196–201.

Gitelson, A. a. et al. 2002. Novel algorithms for remote estimation of vegetation fraction. - Remote Sens. Environ. 80: 76–87.

Gotelli, N. J. and Colwell, R. K. 2001. Quantifyinf biodiversity: procedures and pitfalls in the measurement and comparison of species richness. - Ecol. Lett. 4: 379–391.

Gotelli, N. J. and Colwell, R. K. 2010. Estimating species richness. - In: Magurran, A. E. and McGill, B. J. (eds), Biological Diversity: Frontiers In Measurement And Assessment. pp. 39–54.

Gould, W. 2000. Remote sensing of vegetation , plant species richness , and regional biodiversity hotspots. - Ecol. Appl. 10: 1861–1870.

Griffiths, G. H. and Lee, J. 2000. Landscape pattern and species richness; regional scale analysis from remote sensing. - Int. J. Remote Sens. 21: 2685–2704.

Grime, J. P. 1973. Competitive exclusion in herbaceous vegetation. - Nature 242: 344–347.

Haddad, N. M. et al. 2009. Plant species loss decreases arthropod diversity and shifts trophic structure. - Ecol. Lett. 12: 1029–1039.

Hamilton, A. J. 2005. Species diversity or biodiversity? - J. Environ. Manage. 75: 89–92.

Hector, A. and Bagchi, R. 2007. Biodiversity and ecosystem multifunctionality. - Nature 448: 188–190.

Hector, A. et al. 1999. Plant diversity and productivity experiments en European grasslands. - Science. 286: 1123–1127.

Hector, A. et al. 2011. BUGS in the analysis of biodiversity experiments: Species richness and composition are of similar importance for grassland productivity. - PLoS One in press.

Helmus, M. R. et al. 2007. Phylogenetic measures of biodiversity. - Am. Nat. 169: E68-83.

Heywood, V. H. 1995. Global biodiversity assessment. - Cambridge University Press.

Hill, M. J. 2013. Vegetation index suites as indicators of vegetation state in grassland and savanna: An analysis with simulated SENTINEL 2 data for a North American transect. - Remote Sens. Environ. 137: 94–111.

Hillebrand, H. 2004. On the generality of the latitudinal diversity gradient. - Am. Nat. 163: 192–211.

Hillebrand, H. and Matthiessen, B. 2009. Biodiversity in a complex world: Consolidation and progress in functional biodiversity research. - Ecol. Lett. 12: 1405–1419.

Hooper, D. U. et al. 2005. Effects of biodiversity on ecosystem functioning: a consensus of current knowledge. - Ecol. Monogr. 75: 3–35.

Huemmrich, K. F. et al. 1999. High temporal resolution NDVI phenology from micrometeorological radiation sensors. - J. Geophys. Res. 104: 27935.

Huete, A. R. 1988. A soil-adjusted vegetation index (SAVI). - Remote Sens. Environ. 25: 295–309.

Hunt, E. R. et al. 2003. Applications and research using remote sensing for rangeland management. - Photogramm. Eng. Remote Sens. 69: 675–693.

Huston, M. A. 1997. Hidden treatments in ecological experiments: re-evalutating the ecosystem function of biodiverstiy. - Oecologia 110: 449–460.

Isbell, F. I. et al. 2009. Biodiversity, productivity and the temporal stability of productivity: Patterns and processes. - Ecol. Lett. 12: 443–451.

Isbell, F. et al. 2011. High plant diversity is needed to maintain ecosystem services. - Nature 477: 199–202.

Isbell, F. et al. 2015. Biodiversity increases the resistance of ecosystem productivity to climate extremes. - Nature 526: 574–577.

Jacquemoud, S. et al. 2009. PROSPECT+SAIL models: A review of use for vegetation characterization. - Remote Sens. Environ. 113: S56–S66.

Jennings, M. D. 2000. Gap analysis: Concepts, methods, and recent results. - Landsc. Ecol. 15: 5–20.

Jetz, W. et al. 2016. Monitoring plant functional diversity from space. - Nat. Plants 2: 16024.

Jiménez, M. and Díaz-Delgado, R. 2015. Towards a standard plant species spectral library protocol for vegetation mapping: A case study in the shrubland of Doñana National Park. - ISPRS Int. J. Geo-Information 4: 2472–2495.

Joel, G. et al. 1997. Production efficiency in sunflower: The role of water and nitrogen stress. - Remote Sens. Environ. 62: 176–188.

John, R. et al. 2008. Predicting plant diversity based on remote sensing products in the semi-arid region of Inner Mongolia. - Remote Sens. Environ. 112: 2018–2032.

Karlsson, A. 2006. The pls package: Principal component and partial least squares regression in R. - J. Stat. Softw. 17: 1–11.

Kembel, S. W. et al. 2010. Picante: R tools for integrating phylogenies and ecology. - Bioinformatics 26: 1463–1464.

Kerr, J. T. and Ostrovsky, M. 2003. From space to species: Ecological applications for remote sensing. - Trends Ecol. Evol. 18: 299–305.

Kerr, J. T. et al. 2001. Remotely sensed habitat diversity predicts butterfly species richness and community similarity in Canada. - Proc. Natl. Acad. Sci. U. S. A. 98: 11365–11370.

Kirwan, L. et al. 2007. Evenness drives consistent diversity effects in intensive grassland systems across 28 European sites. - J. Ecol. 95: 530–539.

Kljun, N. et al. 2004. A simple parameterisation for flux footprint predictions. - Boundary-Layer Meteorol. 112: 503–523.

Kuhn, T. S. 1970. The structure of scientific revolutions. - University of Chicago.

Kuhn, M. 2016. caret: Classficication and regression training. in press.

Lary, D. J. et al. 2016. Machine learning in geosciences and remote sensing. - Geosci. Front. 7: 3–10.

Leclerc, M. Y. and Thurtell, G. W. 1990. Footprint prediction of scalar fluxes using a markovian analysis. - Boundary-Layer Meteorol. 52: 247–258.

Lee, M. S. Y. 1997. Documenting present and past biodiversity: conservation biology meets palaeontology. - Trends Ecol. Evol. 12: 132–133.

Legendre, P. and Legendre, L. 1998. Numerical Ecology. - Elsevier.

Lehman, C. L. and Tilman, D. 2000. Biodiversity, stability, and productivity in competitive communities. - Am. Nat. 156: 534–552.

Levin, N. et al. 2007. Predicting mountain plant richness and rarity from space using satellite-derived vegetation indices. - Divers. Distrib. 13: 692–703.

Levrel, H. et al. 2010. Balancing state and volunteer investment in biodiversity monitoring for the implementation of CBD indicators: A French example. - Ecol. Econ. 69: 1580–1586.

Lord, D. et al. 1985. Influence of wind on crop canopy reflectance measurements. - Remote Sens. Environ. 18: 113–123.

Loreau, M. and Hector, A. 2001. Partitioning selection and complementarity in biodiversity experiments. - Nature 412: 72–76.

Lucas, K. and Carter, G. 2008. The use of hyperspectral remote sensing to assess vascular plant species richness on Horn Island, Mississippi. - Remote Sens. Environ. 112: 3908–3915.

Lucas, R. et al. 2008. Classification of Australian forest communities using aerial photography, CASI and HyMap data. - Remote Sens. Environ. 112: 2088–2103.

Lucas, R. et al. 2015. The Earth Observation Data for Habitat Monitoring (EODHaM) system. - Int. J. Appl. Earth Obs. Geoinf. 37: 17–28.

Luoto, M. et al. 2002. Modelling butterfly distribution based on remote sensing data. - J Biogeogr. 29: 1027–1037.

Maestre, F. T. et al. 2012. Plant species richness and ecosystem multifunctionality in global drylands. - Science. 335: 214–218.

Magurran, A. E. 2004. Measuring biological diversity. - Blackwell Publishing.

Magurran, A. E. 2007. Species abundance distributions over time. - Ecol. Lett. 10: 347–354.

Magurran, A. E. 2008. Diversity over time. - Folia Geobot. 43: 319–327.

Magurran, A. E. 2013. Open questions: some unresolved issues in biodiversity. - BMC Biol. 11: 118.

Magurran, A. E. and Dornelas, M. 2010. Biological diversity in a changing world. - Philos. Trans. R. Soc. Lond. B. Biol. Sci. 365: 3593–3597.

Magurran, A. E. and McGill, B. J. 2011. Biological diversity: frontiers in measurement and assessment. - Oxford University Press.

Marceau, D. J. and Hay, G. J. 1999. Contributions of remote sensing to the scale issue. - Can. J. Remote Sens. 25: 357–366.

Midgley, G. F. 2012. Biodiversity and ecosystem function. - Science. 335: 174–176.

Mittelbach, G. G. 2012. Biodiversity and ecosystem functioning. - In: Community Ecology. 1st ed.n. Sinauer Associates, Inc., pp. 41–62.

Mittelbach, G. G. et al. 2001. What is the observed relationship between species richness and productivity? - Ecology 82: 2381–2396.

Möckel, T. et al. 2016. Airborne hyperspectral data predict fine-scale plant species diversity in grazed dry grasslands. - Remote Sens. 8: 133.

Monteith, J. L. 1972. Solar radition and productivity in tropical ecosystems. - J. Appl. Ecol. 9: 747–766.

Monteith, J. L. and Moss, C. J. 1977. Climate and the efficiency of crop production in Britain. - Philos. T. Roy. Soc. B 281: 277–294.

Naeem, S. and Li, S. 1997. Biodiversity enhances ecosystem reliability. - Nature 390: 507–510.

Naeem, S. et al. 1994. Declining biodiversity can alter the performance of ecosystem. - Nature 368: 734–737.

Naeem, S. et al. 2000. Plant diversity increases resistance to invasion in the absence of covarying extrinsic factors. - Oikos 91: 97–108.

Nagendra, H. 2001. Using remote sensing to assess biodiversity. - Int. J. Remote Sens. 22: 2377–2400.

Nagendra, H. 2002. Opposite trends in response for the Shannon and Simpson indices of landscape diversity. - Appl. Geogr. 22: 175–186.

Nash, R. F. 1989. The rights of nature: A history of environmental ethics. - University of Wisconsin Press.

Negi, H. R. and Gadgil, M. 2002. Cross-taxon surrogacy of biodiversity in the Indian Garhwal Himalaya. - Biol. Conserv. 105: 143–155.

Nguyen, D. V and Rocke, D. M. 2002. Multi-class cancer classification via partial least squares with gene expression profiles. - Bioinformatics 18: 1216–1226.

Nijs, I. and Roy, J. 2000. How important are species richness, species evenness and interspecific differences to productivity? A mathematical model. - Oikos 88: 57–66.

Noss, R. 1990. Indicators for monitoring biodiversity: A hierarchical approach. - Conserv. Biol. 4: 355–364.

O'Neill, R. V. and King, A. W. 1998. Homage to ST. Michael; Or, Why are there so many books on scale? (DL Peterson and VT Parker, Eds.). - Columbia University Press.

O'Neill, R. V. et al. 1986. A Hierarchical concept of ecosystems. - Princeton University Press.

Ohtomo, Y. et al. 2014. Evidence for biogenic graphite in early Archaean Isua metasedimentary rocks. - Nat. Geosci. 7: 25–28.

Oldeland, J. et al. 2010. Does using species abundance data improve estimates of species diversity from remotely sensed spectral heterogeneity? - Ecol. Indic. 10: 390–396.

Ollinger, S. V 2011. Sources of variability in canopy reflectance and the convergent properties of plants. - New Phytol. 189: 375–394.

Palmer, M. W. et al. 2002. Quantitative tools for perfecting species lists. - Environmetrics 13: 121–137.

Parviainen, M. et al. 2009. The role of local and landscape level measures of greenness in modelling boreal plant species richness. - Ecol. Modell. 220: 2690–2701.

Pavlick, R. et al. 2013. The Jena Diversity-Dynamic Global Vegetation Model (JeDi-DGVM): a diverse approach to representing terrestrial biogeography and biogeochemistry based on plant functional trade-offs. - Biogeosciences 10: 4137–4177.

Peet, R. K. 1974. The measurement of species diversity. - Annu. Rev. Ecol. Syst. 5: 285–307.

Pereira, H. M. et al. 2010. Global biodiversity monitoring. - Front. Ecol. Environ. 8: 458–460.

Pereira, H. M. et al. 2013. Essential biodiversity variables. - Science. 339: 277–278.

Petchey, O. L. and Gaston, K. J. 2002. Functional diversity (FD), species richness and community composition. - Ecol. Lett. 5: 402–411.

Pettorelli, N. et al. 2014. Satellite remote sensing, biodiversity research and conservation of the future. - Philos. Trans. R. Soc. B Biol. Sci. 369: 1–5.

Pickett, S. T. A. et al. 2007. Ecological understnding: The nature of theory and the theory of nature. - Academic Press.

Pielou, E. C. 1966. The measurement of diversity in different types of biological collections. - J. Theor. Biol. 13: 131–144.

Pigliucci, M. et al. 2006. Phenotypic plasticity and evolution by genetic assimilation. - J. Exp. Biol. 209: 2362–2367.

Pimm, S. L. et al. 1995. The future of biodiversity. - Science. 269: 347–350.

Piñeiro, G. et al. 2006. Seasonal variation in aboveground production and radiation-use efficiency of temperate rangelands estimated through remote sensing. - Ecosystems 9: 357–373.

Pottier, J. et al. 2014. Modelling plant species distribution in alpine grasslands using airborne imaging spectroscopy. - Biol. Lett. 10: 1–4.

Power, M. E. et al. 1996. Challenges in the quest for keystones. - Bioscience 46: 609–620.

Price, J. C. 1994. How unique are spectral signatures? - Remote Sens. Environ. 49: 181–186.

Reich, P. B. and Hobbie, S. E. 2013. Decade-long soil nitrogen constraint on the CO2 fertilization of plant biomass. - Nat. Clim. Chang. 3: 278–282.

Reich, P. B. et al. 2012. Impacts of biodiversity loss escalate through time as redundancy fades. - Science. 336: 589–592.

Reichman, O. J. et al. 2011. Challenges and opportunities of open data in ecology. - Science. 331: 703–705.

Roberts, D. A. et al. 1998. Mapping Chaparral in the Santa Monica Mountains using multiple endmember spectral mixture models. - Remote Sens. Environ. 65: 267–279.

Roberts, D. A. et al. 2004. Spectral and structural measures of Northwest forest vegetation at leaf to landscape scales. - Ecosystems 7: 545–562.

Rocchini, D. 2007. Effects of spatial and spectral resolution in estimating ecosystem α-diversity by satellite imagery. - Remote Sens. Environ. 111: 423–434.

Rocchini, D. and Neteler, M. 2012. Spectral rank–abundance for measuring landscape diversity. - Int. J. Remote Sens. 33: 4458–4470.

Rocchini, D. et al. 2004. Testing the spectral variation hypothesis by using satellite multispectral images. - Acta Oecologica 26: 117–120.

Rocchini, D. et al. 2010. Remotely sensed spectral heterogeneity as a proxy of species diversity: Recent advances and open challenges. - Ecol. Inform. 5: 318–329.

Rocchini, D. et al. 2011. Landscape complexity and spatial scale influence the relationship between remotely sensed spectral diversity and survey-based plant species richness. - J. Veg. Sci. 22: 688–698.

Rocchini, D. et al. 2015. Advancing species diversity estimate by remotely sensed proxies: a conceptual review. - Ecol. Inform. 25: 22–28.

Rockström, J. et al. 2009. A safe operating space for humanity. - Nature 461: 472--475.

Roth, K. L. et al. 2015. Differentiating plant species within and across diverse ecosystems with imaging spectroscopy. - Remote Sens. Environ. 167: 135–151.

Sala, O. E. et al. 1996. Biodiversity and ecosystem functioning in grasslands. - In: Mooney, H. A. et al. (eds), Functional Roles of Biodiversity: A Global Perspective. John Wiley and Sons Ltd, pp. 129–149.

Sala, O. E. et al. 2000. Global biodiversity scenarios for the year 2100. - Science. 287: 1770–1774.

Sanchez-Azofeifa, G. A. et al. 2009. Differences in leaf traits, leaf internal structure, and spectral reflectance between two communities of lianas and trees: Implications for remote sensing in tropical environments. - Remote Sens. Environ. 113: 2076–2088.

Saveraid, E. H. et al. 2001. A comparison of satellite data and landscape variables in predicting bird species occurrences in the Greater Yellowstone Ecosystem, USA. - Landsc. Ecol. 16: 71–83.

Schäfer, E. et al. 2016. Mapping tree species diversity of a tropical montane forest by unsupervised clustering of airborne imaging spectroscopy data. - Ecol. Indic. 64: 49–58.

Schmid, H. P. 2002. Footprint modeling for vegetation atmosphere exchange studies : a review and perspective. - Agric. For. Meteorol. 113: 159–183.

Scholes, R. J. et al. 2012. Building a global observing system for biodiversity. - Curr. Opin. Environ. Sustain. 4: 139–146.

Scurlock, J. M. O. et al. 2002. Estimating net primary productivity from grassland biomass dynamics measurements. - Glob. Chang. Biol. 8: 736–753.

Sellers, P. J. 1987. Canopy reflectance, photosynthesis, and transpiration. II - The role of biophysics in the linearity of their interdependence. - Remote Sens. Environ. 21: 143–183.

Shannon, C. E. 1948. A mathematical theory of communication. - Bell Syst. Tech. J. 27: 379–423, 623–656.

Shen, M. et al. 2010. Do flowers affect biomass estimate accuracy from NDVI and EVI? - Int. J. Remote Sens. 31: 2139–2149.

Siemann, E. et al. 1998. Experimental tests of the dependence of arthropod diversity on plant diversity. - Am. Nat. 152: 738–750.

Simpson, E. H. 1949. Measurement of diversity. - Nature 163: 688–688.

Sims, P. L. and Risser, P. G. 2000. Grasslands. - In: Barbour, M. G. and Billings, W. D. (eds), Northern American Terrestrial Vegetation. 2nd ed.n. Cambridge University Press, pp. 323–356.

Srivastava, D. S. et al. 2012. Phylogenetic diversity and the functioning of ecosystems. - Ecol. Lett. 15: 637–648.

Stickler, C. M. and Southworth, J. 2008. Application of multi-scale spatial and spectral analysis for predicting primate occurrence and habitat associations in Kibale National Park, Uganda. - Remote Sens. Environ. 112: 2170–2186.

Stoms, D. M. and Estes, J. E. 1993. A remote sensing research agenda for mapping and monitoring biodiversity. - Int. J. Remote Sens. 14: 1839–1860.

Team, R. C. 2015. R: A language and environment for statistical computing. in press.

Thomas, C. D. et al. 2004. Extinction risk from climate change. - Nature 427: 145–148.

Thompson, S. D. 2015. Mapping and monitering indicators of terrestrial biodiversity with remote sensing.

Tiede, D. et al. 2010. Object-based class modeling for Cadastre-constrained delineation of Geo-objects. - Photogramm. Eng. Remote Sens. 76: 193–202.

Tilman, D. 1997. The influence of functional diversity and composition on ecosystem processes. - Science. 277: 1300–1302.

Tilman, D. and Haddi, A. El 1992. Drought and biodiversity in Grasslands. - Oecologia 89: 257–264.

Tilman, D. and Downing, J. A. 1994. Biodiversity and stability in grasslands. - Nature 367: 363–365.

Tilman, D. et al. 1994. Habitat destruction and the extinction debt. - Nature 371: 65–66.

Tilman, D. et al. 1996. Productivity and sustainability influenced by biodiversity in grassland ecosystems. - Nature 379: 718–720.

Tilman, D. et al. 2001. Diversity and productivity in a long-term grassland experiment. - Science. 294: 843–845.

Tilman, D. et al. 2006. Biodiversity and ecosystem stability in a decade-long grassland experiment. - Nature 441: 629–632.

Tucker, C. J. 1979. Red and photographic infrared linear combinations for monitoring vegetation. - Remote Sens. Environ. 8: 127–150.

Tucker, C. J. et al. 1985. African land-cover classification using satellite data. - Science. 227: 369–375.

Tuomisto, H. 2010a. A diversity of beta diversities: Straightening up a concept gone awry. Part 1. Defining beta diversity as a function of alpha and gamma diversity. - Ecography (Cop.). 33: 2–22.

Tuomisto, H. 2010b. A diversity of beta diversities: Straightening up a concept gone awry. Part 2. Quantifying beta diversity and related phenomena. - Ecography (Cop.). 33: 23–45.

Turner, W. 2014. Sensing biodiversity. - Science. 346: 301–303.

Turner, M. G. et al. 1989. Predicting across scales: Theory development and testing. - Landsc. Ecol. 3: 245–252.

Turner, W. et al. 2003. Remote sensing for biodiversity science and conservation. - Trends Ecol. Evol. 18: 306–314.

Turner, W. et al. 2015. Free and open-access satellite data are key to biodiversity conservation. - Biol. Conserv. 182: 173–176.

US Congress Office of Technology 1987. Technologies to maintain biological diversity.

Ustin, S. L. 2013. Remote sensing of canopy chemistry. - Proc. Natl. Acad. Sci. U. S. A. 110: 804–805.

Ustin, S. L. and Gamon, J. A. 2010. Remote sensing of plant functional types. - New Phytol. 186: 795–816.

Ustin, S. L. et al. 2004. Using imaging spectroscopy to study ecosystem processes and properties. - Bioscience 54: 523–534.

Ustin, S. L. et al. 2009. Retrieval of foliar information about plant pigment systems from high resolution spectroscopy. - Remote Sens. Environ. 113: S67–S77.

van Leeuwen, W. J. D. and Huete, A. R. 1996. Effects of standing litter on the biophysical interpretation of plant canopies with spectral indices. - Remote Sens. Environ. 55: 123–138.

Violle, C. et al. 2012. The return of the variance: Intraspecific variability in community ecology. - Trends Ecol. Evol. 27: 244–252.

Waide, R. B. et al. 1999. The relationship between productivity and species richness. - Annu. Rev. Ecol Syst 30: 257–300.

Wake, D. B. and Vredenburg, V. T. 2008. Are we in the midst of the sixth mass extinction? A view from the world of amphibians. - Proc. Natl. Acad. Sci. U. S. A. 105: 11466–11473.

Wang, R. et al. 2016a. Integrated analysis of productivity and biodiversity in a southern Alberta prairie. - Remote Sens. 8: 214.

Wang, R. et al. 2016b. Seasonal variation in the NDVI–species richness relationship in a prairie grassland experiment (Cedar Creek). - Remote Sens. 8: 128.

Wardle, D. A. 1999. Is “sampling effect” a problem for experiments investigating biodiversity-ecosystem function relationships? - Oikos 87: 403–407.

Wehlage, D. C. 2012. Monitoring year-to-year variability in dry mixed-grass prairie yield using multi-sensor remote sensing.

Westman, W. E. et al. 1989. Tropical deforestation and species endangerment: the role of remote sensing. - Landsc. Ecol. 3: 97–109.

Whittaker, R. H. 1960. Vegetation of the Sisiyou Mountains, Orgeon and California. - Ecol. Monogr. 30: 279–338.

Whittaker, R. H. 1972. Evolution and measurement of species diversity. - Taxon 21: 213–251.

Whittaker, R. J. et al. 2001. Scale and species richness : towards a general , theory of species diversity hierarchical. - Diversity 28: 453–470.

Williams, C. B. 1964. Patterns in the balance of nature and related problems in quantitative ecology. - Academic Press.

Wilsey, B. J. and Potvin, C. 2000. Biodiversity and ecosystem functioning: importance of species evenness in an old field. - Ecology 81: 887–892.

Woodcock, C. E. and Strahler, A. H. 1987. The factor of scale in remote sensing. - Remote Sens. Environ. 21: 311–332.

Wright, I. J. et al. 2004. The worldwide leaf economics spectrum. - Nature 428: 821–827.

Wu, J. and Loucks, O. L. . 1995. From balance of nature to hierarchical patch dynamics : A paradigm shift in ecology. - Q. Rev. Biol. 70: 439–466.

Wulder, M. A. et al. 2004. High spatial resolution remotely sensed data for ecosystem characterization. - Bioscience 54: 511–521.

Xiao, Q. et al. 2004. Using AVIRIS data and multiple-masking techniques to map urban forest tree species. - Int. J. Remote Sens. 25: 5637–5654.

Yuan, W. et al. 2007. Deriving a light use efficiency model from eddy covariance flux data for predicting daily gross primary production across biomes. - Agric. For. Meteorol. 143: 189–207.

Zanne, A. E. et al. 2014. Three keys to the radiation of angiosperms into freezing environments. - Nature 506: 89–92.

Zhang, Y. et al. 2012. Forest productivity increases with evenness, species richness and trait variation: A global meta-analysis. - J. Ecol. 100: 742–749.

Zhang, L. et al. 2016. Deep learning for Remote Sensing Data. - IEEE Geosci. Remote Sens. Mag. 4: 22–40.

Zomer, R. et al. 2009. Building spectral libraries for wetlands land cover classification and hyperspectral remote sensing. - J. Environ. Manage. 90: 2170–2177.

# Appendices

## Chapter 2

Table S2.1 Planted species richness and composition of each plot used in this study. Two species were not germinated in 1994, so plots were reseeded with different species in the same functional groups in 1995. Two woody species (*Quercus ellipsoidalis* and *Quercus macrocarpa*) occurred infrequently and did not exist in the selected plots in this study. The species abbreviations and identities are summarized in Table S2.2.

| Plot # | Species richness | Species |
|---|---|---|
| 2 | 1 | Lesca |
| 3 | 4 | Asctu Liaas Monfi Panvi Solri |
| 5 | 1 | Andge |
| 6 | 2 | Panvi Schsc |
| 11 | 1 | Achmi |
| 12 | 8 | Achmi Koecr Luppe Monfi Petca Petvi Poapr Schsc Solri Sornu |
| 15 | 8 | Agrsm Elyca Monfi Petca Petpu Petvi Poapr Queel Quema Solri |
| 16 | 1 | Asctu |
| 20 | 1 | Amoca |
| 30 | 16 | Achmi Agrsm Amoca Andge Asctu Elyca Koecr Liaas Luppe Monfi Panvi Poapr Queel Quema Schsc Solri Sornu |
| 31 | 1 | Schsc |
| 33 | 4 | Agrsm Andge Liaas Petca Petvi |
| 34 | 16 | Achmi Agrsm Amoca Andge Asctu Elyca Koecr Luppe Monfi Panvi Petpu Poapr Queel Quema Schsc Solri Sornu |
| 35 | 16 | Agrsm Amoca Andge Asctu Elyca Koecr Lesca Liaas Luppe Monfi Panvi Petpu Queel Quema Schsc Solri Sornu |
| 44 | 4 | Asctu Panvi Petca Petpu Petvi |
| 45 | 4 | Andge Liaas Petpu Quema |
| 56 | 2 | Luppe Schsc |

| | | |
|---|---|---|
| 57 | 8 | Achmi Agrsm Koecr Lesca Monfi Petca Petvi Poapr Schsc Solri |
| 58 | 4 | Andge Monfi Poapr Solri Sornu |
| 67 | 8 | Agrsm Koecr Luppe Monfi Petca Petvi Queel Quema Solri Sornu |
| 68 | 16 | Achmi Agrsm Asctu Elyca Koecr Lesca Liaas Luppe Monfi Panvi Petpu Poapr Queel Quema Schsc Solri Sornu |
| 92 | 1 | Sornu |
| 93 | 4 | Agrsm Koecr Luppe Petpu |
| 117 | 2 | Asctu Luppe |
| 118 | 8 | Achmi Agrsm Andge Asctu Koecr Monfi Petpu Quema Solri |
| 129* | 1 | Liaas |
| 142 | 1 | Koecr |
| 164 | 16 | Agrsm Amoca Andge Asctu Elyca Koecr Lesca Liaas Monfi Panvi Petpu Poapr Queel Quema Schsc Solri Sornu |
| 165 | 2 | Poapr Sornu |
| 168 | 2 | Andge Koecr |
| 169 | 16 | Achmi Agrsm Andge Asctu Elyca Koecr Lesca Liaas Luppe Monfi Panvi Petpu Poapr Queel Quema Solri Sornu |
| 170 | 8 | Achmi Asctu Elyca Koecr Monfi Petca Petpu Petvi Queel Solri |
| 171 | 2 | Koecr Luppe |
| 205 | 1 | Petpu |
| 265* | 1 | Luppe |

* indicates the plot was not included in the whole-plot reflectance sampling campaign.

Table S2.2 Species abbreviations and identities in table S2.1.

| Abbreviations | Identities |
|---|---|
| Achmi | *Achillea millefolium* |
| Agrsm | *Agropyron smithii* |
| Amoca | *Amorpha canescens* |
| Andge | *Andropogon gerardii* |
| Asctu | *Asclepias tuberosa* |
| Elyca | *Elymus canadensis* |
| Koecr | *Koeleria cristata* |
| Lesca | *Lespedeza capitata* |
| Liaas | *Liatris aspera* |
| Luppe | *Lupinus perennis* |
| Monfi | *Monarda fistulosa* |
| Panvi | *Panicum virgatum* |
| Petca | *Petalostemum candidum* |
| Petpu | *Petalostemum purpureum* |
| Poapr | *Poa pratensis* |
| Queel | *Quercus ellipsoidalis* |
| Quema | *Quercus macrocarpa* |
| Schsc | *Schizachyrium scoparium* |
| Solri | *Solidago rigida* |
| Sornu | *Sorghastrum nutans* |

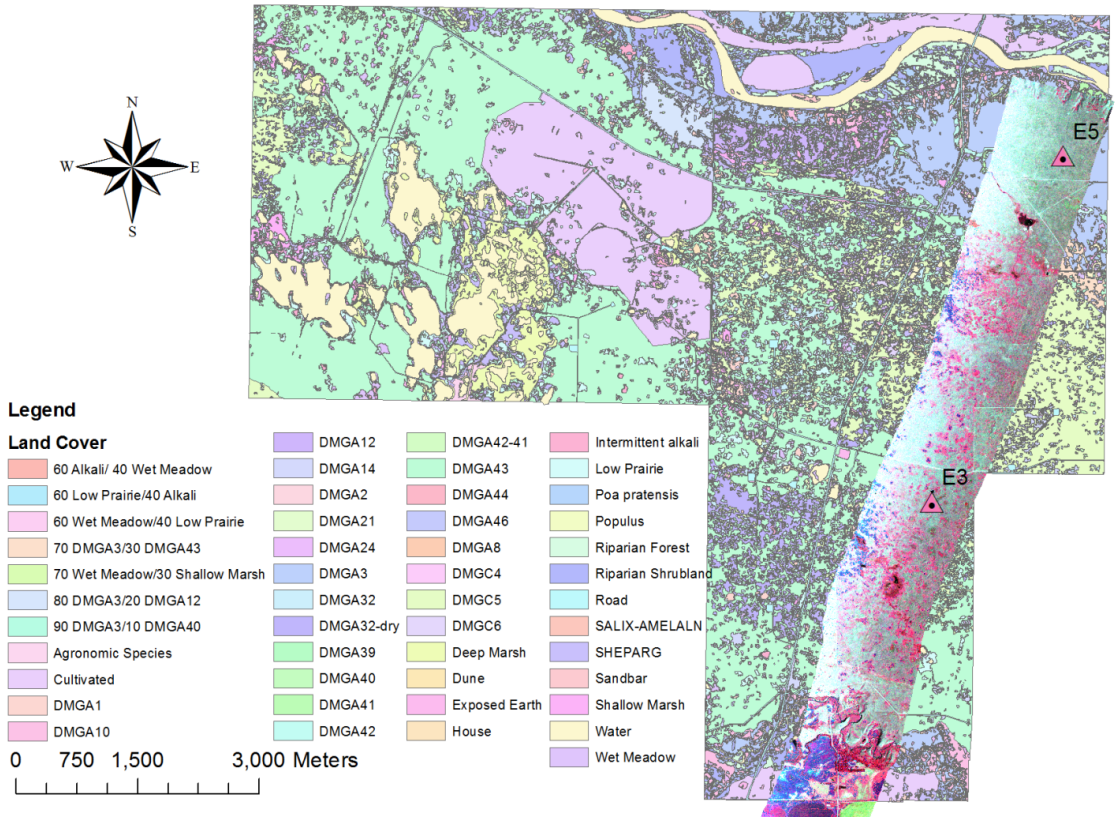


Figure S3.1 The dominant vegetation cover map (1:15,000) at Mattheis Research ranch (Becker 2013), false color (Near Infrared-Red-Green) airborne image and code (Becker 2013) for dominant species in both phenology sites (E3 and E5). The dominant vegetation cover map was derived from a combination of aerial photos and field sampling begun in 2010 but published in 2013 (Becker 2013).

Table S3.1 Code (Becker 2013) for dominant species at two phenology and flux sites

| Code | Dominant species |
|---|---|
| DMGA32 | *Glycyrrhiza lepidota* |
| DMGA32-dry | *Stipa comata*, *Glycyrrhiza lepidota* |
| DMGA43 | *Stipa comata*, *Carex stenophylla*, *Calamovilfa longifolia* |
| DMGC5 | *Rosa woodsii*, *Stipa comata*, *Calamovilfa longifolia*, *Carex stenophylla* |
| DMGA3 | *Stipa comata*, *Koeleria macrantha*, *Bouteloua* |

| | |
|---|---|
| | *gracilis* |
| DMGA46 | *Stipa comata*, *Bouteloua gracilis, Agropyron cristatum* |
| DMGA 40 | *Agropyron smithii*, *Carex stenophylla* |

Table S3.2 Percent cover of dominant vegetation types at E3 site

| Species/ Community code | Percent Cover (200 m radius) | Percent Cover (500 m radius) |
|---|---|---|
| DMGA32 | 0.072519 | 0.084158 |
| DMGA32-dry | 0.03564 | 0.042891 |
| DMGA43 | 0.76665 | 0.750265 |
| DMGC5 | 0.029128 | 0.055279 |
| Intermittent alkali | 0.003819 | 0.000849 |
| Low Prairie | 0.078827 | 0.043499 |
| Shallow Marsh | 0.001032 | 0.001911 |
| water | 0.003258 | 0.001809 |
| Wet Meadow | 0.009125 | 0.010522 |
| Exposure earth | 0 | 0.001233 |
| Others | 0 | 0.007584 |
| Total | 1 | 1 |

Table S3.3 Percent cover of dominant vegetation types at E5 site

| Species/ Community code | Percent Cover (200 m radius) | Percent Cover (500 m radius) |
|---|---|---|
| DMGA3 | 0.969884 | 0.843248 |
| DMGA46 | 0.019399 | 0.055221 |
| Wet Meadow | 0.010716 | 0.007673 |
| Exposure earth | 0 | 0.005448 |
| Low Prairie | 0 | 0.007682 |
| Shallow Marsh | 0 | 0.001349 |
| water | 0 | 0.000213 |
| 90DMGA3/10DMGA40 | 0 | 0.070067 |
| Others | 0 | 0.0091 |
| Total | 1 | 1 |

## Chapter 4

### 4.1 Cedar Creek BigBio plots composition

Table S4.1 Planted species richness and composition of each plot used in this study. Two species were not germinated in 1994, so plots were reseeded with different species in the same functional groups in 1995. Two woody species (*Quercus ellipsoidalis* and *Quercus macrocarpa*) occurred infrequently and did not exist in the selected plots in this study. The species abbreviations and identities are summarized in Table S4.2.

| Plot # | Species richness | Species |
|---|---|---|
| 2 | 1 | Lesca |
| 3 | 4 | Asctu Liaas Monfi Panvi Solri |
| 5 | 1 | Andge |
| 6 | 2 | Panvi Schsc |
| 11 | 1 | Achmi |
| 12 | 8 | Achmi Koecr Luppe Monfi Petca Petvi Poapr Schsc Solri Sornu |
| 15 | 8 | Agrsm Elyca Monfi Petca Petpu Petvi Poapr Queel Quema Solri |
| 16 | 1 | Asctu |
| 20 | 1 | Amoca |
| 30 | 16 | Achmi Agrsm Amoca Andge Asctu Elyca Koecr Liaas Luppe Monfi Panvi Poapr Queel Quema Schsc Solri Sornu |
| 31 | 1 | Schsc |
| 33 | 4 | Agrsm Andge Liaas Petca Petvi |
| 34 | 16 | Achmi Agrsm Amoca Andge Asctu Elyca Koecr Luppe Monfi Panvi Petpu Poapr Queel Quema Schsc Solri Sornu |
| 35 | 16 | Agrsm Amoca Andge Asctu Elyca Koecr Lesca Liaas Luppe Monfi Panvi Petpu Queel Quema Schsc Solri Sornu |
| 44 | 4 | Asctu Panvi Petca Petpu Petvi |
| 45 | 4 | Andge Liaas Petpu Quema |

| | | |
|---|---|---|
| 56 | 2 | Luppe Schsc |
| 57 | 8 | Achmi Agrsm Koecr Lesca Monfi Petca Petvi Poapr Schsc Solri |
| 58 | 4 | Andge Monfi Poapr Solri Sornu |
| 67 | 8 | Agrsm Koecr Luppe Monfi Petca Petvi Queel Quema Solri Sornu |
| 68 | 16 | Achmi Agrsm Asctu Elyca Koecr Lesca Liaas Luppe Monfi Panvi Petpu Poapr Queel Quema Schsc Solri Sornu |
| 92 | 1 | Sornu |
| 93 | 4 | Agrsm Koecr Luppe Petpu |
| 117 | 2 | Asctu Luppe |
| 118 | 8 | Achmi Agrsm Andge Asctu Koecr Monfi Petpu Quema Solri |
| 129* | 1 | Liaas |
| 142 | 1 | Koecr |
| 164 | 16 | Agrsm Amoca Andge Asctu Elyca Koecr Lesca Liaas Monfi Panvi Petpu Poapr Queel Quema Schsc Solri Sornu |
| 165 | 2 | Poapr Sornu |
| 168 | 2 | Andge Koecr |
| 169 | 16 | Achmi Agrsm Andge Asctu Elyca Koecr Lesca Liaas Luppe Monfi Panvi Petpu Poapr Queel Quema Solri Sornu |
| 170 | 8 | Achmi Asctu Elyca Koecr Monfi Petca Petpu Petvi Queel Solri |
| 171 | 2 | Koecr Luppe |
| 205 | 1 | Petpu |
| 265* | 1 | Luppe |

* indicates the plot was not included in the whole-plot reflectance sampling campaign.

Table S4.2 Species abbreviations and identities in table S4.1.

| Abbreviations | Identities |
|---|---|
| Achmi | *Achillea millefolium* |
| Agrsm | *Agropyron smithii* |
| Amoca | *Amorpha canescens* |
| Andge | *Andropogon gerardii* |
| Asctu | *Asclepias tuberosa* |
| Elyca | *Elymus canadensis* |
| Koecr | *Koeleria cristata* |
| Lesca | *Lespedeza capitata* |
| Liaas | *Liatris aspera* |
| Luppe | *Lupinus perennis* |
| Monfi | *Monarda fistulosa* |
| Panvi | *Panicum virgatum* |
| Petca | *Petalostemum candidum* |
| Petpu | *Petalostemum purpureum* |
| Poapr | *Poa pratensis* |
| Queel | *Quercus ellipsoidalis* |
| Quema | *Quercus macrocarpa* |
| Schsc | *Schizachyrium scoparium* |
| Solri | *Solidago rigida* |
| Sornu | *Sorghastrum nutans* |

**4.2 Signal noise ratio effects on CV**

In the simulation work, scaling up (aggregating) the 1 mm pixel sizes also smoothed the data, reducing instrument noise. This analysis explored how this noise affected the CV.

The method of this analysis:

To evaluate noise effects, we a) estimated the signal power of the 1 mm reflectance image. b) generated white Gaussian noise according to the signal power and fixed SNR.

c) added the noise back to reflectance at large scales, and d) calculated CV from reflectance spectra with and without the added noise.

The SNR of the image can be affected by the camera settings, environment and the properties of the targets. A fixed Signal-to-Noise ratio (SNR) was used to simulate the noise, instead of assessing the true noise properties of the instrument. The SNR of the instrument was set to 500 in this test.

$$\mathrm{SNR} = \frac{\text{Signal Power}}{\text{Noise Power}} \qquad \text{(Equation S4.1)}$$

The signal power for each wavelength was estimated with the 1mm Headwall reflectance image.

$$\mathrm{SignalPower_i} = \frac{\sum \rho_i^2}{\text{Signal Length}} \qquad \text{(Equation S4.2)}$$

where $SignalPower_i$ and $\rho_i$ indicate the signal power and reflectance value at wavelength $i$, respectively. Signal length indicates the number of pixels included in the signal power estimation. In this analysis, 10, 000 pixels were used to estimate the signal power at each wavelength.

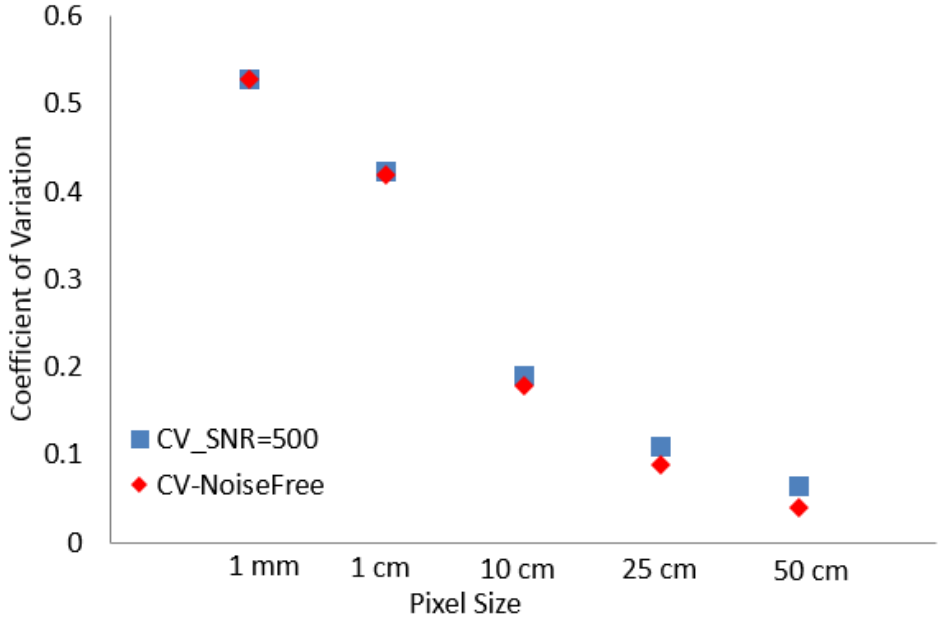


Figure S4.1 Noise effects on the scaling CV results.

The synthetic images represent an idealized situation, but the added noise had a minor effect on the calculated CV (Figure S4.1). Relative to the CV without additional noise, adding a SNR of 500 increased the CV at larger scales, but the decreasing CV value was mostly dominated by the loss of information when scaling up. From this, we conclude that the trend is primarily due to reduced spectral variability (and not reduced SNR) with increasing pixel size.

### 4.3. Spectral range effects on CV

Our imaging spectrometer covered the visible-NIR range, so cannot address the relative benefits of the SWIR for biodiversity detection. This test used a non-imaging full range spectrometer to evaluate the effects of spectral range on CV. A main goal was to see if a SWIR detector added additional information (present in the CV) to assist in biodiversity detection.

A full range spectrometer (PSR 3500, Spectral Evolution, Lawrence, MA, USA) was used to collect data in 30 BigBio plots (6 replicates at each richness levels) in July 2016, which were the same plots used in the primary study reported in the paper. The spectral range of the spectrometer covered 350 to 2500 nm. The spectral resolution was less than 3 nm at 350 to 1000 nm, less than 9 nm at 1500 nm and less than 6.5 nm at 2100nm. A white reference panel (Spectralon, Labsphere, North Sutton, NH, USA) was used to calculate the reflectance. The spectrometer was carried by a tram system (Gamon 2006) to collect data along a transect 2 m from the north edge of each plot. A 6 degree lens (PP system, Amesbury, MA, USA) was mounted on the tram cart at a height of 2 meters, yielding a ground pixel size (IFOV) of approximately 20 cm. Data were collected every 20 cm and the first and last half meters at the east and west end of each transect were skipped to avoid edge effects, yielding 40 samples for each plot. All the measurements were done on clear sunny days and between 10 a.m. and 3 p.m. to minimize shadow effects. For each plot, the CV was calculated for different spectral regions (Table S4.3) and compared to independent metrics: planted species richness, Shannon's Index, and Simpson's Index.

Table S4.3 $R^2$ and *P* value (in parentheses) of the CV-biodiversity metrics relationships for different spectral ranges (in nm). The biodiversity metrics were calculated with biomass data from 2014 and 2015. The strongest correlations and the associated spectral range are shown in bold.

| | 400-1000 | 400-700 | **700-1000** | 400-1765 | 400-2350 | 1000-1765 | 1765-2350 |
|---|---|---|---|---|---|---|---|
| Planted Richness | 0.09 (0.12) | 0.02 (0.40) | **0.21 (0.01)** | 0.10 (0.10) | 0.11 (0.08) | 0.10 (0.10) | 0.12 (0.06) |
| Shannon's Index | 0.04 (0.16) | 0.04 (0.28) | **0.20 (0.01)** | 0.08 (0.12) | 0.10 (0.09) | 0.11 (0.08) | 0.11 (0.09) |
| Simpson's Index | 0.10 (0.09) | 0.02 (0.45) | **0.23 (0.007)** | 0.11 (0.08) | 0.11 (0.07) | 0.1 (0.09) | 0.12 (0.07) |

In this test, using the full range data didn't appear to add much extra information to CV. The strongest R2 arose from 700-1000 (not the full range), and adding data above 1000 nm didn't improve CV for diversity estimation (Table S4.3). This higher correlation using the 700-1000 nm range suggests a strong influence of canopy structure (evident in the 700-1000 nm range) on optical diversity. While not a conclusive test, these results suggest that a full-range spectrometer may not add much power to this particular method of assessing biodiversity based on CV. We note that full-range spectrometers have many vegetation absorption features not present in the VIS-NIR range, and these can play an important role in some methods of biodiversity assessment (Asner, 1998; Ollinger, 2011; Ustin, 2013).

**4.4. Sample size effects on CV**

Since sample size varies with degree of aggregation used for the synthetic image, this simple study aims to test how the sample size affects the coefficient of variation.

Methods

Two images with different species richness level were selected. One is from plot 5, SR=1. The other is from plot 34, SR=16 (Figure S4.2). 100 pixels were randomly picked from each image and used to calculate $CV_{sample}$. 10000 samples were taken to calculate the sampling distribution (Figure S4.2). We then changed the sample size to 64, 81, 400, 900, 1600, and 2500 and calculated the CV of the two plots with 10000 iterations to evaluate sample size effects on CV (Figure S4.2). Because the estimated CV tends to be low when applied to a small or moderate sized sample, we calculated the unbiased estimated CV at each sample size (Sokal & Rohlf, 1995) as:

$$\widehat{cv}^* = \widehat{CV}\left(1 + \frac{1}{4n}\right) \qquad \text{(Equation S4.3)}$$

*where* n indicated the sample size.

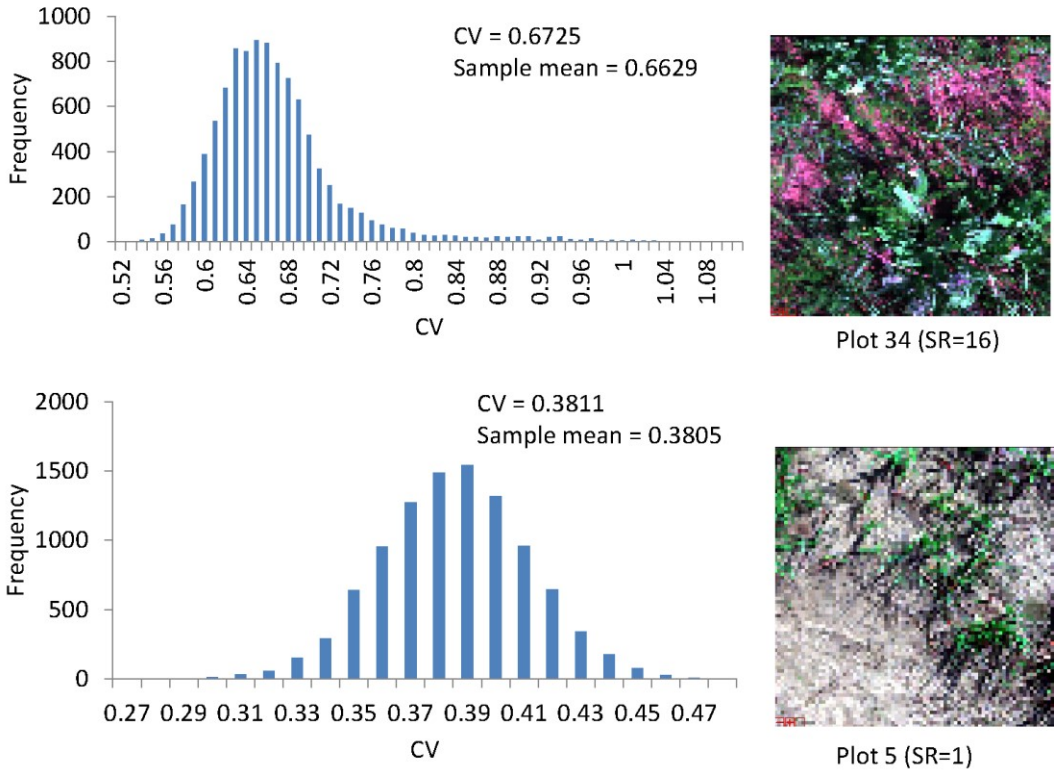


Figure S4.2 Histogram of CV calculated with synthetic images. Sampling iterations = 10000. CV: CV calculated with the simulated image; Sample mean: average CV of 10000 samples.

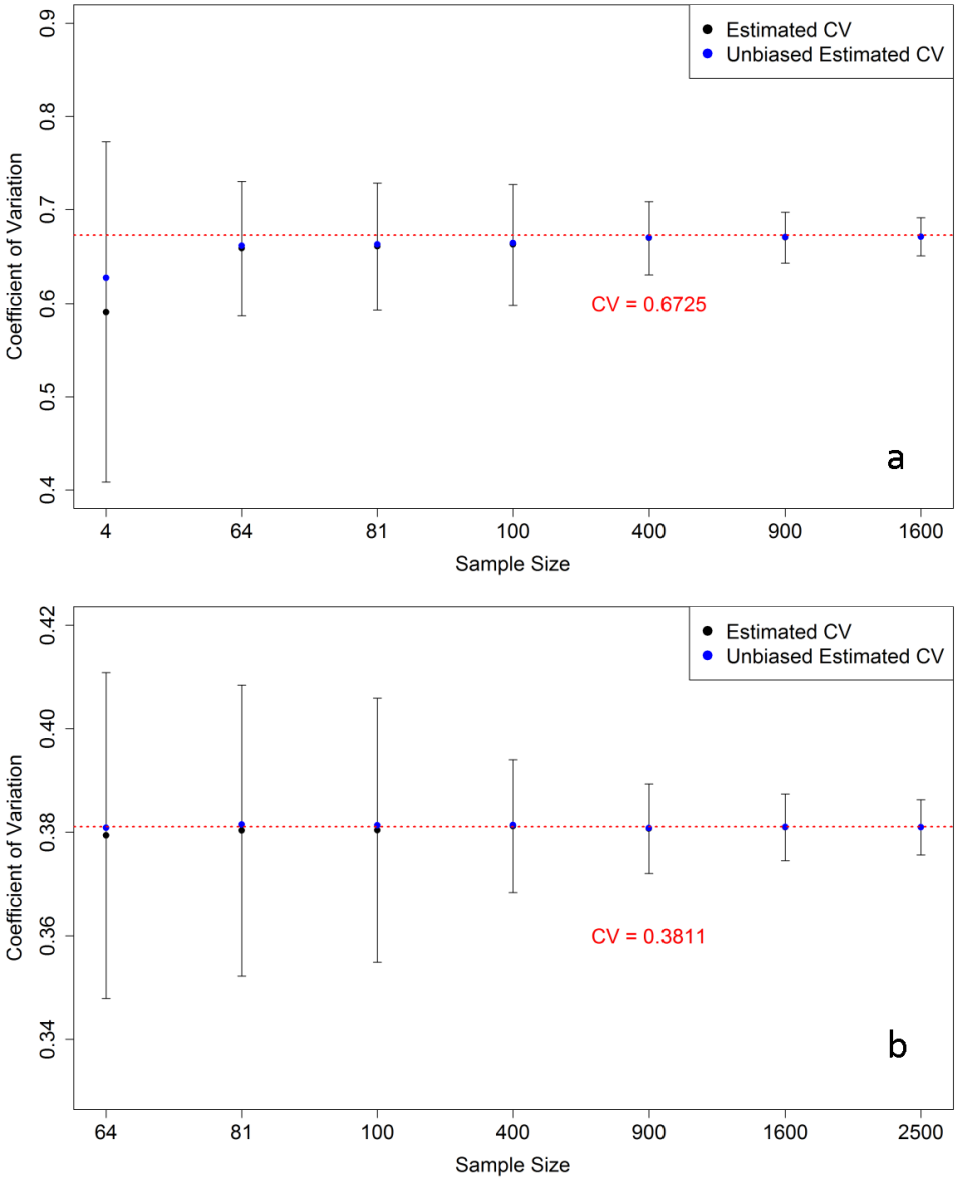


Figure S4.3 The sample size effects on CV. a: estimated CV of plot 34 (SR=16); b: estimated CV of plot 5 (SR=1). The estimated CV was calculated by averaging 10 000 iterations at each sample size (mean of the "sampling distribution"). The unbiased estimated CV was calculated using Equation S4.3 at each sample size. At a small sized sample (64), the estimated CV underestimated the CV by 2%.

We can estimate the CV of the raw image by repeating the sampling process and calculating the mean. The more complex the plot is, the higher chance to get extreme CV

values when take a sample. Samples from high richness plots have a wide range in the frequency plot, visible as a large standard deviation of the normal distribution.

The variation in CV decreased with increasing sample size (from 64 to 2500 (Figure S4.3). In this test, the estimated CV from 1000 iterations underestimated the population CV by around 2% with the smallest sample size (64). The underestimation can reach 6% when a very small sample size is used (sample size = 4). This test indicates that CV is not very sensitive to the sample size and the CV-scale trend is mainly driven by the spectral variability.

## Chapter 5

Table S5.1 Species and mean distance from centroid in the spectral space of each species using two sampling methods (image-derived and leaf-clip-derived spectra) and two spectral ranges (vis-NIR and full-range)

| Species | Abbrev | Image-derived (vis-NIR) | Leaf Clip (vis-NIR) | Leaf Clip (full range) |
|---|---|---|---|---|
| *Achillea millefolium* | ACHMI | 1.256001015 | 0.813613 | 1.160409 |
| *Amorpha canescens* | AMOCA | 1.167630003 | 0.890453 | 1.37737 |
| *Andropogon gerardii* | ANDGE | 1.240865428 | 0.561511 | 0.876769 |
| *Asclepias tuberosa* | ASCTU | 1.920660501 | 0.780499 | 1.18425 |
| *Koeleria cristata* | KOECR | 1.934593559 | 0.677192 | 1.208055 |
| *Lespedeza capitata* | LESCA | 1.885387576 | 0.813369 | 1.23377 |
| *Liatris aspera* | LIAAS | 1.173263778 | 0.599524 | 0.885812 |
| *Lupinus perennis* | LUPPE | 1.038683238 | 0.686042 | 1.053653 |
| *Monarda fistulosa* | MONFI | 1.03093993 | 0.591716 | 0.912182 |
| *Panicum virgatum* | PANVI | 1.058286603 | 0.518749 | 0.809089 |
| *Petelostemum candidum* | PETCA | 0.848094812 | 0.680564 | 1.017332 |
| *Petalostemum purpureum* | PETPU | 0.875418829 | 0.689497 | 0.992343 |
| *Petalostemum villosum* | PETVI | 3.818134861 | 0.802017 | 1.272249 |
| *Poa pratensis* | POAPR | 1.634507667 | 0.795865 | 1.221838 |
| *Schizachyrium scoparium* | SCHSC | 1.165955337 | 0.659302 | 1.056764 |
| *Solidago rigida* | SOLRI | 0.878025491 | 0.565257 | 0.837494 |
| Average | - | 1.43290304 | 0.69532 | 1.06871 |

Plot-level contribution of between- species variation to the total variation

To estimate the contribution of between-species variation to the total variation, we calculated the mean distance to the centroid in the spectral space for each species (Price 1994, Anderson 2001) :

$$Percent_{between\ species} = \sum_{i=0}^{S} d_i^2 * n_i \Big/ \sum_{j=0}^{N} d_j^2 \quad \text{(S5.1)}$$

where *S* indicated the species richness and *N* indicated the total measurements in a simulated plot. $d_i$ indicated the distance from the centroid of each species to the centroid of the plot and $n_i$ indicated the number of points it represents, which is the number of individuals of the *i*th species.

The average contribution of between-species variation increased when species richness got higher (Figure S5.1). The variation of between species variation was smaller among the high richness plots than low richness plots. The plot-level between species variation calculated using leaf clip-derived full range spectra was slightly higher than using leaf clip-derived visible-NIR wavelengths indicated that using full range spectra added useful information to separate different species. The contribution of between species variation was larger in the plots created using the image-derived reflectance than leaf clip-derived reflectance. For both reflectance measurements, the within-species variation was generally larger than the between-species variation at all species richness levels. The between-species variation contributed less than 40% of the total variation for most of the simulated plots.

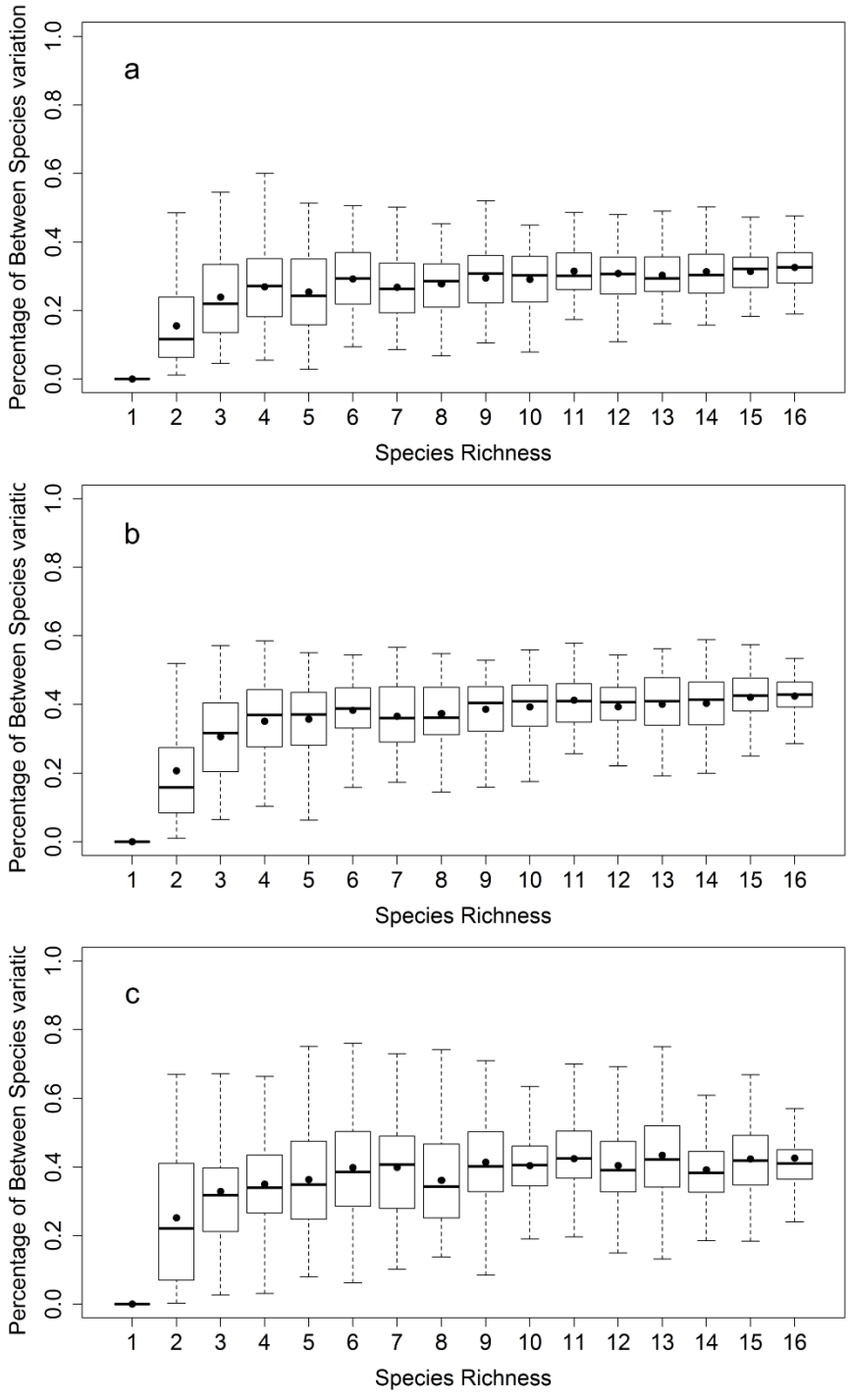


Figure S5.1 Contribution of between-species variation to the total variation

a: Leaf clip-derived (visible-NIR); b: Leaf clip-derived (full range); c: Image-derived (visible-NIR)

Table S5.2 Distance between the mean reflectance of different species in the spectral space (Image-derived reflectance). The species abbreviations and identities are summarized in Table S5.1.

| | ACHMI | AMOCA | ANDGE | ASCTU | KOECR | LESCA | LIAAS | LUPPE | MONFI | PANVI | PETCA | PETPU | PETVI | POAPR | SCHSC | SOLRI |
|---|---|---|---|---|---|---|---|---|---|---|---|---|---|---|---|---|
| ACHMI | -1.00 | 0.58 | 4.31 | 3.89 | 1.60 | 2.52 | 2.63 | 5.08 | 2.56 | 1.77 | 2.52 | 0.74 | 1.80 | 0.51 | 0.38 | 2.35 |
| AMOCA | | -1.00 | 4.02 | 3.59 | 1.33 | 2.15 | 2.35 | 4.73 | 2.33 | 1.70 | 2.23 | 0.49 | 2.15 | 0.77 | 0.69 | 2.10 |
| ANDGE | | | -1.00 | 0.67 | 2.71 | 1.99 | 1.69 | 1.01 | 1.87 | 2.68 | 1.79 | 3.65 | 6.08 | 4.71 | 4.13 | 2.03 |
| ASCTU | | | | -1.00 | 2.32 | 1.48 | 1.29 | 1.24 | 1.39 | 2.38 | 1.44 | 3.21 | 5.68 | 4.28 | 3.76 | 1.56 |
| KOECR | | | | | -1.00 | 1.03 | 1.04 | 3.49 | 1.07 | 0.64 | 0.92 | 0.97 | 3.38 | 2.01 | 1.45 | 0.86 |
| LESCA | | | | | | -1.00 | 0.57 | 2.60 | 0.68 | 1.42 | 0.62 | 1.81 | 4.28 | 2.86 | 2.44 | 0.57 |
| LIAAS | | | | | | | -1.00 | 2.47 | 0.46 | 1.16 | 0.19 | 1.98 | 4.42 | 3.04 | 2.48 | 0.47 |
| LUPPE | | | | | | | | -1.00 | 2.62 | 3.57 | 2.60 | 4.39 | 6.85 | 5.44 | 4.94 | 2.78 |
| MONFI | | | | | | | | | -1.00 | 1.15 | 0.55 | 1.91 | 4.35 | 2.96 | 2.44 | 0.24 |
| PANVI | | | | | | | | | | -1.00 | 1.03 | 1.32 | 3.51 | 2.24 | 1.55 | 1.03 |
| PETCA | | | | | | | | | | | -1.00 | 1.87 | 4.30 | 2.92 | 2.35 | 0.50 |
| PETPU | | | | | | | | | | | | -1.00 | 2.48 | 1.07 | 0.77 | 1.69 |
| PETVI | | | | | | | | | | | | | -1.00 | 1.43 | 1.98 | 4.14 |
| POAPR | | | | | | | | | | | | | | -1.00 | 0.82 | 2.75 |
| SCHSC | | | | | | | | | | | | | | | -1.00 | 2.25 |
| SOLRI | | | | | | | | | | | | | | | | -1.00 |